2-1-2012

A novel method for modeling the neutron Time of Flight (nTOF) detector response in current mode to inertial confinement fusion experiments

Alan Nelson

Alan John Nelson
Candidate

Department of Chemical and Nuclear Engineering
Department

This dissertation is approved, and it is acceptable in quality and form for publication:

Approved by the Dissertation Committee:

Dr. Gary Cooper, *Chairperson*

Dr. Carlos Ruiz

Dr. Anil Prinja

Dr. Mark Gilmore

A NOVEL METHOD FOR MODELING THE NEUTRON TIME OF FLIGHT (nTOF) DETECTOR RESPONSE IN CURRENT MODE TO INERTIAL CONFINEMENT FUSION EXPERIMENTS

By

ALAN JOHN NELSON

B.S. NUCLEAR ENGINEERING
THE UNIVERSITY OF NEW MEXICO, 1988
M.S. NUCLEAR ENGINEERING
THE UNIVERISITY OF NEW MEXICO, 2003

DISSERTATION

Submitted in Partial Fulfillment of the
Requirements of the Degree of

Doctor of Philosophy
Engineering

The University of New Mexico
Albuquerque, New Mexico

December, 2011

DEDICATION

To Kathleen, the love of my life.

And to my family. To my mother Joyce and father Henry, to Uncle Lou and Iyay (Aunt Alice), and to my brothers Eric, Jay and Tim, to my sister Rosie and her husband Bill, to my nephew Robby (son of Hip) and his mother Ann. To my nephews on the west coast, Zack, his wife Cyndy and their son Sam, and Ike (sons of Eric), their stepsister Molly and her mother Caren. And especially to my identical twin brother Lou.

I would like to thank them all for their support and encouragement.

And finally, to all MCNP users everywhere who have ever tried to read – and understand – an MCNP manual. Believe me, I feel your pain.

Umpïyeo!!

ACKNOWLEDGEMENTS

I would like to acknowledge Dr. Gary Cooper, my faculty advisor, and Dr. Carlos Ruiz of Sandia National Laboratories (PMTS), for their never-ending patience and unwavering support and encouragement during the course of this work. I would also like to thank Carlos for all our countless conversations where he “set me straight” on a myriad of topics. I would also like to thank Dr. Ray Leeper for his steadfast support. In addition, I would like to acknowledge Sandia National Laboratories, and in particular, Dr. Keith Matzen and Dr. John Porter for providing funding for this work. Also, special thanks go to Dr. Gordon Chandler, Dr. Kelly Hahn, and technologists José Torres and Ruth Smelser for providing support and encouragement. Great thanks goes out to Dr. Dave Fehl for all his assistance as well.

And finally, I would like to thank Brent Davis, Irene Garza, Larry Robbins, Dr. Chris Hagen, Dr. Lee Ziegler, Steve Molnar and Tim Meehan of National Security Technologies (NSTec) for not only building the nTOF detectors, but also testing and characterizing them, and providing the support and facilities necessary for calibrating them as well.

A Novel Method for Modeling the Neutron Time of Flight (nTOF)

Detector Response in Current Mode to Inertial Confinement Fusion Experiments

By

Alan John Nelson

B.S., Nuclear Engineering, University of New Mexico, 1988

M.S., Nuclear Engineering, University of New Mexico, 2003

Ph.D., Engineering, University of New Mexico, 2011

ABSTRACT

There are several machines in this country that produce short bursts of neutrons for various applications. A few examples are the Z-machine, operated by Sandia National Laboratories in Albuquerque, NM[†]; the OMEGA Laser Facility at the University of Rochester in Rochester, NY[§]; and the National Ignition Facility (NIF) operated by the Department of Energy at Lawrence Livermore National Laboratory in Livermore, California[‡]. They all incorporate neutron time of flight (nTOF) detectors which measure neutron yield, and the shapes of the waveforms from these detectors contain germane information about the plasma conditions that produce the neutrons. However, the signals can also be "clouded" by a certain fraction of neutrons that scatter off structural components and also arrive at the detectors, thereby making analysis of the plasma

---

[†]Matzen, K., Phys. Plasmas **4**, 1519 (1997).
[§]T.R. Boehly, D.L. Brown, R.S. Craxton, R.L. Keck, J.P. Knauer, J.H. Kelly, T.J. Kessler, S.A. Kumpan, S.J. Loucks, S.A. Letzring, F.J. Marshall, R.L. McCrory, S.F.B. Mose, W. Seka, J.M. Soures, and C.P. Verdon, "Initial performance results of the OMEGA laser system," *Opt. Commun*., vol. 133, pp. 495-506, 1997.
[‡]E.I. Moses, "The National Ignition Facility: Status and plans for the experimental program," *Fusion Sci. Technol*., vol 44, pp. 11-18, 2003.

conditions more difficult. These detectors operate in current mode – i.e., they have no discrimination, and all the photomultiplier anode charges are integrated rather than counted individually as they are in single event counting. Up to now, there has not been a method for modeling an nTOF detector operating in current mode. MCNP-PoliMi[∇] was developed in 2002 to simulate neutron and gamma-ray detection in a plastic scintillator, which produces a collision data output table about each neutron and photon interaction occurring within the scintillator; however, the post-processing code which accompanies MCNP-PoliMi assumes a detector operating in *single-event counting mode* and not current mode. Therefore, the idea for this work had been born: could a new post-processing code be written to simulate an nTOF detector operating in current mode? And if so, could this process be used to address such issues as the impact of neutron scattering on the primary signal? Also, could it possibly even identify sources of scattering (i.e., structural materials) that could be removed or modified to produce "cleaner" neutron signals?

This process was first developed and then applied to the axial neutron time of flight detectors at the Z-Facility mentioned above. First, MCNP-PoliMi was used to model relevant portions of the facility between the source and the detector locations. To obtain useful statistics, variance reduction was utilized. Then, the resulting collision output table produced by MCNP-PoliMi was further analyzed by a MATLAB post-processing code. This converted the energy deposited by neutron and photon interactions in the plastic scintillator (i.e., nTOF detector) into light output, in units of

[∇]S.A. Pozzi, E. Padovani, M. Marsequerra, Nucl. Instr. and Meth. A 513 (2003) 550-558.

MeVee[ϕ] (electron equivalent) vs time. The time response of the detector was then folded into the signal via another MATLAB code. The simulated response was then compared with experimental data and shown to be in good agreement.

To address the issue of neutron scattering, an "Ideal Case," (i.e., a plastic scintillator was placed at the same distance from the source for each detector location) with no structural components in the problem. This was done to produce as "pure" a neutron signal as possible. The simulated waveform from this "Ideal Case" was then compared with the simulated data from the "Full Scale" geometry (i.e., the detector at the same location, but with all the structural materials now included).   The "Ideal Case" was subtracted from the "Full Scale" geometry case, and this was determined to be the contribution due to scattering. The time response was deconvolved out of the empirical data, and the contribution due to scattering was then subtracted out of it. A transformation was then made from *dN/dt* to *dN/dE* to obtain neutron spectra at two different detector locations.

___

[ϕ]1 MeVee = amount of light produced by 1 MeV deposited by a Compton scattered electron.

TABLE OF CONTENTS

LIST OF FIGURES

LIST OF TABLES

CHAPTER 1

INTRODUCTION

Neutron Time of Flight (nTOF) detectors are fielded on neutron producing experiments on Sandia National Laboratories' Z machine [1,2]. Some of these are Inertial Confinement Fusion [3] (ICF) experiments using deuterium filled capsules. In addition, these detectors are used to measure the neutron yield and neutron energy from the reaction:

$$D + D \rightarrow He^3(0.82\ MeV) + n(2.45\ MeV) \quad (1)$$

The detectors consist of 2.54 cm (1 inch) thick by 7.62 cm (3 inch) diameter Bicron 418 plastic scintillator coupled via UVT plastic light guides to fast Hamamatsu R5945 mesh-type photomultiplier tubes. Two of these ("side-on") detectors were located along a single line-of-sight at 102° with respect to the z-pinch axis at distances of 742 cm (24.34 ft) and 839 cm (27.53 ft). Another pair of "on-axis" detectors were located on a single line of sight along the z-axis at distances of 730 cm (23.95 ft) and 809 cm (26.54 ft), below the target chamber center (TCC). A schematic of all the nTOF detector positions relative to the ICF capsule is shown in Figure 1.

The physical dimensions of the Z-Facility are quite large, with meters of distance between the source and the detectors. An axial cross-sectional diagram of the facility is shown below in Figure 2, which includes the "on-axis" nTOF detectors located in the basement "pig," which actually had to be fielded 3 ° off axis, to allow space for other

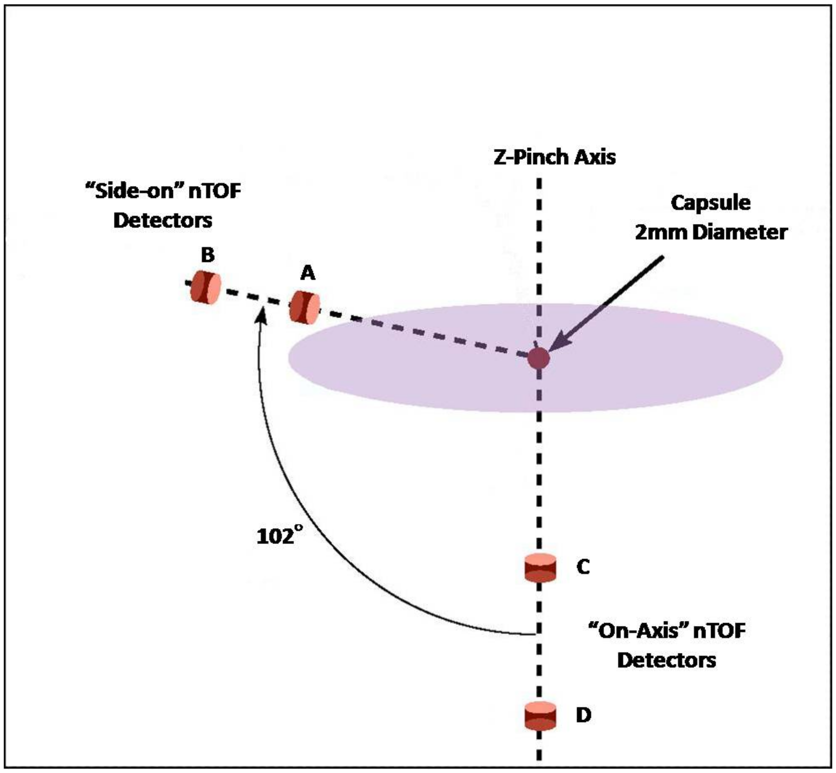

Figure 1. Schematic of nTOF Detector Positions relative to ICF Capsule.

diagnostics sharing the axial view. Due to the intense bremsstrahlung background characteristically produced by Z pinches [4], 20.32 cm (8 inches) of lead shielding was required to prevent the detectors from producing a non-linear response due to saturation of the PMT in the extreme x-ray pulse and not recovering before the neutron signal arrived.

To acquire realistic nTOF signals at the detector, part of the Z-Facility, particularly between the source (Z-pinch) and detector locations would have to be modeled with MCNP [5], with a reasonable degree of detail. To include the axial nTOF detectors in the basement below TCC, the model would extend from the pinch location downward, comprising three of the magnetically insulated transmission lines (MITLs), the stack (which makes up the vacuum chamber), the bottom lid, and the radiation

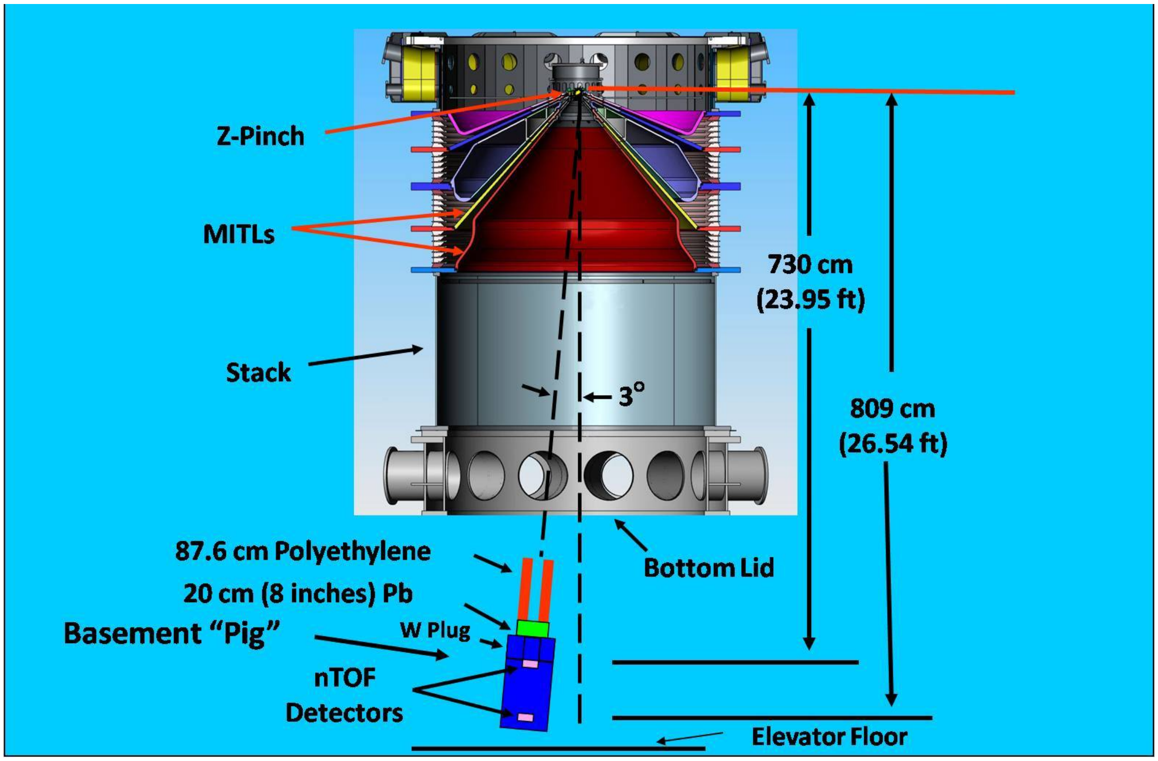

Figure 2. Axial Cross Sectional Diagram of the Z-Facility from the Z-pinch to the Basement "Pig," three degrees off-axis, and ~7m – 8m (23 ft – 26 ft) away from the pinch (TCC).

shield in the basement (i.e., the "pig") housing the two nTOF detectors. In addition to the pig, a polyethylene collimator 87.6 cm (34.49 in) long with an inner diameter of 7.62 cm (3in) that was fixed to the top of the pig was also included. A cross section view near TCC of the model used is shown in Figure 3; the entire model comprises over 2400 cells, and more than 900 surfaces. The great number of cells and surfaces were required due to the large scope of the machine. Although the basic *geometry* of the machine is straightforward – the vacuum chamber is a large cylinder, the MITLs (magnetically insulated transmission lines, shown in Figure 2) are large cones; even the "pig" in the basement has a cylindrical geometry, and these basic shapes all exist within MCNP, however, one cannot assign, for example, one cylindrical cell to be the vacuum

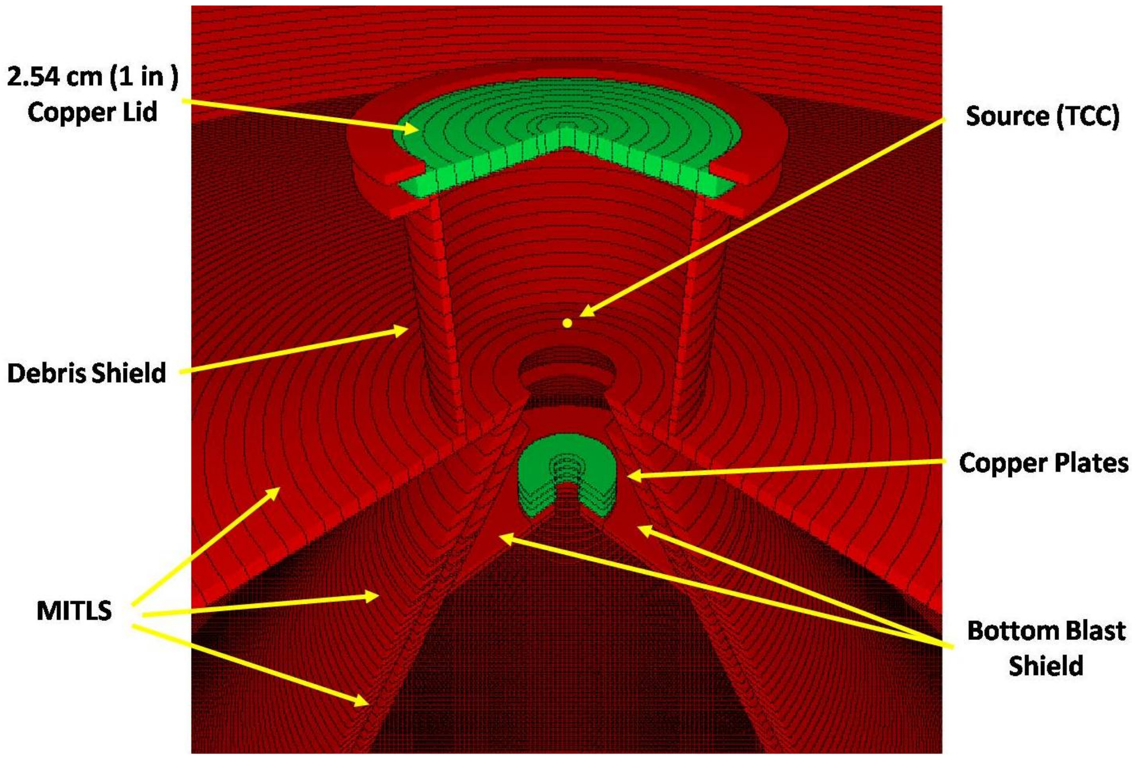

Figure 3. 3-D View near Source (TCC). The MCNP-PoliMi model comprised of over more than 2400 cells and 900 surfaces. The overall geometry is cylindrical, and the lines seen in the figure are individual surfaces making up each slice, or cell.

chamber, with an inner diameter of 3.20 m (10 ft, 6 inches) and a length from TCC downward of 5.3 m (17 feet, 5 inches). To track particles effectively, MCNP requires that the optical thickness of cell dimensions be on the order of *one mean free path* [5]. For DD neutrons of 2.45 MeV through stainless steel, the mean free path is 3.33 cm (1.31 inches). Therefore, a great number of cells and surfaces were needed to divide the vacuum chamber into thin *slices* (cells) – the same with the MITLs, and the same with the basement "pig" – in fact, the same with the entire geometry of the problem. Making simple slices of the geometry also allowed MCNP to run faster, since it prefers the problem geometry made up of many simple cells rather than fewer more complicated cells [5]. The slices can be seen in the three-dimensional view near the source, in Figure 3. The overall geometry was cylindrical, and the lines seen in Figure 3 are individual surfaces making up each slice, or cell.

The “pig” which housed the two nTOF detectors was originally designed to field an x-ray camera, and was not designed as a neutron shield; however, it was the only shield available at the time, and had ample space to accommodate the two nTOF detectors. Also, being comprised of high Z materials – namely lead and tungsten – made it an effective shield against the intense bremsstrahlung background. The original basement pig compared to its MCNP model are shown in Figure 4. As seen in the

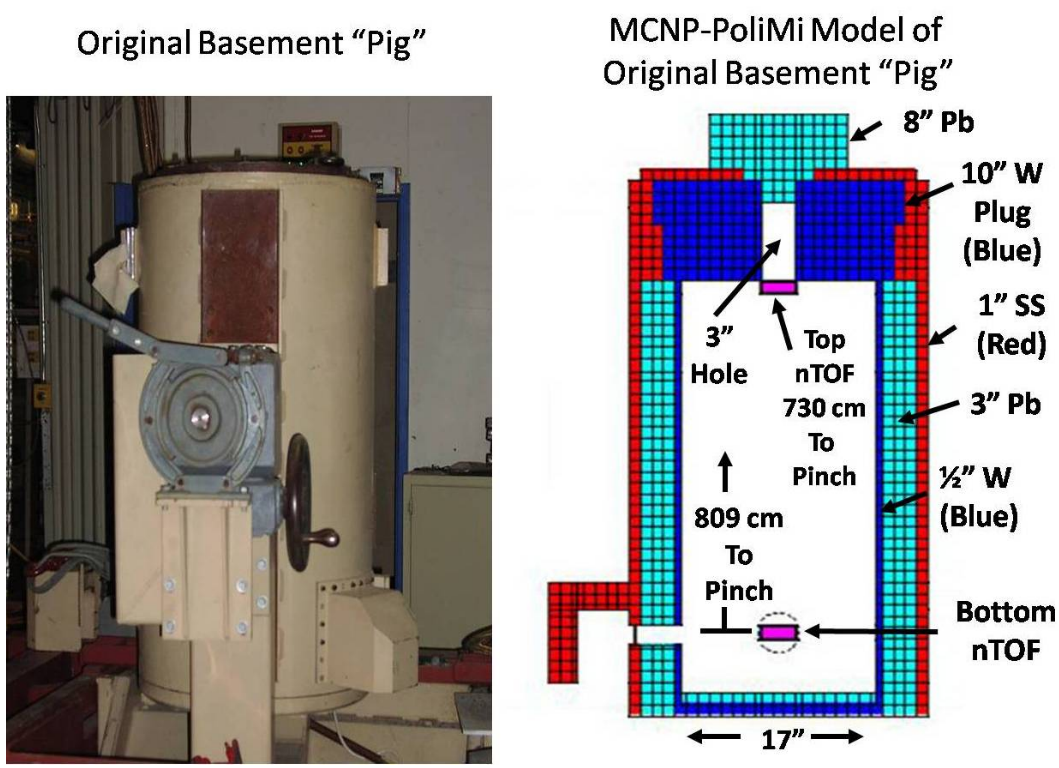

Figure 4. Original Basement “Pig” and its MCNP-PoliMi model. It was not designed as a neutron shield; it originally housed an x-ray camera. The lead plug located on top (right) was necessary to attenuate the intense x-ray pulse at shot time so the detectors would not saturate.

figure, an additional 20.32 cm (8 in) of lead were added to the top of the pig to cover the 7.62 cm (3 in) aperture. This shielding was necessary to reduce the bremsstrahlung pulse in the detectors. Without it, that intense x-ray pulse would saturate the two nTOFs, and they would not recover in time to see the DD neutron pulse arriving over 300 ns later.

As mentioned above, a polyethylene collimator 87.6 cm (34.49 in) long with a 7.62 cm (3 in) inner aperture was located on top of the pig. A cross section of the polyethylene collimator and top of the pig is shown in Figure 5. Below the 20.32 cm (8

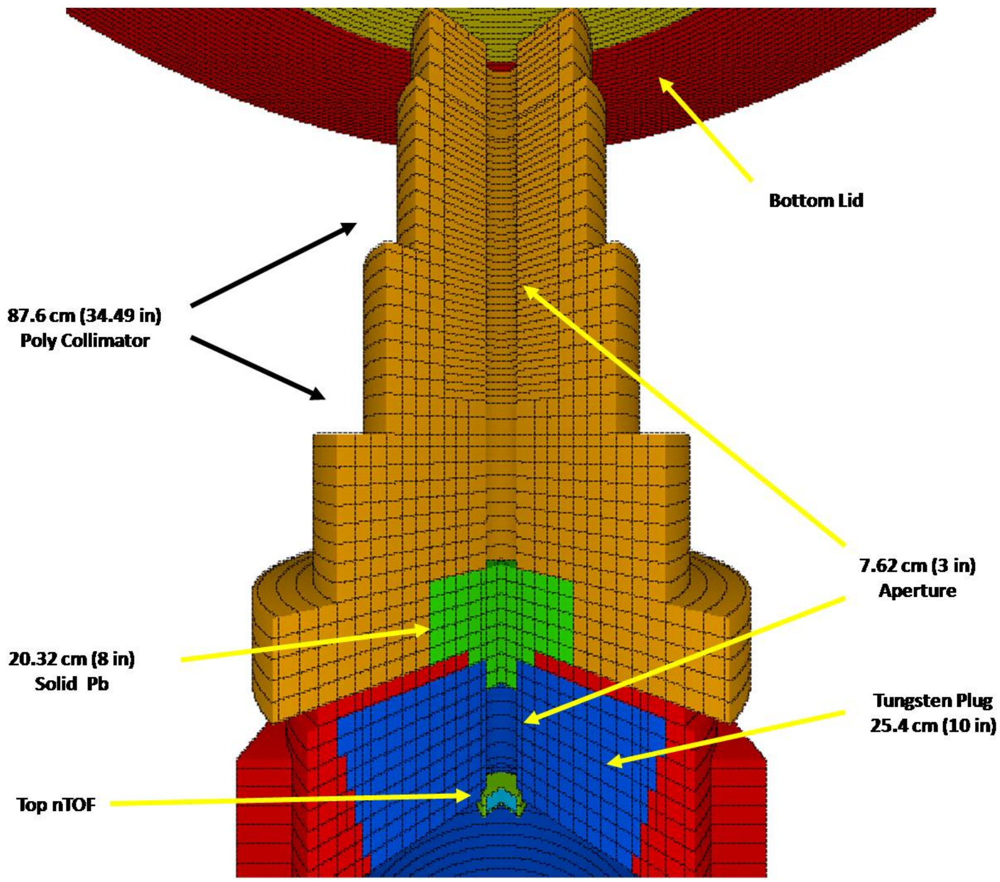

Figure 5. 3-D View of Polyethylene Collimator and Top nTOF. The detector is located at the base of the 7.62 cm (3 in) aperture.

in) of lead is a tungsten plug 25.4 cm (10 in) long with a 7.62 cm (3 in) aperture. The top nTOF detector is located at the base of the aperture. A cross section of the lower part of the pig showing both the top and bottom nTOF detectors, part of the pig chassis and elevator floor is shown in Figure 6.

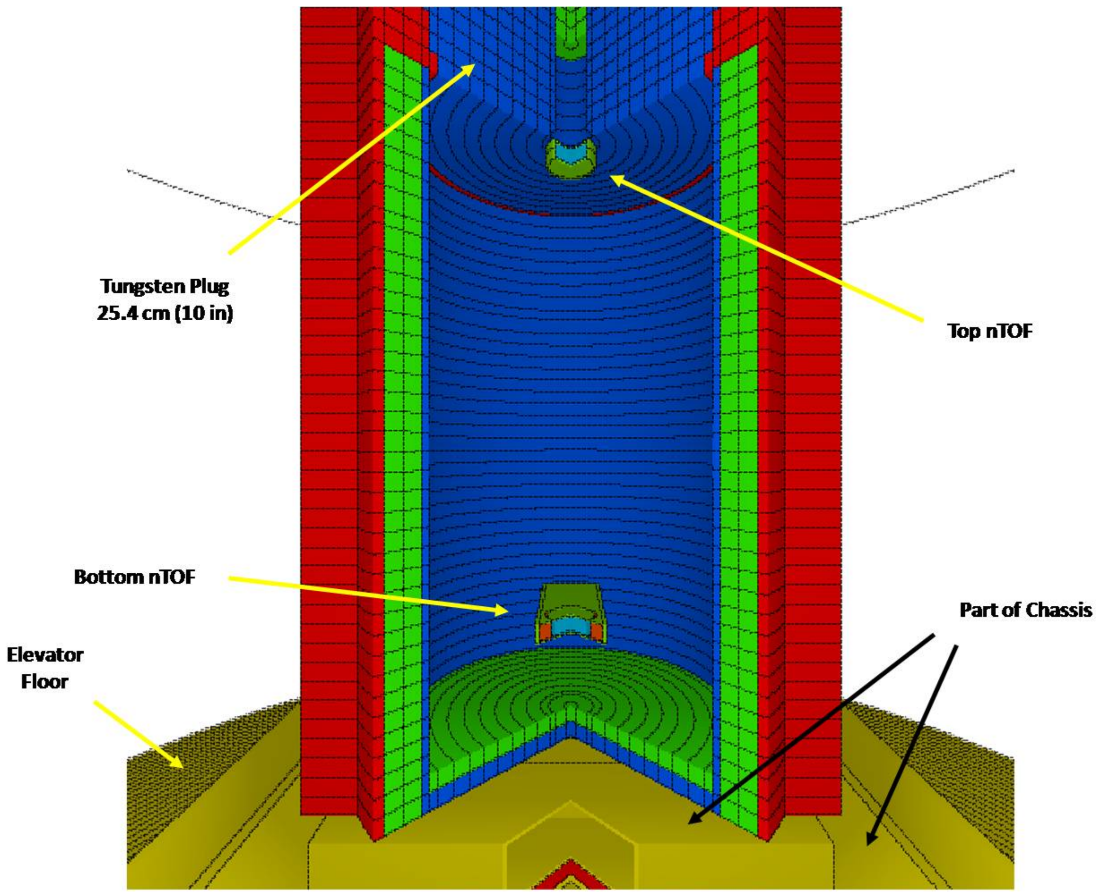

Figure 6. 3-D View of Top and Bottom nTOF Detectors. Part of the chassis, the elevator floor and tungsten plug can also be seen.

CHAPTER 2

MCNP-PoliMi

MCNP-PoliMi [6] is a user-modified version of a general purpose, continuous-energy, time-dependent, Monte Carlo N-Particle code, version 4C [5] that can be used for neutron, photon, electron, or coupled neutron/photon/electron transport. In it, the user creates an input file which contains: the geometry of the problem, description of materials in the problem, the location and characteristics of the source, and the type of answers or tallies desired. It has been used to simulate measurements made by the Nuclear Materials Identification System (NMIS) [7], and has been validated [8]. It was developed at the Polytechnic of Milan, Italy (which gives rise to its name; PoliMi stands for "**Poli**tecnico di **Mi**lano") by E. Padovani and S.A. Pozzi, in 2002 [9]. It is a versatile tool to simulate particle interactions and detection processes, and consists of two stages: first, an input file is run which produces a collision data output table, then the PoliMi MATLAB post-processing code [9] analyzes the table and produces a detector response. In this case, the MATLAB post-processing code was rewritten for this work to simulate a detector response produced by an nTOF detector operated in current mode [10].

Detailed information about each neutron and photon interaction occurring in user-specified cells is reported in the collision data output table. Interaction type, target nucleus, energy deposited in the collision, time at which the collision occurred, and number of scatterings are among the pertinent data. A partial sample of the collision data output table is shown below in Table I. The modified MATLAB post-processing code reads the collision data output table, and converts the energy deposited in MeV to MeVee (electron equivalent) [11] according to the incident particle's *response function*.

Table I.

Excerpt from MCNP-PoliMi Collision Data Output Table.

Projectile Type[§]	Interaction Type[∇]	Target Nucleus[†]	Energy Deposited in Collision (MeV)	Time (Shakes)[Φ]	Number Of Scatterings
1	-99	1001	0.52526	43.55	1
1	-99	1001	0.18983	84.74	2
1	-99	1001	0.01374	84.76	1
1	-99	6000	0.01628	75.01	3
1	-99	6000	0.00892	75.13	3
1	-99	1001	0.02221	75.27	3
1	-99	1001	0.01146	75.31	4
1	-99	6000	0.00028	75.43	2
1	-99	1001	0.00036	75.49	1
1	-99	1001	0.00080	78.30	3
1	-99	6000	0.00012	78.74	2
1	-99	6000	0.01170	74.81	1
2	1	6	1.94631	62.74	1

[§]1 = Neutron; 2 = photon; [∇]-99 = elastic scattering; 1 = Compton scattering; -1 = inelastic scattering; [†]1001 and 1 = Hydrogen; 6000 and 6 = Carbon; [Φ]1 Shake = 10 ns = 10^{-8} sec.

CHAPTER 3

RESPONSE FUNCTIONS

The simulation of the detector pulse requires that the energy deposited in the detector by neutrons and photons be converted into light output by using measured detector response functions [9]. Neutrons are detected primarily by elastic scattering on hydrogen, with the measured response function fit to the following quadratic equation for a plastic scintillator as shown in equation (2):

$$L = 0.0364 * {E_n}^2 + 0.125 * E_n \quad (2)$$

where E_n is the energy deposited by the neutron on hydrogen (MeV) and L is the measured light output (MeVee). The resulting recoil protons quickly transfer their kinetic energy to luminescent states in the scintillator [12]. Neutron interactions with carbon are assumed to generate a very small light output equal to:

$$L = 0.02 * E_n \quad (3)$$

where E_n is the energy deposited by the neutron on carbon (MeV) and L is the corresponding light output (MeVee). (This is an approximation by the authors of PoliMi, due to the fact that the light conversion of the recoil carbons is roughly one order of magnitude lower than that of the recoil protons; in the post-processing program they arbitrarily imposed that the kinetic energy of carbon nuclei be converted to light with a constant efficiency factor of 0.02 MeVee per MeV [13]). In these reactions, energy is lost by the neutron without significant light production.

Photons, on the other hand, are detected primarily by Compton scattering, and the pulse-height to energy deposited response is very close to linear:

$$L = E_{\gamma} \tag{4}$$

where E_{γ} is the energy deposited by the photon (MeV) and L is the measured light output (MeVee). A plot of the response function for a neutron on hydrogen according to the response functions of PoliMi (equation 2 above) and Stanton [14] as well as Czirr [15] and Verbinski [16] are shown in Figure 7. This displays not only the comparison of PoliMi's, Stanton's, Czirr's and Verbinski's response functions, but also the nonlinear nature of scintillator light output for non-photons.

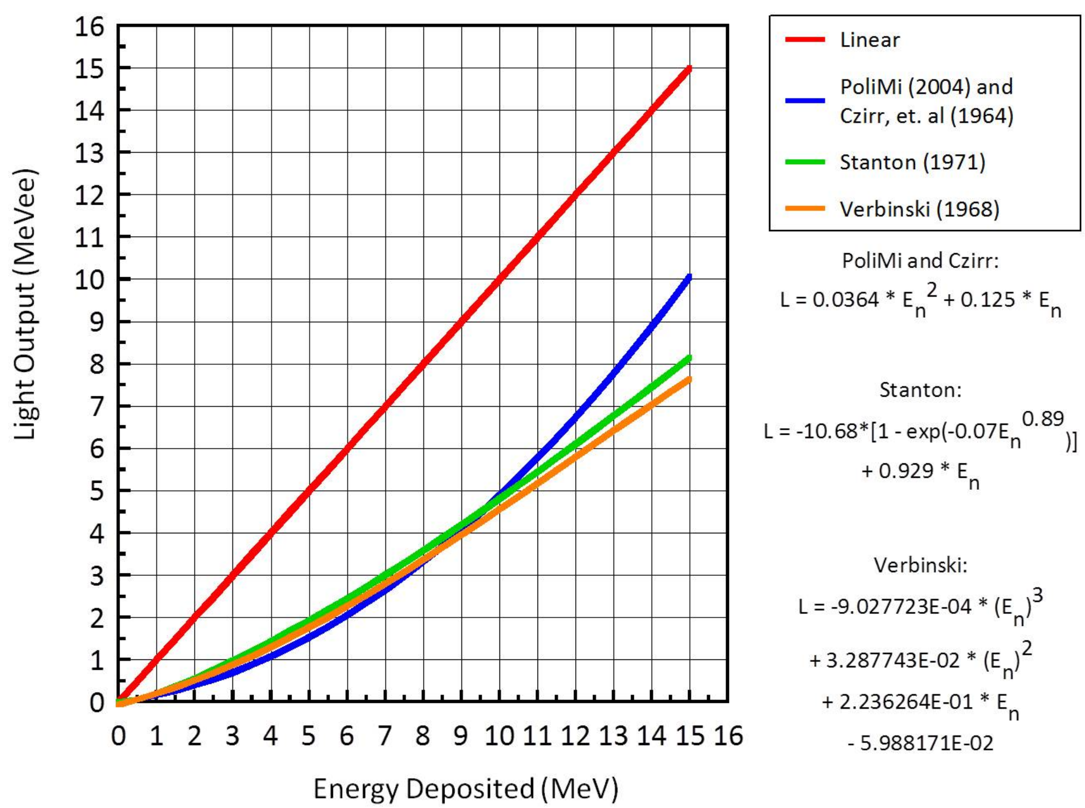

Figure 7. The nonlinearity of Scintillator Light Output. Comparison of the response functions of PoliMi, Czirr, Stanton and Verbinski for a neutron on hydrogen. PoliMi and Czirr compare well with each other, and Stanton and Verbinski are similar. They all produce light output which is decidedly nonlinear in nature.

ENERGY DEPOSITED VS LIGHT OUTPUT

There has been a trend in the community when doing calculations of this nature to only look at the energy deposited in the scintillator as opposed to the light output produced from neutron interactions with hydrogen and carbon (in MeVee). Certainly, MCNP accommodates energy deposition tallies, such as an F6 (MeV/gram) [5], but in reality, this is not the true "output" from the scintillator. Without the correct response functions listed above, which have been measured by Stanton [14], Czirr [15], Verbinski [16] and Polimi [17] which convert energy deposited (MeV) to light output (MeVee), one will *grossly overestimate* the amount of light output which is produced. An illustrative example is shown in Figure 8. For the same MCNPX [18] calculation, the F6 Tally (MeV/gram) was compared to the light output produced by the process discussed in this work. At the left in Figure 8 is the F6 Tally (red) compared to the calculated light output (blue). As can be seen, the F6 Tally crudely resembles the calculated light output, but once they are area normalized (on the right) there is no longer any resemblance, showing that the F6 Tally is overestimating the amount of light output produced greater than an order of magnitude. When the calculated light output in Figure 8 (blue, left) is compared with the actual data and area normalized (as shown, for example, in Figure 15 on page 30) one can see that the calculation is very close to the data, both in terms of shape and magnitude.

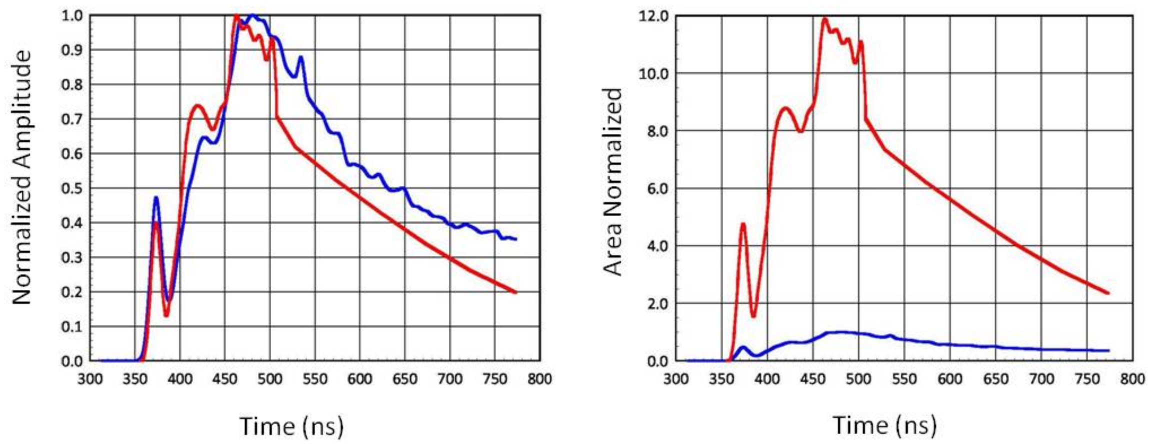

Figure 8. Energy Deposition (MeV) vs Light Output (MeVee). For the same number of histories, light output was produced using the response functions above, and shown in blue; this is compared to an F6 energy deposition tally in MCNPX (MeV/gram, red). On the left one can see that the red crudely resembles the blue *in shape*, but once they are area normalized (on the right) there is no longer any resemblance, showing that the F6 Tally is overestimating the amount of light produced greater than an order of magnitude. When the calculated light output (blue, left) is compared to the actual data and area normalized (Figure 15, p. 30) the calculation compares well to the data, both in terms of shape and magnitude.

CHAPTER 4

THE POST-PROCESSING CODE

The post-processing code was written in MATLAB, which loads the collision data output table, then sorts it in terms of increasing time (column 6 in Table I, p. 9), then converts the energy deposited in MeV into light output (MeVee) according to the incident particle (either a neutron or photon) and the target nucleus (H or C), then sums all the light outputs into time bins which correspond to the resolution of the data digitizer recording (in this case, 200 ps time bins used on Tektronix TVS645 digitizers [19]), then plots the light output versus time. An additional code written for this work convolves the actual time response of the detector with the MATLAB output where it can be compared with empirical data. A flowchart of the post-processing code with these additional steps is shown in Figure 9.

Figure 10 shows an early plot of light output versus time only (with no convolved detector response) for an analog Monte Carlo run. The term “analog” means assigning weight equal to unity to all of the particles generated at the source and to each of the secondary particles born at a collision. The analog model is the simplest Monte Carlo model for particle transport problems because it uses natural probabilities that various events occur (e.g., collision, capture, scattering, etc.). Particles are followed from event to event, and the next event is always sampled (using the random number generator) from a number of possible next events according to the natural event probabilities.

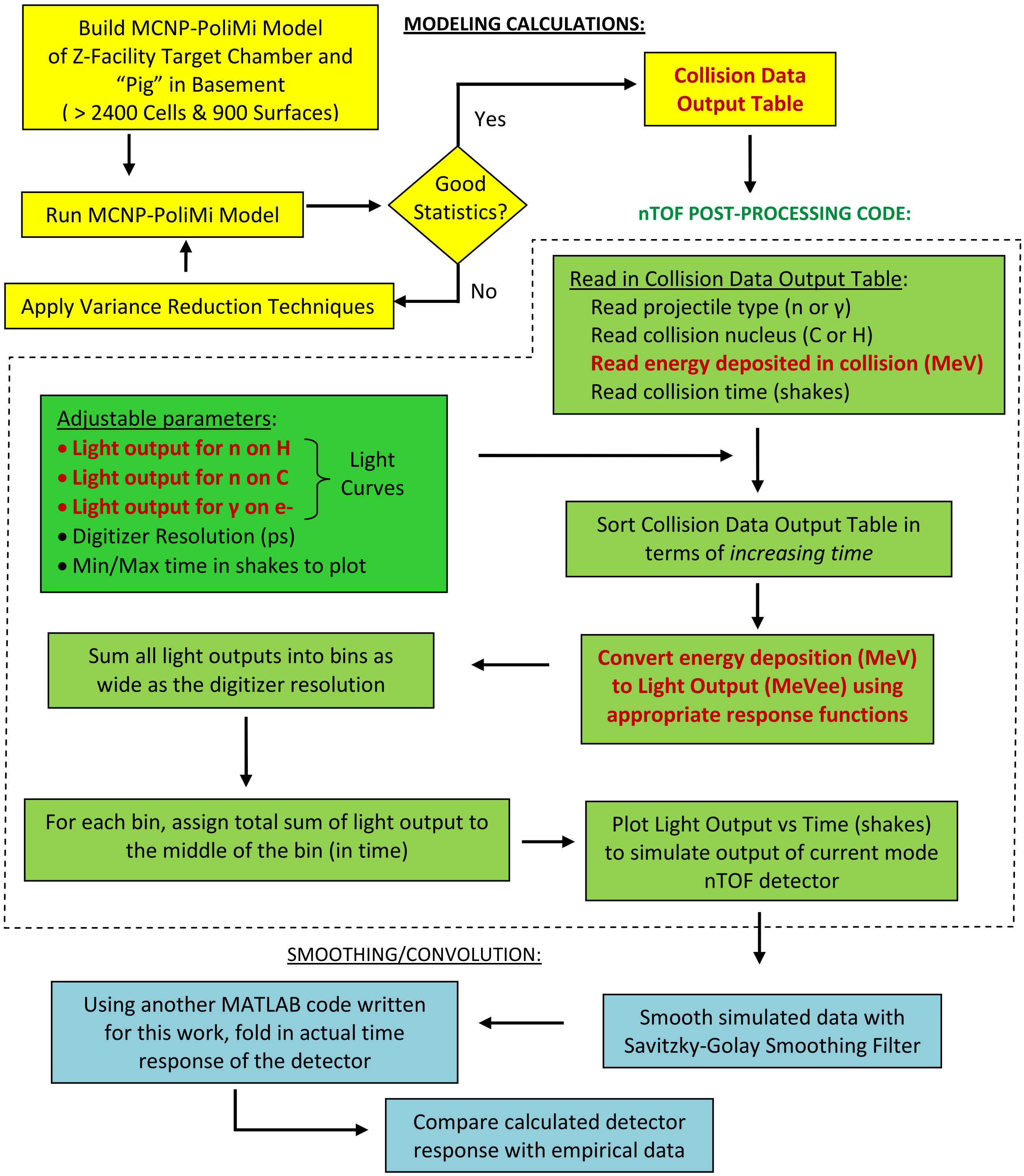

Figure 9. Flowchart of the post-processing code. It reads the collision output table produced in an MCNP-PoliMi model, sorts is in terms of increasing time, converts energy deposited (MeV) into light output (MeVee) with appropriate response functions, sums the light output into time bins equal to the digitizer's resolution, and plots the result. The raw data is then smoothed with a Savitzky-Golay smoothing filter. An additional code then convolves the smoothed data with the actual time response of the detector, where it can then be compared with empirical data.

This way, analog Monte Carlo is directly analogous to naturally occurring transport. It works well when a significant fraction of the particles contribute to the tally estimate; however, in most real-world type problems with complicated geometries and large source-to-detector distances, the fraction of particles detected can be very small (less than 10^{-06}). For these cases analog Monte Carlo fails because few, if any, of the particles get tallied, and the statistical uncertainty in the answer is unacceptable. The MCNP results in Figure 10 is a case in point; on a desktop PC, it ran the maximum amount of particles (2.0E09), and it took 43 hours. Due to the distance from the source (~8m) and amount of material between the detectors and source (20.32 cm Pb, the bottom lid, etc.), the probability of transporting a particle from the Z-pinch (TCC) to an nTOF detector in the basement becomes *vanishingly small* when using analog Monte Carlo. Therefore, *non-analog* Monte Carlo techniques had to be implemented. Non-analog Monte Carlo models estimate the same average value as the analog Monte Carlo model, but often make the variance (uncertainty) of the estimate much smaller than the variance for the analog estimate. In practical terms, this means that problems that would be impossible to solve in *days* of computer time can now be solved in *minutes* of computer time.

There are many non-analog techniques, and they all are meant to increase the odds that a particle contributes to a tally. To ensure that the average score is the same in the nonanalog model as in the analog model, the score is modified to remove the effect of biasing (changing) the natural odds. Thus, if a particle is artificially made q times as likely to execute a given random walk (i.e., travel in a particular direction toward a detector), then the particle's score is weighted by (multiplied by) 1/q. The average score is thus preserved, because it is the sum over all random walks. In this way, nonanalog – or variance reduction – techniques (VRTs) can often decrease the

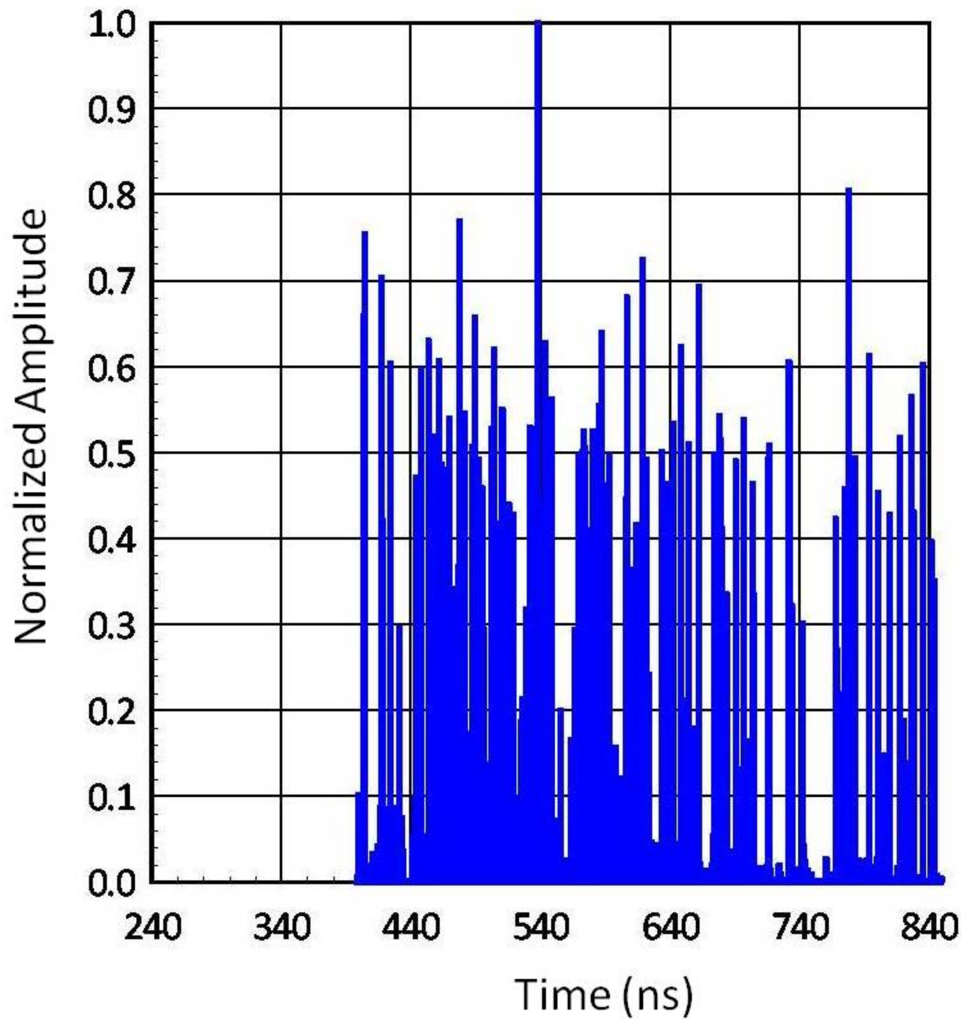

Figure 10. An analog MCNP-PoliMi model (i.e., without any Variance Reduction Techniques applied). This was run with the maximum amount of particles (2.0E09), and it took 43 hours of computer time.

relative error by sampling naturally *rare* events with an *unnaturally high frequency* and weighting the tallies appropriately.

CHAPTER 5

VARIANCE REDUCTION

Central to the art of variance reduction is the concept of particle weight [20]. To simulate the transport of a large number of particles, it is not necessary to follow all of them. Rather, it is only necessary to follow a statistically significant sample of particle "histories." Each history is assigned a weight that, in some sense, represents the number of particles modeled. At any time during the random walk of the particle, it may be split into N particle "tracks" provided that the weight is divided by N. Alternatively, it may be killed with probability 1/N ("Russian Roulette") at any time provided the weight of surviving particles is multiplied by N. All variance reduction schemes work by putting a large number of particles of low weight in regions of interest and allowing only a small number of particles with high weight in unimportant regions of the problem. A summary of all the VRTs that proved useful for this work are shown below.

WEIGHT WINDOWS

The weight windows method is a *population control method* which artificially increases/decreases the number of particles in spatial or energy regions that are important/unimportant to the tally score. It is another form of geometry splitting and Russian Roulette, where a particle crossing into a cell of higher importance is split, whereas a particle crossing into a cell of lower importance undergoes Russian Roulette. In this way, particles from the source migrate toward the tally region. The user can also employ a mesh-based weight window (or "importance") generator, where a mesh is superimposed over the entire geometry of the problem; this causes an optimum performance function to be generated. This importance function is usually superior to anything an experienced user can guess for cell importances (especially when *thousands* of cells make up the problem, manually assigning an importance to each one becomes non-trivial). All regions in the problem are assigned a set of upper and lower weight window bounds. Particles with weights greater than the upper bound are split so that all split particles are within the window; particles with weights below the lower bound play Russian Roulette to increase their weight until they lie within the window or are killed [21]. This causes more particles with lower weight to drift toward the tally region.

POINT/RING DETECTOR

The use of a point detector (or a ring detector if the problem has axial symmetry) is a *partially deterministic method* where the random walk process is replaced by a deterministic process to move particles from one region to another. It is a necessity in situations where the analog random walk is inefficient. Often, the point is in a region far from the source in an area where it would otherwise be difficult to transport particles. It deterministically estimates the fluence at the specified point in the problem. At every collision site, the probability of a particle scattering toward the point detector is calculated. There are three factors that affect this probability: the distance between the collision site and the point/ring detector; the probability of scattering toward the point/ring detector, rather than in the original direction; and the optical thickness of material between the collision site and the point/ring detector. In this case the point detector was placed at the center of each 7.62 cm (3 in) diameter, 2.54 cm (1 in) thick plastic nTOF scintillator. However, to eliminate cross-talk, only one point detector was used at a time. Also, since the bottom pig was 3°off axis as shown in Figure 2, a ring detector could not be used (the problem was not axially symmetric); a point detector was used instead.

DXTRAN

Like the point/ring detector, DXTRAN is a *partially deterministic* method. It stands for "deterministic transport," and is a "next event estimator" which is used to deterministically transport the uncollided weight from collision and source points to a spherical surface, known as a DXTRAN sphere. Thus, source particles upon being born, or upon collision during their random walk, generate "pseudoparticles" which are *deterministically transported*, without collision, to the DXTRAN sphere. The random walk is then continued *inside* the sphere for these DXTRAN particles. If non-DXTRAN particles try to enter the DXTRAN sphere, they are killed (i.e., removed from the problem) to balance the particle weight contribution to the cells inside the sphere. In this way, one can obtain many particles in a small region of interest that would otherwise be difficult to sample. For this case, a DXTRAN sphere was made just to encompass each 7.62 (3in) diameter, 2.54 cm (1in) thick plastic nTOF scintillator. And similarly with using point detectors, only one DXTRAN sphere was used at a time to eliminate cross-talk between multiple spheres.

FORCED COLLISIONS

Forced Collisions is a *modified sampling method* which artificially increases the sampling of collisions in specified cells, generally those near a DXTRAN sphere and/or point/ring detector. This method splits particles into collided and uncollided parts, where the collided part is forced to interact within the specified cell while the uncollided particle exits the cell without collision. In combination with a DXTRAN sphere and a point/ring detector, this method produces large numbers of collisions which are desirable to more efficiently approach the problem solution. For this model, the specified cell on the forced collisions card was the cell assigned to the actual nTOF plastic scintillator with a point detector located at its center, which was encompassed by a DXTRAN sphere.

IMPLICIT CAPTURE

Like Forced Collisions, implicit capture is a *modified sampling method*. When a particle collides, there is a probability that it is captured by the nucleus. In analog capture, the particle is killed with that probability. In implicit capture (also known as "survival biasing," and "absorption by weight reduction") the particle is never killed by capture; instead, its weight is reduced by the capture probability at each collision. In this way, no particles are lost to absorption, but absorption effects are properly accounted for. The advantage of implicit capture is that important particles are not killed after a great deal of effort has been expended to transport them long distances, and that when a particle has finally, against considerable odds, reached the tally region, it is not absorbed just before a tally contribution is made. Also, particles that loose energy through multiple collisions and are no longer considered useful, analog capture can efficiently get rid of them – the user can specify the energy at which analog capture takes over. In fact, implicit capture is so powerful that it is one of two MCNP variance reduction options that is turned on by default. The other is Russian Roulette [5].

Using the above variance reduction methods, generally two runs were required to satisfy the requirements of a "good" calculation, namely, that the relative error on the point/ring detector tally (located at the center of the nTOF scintillators) were less than 5%, the Figure of Merit (FOM), or measure of efficiency, was maximized, and that all ten statistical checks in the output were passed. The Figure of Merit is defined as:

$$FOM = 1/R^2T \tag{5}$$

where T is the run time, and R is the relative error generated by the point/ring detector tally. For different VRTs, the one with the largest FOM is preferred.

VARIANCE REDUCTION CAVEATS

While some problems can only be solved by using variance reduction methods, the user should proceed cautiously when applying them. When they are used correctly they can greatly help the user produce a more efficient calculation. Used poorly, however, and they can result in a wrong answer with good statistics and few clues that anything is amiss. The user should proceed cautiously when applying VRTs. A few precautions a user should heed when using VRTs are the following:

- The user should err on the conservative side when using VRTs (some techniques are not recommended for the inexperienced user, such as forced collisions, point/ring detectors, and DXTRAN spheres).
- The output should be studied for peculiarities (large fluctuations, etc.)

- One of the key parameters for assessing the effectiveness of a VRT is the Figure of Merit (FOM) – generally the better the improvement of the FOM, the better is the VRT.
- Also, the FOM table should not be erratic; this indicates poor sampling. The FOM should rapidly approach a constant value (except for fluctuations early on in the simulation).

SMOOTHING THE RAW SIMULATED DATA

Once the variance reduction techniques listed above were implemented, and the output was examined to make sure the relative error on the point detector tally was < 5%, the FOM was maximized, and the ten statistical checks passed, the post-processing code was used to plot light output (MeVee) vs time (ns). An example of a plot produced is shown in Figure 11 for detector location "D" as indicated in Figure 1. It should be noted that this data indicated the largest amount of scattering seen in an nTOF signal for this type of experiment. Note that after the initial neutron peak there is a very large, second scattering peak. This was a model of the machine as shown in Figure 3. MCNP- PoliMi models were run at each axial detector location ("C" and "D" in Figure 1), each before and after the collimator was implemented, and will be compared with the experimental data in Chapter 6.

As can be seen in Figure 11, despite all the efforts with variance reduction to obtain as good a signal as possible at the detector, due to the complexity of the problem with large source-to-detector distances, and abundant scattering material throughout

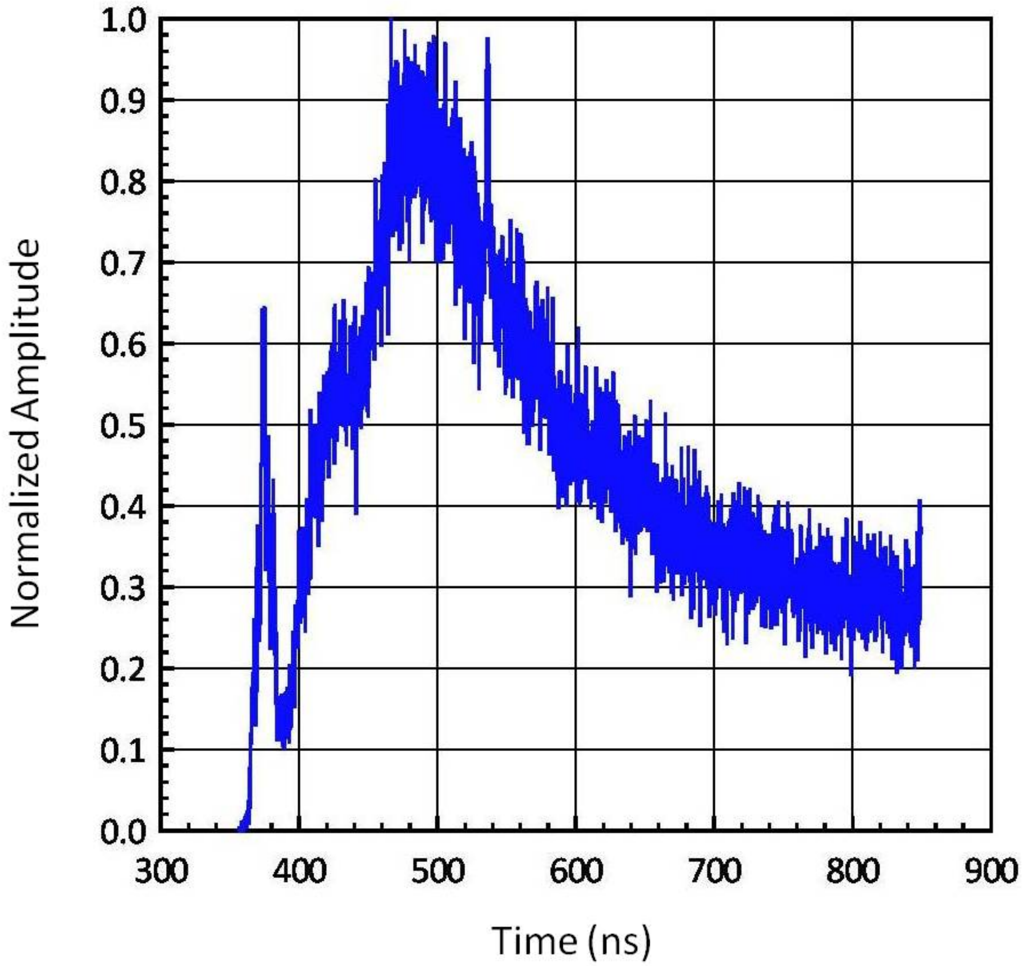

Figure 11. Output of the post-processing code for the largest amount of scattering seen in an nTOF signal for this type of experiment. Light output in MeVee is plotted vs time in ns. This particular case is for detector location "D" in Figure 1. Note that after the primary neutron peak there is a very large, second scattering peak.

the model, the raw simulated data is too noisy. To smooth out this noise, a Savitzky-Golay smoothing filter was used [22]. The advantage of this method is that it tends to preserve features of the distribution such as relative minima, maxima, and width, which are usually 'flattened' by other adjacent averaging techniques [23]. The raw simulated data before and after smoothing are shown in Figure 12.

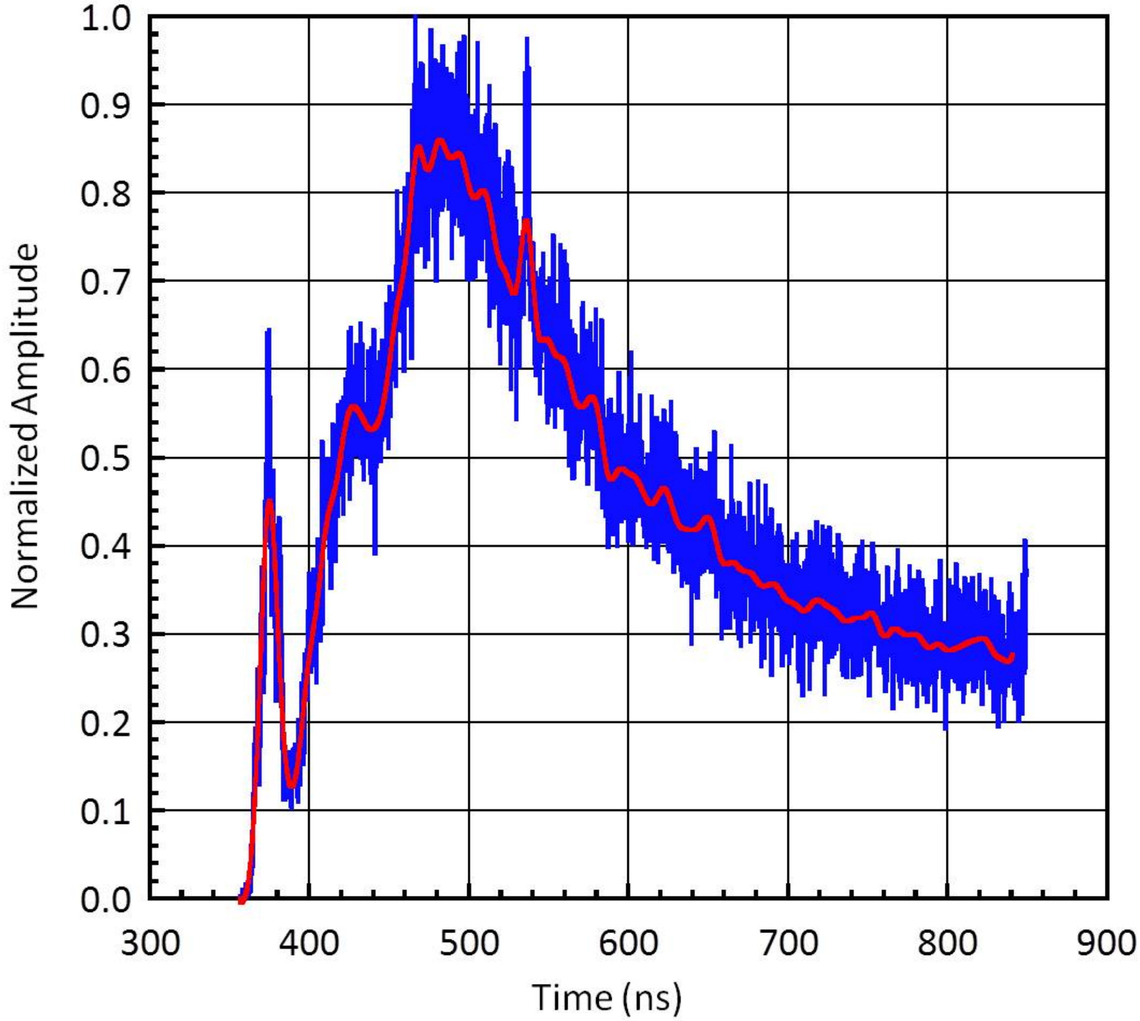

Figure 12. Despite using numerous variance reduction techniques to obtain the best signal possible at the detector, the raw simulated data from Figure 11 (blue) is still too noisy. The Savitzky-Golay smoothing filter was applied to help smooth out the noisy simulated data and is shown in red.

CHAPTER 6

CONVOLVING THE TIME RESPONSE

The next step was to "fold in" – or convolve – the actual time response of the detector with the post-processor output. This required another code to be written in MATLAB. The time response of the detectors used was found experimentally at the Idaho Accelerator Center (IAC) using their 15 MeV Linac producing a 50 ps photon beam [24]; (see also Appendix E). A plot of a detector time response is shown in Figure 13.

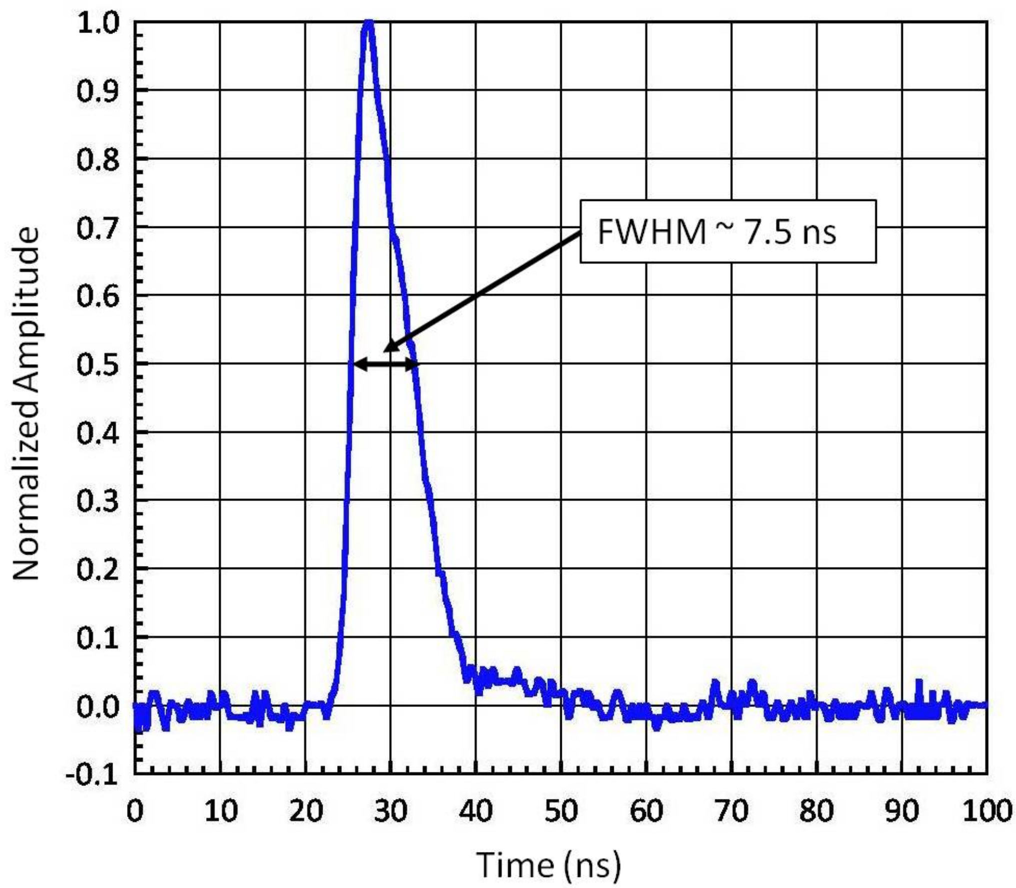

Figure 13. Time response of an nTOF detector found at the Idaho Accelerator Center (IAC). The FWHM is approximately 7.5 ns. This was made with 50 picosecond bursts of x-rays. It will be convolved with a neutron impulse response later in order to include both *timing* and *neutron impulse response information.*

The convolution of two functions r(t) and s(t), is denoted by:

$$(r \otimes s)_j \equiv \sum_{k=-\frac{M}{2}+1}^{\frac{M}{2}} s_{j-k}\, r_k \tag{6}$$

Typically *s* is a signal or data stream, and *r* is a response function of finite duration M. The effect of convolution is to smear – or broaden – the signal *s(t)* in time according to the response function *r(t)* [25].

BROADENING DUE TO TEMPERATURE AND TIME RESPONSE

In an "Ideal Case," an nTOF detector at 809 cm (26.54 ft), location "D" in Figure 1, from a 4 keV DD fusion source would produce a FWHM according to:

$$Temp = 16578.1944 * \frac{(FWHM)^2}{D^2} \tag{7}$$

where Temp is in keV, D is in cm, and FWHM is in ns. Thus, the broadening due to temperature alone would be 12.57 ns for the parameters listed above. Then, folding in a time response of 7.5 ns, in quadrature [26], the FWHM becomes:

$$FWHM = \sqrt{(Temp\ FWHM)^2 + (Time\ Response\ FWHM)^2} \tag{8}$$

$$or, FWHM = 14.64\ ns$$

Broadening due to temperature and temperature *plus* time response is shown in Figure 14. Note how the time response broadens the signal and adds a small "tail" to the waveform. Also, the peak shifts to the right in time from 373.16 ns to 379.76 ns due to the convolution of the time response.

Another contributor to broadening in the real world is the thickness of scintillator *itself*. This is shown in Table II for plastic scintillator thicknesses ranging from 0.3175 cm (1/8") to 20.32 cm (8"). This data was obtained by running an "Ideal Case" – i.e., a scintillator of varying thickness at a distance of 809 cm from a 4 keV DD fusion source, and producing a waveform by the technique described herein. Also shown in the table is the broadening due to the convolution of the time response.

However, what role does *neutron scattering* play in the broadening of the detector response? It cannot be subtracted out in quadrature, since it is not a Gaussian phenomenon. Nevertheless, since it is entirely a function of how much structural and shielding material are near the detector, it would be unique in every location, and totally dependent on the local geometry. Therefore, the simplest approach would be to take the total FWHM and subtract out the FWHM due to temperature and time

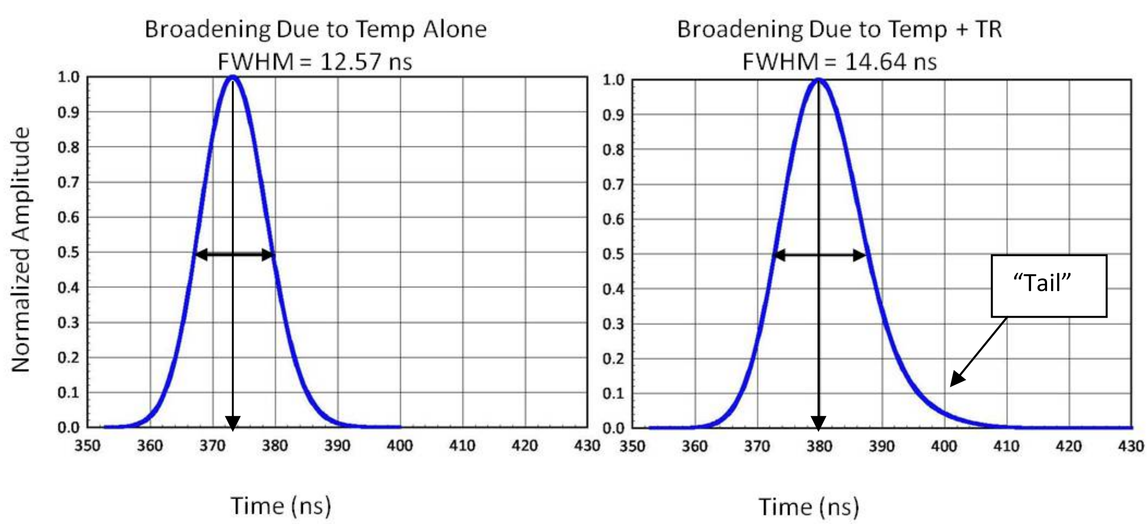

Figure 14. Broadening due to 4 keV temperature alone (right), and a 4 keV temperature and a time response of 7.5 ns (left). In the first case, the FWHM = 12.57 ns; in the second, the FWHM = 14.64 ns. Note that the peak shifts to the right in time from 373.16 ns (left) to 379.76 ns (right) due to the folding in of the time response, which broadens the signal, and produces a small "tail" (right).

response; the remainder would be the broadening due to neutron scattering at that particular detector location.

Table II.

Temporal Broadening due to Scintillator Thickness and Time Response for a 4 keV DD Fusion Source placed at 809 cm.†

Thickness of Scintillator	**Broadening due to Thickness (ns)**	**Broadening due to Time Response (ns) Ave: < 2.437 >**
0.3175 cm (1/8”)	---	2.394
1.27 cm (1/2”)	0.03	2.425
2.54 cm (1”)	0.03	2.43
5.08 cm (2”)	0.08	2.518
7.62 cm (3”)	0.33	2.441
10.16 cm (4”)	0.53	2.418
15.24 cm (6”)	0.83	2.425
20.32 cm (8”)	1.03	2.441

†Ideally, for a 4 keV DD Fusion Source, broadening due to temperature alone is given by equation (7) above to be 12.57 ns, and broadening due to convolution with the time response is given by equation (8) above to be 14.64 ns.

COMPARING CALCULATIONS WITH EMPIRICAL DATA

Using the MATLAB code written for convolution, the time response was convolved (“folded in”) with the post-processor output and compared with empirical data. In Figure 15, the calculated detector response is compared to shot z1217, with the machine in a configuration as shown in Figure 3. The plots are area normalized. The neutron source used in the MCNP-PoliMi model was a 4 keV DD Fusion Source.

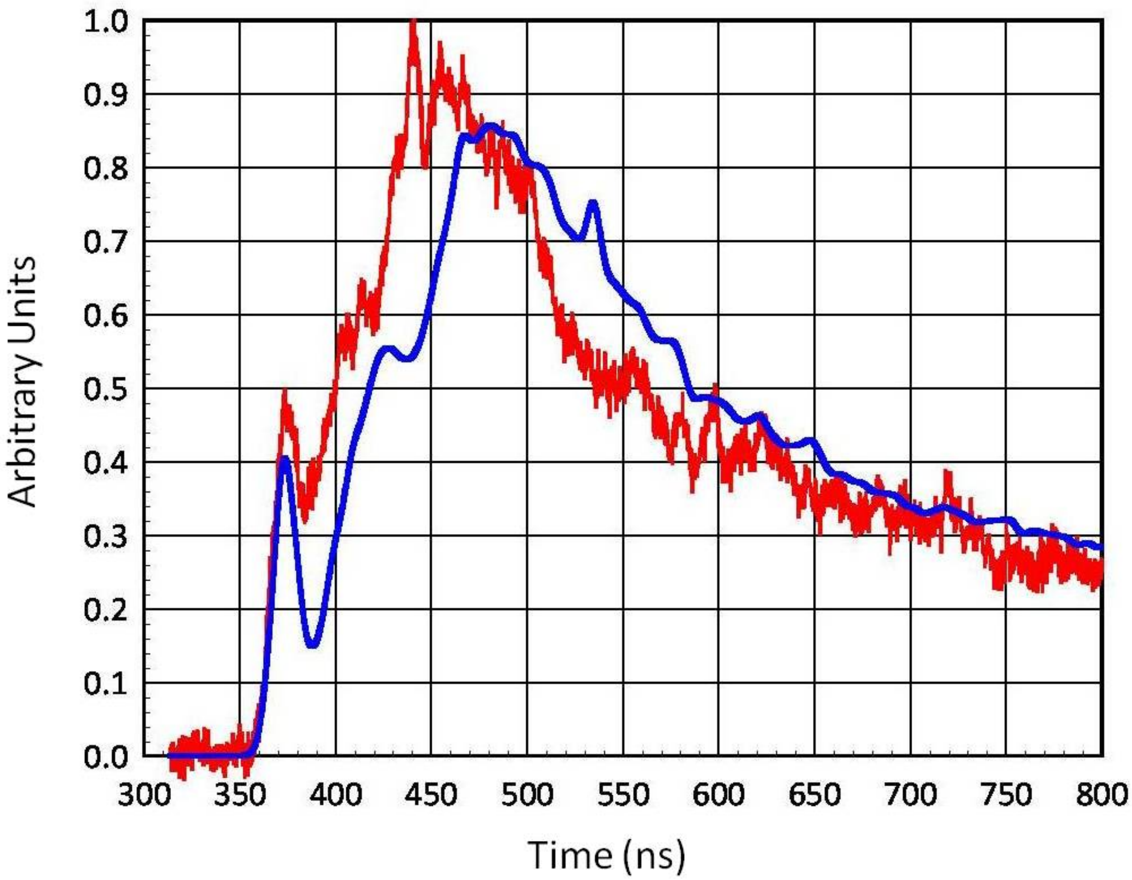

Figure 15. Area normalized comparison between shot z1217 without TIVAR 1000 Collimator (red) and MCNP-PoliMi model with folded-in time response for a 4 keV DD fusion source (blue) for a detector located at "D" in Figure 1. The same features can be observed: a primary neutron peak followed by a very large, second scattering peak.

A close up of the neutron peak from shot z1217 at detector location "D" in Figure 1 is compared to the model in Figure 16 below. The model shows a full width at half maxima of 16.38 ns. A FWHM cannot be extracted from the data due to the large, second scattering peak. Both plots are area normalized.

For the nTOF detector located at "C" in Figure 1, an MCNP-PoliMi model produced a neutron detector response and the detector time response was folded in as described above. A plot of the MCNP-PoliMi model compared with the actual empirical data for the nTOF detector located at "C" for shot z1217 is shown in Figure 17. As can be seen, there is better separation between the primary neutron peak and the secondary scattering peak compared to Figure 15. Also, the neutron peak has a greater amplitude relative to the scattering peak. Both plots are area normalized.

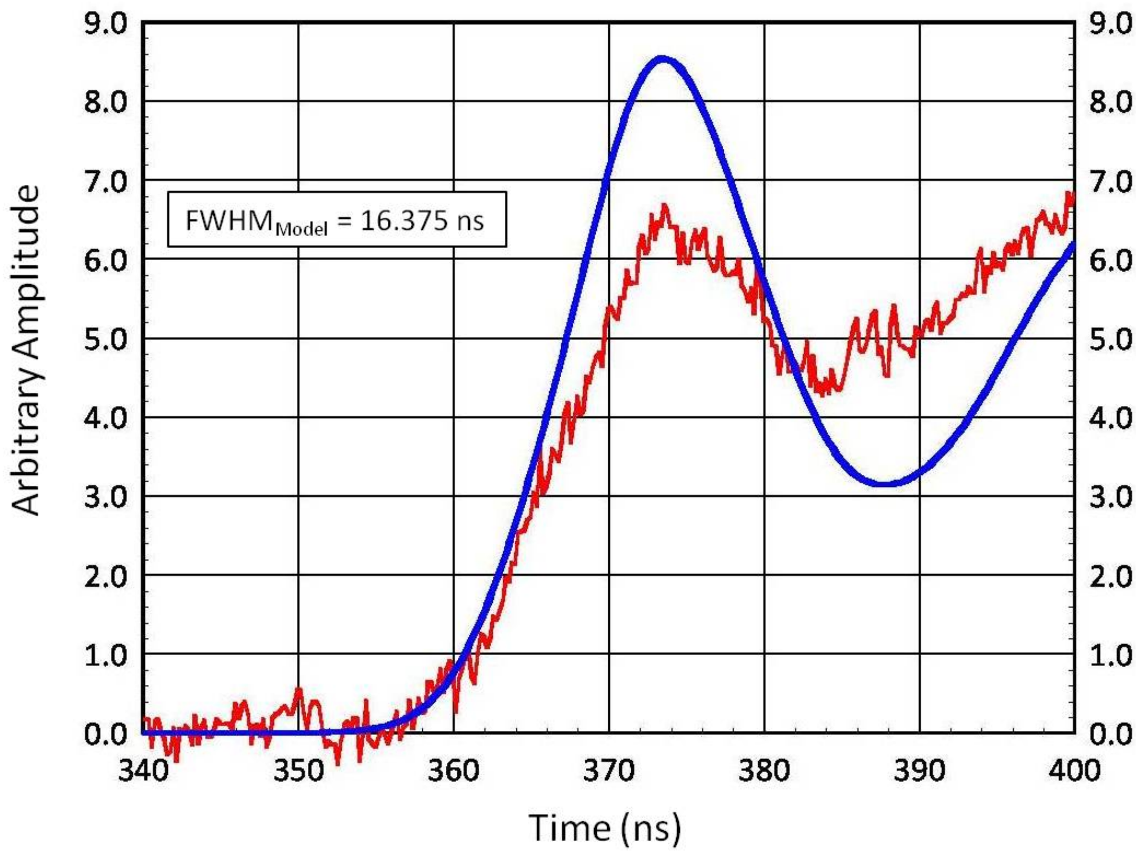

Figure 16. Close-up of the primary neutron peak in Figure 15, for the bottom nTOF detector located at "D" in Figure 1. The model was run at a temperature of 4 keV, and its full width at half maxima is 16.38 ns. A FWHM from the data cannot be extracted due to the large, second scattering peak following the neutron peak.

A close up of the neutron peak for shot z1217 located at "C" in Figure 1 is compared to the model in Figure 18. The FWHM of the data is 14.89 ns, while the FWHM of the model is 15.11 ns. Both plots are area normalized.

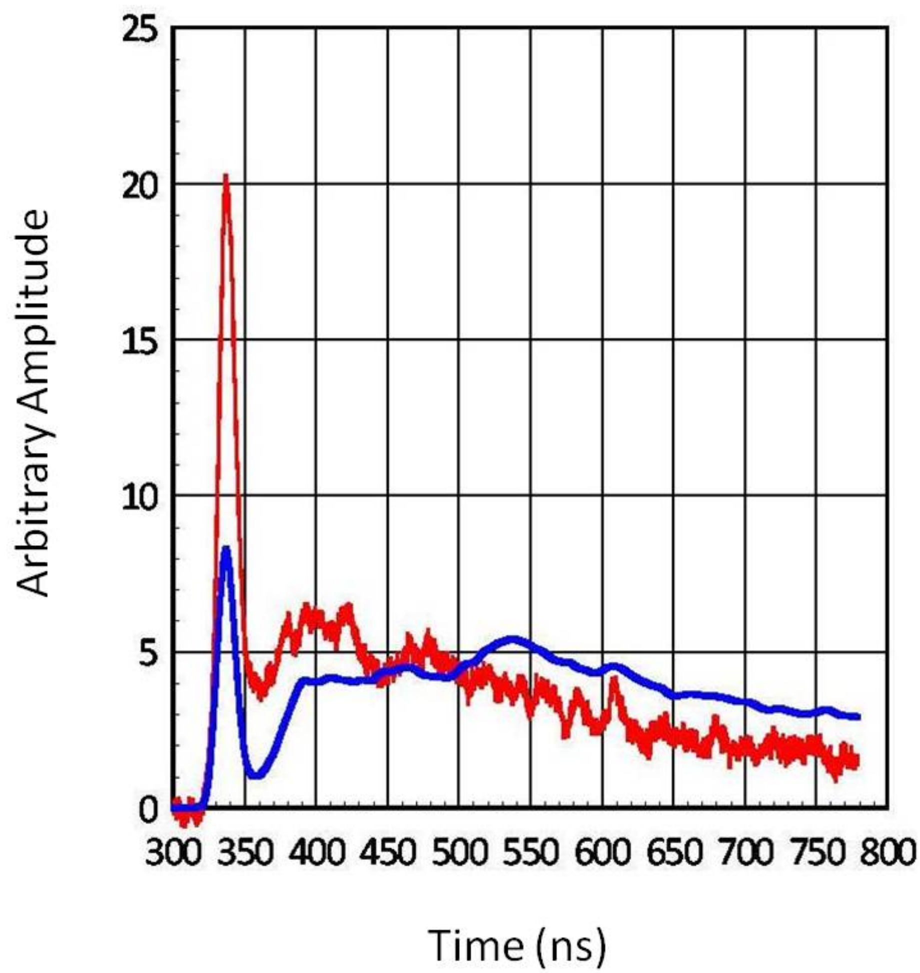

Figure 17. Area normalized comparison between shot z1217 without Tivar Collimator (red) and MCNP-PoliMi model with folded-in time response for a 4 keV DD fusion source (blue) for a detector located at “C” in Figure 1. There is better separation between the primary neutron peak and the second scattering peak than shown in Figure 15. Also, the neutron peak has a greater amplitude relative to the scattering peak than that shown in Figure 15.

To reduce the second scattering peak seen in Figure 17 for the detector located at “C” (in Figure 1) and to lessen the second scattering tail seen in Figure 15 for the other detector located at “D” (in Figure 1), a collimator made of UHMW TIVAR 1000 was built and placed under TCC as seen in Figure 19. This material was chosen over regular polyethylene because it does not outgas under vacuum [27]; (see also Appendix F). The collimator was 25.4 cm (10 in) long and had a tungsten insert on axis serving as a gamma ray collimator for the intense bremsstrahlung background. The length of 25.4 cm (10 in) was chosen to be manageable to install; also MCNPX calculations showed that that length would attenuate DD neutrons by approximately a factor of 1000.

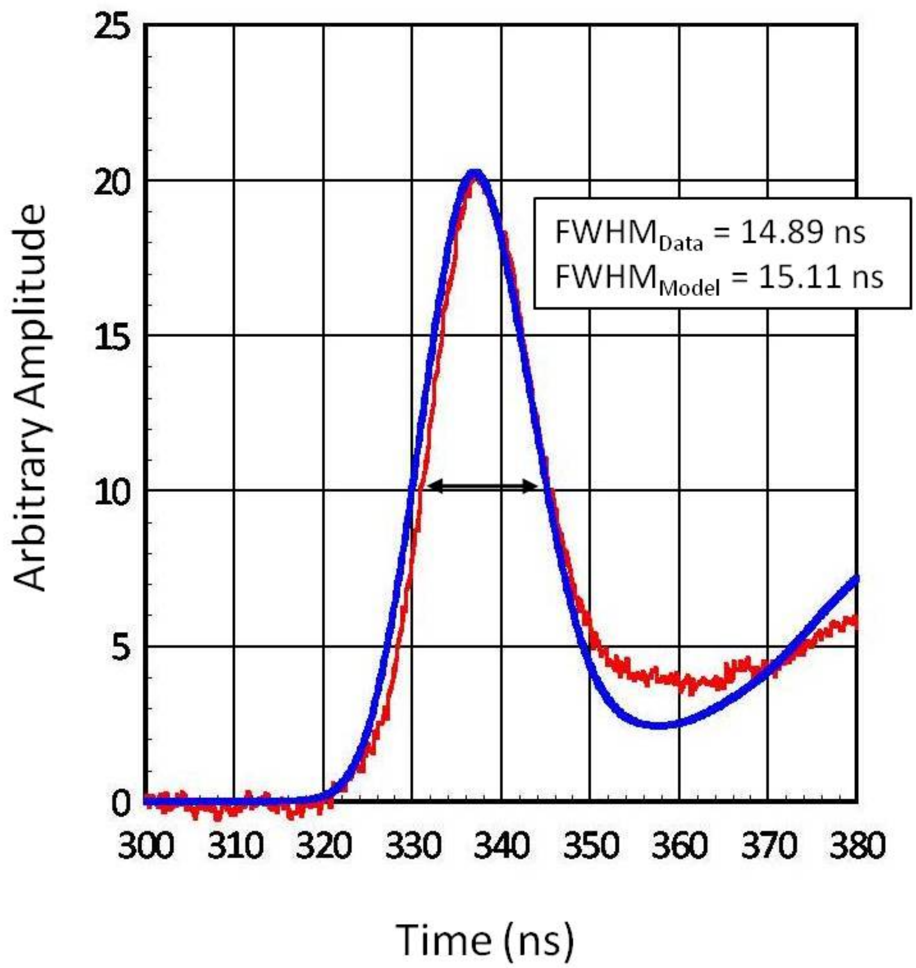

Figure 18. Close-up of the primary neutron peak in Figure 17, for the top nTOF detector located at "C" in Figure 1. The model was run at a temperature of 4 keV, and its full width at half maxima is 15.11 ns, while the data from shot z1217 has a full width at half maxima of 14.89 ns. Both plots are area normalized.

The exit aperture on the collimator was 7.62 cm (3 in). When projected downward, the collimator would cast a "shadow" all the way down to the basement floor, 880.76 cm (28.9 ft) below the pinch (TCC). This is shown in Figure 20. With the pig being 3 degrees off-axis, this made both nTOF detectors just fit inside the collimator “cone,” as shown in Figure 21. However, it was hoped the collimator would reduce neutron scattering off the elevator floor that may have been contributing to the second scattering peak for the nTOF detector located at “D” in Figure 1 (i.e., the detector closest to the floor) as seen in Figure 6.

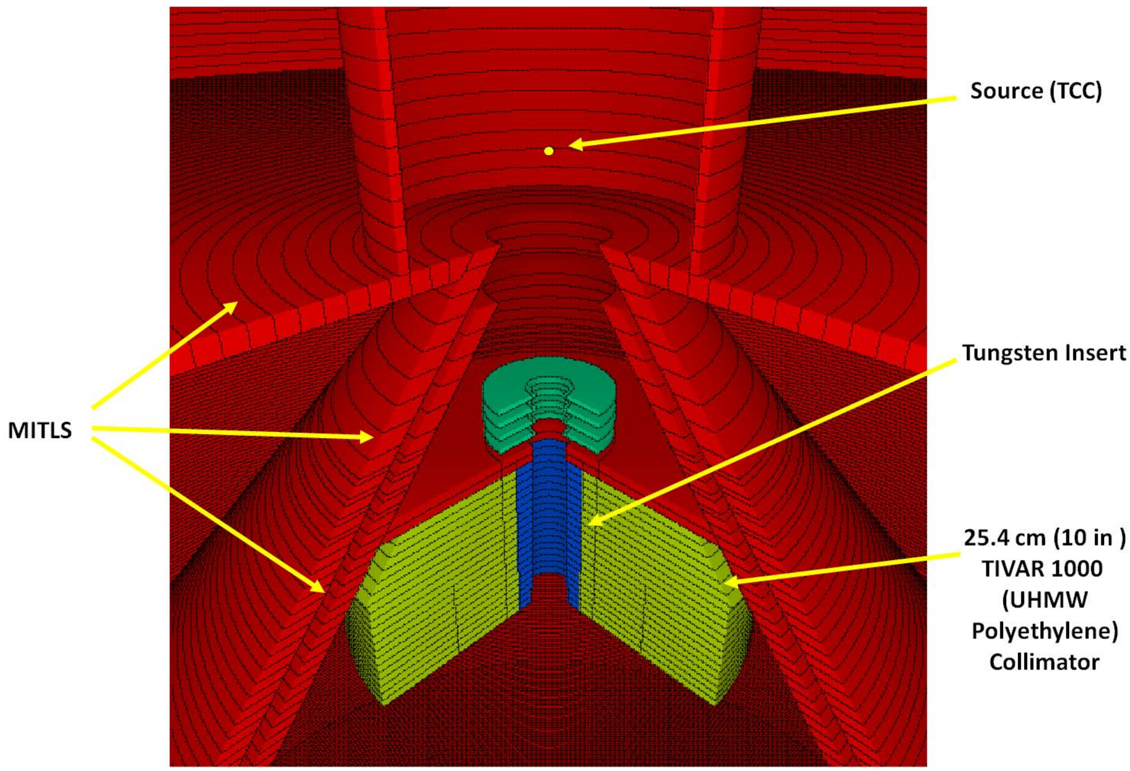

Figure 19. A closer view of the UHMW TIVAR 1000 collimator incorporated into the machine on neutron producing shots in order to help “clean up” neutron signals. MCNPX calculations showed that Its length of 25.4 cm (10 in) would attenuate DD neutrons by approximately a factor of 1000. The tungsten insert is serving as a gamma ray collimator.

A plot of an MCNP-PoliMi model with the collimator in place, and the detector response convolved with the calculated signal (blue) compared to shot z1549 when the collimator was fielded on the machine (red) is shown in Figure 22. As can be seen, use of the collimator greatly reduced the second scattering peak and produced a much greater amplitude of the primary neutron signal relative to the second peak as compared to Figure 15.

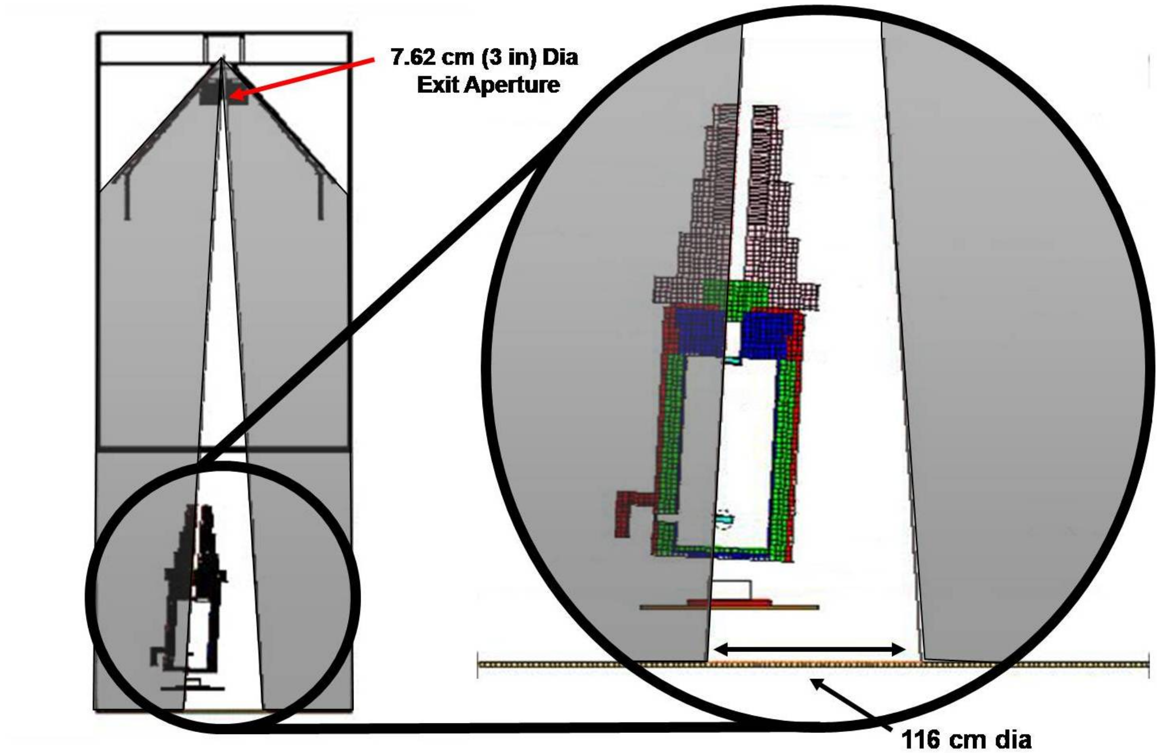

Figure 20. “Shadow” of TIVAR 1000 Collimator. With a 7.62 cm (3 in) diameter exit aperture growing to a 116 cm (45.7 in) diameter spread at the basement floor 880.76 cm (28.9 ft) below TCC.

A close up of the neutron peak for shot z1549 located at “D” in Figure 1 is compared to the model in Figure 23. The FWHM of the data is 12.75 ns, while the FWHM of the model is 11.84 ns. The model was run at a temperature of 2 keV for a DD fusion neutron source. Both plots are area normalized.

For the top nTOF detector located at “C” in Figure 1, a plot of its MCNP-PoliMi model with folded in time response (blue) is compared with shot z1549 for a fielded detector in the same location (red) in Figure 24. As can be seen, the effect of the collimator was to virtually eliminate the second scattering tail that was seen in Figure 17 (before the collimator was added). A close-up of the neutron scattering peak is shown in Figure 25. The full width at half maxima for the data is 12.70 ns, while the full width at half maxima for the model is 11.20 ns. Of note is that the temperature of the actual experiment is unknown, while the model was run with a 2 keV DD fusion neutron source.

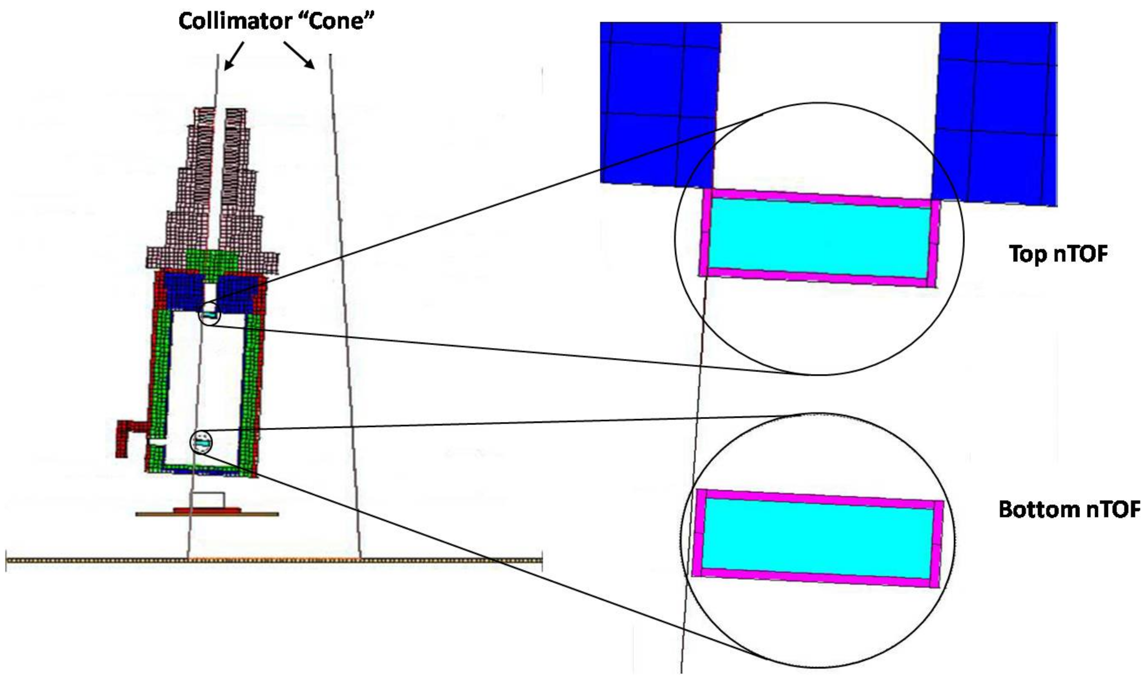

Figure 21. With the pig aligned 3 degrees off-axis, the collimator "cone" just encompassed both detectors. However, it was still hoped that the addition of the collimator would reduce neutron scattering off the elevator floor that may be contributing to the second scattering peak seen in Figure 15.

As can be seen from Figures 23 and 25, collimation is essential to produce "cleaner" neutron signals. It will be shown later that it does indeed reduce shallow-angle scattering in the neutron peak, and it helps eliminate the bulk of scattering arriving later in time. As shown by the "shadow" in Figure 20, neutrons removed early in time by the collimator near the source therefore cannot arrive later in time at the detectors by scattering.

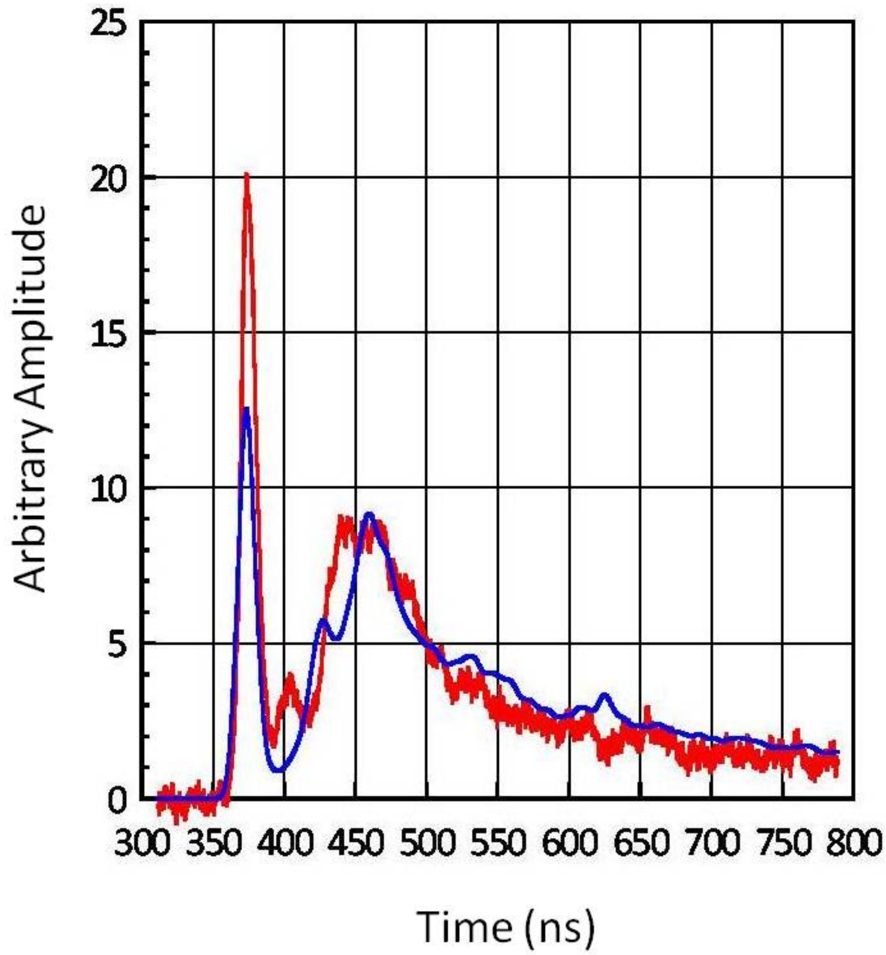

Figure 22. Area normalized comparison of shot z1549 (red) for detector at location "D" in Figure 1 with TIVAR 1000 Collimator in place and MCNP-PoliMi model with folded in time response of 7.5 ns (blue). Use of the collimator greatly reduced the second scattering peak and produced a much greater amplitude of the primary neutron signal compared to the second peak as compared to Figure 15.

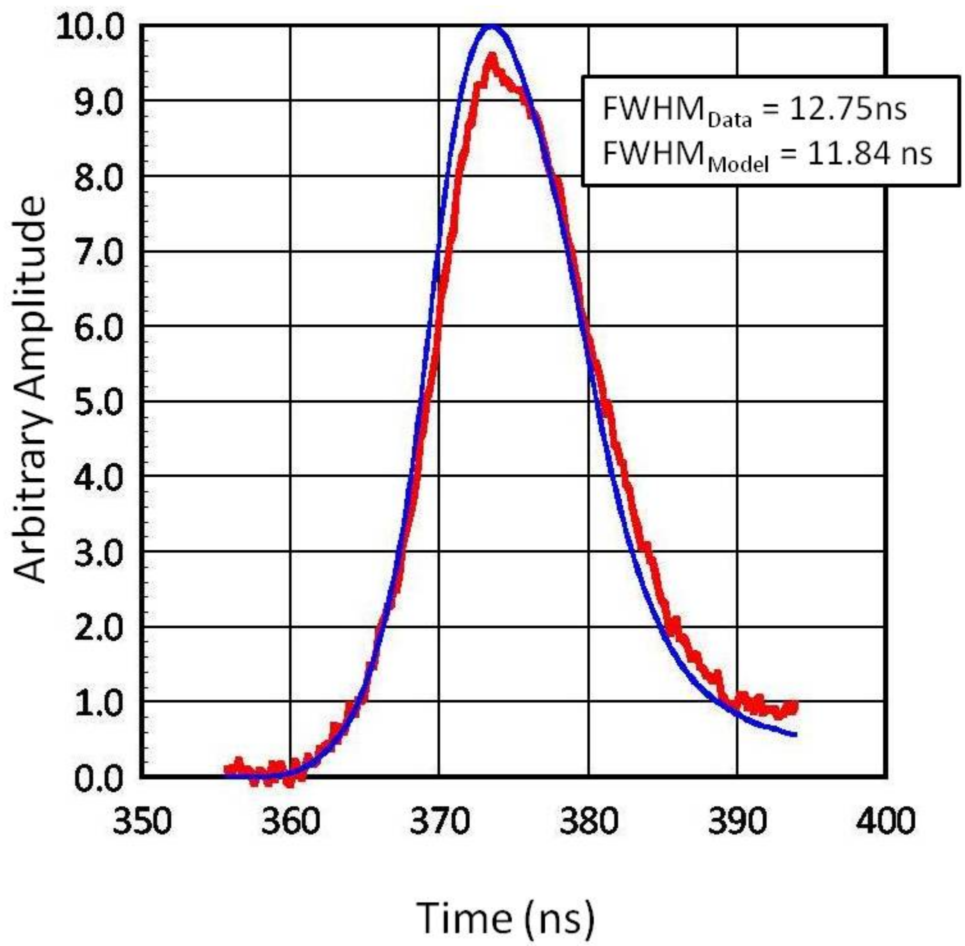

Figure 23. Close-up of primary neutron peak in Figure 22, for the bottom nTOF detector located at "D" in Figure 1. The full width at half maxima of the data is 12.75 ns, while the full width at half maxima for the model is 11.84 ns. The model was run with a 2 keV DD fusion neutron source.

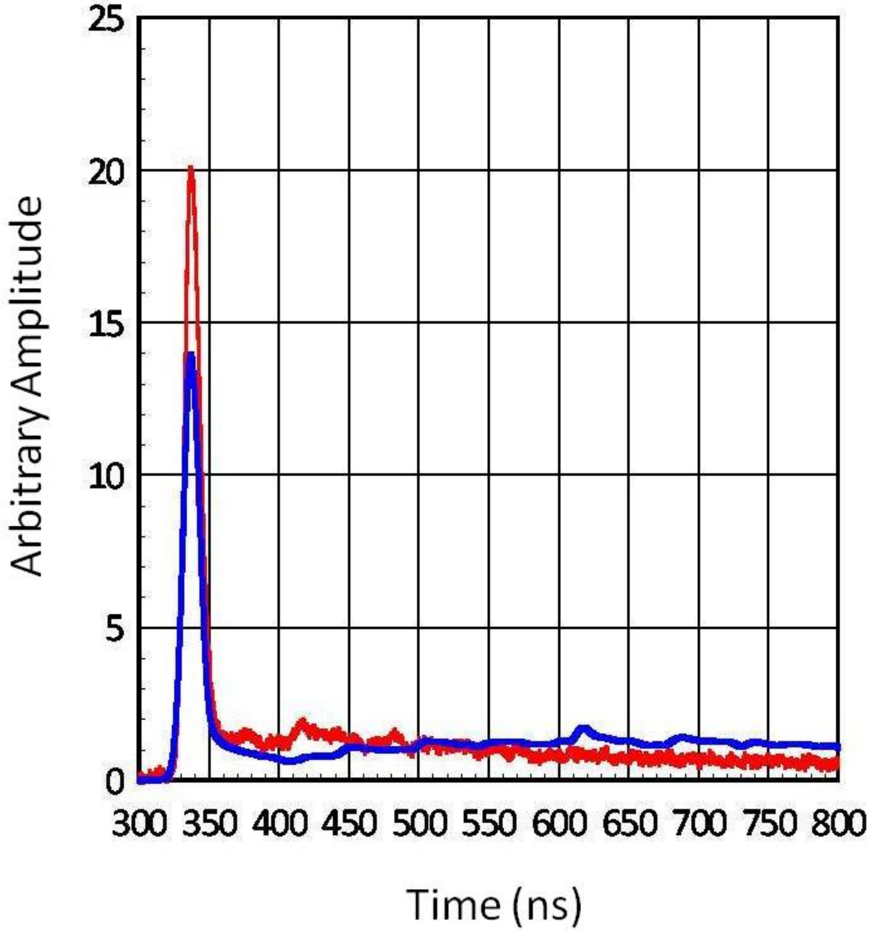

Figure 24. Area normalized comparison of shot z1549 (red) for detector at location "C" in Figure 1 with Tivar 1000 Collimator in place and MCNP-PoliMi model with folded in time response of 7.5 ns (blue). The effect of the collimator was to virtually eliminate the second scattering tail that was seen in Figure 17.

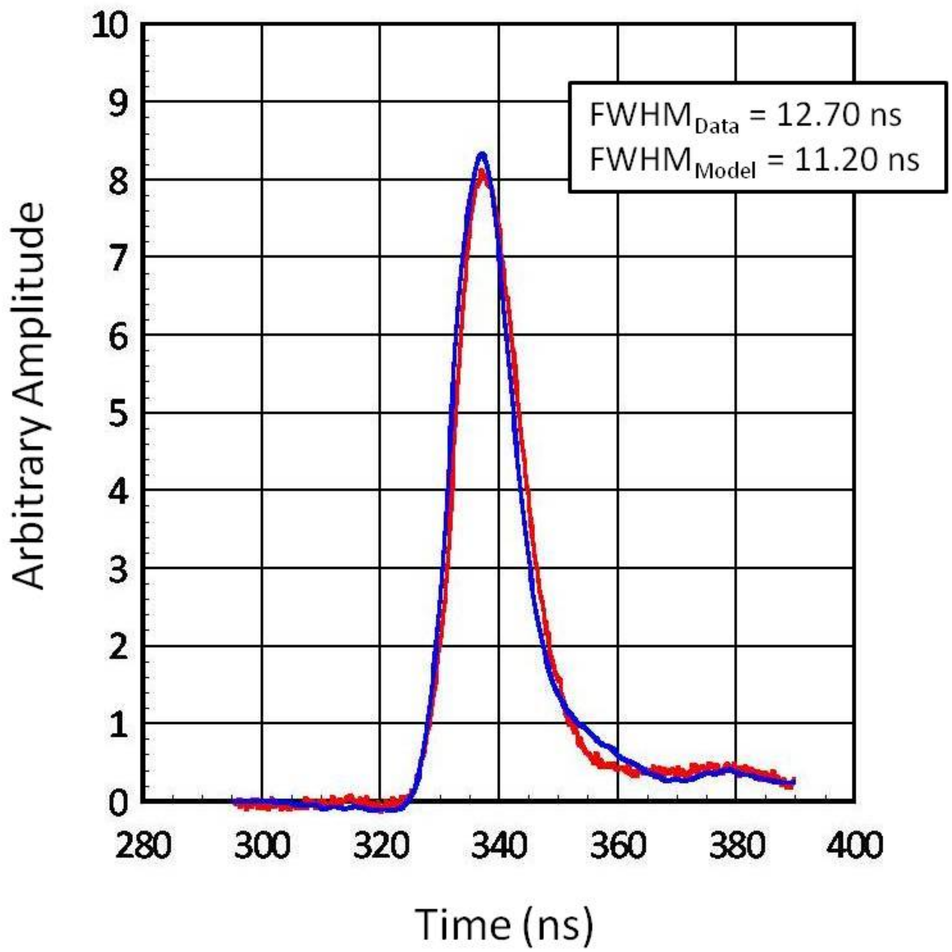

Figure 25. Close-up of primary neutron peak in Figure 21, for the top nTOF detector located at "C" in Figure 1 with the TIVAR 1000 Collimator in place. The full width at half maxima for the data is 12.70 ns, while the full width at half maxima for the model is 11.20. The model was run with a temperature of 2 keV DD fusion neutron source.

CHAPTER 7

DECONVOLVING THE TIME RESPONSE FROM THE SIMULATED DATA

It was shown above that a detector's intrinsic time response will broaden the detector's signal – in effect, it "smears" the data in time to some degree. To further analyze the data, however, this time response must be deconvolved – or "unfolded" – from the data. Deconvolution is a process of *undoing* the smearing in the data that has occurred due to the influence of a known response function. The equation for deconvolution is the same as that for convolution, namely equation (6), except that now the left hand side is taken to be known, and (6) is to be considered as a set of N linear equations for the unknown quantities s_j. This can be accomplished using Fast Fourier Transforms. First, the transform of the signal (which is convolved with the response function) is taken. Next the transform of the response function is taken. The transform of the signal is now *divided* by the transform of the response – this gives the transform of the deconvolved signal. The last step is to take the inverse FFT to finally obtain the raw signal.

To make sure the process was correct, the time response in Figure 13 was deconvolved from the MCNP-PoliMi model with folded-in time response for a 4 keV DD fusion source (blue), shown in Figure 15. After deconvolving, the result was compared with the smoothed calculated data shown in Figure 12 (red) and will be discussed below. A set of codes from *Numerical Recipes* was used to accomplish this [25].

Prior to attempting Fast Fourier Transforms, the signal and time response have to be "prepared." The number of points in the signal must be an integer power of 2, and "zero-padded" (i.e., extended with zeros) at its extreme end in time. The amount of zero-padding at the end of the data must equal the number of data points in region "A" or "B" in Figure 27 – *whichever is larger*. This is shown in Figure 26 below.

The time response has to be placed in "wrap-around order," meaning the data is considered as being wrapped around a cylinder with the ends touching – this means

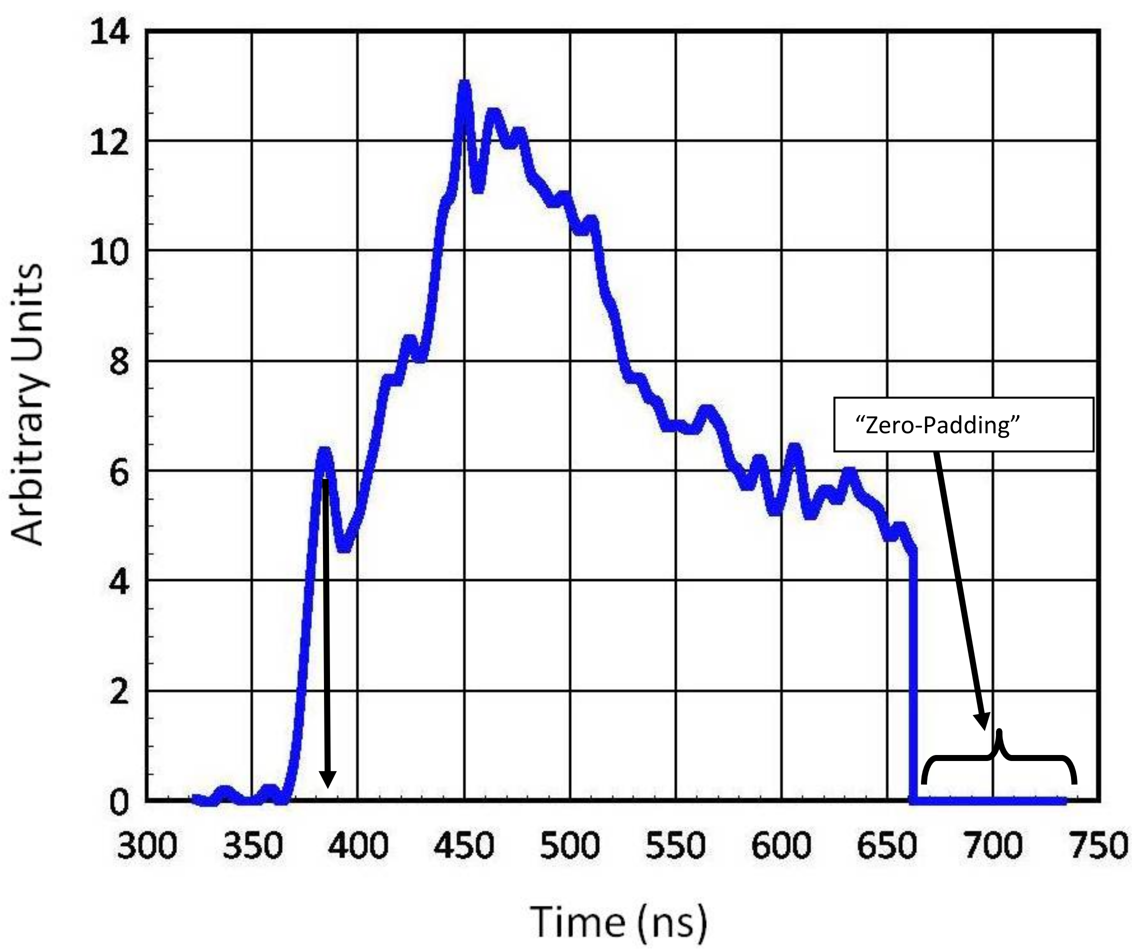

Figure 26. Preparation for the signal prior to taking Fast Fourier Transforms. This is the empirical data from shot z1217. The total number of points in the signal must be an integer power of 2, and "zero-padded" – or extended with zeros at its extreme end in time. The amount of zero padding must equal the number of points in region "A" or "B" in Figure 27 – *whichever is larger*. (Note that the neutron peak is at 383.13 ns – see arrow.)

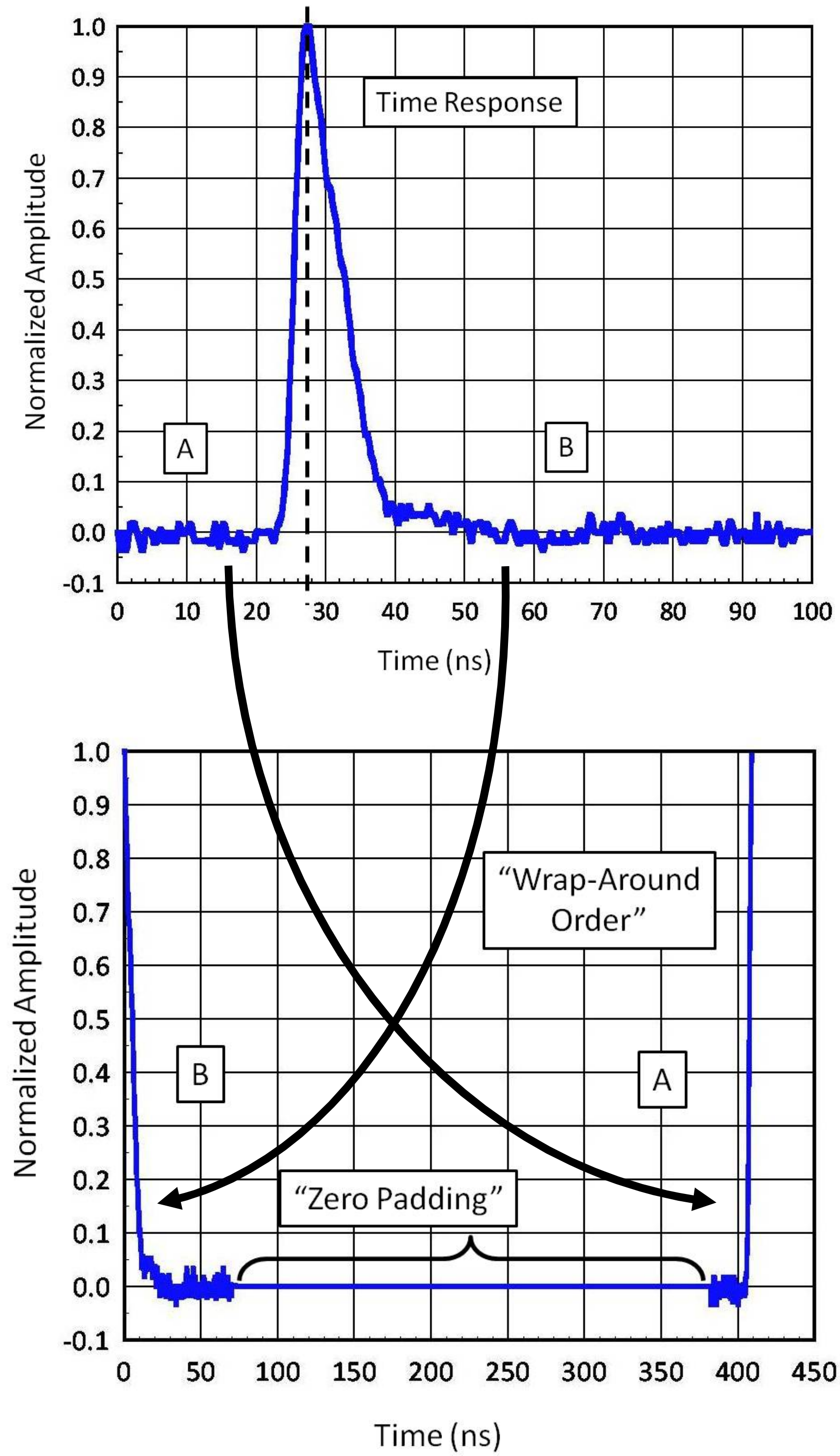

Figure 27. "Wrap-Around Order." First the time response (above, and the same as shown in Figure 13), is cut in half at its peak. Then each side of the time response is *flipped left-for-right* (see arrows), then "zero-padded" in the middle. The total number of points, M, can be any odd integer less than or equal to N, the number of points in the data, which must be an integer power of 2.

that a large center section in the middle of the data, is zero, with nonzero values clustered at the two extreme ends. This is shown in Figure 27.

Once the data and the response function have been prepared properly, the deconvolution can be accomplished by Fast Fourier Transforms. A plot of the smoothed, calculated data (blue) is compared with the deconvolved fit (red), and the smoothed, deconvolved fit (green) is shown in Figure 28. The blue and green traces fall neatly on top of each other, showing good agreement.

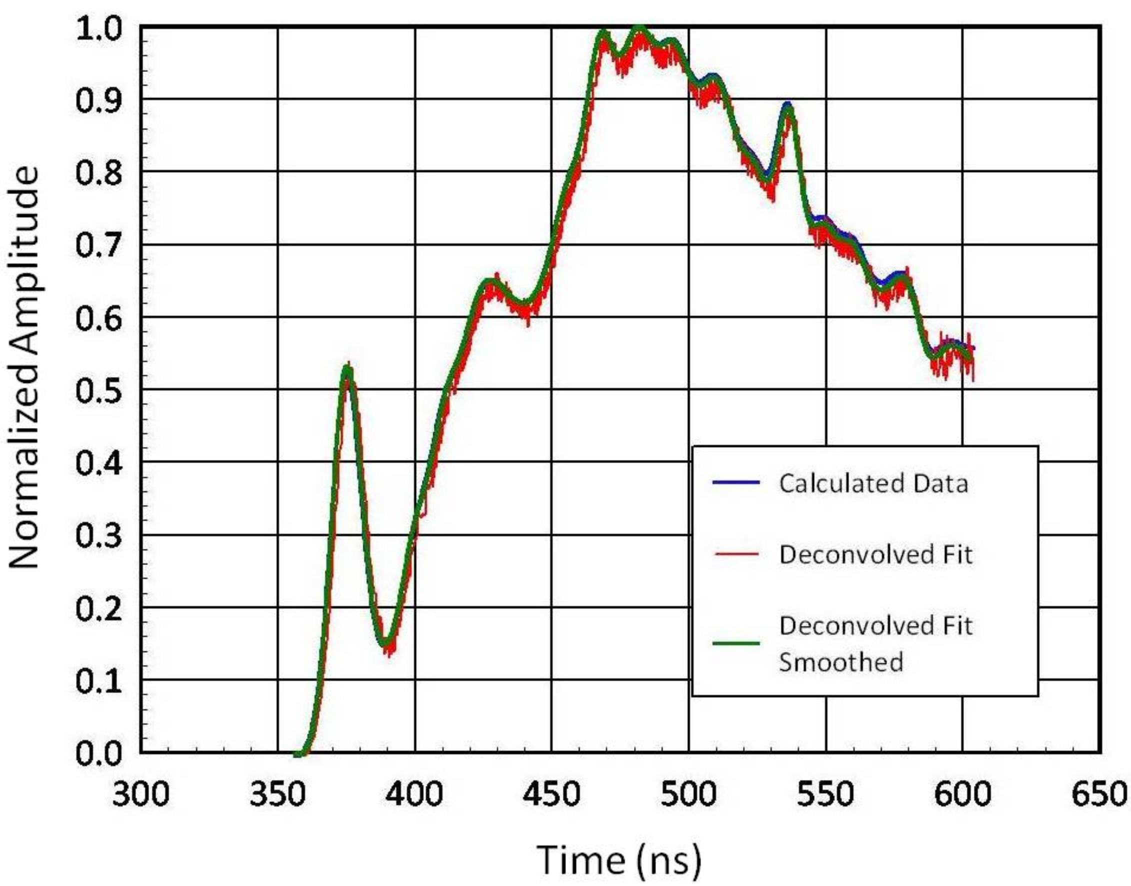

Figure 28. The smoothed calculated data (blue, also shown in Figure 12 with a red trace) is compared to the deconvolved fit using Fast Fourier Transforms (red). The deconvolved fit is smoothed (green) and can be seen laying on top of the calculated data, showing good agreement. Both blue and green traces have been smoothed with the Savitsky-Golay smoothing filter.

CHAPTER 8

CONVOLVING A NEUTRON IMPULSE RESPONSE WITH THE KNOWN TIME RESPONSE

Using the techniques described herein, a *monoenergetic* source of neutrons of 2.45 MeV were run with a 2.54 cm (1 inch) scintillator placed at 809 cm. The resulting waveform can be described as the *calculated neutron impulse response* for the scintillator, and is shown in Figure 29 below. The shape of the waveform from 374.51 ns (where it begins) down to 375.71 ns (both indicated by arrows) is a time span of 1.2 ns.

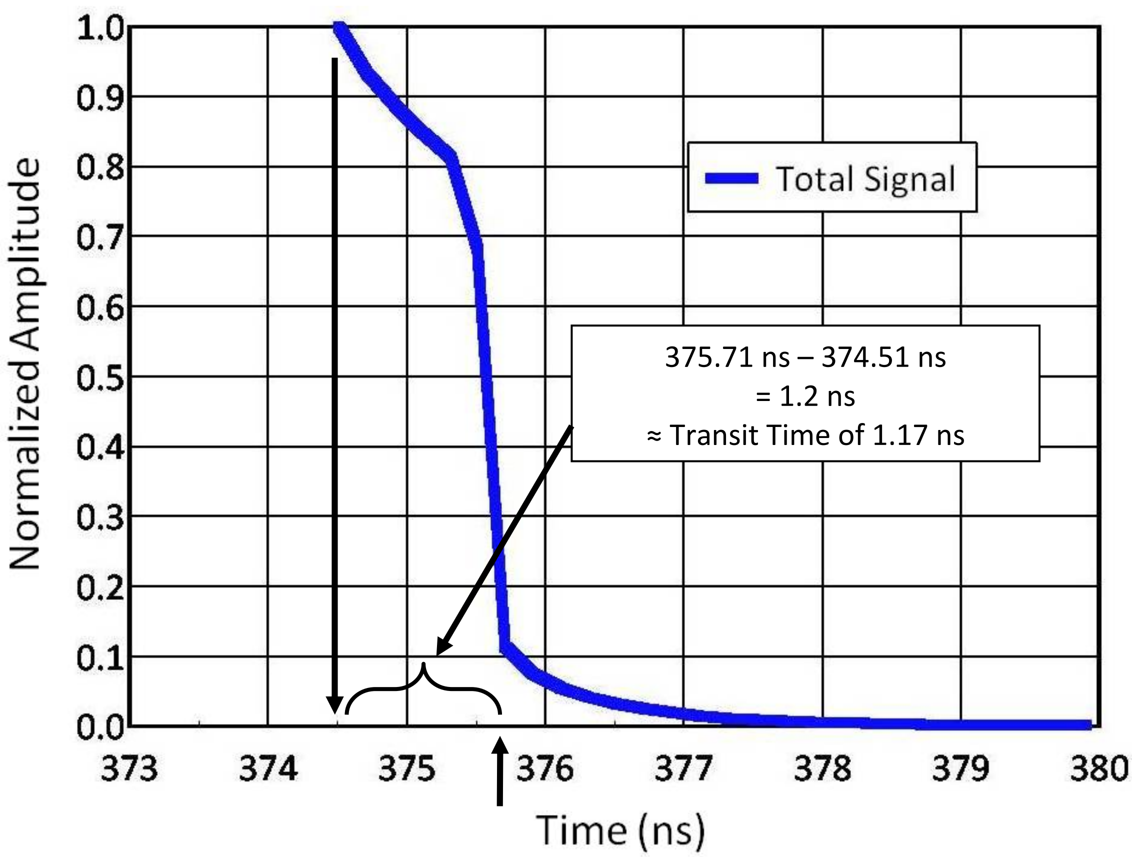

Figure 29. The neutron impulse response for a 2.54 cm (1 inch) scintillator placed 809 cm from a monoenergetic source of 2.45 MeV DD neutrons. The region in time indicated by the bracket is 1.2 ns, which is due to the transit time of a 2.45 MeV neutron traversing the scintillator. The curved portion of the waveform which follows is due explicitly to secondary scattering in the scintillator, and is described in Figure 30.

This value of 1.2 ns correlates to the *transit time* of a 2.45 MeV neutron passing through a 2.54 cm (1 inch) scintillator, and can be found by:

$$KE = \frac{1}{2}mv^2 \tag{9}$$

Substituting 2.45 MeV for *KE*, letting m = m_0, and multiplying by c^2/c^2 gives:

$$2.45\ MeV = \frac{1}{2}\frac{v^2}{c^2}m_0c^2 \tag{10}$$

Solving for v/c:

$$\frac{v}{c} = \sqrt{\frac{(2)(2.45\ MeV)}{m_0c^2}} \tag{11}$$

Letting c = 2.9979E10 cm/sec, and m_0c^2 = 939.5653 MeV for a neutron and solving for v:

$$v = \sqrt{\frac{(2)(2.45\ MeV)}{939.5653\ MeV}}\,(2.9979E10\,\frac{cm}{sec}) \tag{12}$$

v becomes:

$$v = 2.166E09\,\frac{cm}{sec}\,(\frac{1\ sec}{10^9\ ns}) \tag{13}$$

Thus, the velocity of a 2.45 MeV neutron is:

$$v = 2.166\ cm/ns \tag{14}$$

And the transit time through a 2.54 cm (1 inch) thick scintillator becomes:

$$Transit\ Time = \frac{2.54\ cm}{2.166\ cm/ns} \tag{51}$$

or:

$$\boxed{Transit\ Time = 1.17\ ns} \qquad (16)$$

PRIMARY AND SECONDARY NEUTRON SCATTERING

One of the versatile features of the collision data output table (Table I), is that it contains so much germane information. As noted in this work, the incident particle, target nucleus, energy deposited and time of the event were used to model the nTOF detector response. Other information in the table includes the *number of scatterings* which have occurred. Using this information, Figure 29 can be further analyzed in terms of *primary and secondary neutron scattering*. In this context, primary scattering refers to the number of scatterings in Table I to be equal to one, and secondary scattering refers to the number of scatterings in Table I to be greater than one. The post-processing code was easily modified to plot the light output due only to primary scattering in one case (i.e., number of scatterings = 1), and only secondary scattering (i.e., number of scatterings > 1) in the other. The result is shown in Figure 30. The total signal (blue) is the same as that shown in Figure 29. The green, however, shows only the light output produced by primary scattering, and the red shows only the light output produced by secondary scattering. If both signals are summed (red and green), they equal the total signal (blue). In the span of transit time shown in Figure 30 of 1.2 ns, 85.6 % of light output is due to primary scattering, and 14.4% of light output is due to secondary scattering (this was done by summing amplitudes of the total signal, primary and secondary scattering and determining the contribution of each). Upon arriving at the scintillator, a neutron may collide with a hydrogen atom on the front face of the scintillator (in which case, the transit time is much less than 1.2 ns), or it may traverse through the scintillator and collide with a hydrogen atom in the middle (in which case, the transit time would be 1.2ns/2 = 0.6 ns), or it may interact at the back face of the scintillator (in which case, the transit time would be 1.2 ns). Of note in Figure 30 is that after 375.71 ns the light output produced is due to secondary scattering only, since the green trace (primary scattering) drops to zero and the red trace (secondary scattering) lies on top of the blue trace (i.e., the total signal).

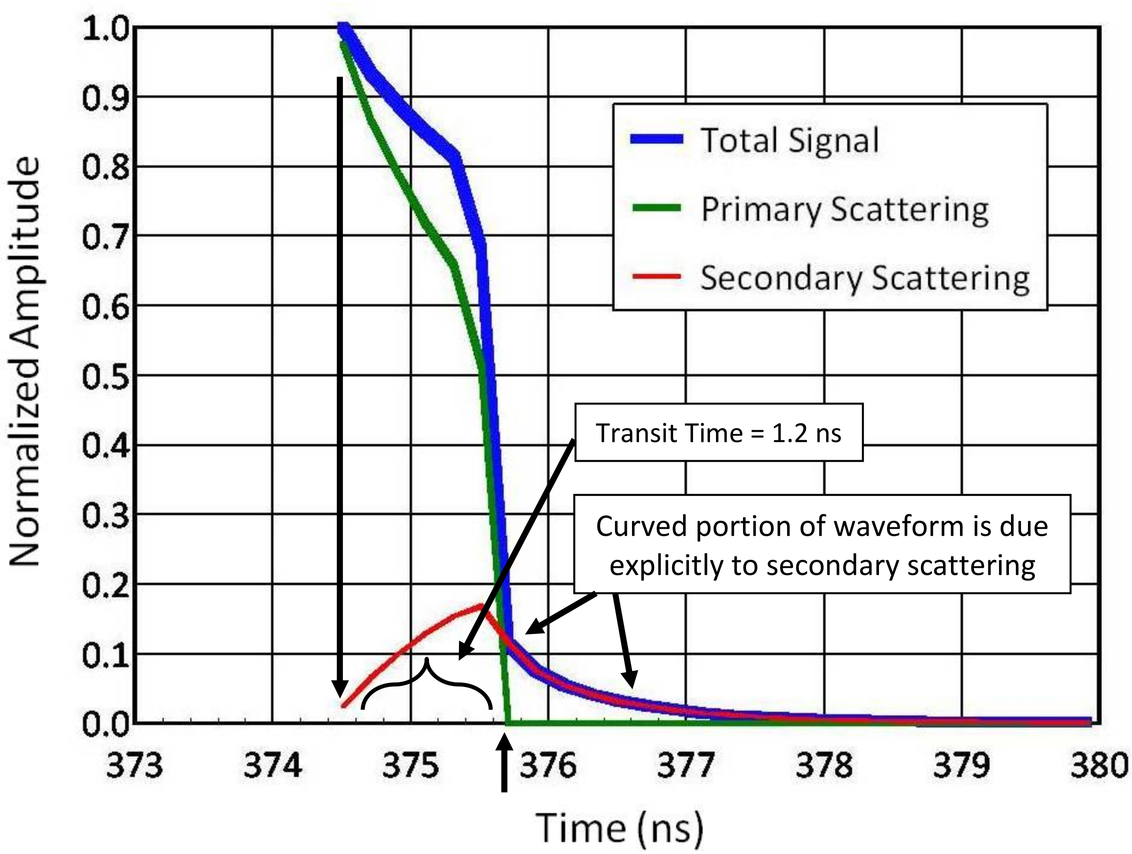

Figure 30. The neutron impulse response divided up into its component parts: primary and secondary scattering. In the span of the transit time of 1.2 ns, 85.6% of the light output is produced by primary scattering, while 14.4% of the light output is produced by secondary scattering. After 1.2 ns of transit time, the green trace (primary scattering) drops to zero and all light output produced is due to secondary scattering only.

To analyze the data as correctly as possible, it was then necessary to convolve the neutron impulse response (Figure 29) with the time response (Figure 13). The reason to include both these waveforms is that they each contain information necessary for a "total" signal. Figure 13, the time response, was found by pulsing x-rays with a 50 picosecond width into the nTOF detector at the Idaho Accelerator Center (IAC) using their 15 MeV short pulse Linac [24]; (see also Appendix E). This provided *timing information* due to impinging x-rays, but it did not provide any *neutron impulse information*. Therefore, the monoenergetic 2.45 MeV neutron impulse response (Figure 29) is necessary to be included, which is why it was convolved with the time response and shown in Figure 31 below.

The FWHM of 7.607 ns in Figure 31 compares favorably with finding it analytically in quadrature:

$$FWHM = \sqrt{(7.5\,ns)^2 + (1.2\,ns)^2} \quad (17)$$

The full width at half maxima of the monoenergetic neutron impulse response convolved with the time response becomes:

$$FWHM = 7.60\,ns \quad (18)$$

Once the neutron impulse response was convolved with the time response, it was then necessary to find the *time delay* -- i.e., the delay from neutrons impinging on the face of the scintillator to the electronic signal coming out of the base of the photomultiplier tube. This consists of three components: (1) the average transit time of a 2.45 MeV neutron through a 2.54 cm (1 inch) scintillator (which is found from the value above); (2) the transit time of light produced in the scintillator that travels through

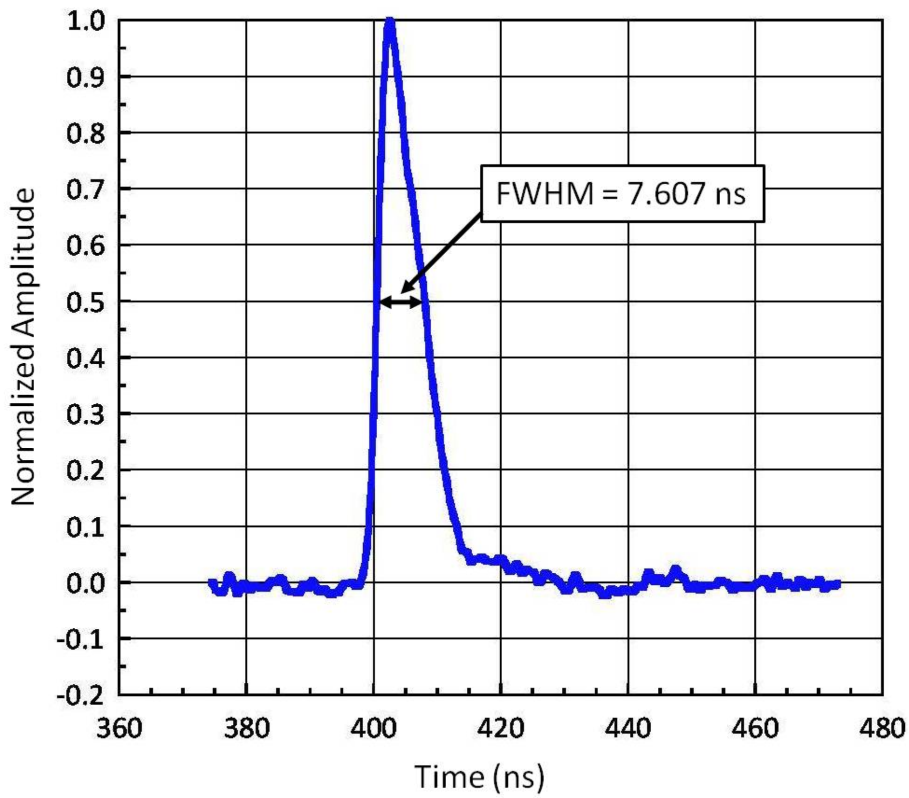

Figure 31. The convolution of the neutron impulse response (Figure 29) with the time response (Figure 13) found at the Idaho Accelerator Center (IAC). Together, both provide *timing* and *neutron impulse* response information necessary to be deconvolved out of the real data.

the light guide; and (3), the transit time through the photomultiplier tube and base, which has been measured by National Security Technologies (NSTec) [28]. A schematic of this is shown in Figure 32.

As mentioned, the transit time of a 2.45 MeV neutron through a 2.54 cm (1 inch) scintillator is 1.2 ns; thus, *the average is half that value*, since a neutron can interact on the front face or it can interact on the back face – therefore, it is taken to be 0.6 ns. The transit time of the light that is produced and travels through the light guide is merely the length of the light guide, l, divided by c/n, where c is the speed of light and n is the index of refraction for the light guide material. This is known to be 1.2 ns. This was

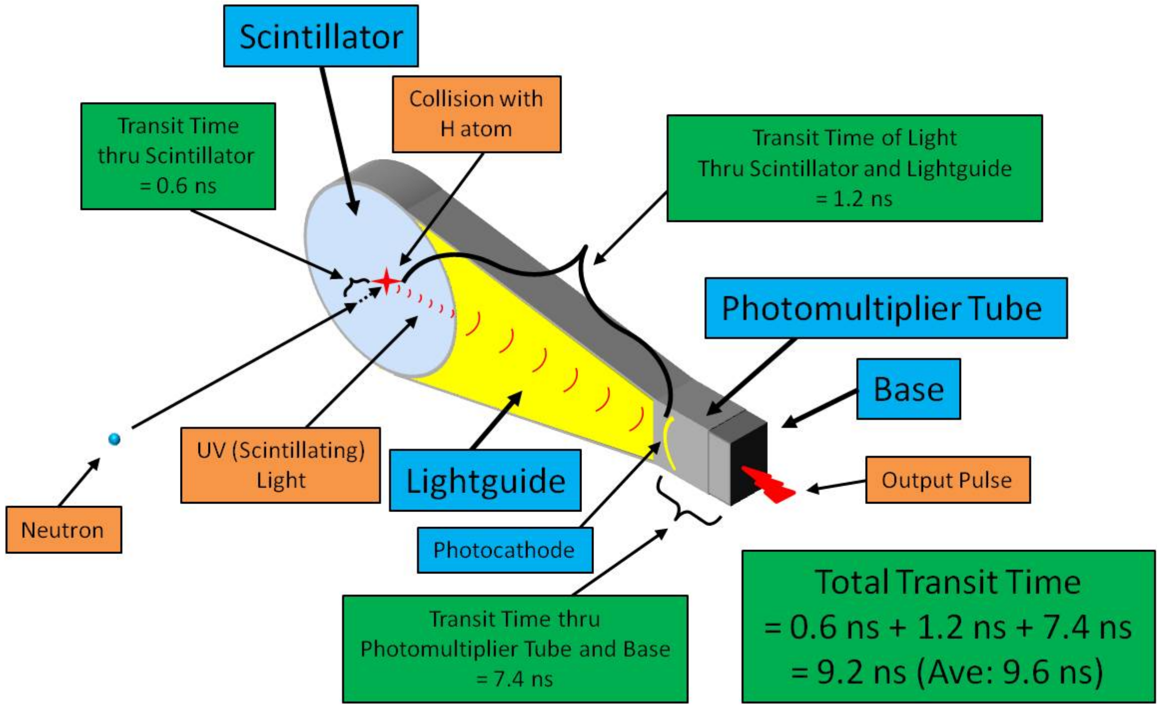

Figure 32. Schematic of the time delays that need to be taken into account (green boxes). The detector shown is a "single paddle" nTOF detector. A neutron (at left) penetrates the center of the scintillator and has a collision with a hydrogen atom. The time from the neutron entering the scintillator to when it interacts is its *transit time*, and was found above to be 0.6 ns. The time the UV (scintillating) light reaches the light guide (yellow), and travels the length of the light guide is 1.2 ns. Upon reaching the photocathode in the photomultiplier tube, the light is converted into an electronic signal, emerging from the base with a transit time of 7.4 ns, measured by National Security Technologies (NSTec) [28]. The sum of all transit times are 9.2 ns, but with fielding several nTOF detectors, it was considered that the average transit time to be 9.6 ns.

taken from the center of the scintillator as an average value. Finally, the transit time through the photomultiplier tube and base, measured by NSTec [28], is 7.4 ns. The sum of all these delays is 9.2 ns. This was done for every nTOF detector fielded, with an average value to be 9.6 ns to be the total delay from when radiation impinges upon the face of the scintillator to the electronic signal coming out of the base of the photomultiplier tube.

Once all the time delays have been taken into account, it is then necessary to correct Figure 31 in terms *where the actual time/neutron response starts*. This is because when the time responses were found experimentally at Idaho State, there was no fiducial present to indicate the time radiation was impinging upon the detector. Therefore, a value of 5% of the amplitude in Figure 31 was taken to be the start of the output pulse of the detector, and from that point, 9.6 ns earlier in time was taken to be the point at which radiation impinged upon the detector. This is shown in Figure 33.

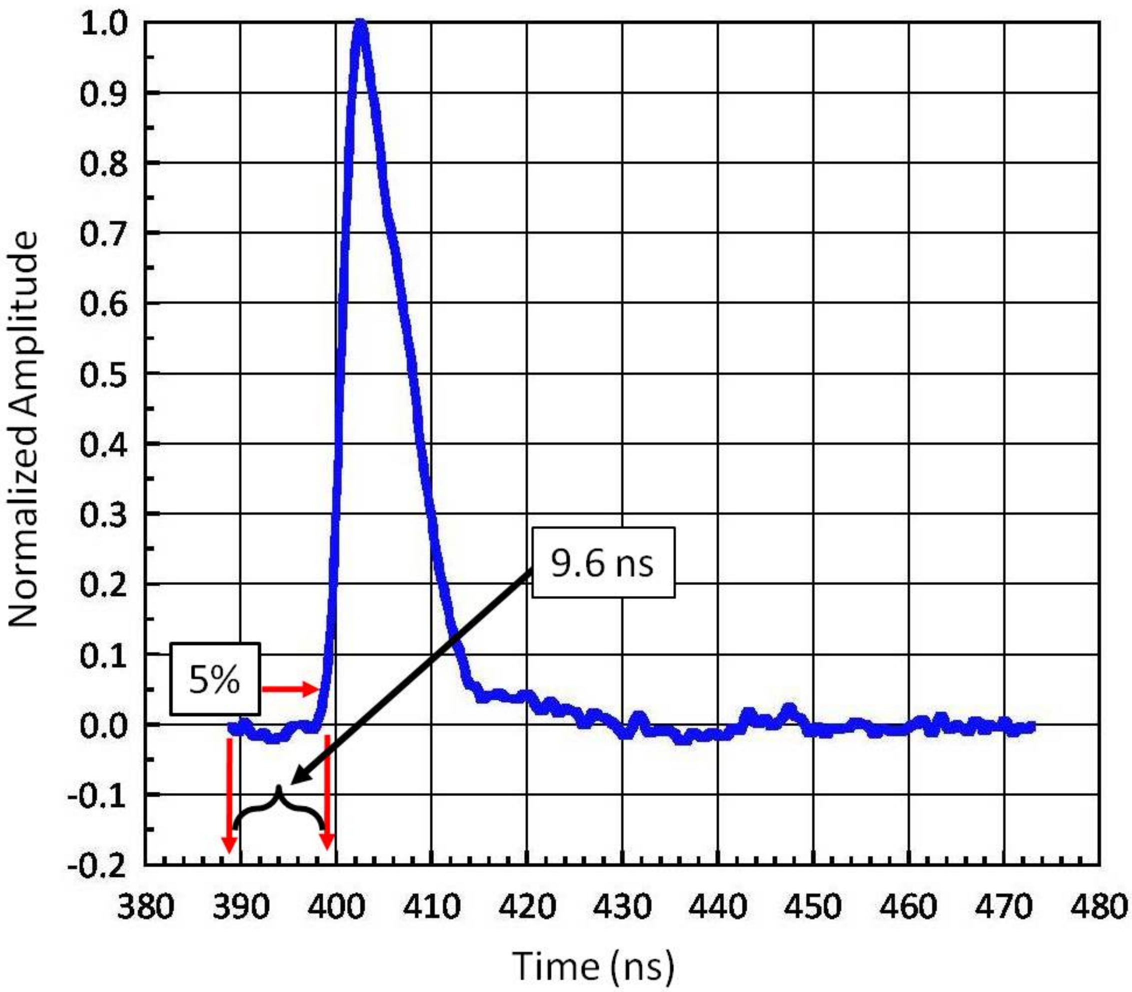

Figure 33. The Neutron Impulse/Time Response corrected for the time when radiation first impinges upon the detector. From the point of 5% of shot breakout, 9.6 ns earlier in time indicates the time in which radiation first impinges upon the detector (In this case, radiation first strikes the detector at 389.11 ns). 9.6 ns is the time it takes for the signal to traverse the entire detector – scintillator, light guide, photomultiplier tube and base – before an electronic signal (the pulse shown above) is produced.

CHAPTER 9

DECONVOLVING THE NEUTRON AND TIMING INSTRUMENT RESPONSE OUT OF THE REAL DATA

The neutron and timing instrument response (the convolution of both timing and neutron impulse information) in Figure 33 was now placed in "wrap-around order" (see Figure 27) and deconvolved out of the empirical data. The result is shown in Figure 34. Note that the neutron peak is at 373.53 ns (see arrow), and that the neutron peak from the empirical data (Figure 26) is at 383.13 shakes. The deconvolution has shifted the waveform *earlier in time*, because the time response information has been removed from the data. The neutron peak has been shifted back in time by 9.6 ns. This is a check that causality has not been violated. Neutrons *must arrive earlier* than the signal that is produced [29].

As a check to see if the deconvolution is correct, the waveform in Figure 34 was convolved with Figure 33 and compared with the empirical data. The results are shown in Figure 35 as an area normalized plot. The blue waveform is the empirical data from z1217, and the red waveform is the convolved signal. As can be seen, the red falls neatly on top of the blue with extremely small variations, indicating a very good fit.

SUBTRACTING THE CONTRIBUTION DUE TO NEUTRON SCATTERING

Once the time and neutron impulse response have been deconvolved out of the data, the contribution due to scattering can then be subtracted out. This is accomplished by running an "Ideal Case" case of a 2.54 cm (1 inch) scintillator 809 cm from a 4 keV DD fusion source (shown in Table II), with no material between the

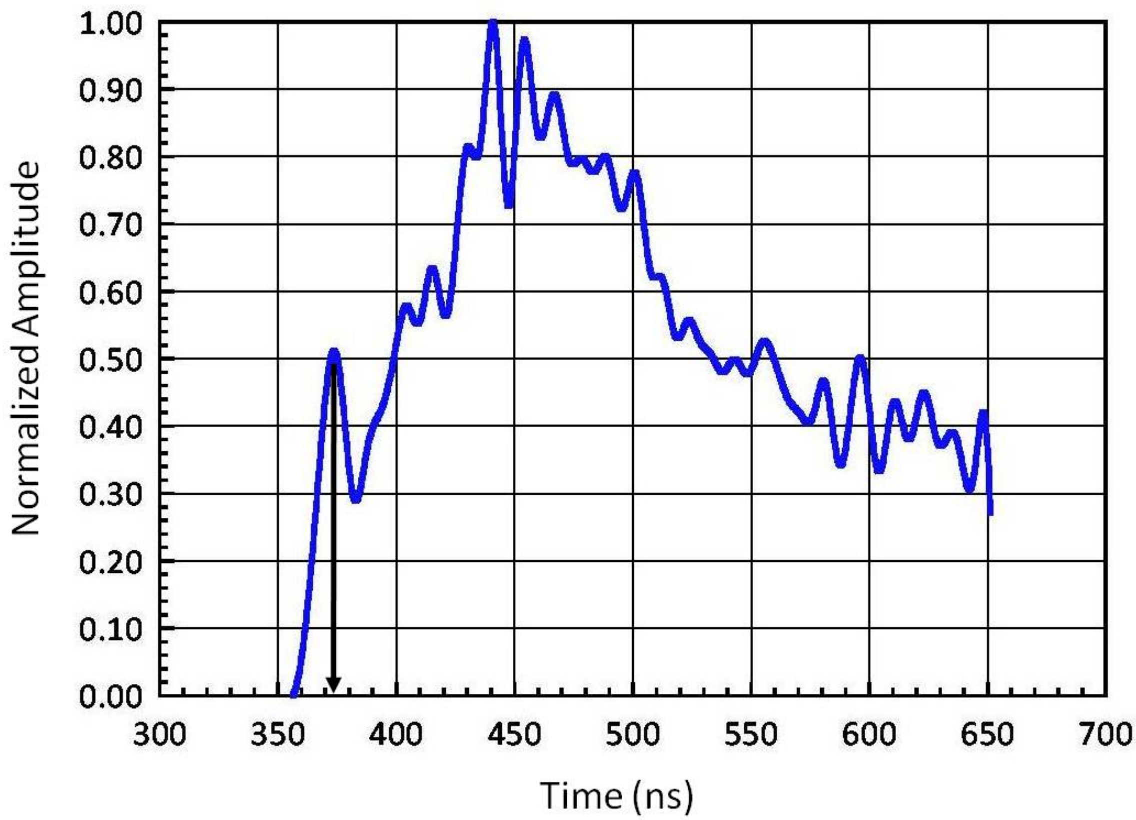

Figure 34. The empirical data from shot z1217 with the neutron impulse and timing information (Figure 31) deconvolved out of it. Note that the neutron peak is at 373.53 ns (see arrow) vs the neutron peak in the empirical data (Figure 26) at 383.13 ns. The deconvolution has shifted the waveform earlier in time by 9.6 ns – indicating that the time response information has been removed from the data. The delay above *must be at least* 9.6 ns, in order that causality not be violated – neutrons *must arrive earlier* than the signal that is produced.

source and scintillator, and comparing a case run with all the geometry and materials in the problem with the 2.54 cm (1 inch) scintillator at the same location (shown in blue in Figure 15). A plot of the “Ideal Case” being subtracted out from the “Full Scale” geometry leaving the contribution to scattering is shown in Figure 36. It is interesting to note that there is a small hump (green) due to scattering early in time, indicating that some shallow angle scattering is occurring, contributing to the signal. Not much can be said for the tail, as this is dominated by the huge, second scattering peak produced from lack of a neutron collimator near the source. Looking at the full width at half maxima in Table III – subtracting the FWHM of the "Ideal Case" from the FWHM of the "Full Scale" geometry in Figure 36 – one sees that the broadening due to scattering is 3.857 ns.

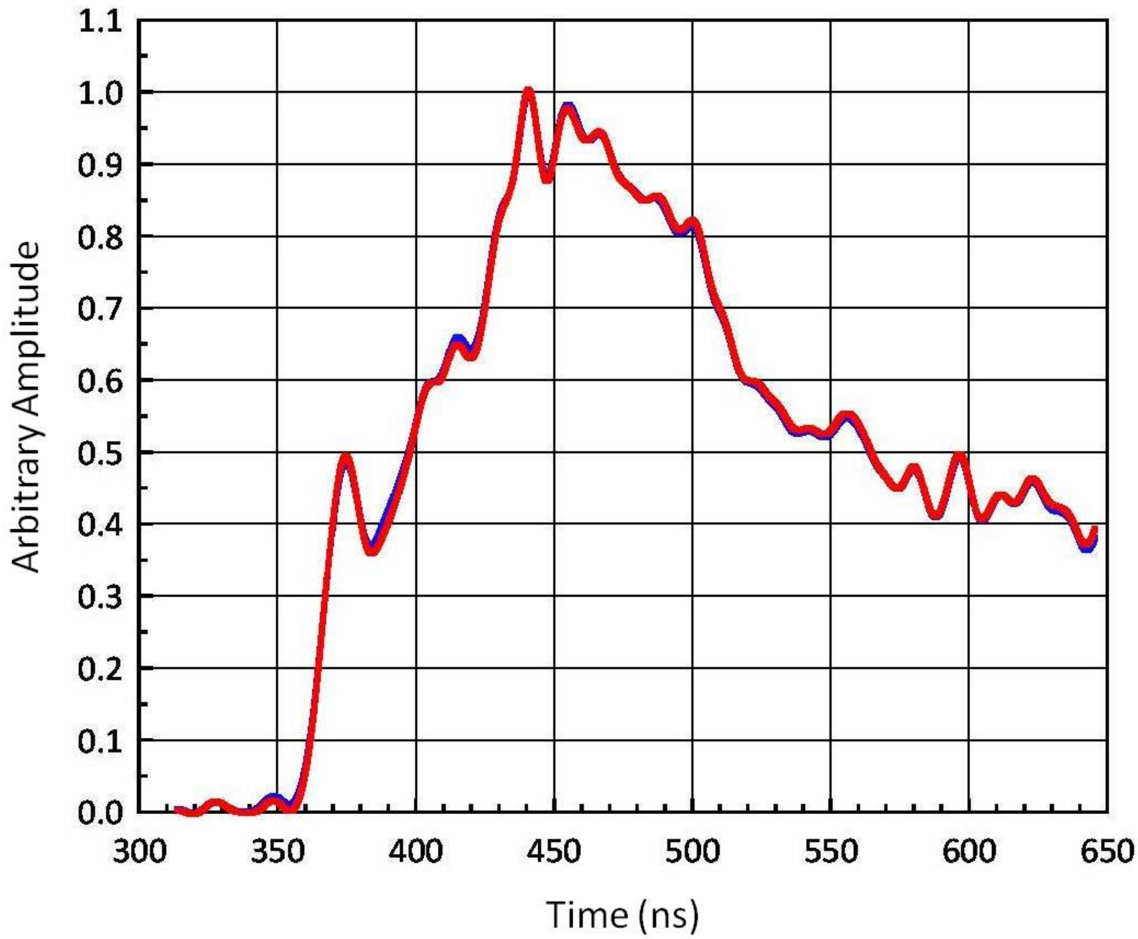

Figure 35. Area Normalized plot of the empirical data from z1217 (blue) compared with Figure 33 and Figure 34 being convolved together (red) as a "check" of the deconvolution. As can be seen, the red falls neatly on top of the blue with extremely small variations, indicating a very good fit.

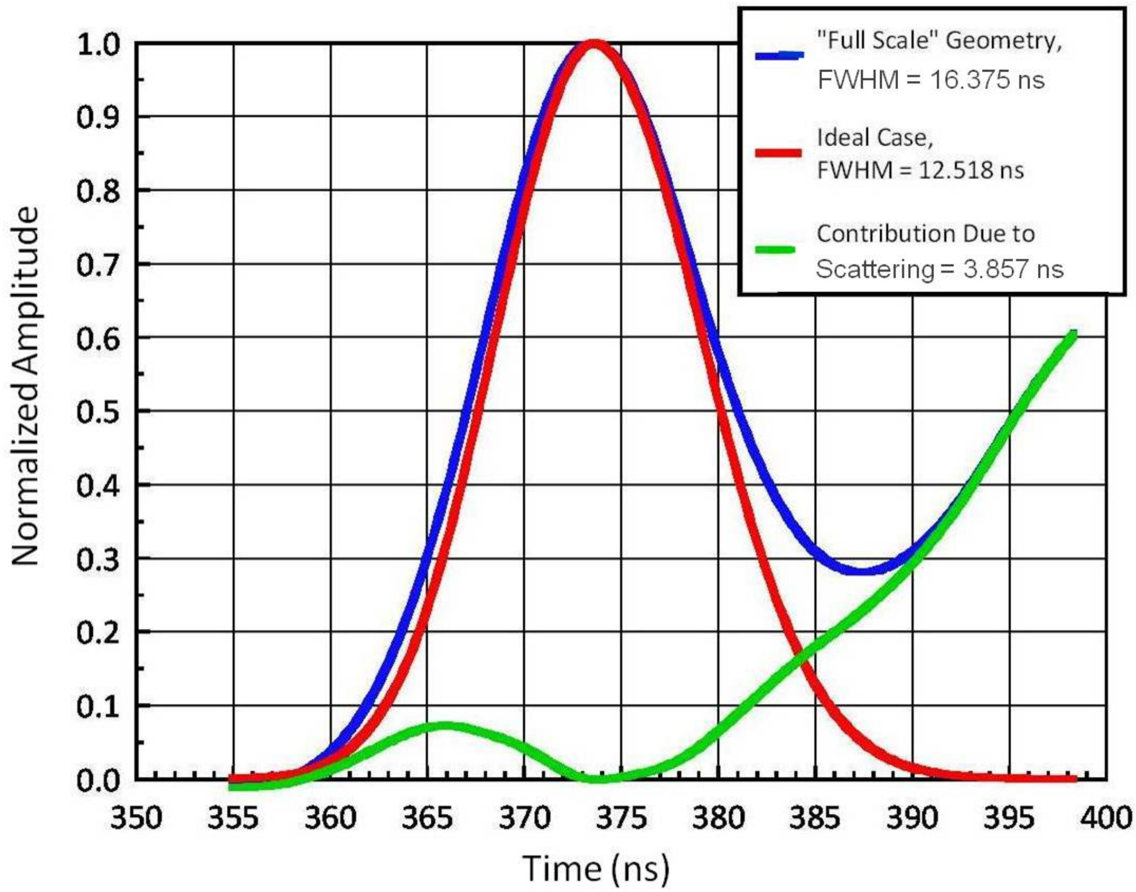

Figure 36. The "Ideal Case" (red) – i.e., a 2.54 cm (1 inch) scintillator placed 809 cm away from a 4 keV DD Fusion Source is subtracted out from the "Full Scale" Geometry (i.e., the scintillator in the same location but now with all the geometry of the problem added; blue). The result is the contribution due to scattering (green). Of interest is the small hump due to scattering early in time, indicating that indeed, there is some shallow-angle scattering contributing to the signal. Not much can be said for the tail, as this is dominated by the huge, second scattering peak produced from lack of a neutron collimator near the source. Subtracting the FWHM of the Ideal Case from the Full Scale Geometry leaves 3.857 ns, which is the amount of broadening that scattering contributes.

Once the contribution due to neutron scattering has been found (green in Figure 36), it could now be subtracted from the waveform in Figure 34 – the empirical data from z1217 with the time response and neutron impulse response deconvolved out of it. This is shown in Figure 37. The data is now ready to be transformed from the time domain *(dN/dt)* to the energy domain *(dN/dE)* to infer a neutron spectrum.

Table III.

Broadening due to Scattering at Detector Location "D" with no Collimator.

<u>Waveform</u>	<u>FWHM (ns)</u>
"Full Scale" Geometry (Bottom nTOF)	16.375
"Ideal Case"	12.518
Broadening Due to Scattering:	16.375 – 12.518 = <u>3.857 ns</u>

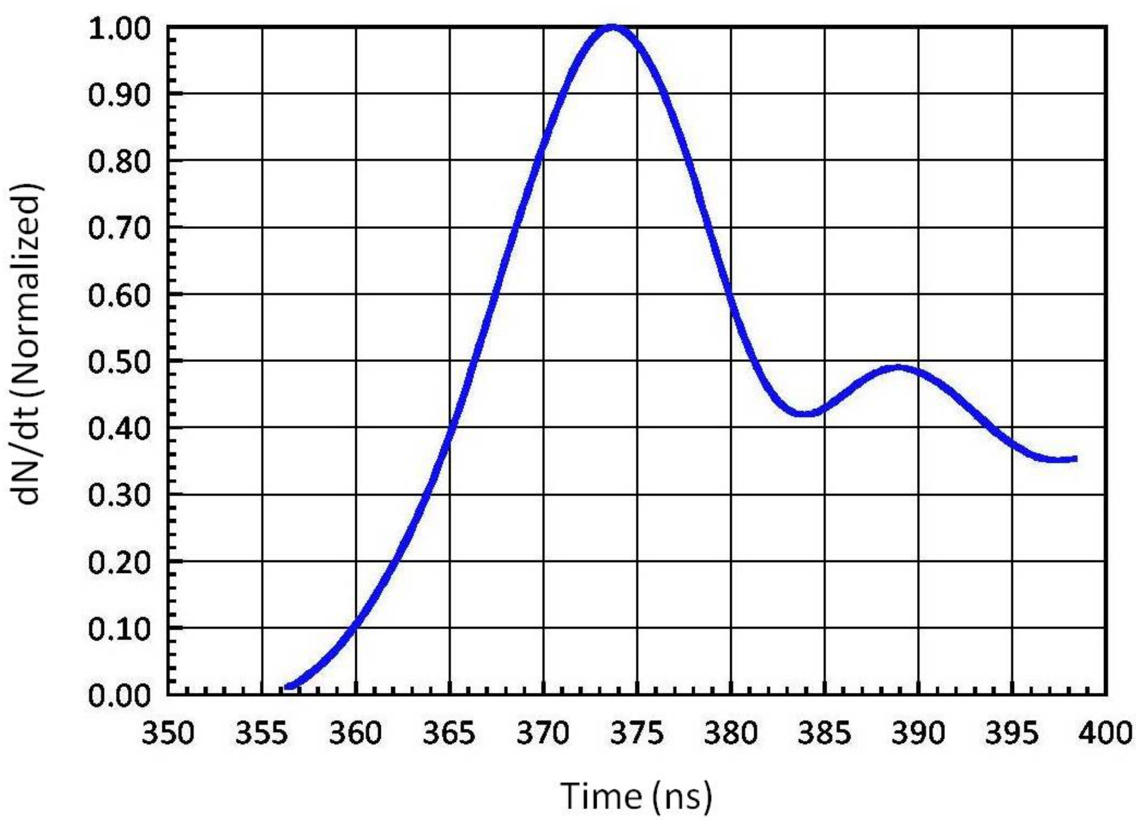

Figure 37. The empirical data from z1217 with the time response and neutron impulse response deconvolved out of it, and now with the contribution due to scattering (green in Figure 36) subtracted out of it. The data is now ready to be transformed from the time domain *(dN/dt)* to the energy domain *(dN/dE)* in order to produce a neutron spectrum.

CHAPTER 10

MAKING THE TRANSFORMATION FROM *(dN/dt)* to *(dN/dE)*

In the real world, the signal produced by an nTOF detector is in *Voltage vs Time*, due to the fact that the small amount of light output produced in the scintillator is converted to an electrical signal in the photomultiplier tube. The amplitude of this waveform is directly related to the number of incident neutrons that interacted in the scintillator. Thus, one could also refer to an nTOF signal as *dN/dt*, or number of neutrons interacting in the scintillator vs time. This is a known quantity. Unfortunately, what is not known is *dN/dE*, which is related to *dN/dt* by:

$$\frac{dN}{dt} = \frac{dN}{dE} * \frac{dE}{dt} \tag{19}$$

Solving for *dN/dE*:

$$\frac{dN}{dE} = \frac{\frac{dN}{dt}}{\frac{dE}{dt}} \tag{20}$$

From equation (9) above:

$$E = \frac{1}{2}\, m\, v^2 \tag{21}$$

Putting v in terms of t:

$$E = \frac{1}{2}\, m_0\, \frac{c^2}{c^2} \left(\frac{l}{t}\right)^2 \tag{22}$$

let $m = m_0\, c^2 = 939.5054\ MeV$, and taking the derivative of (22) with respect to t:

$$\frac{dE}{dt} = -\frac{m}{c^2}\frac{l^2}{t^3} \tag{23}$$

Taking the absolute value of *dE/dt*:

$$\left|\frac{dE}{dt}\right| = +\frac{m}{c^2}\frac{l^2}{t^3} \tag{24}$$

Solving for t in equation (22):

$$t = \sqrt{\frac{ml^2}{2c^2E}} \tag{25}$$

And t^3 becomes:

$$t^3 = \left[\frac{ml^2}{2c^2E}\right]^{3/2} \tag{26}$$

Substituting the value of *dE/dt* in (24) into (20) becomes:

$$\frac{dN}{dE} = \frac{dN}{dt} * \frac{c^2t^3}{ml^2} \tag{27}$$

Substituting the value of t^3 in (26) into (27):

$$\frac{dN}{dE} = \frac{dN}{dt} * \frac{c^2}{ml^2}\left(\frac{ml^2}{2c^2E}\right)^{3/2} \tag{28}$$

Simplifying:

$$\frac{dN}{dE} = \frac{m^{1/2}\,l}{2c\sqrt{2}\,E^{3/2}} * \frac{dN}{dt} \tag{29}$$

Defining constants:

$$K(l)_E = \frac{m^{1/2}\, l}{2c\sqrt{2}}, and\ K(l)_t = \frac{c^2}{ml^2}\ such\ that: \tag{30}$$

$$\frac{dN}{dE} = K(l)_E * \frac{dN}{dt} * E^{-3/2} \tag{31}$$

and:

$$\frac{dN}{dE} = K(l)_t * \frac{dN}{dt} * t^3 \tag{32}$$

Equation (31) is used to solve for *dN/dE* and equation (22) to solve for *E*. The values of *dN/dt* in (31) are those of the ordinate of Figure 37 and the values of t are those of the abscissa of Figure 37. The units of equation (31) must be #/MeV, and those of equation (22) are MeV. A plot of the transformation from *dN/dt* from Figure 37 to *dN/dE* is shown in Figure 38. It is the neutron spectrum for shot z1217 at detector location "D" in Figure 1. The time response (Figure 13), and the neutron impulse response (Figure 29), convolved together (Figure 31) to include both *timing information and neutron impulse information* (Figure 31) was deconvolved out of the data (Figure 34), and the contribution to scattering was subtracted out (Figure 36, green), leaving the true *dN/dt* signal (Figure 37). The transformation to *dN/dE* – the neutron spectrum is shown in Figure 38. It should be noted that the energy bins along the ordinate *are not equal* after the transformation is made, with larger bins at high energies, but the data can be interpolated with the bin width of the smallest energy bin at the extreme end of the data.

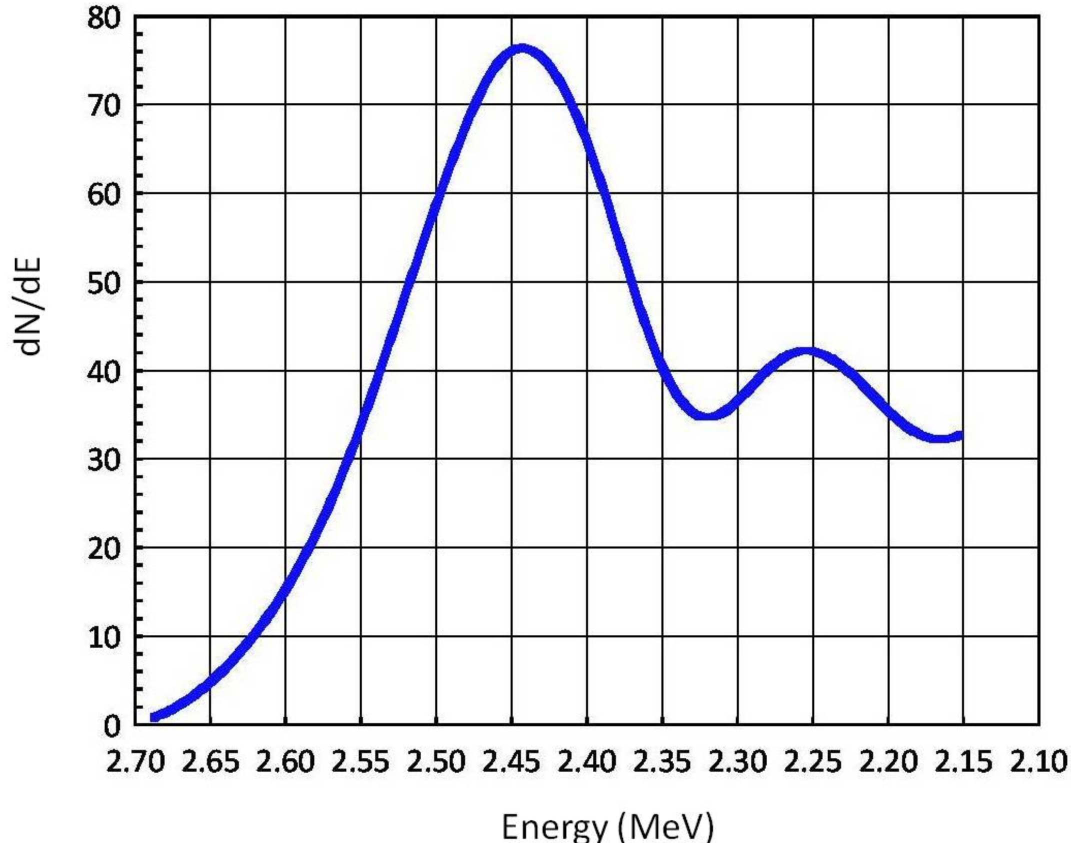

Figure 38. The Transformation from *dN/dt* (Figure 34) to *dN/dE*, the neutron spectrum for shot z1217 at detector location "D" in Figure 1. The time response and neutron impulse response have been deconvolved out of the data, and the contribution due to scattering has been subtracted out. The humped "tail" seen at ~2.25 MeV is not to be believed because of the enormous scattering tail (green in Figure 36).

According to the equation:

$$\int_{E_{min}}^{E^{max}} \frac{dN}{dE}\, dE = \int_{t_{min}}^{t^{max}} \frac{dN}{dt}\, dt \qquad (33)$$

the integral of *dN/dE* in Figure 38 *must equal* the integral of *dN/dt* in Figure 37. Before integrating *dN/*dE (Figure 38), the smallest bin width found at the end of the data must be used to interpolate the data, because all the bin widths need to be the same before integrating. Table IV below shows that both integrals are the same.

Table IV.

Integrals of *dN/dt* (Figure 37) and *dN/dE* (Figure 38)

Waveform	Integral
dN/dt (Figure 37)	1.84385
dN/dE (Figure 38)	1.84386

For the nTOF detector located at position "C" in Figure 1, the top nTOF in the basement "pig", the same analysis was performed, and the contribution due to scattering is shown in Figure 39 (green). It was found by subtracting the "Ideal Case" full width at half maxima from the "Full Scale" geometry full width at half maxima. The broadening due to scattering at detector location "C" in Figure 1 with no collimator is 3.89 ns.

The contribution to scattering in the top nTOF was subtracted from the data after having the time response and neutron impulse response deconvolved out of it, and the transformation from *dN/dt* to *dN/dE* was made. It is shown in Figure 40, plotted alongside the spectrum found at the bottom nTOF location (Figure 38). The Bottom nTOF spectrum's peak is located at 2.46 MeV, and the top nTOF spectrum's peak is at 2.44 MeV. The "tails" are not to be believed, since scattering was such an issue.

Later on in Z's history the Ultra-High Molecular Weight (UHMW) TIVAR collimator (Figure 19) was added to neutron producing shots to "clean up" the neutron signals.

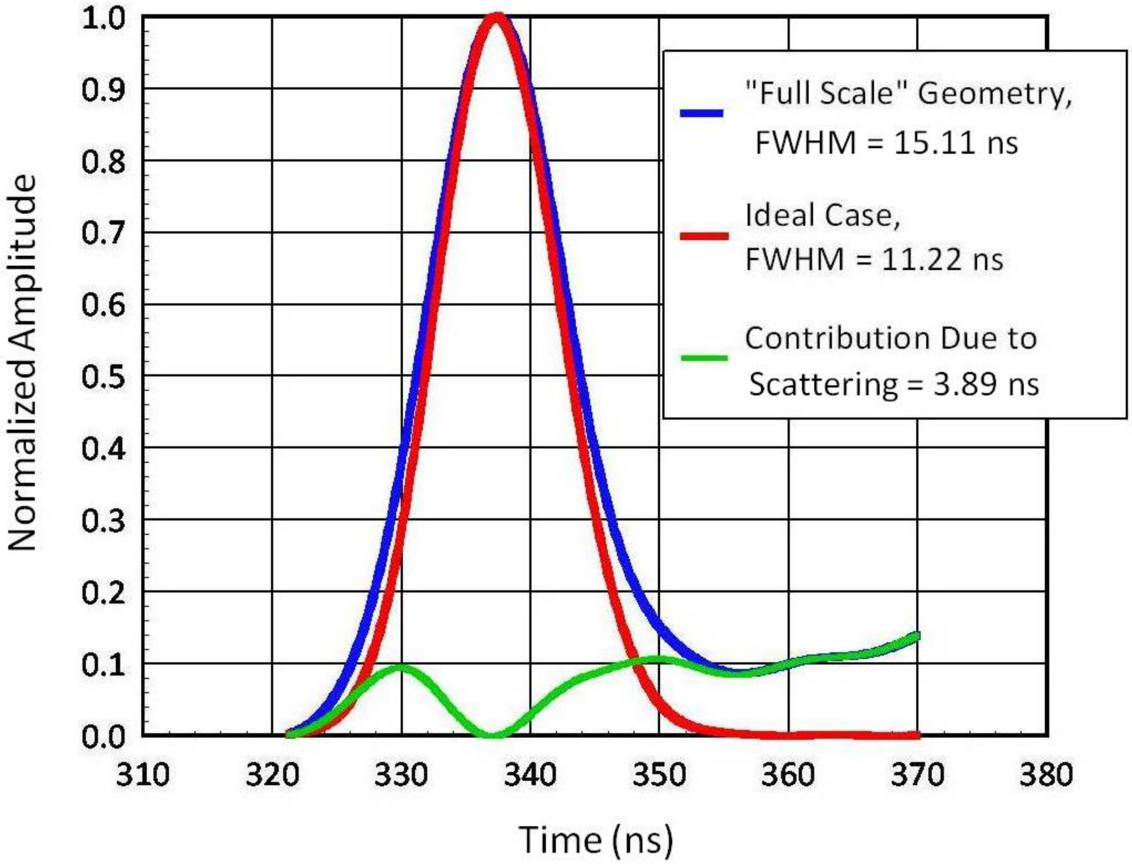

Figure 39. The “Ideal Case” (red) – i.e., a 2.54 cm (1 inch) scintillator placed 730 cm (location “C” in Figure 1) away from a 4 keV DD Fusion Source is subtracted out from the “Full Scale” Geometry (blue). The result is the contribution due to scattering (green). Subtracting the FWHM of the “Ideal Case” from the FWHM of the “Full Scale” Geometry leaves 3.89 ns, which is the amount of broadening that scattering contributes.

And as shown in Figures 22 and 24, it greatly reduced the second scattering “tail” for detector location “D” (Figure 1) and virtually eliminated the second scattering tail at detector location “C” (Figure 1).

On shot z1549 both detector signals from the basement “pig” were analyzed. Once the time response and neutron impulse response was deconvolved out of the data, the contribution to scattering was determined for detector location “D” (Figure 1) and shown in Figure 41. The “Full Scale” geometry (blue) was run with the TIVAR 1000 collimator in place in the model, and it is compared to an "Ideal Case" (red) in Figure 41. The broadening due to scattering (green) is the "Ideal Case" subtracted from the "Full Scale" geometry, and is 2.849 ns.

Table V.

Broadening due to Scattering at Detector Location "C" with no Collimator.

Waveform	FWHM (ns)
"Full Scale" Geometry (Bottom nTOF)	15.11
"Ideal Case"	11.220
Broadening Due to Scattering:	15.11 – 11.220 = 3.89 ns

This is less than the value of 3.857 ns shown in Figure 36 and Table III, indicating that the collimator is reducing some shallow-angle scattering into the detector. Some shallow-angle scattering is still contributing to the signal – this is due to the fact that the "bore" on the collimator is quite large, 7.62 cm (3 inch) diameter, and as shown in Figure 20, the "collimator cone" spreads out to a 116 cm (45.7 in) diameter at the basement floor. The collimator also reduces the second scattering tail drastically in Figure 41 compared to Figure 36.

Analysis of the top nTOF signal when the collimator was added (position "C" in Figure 1) was performed and is shown in Figure 42. The "Full Scale" geometry (blue) was run with the TIVAR 1000 collimator in place, and it is compared to the "Ideal Case"

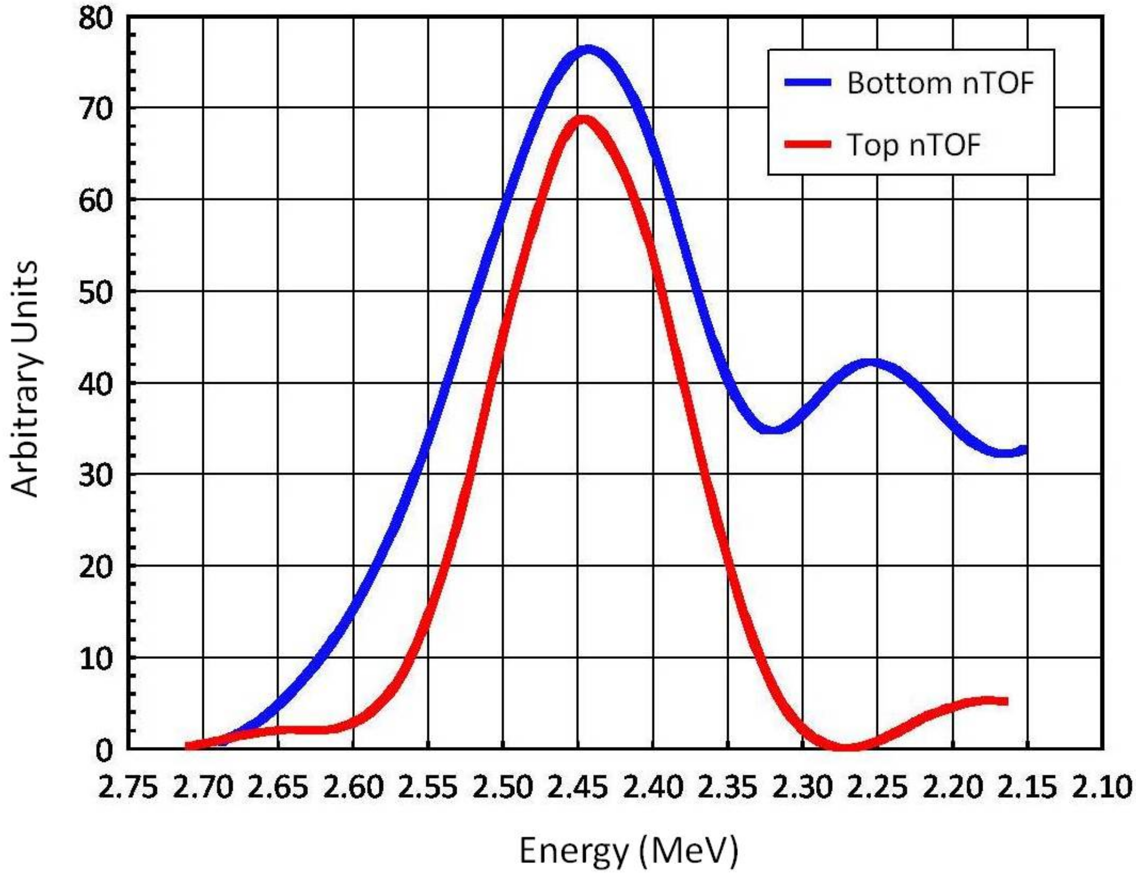

Figure 40. Energy Spectra for both the Top and Bottom nTOF detectors at locations "C" and "D" in Figure 1 from shot z1217. Although not identical, they are similar in shape. The Bottom nTOF spectrum's peak is at 2.46 MeV, while the Top nTOF spectrum's peak is at 2.44 MeV. Note that Energy along the abscissa decreases as one moves to the right. The "tails" are not to be believed, since scattering was such an issue.

(red). The broadening to scattering (green) is the "Ideal Case" subtracted from the "Full Scale" geometry, and is 3.176 ns, shown in Table VII. This is less than 3.89 ns shown in Figure 39 and Table V, indicating that again, the collimator is reducing shallow angle scattering into the detector. And, as in the case of Figure 41, the collimator does effectively reduce the second scattering tail seen in Figure 39.

Table VIII shows the contributions due to scattering for both detectors, with and without the collimator. The addition of the collimator reduced the broadening due to scattering for detector location “D” in Figure 1 (the Bottom nTOF) by 26.1 %. The

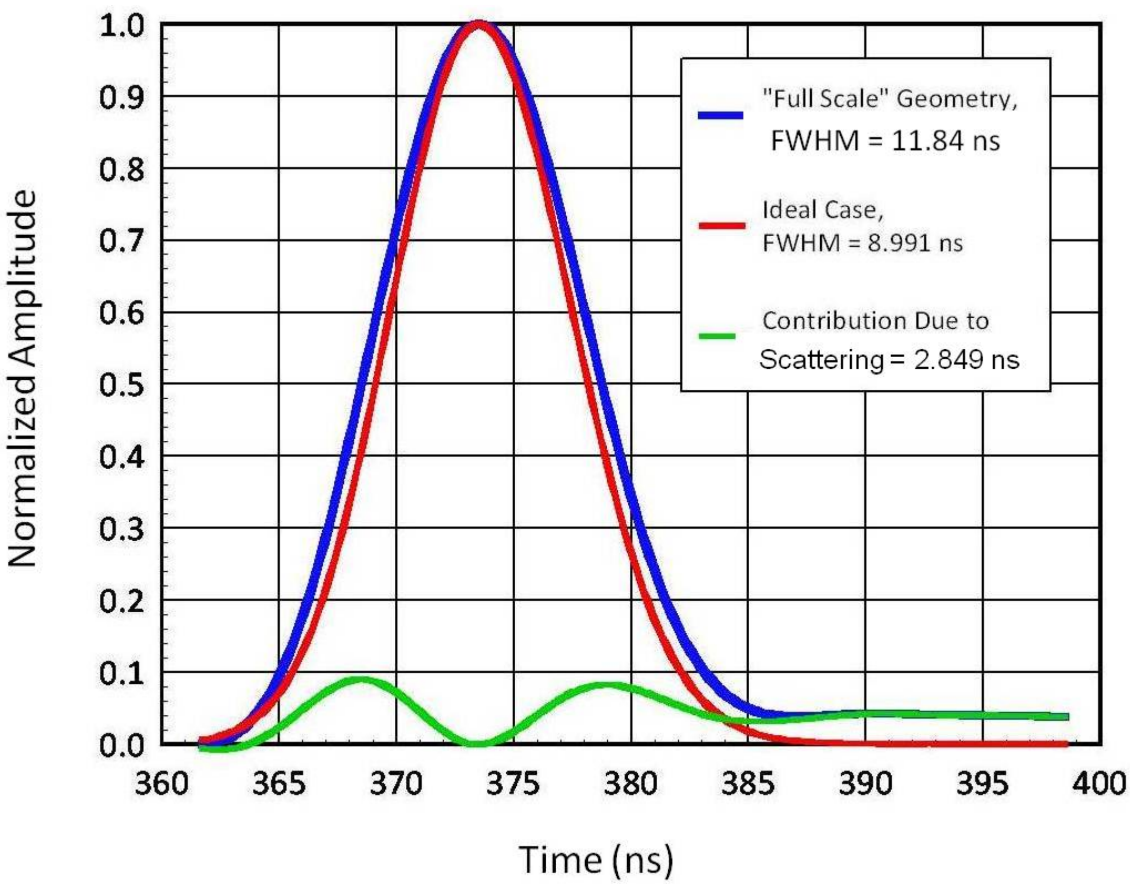

Figure 41. The “Ideal Case” (red) – i.e., a 2.54 cm (1 inch) scintillator placed 809 cm away from a 2 keV DD Fusion Source is subtracted out from the “Full Scale” Geometry (including the TIVAR collimator; blue). The result is the contribution due to scattering (green). What clearly can be seen is the reduction of the scattering tail in Figure 38 compared to Figure 33 – this is a direct result of the addition of the Tivar collimator. Subtracting the FWHM of the “Ideal Case” from the FWHM of the “Full Scale” Geometry leaves 2.849 ns, which is the amount of broadening that scattering contributes at detector location “D” in Figure 1.

addition of the collimator reduced the broadening due to scattering for detector location “C” in Figure 1 (the Top nTOF) by 18.4 %. Reduction of shallow angle scattering could be increased even further if the “bore” of the collimator were reduced in size from 7.62 cm (3 inches) to a smaller diameter, but as shown in Figure 21, reducing the diameter would occlude the scintillators' view of the source, because the "pig" is tilted 3° from vertical.

Table VI.

Broadening due to Scattering at Detector Location "D" with a Collimator.

Waveform	FWHM (ns)
"Full Scale" Geometry (Bottom nTOF)	11.84
"Ideal Case"	8.991
Broadening due to Scattering:	11.84 – 8.991 = 2.849 ns

The contribution to scattering in both the Bottom nTOF and the Top nTOF was subtracted from the data after having the time response and neutron impulse response deconvolved out of them, and the transformation from *dN/dt* to *dN/dE* was made. Both spectra are shown in Figure 43. The Bottom nTOF spectrum's peak is at 2.44 MeV, while the Top nTOF spectrum's peak is located at 2.45 MeV.

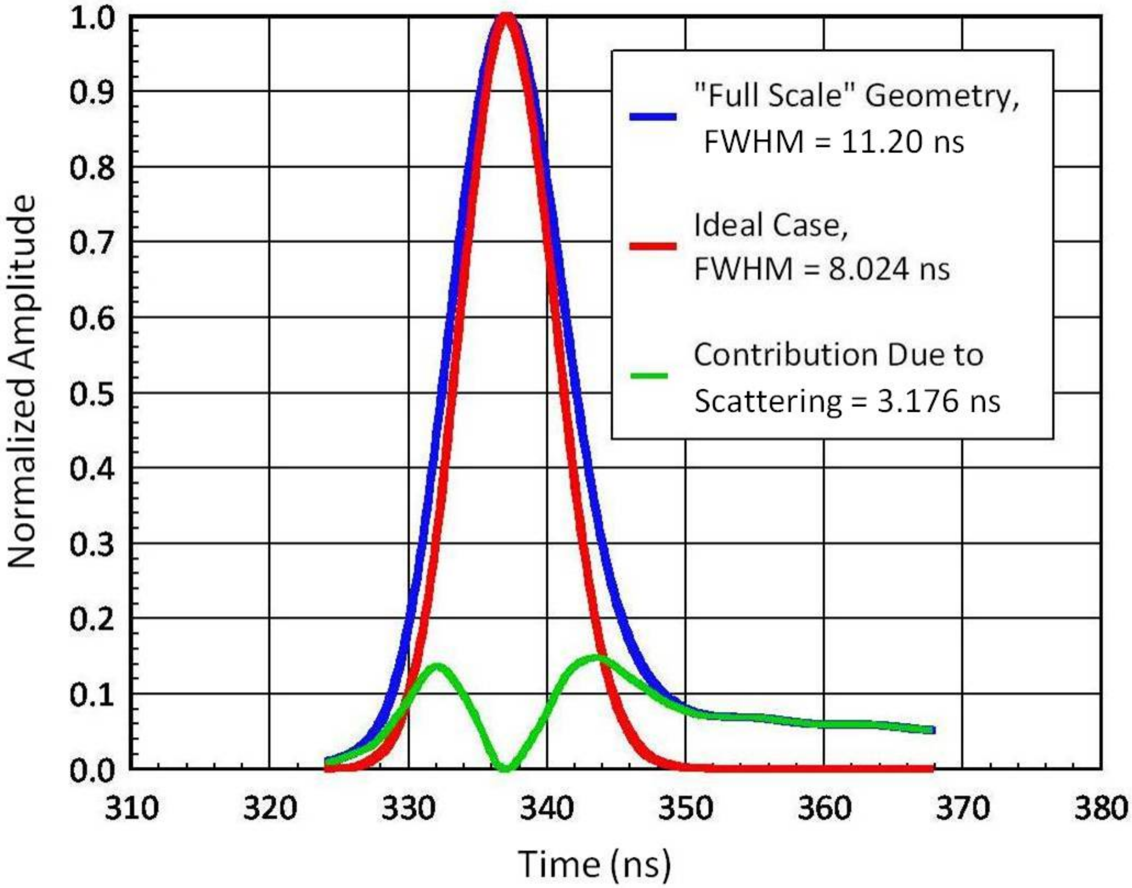

Figure 42. The “Ideal Case” (red) is subtracted from the “Full Scale” geometry (blue) to produce the contribution to scattering (green). This is the top nTOF located at position “C” in Figure 1, and was modeled at a temperature of 2 keV. The collimator does effectively reduce the second scattering peak shown in Figure 22. Subtracting the FWHM of the “Ideal Case” from the “Full Scale” Geometry leaves 3.176 ns, which is the amount of broadening that scattering contributes.

Table VII.

Broadening due to Scattering at Detector Location "C" with a Collimator

Waveform	FWHM (ns)
"Full Scale" Geometry (Top nTOF)	11.20
"Ideal Case"	8.024
Broadening due to Scattering:	11.2 – 8.024 = 3.176 ns

Table VIII.

Broadening Due to Scattering for each Detector Location

	Without Collimator (ns)	With Collimator (ns)	% Reduction
Bottom nTOF, ("D")	3.857	2.849	26.1
Top nTOF, ("C")	3.89	3.176	18.4

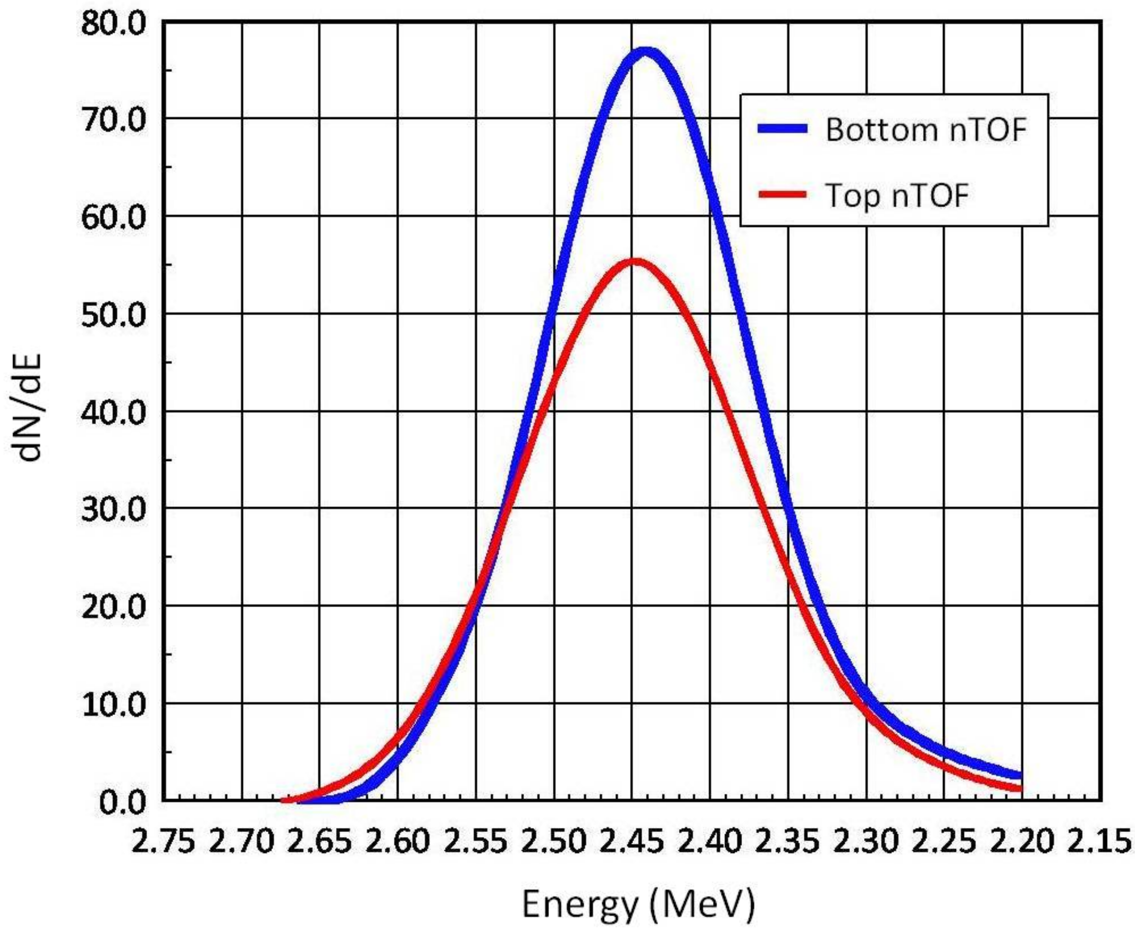

Figure 43. Energy Spectra for both the Top and Bottom nTOF detectors at locations “C” and “D” in Figure 1 from shot z1549. They are similar in shape. The Bottom nTOF spectrum’s peak is located at 2.44 MeV, and the Top nTOF spectrum’s peak is at 2.45 MeV. Note that Energy along the abscissa decreases as one moves to the right.

CHAPTER 11

IDENTIFYING SOURCES OF NEUTRON SCATTERING

An ideal neutron measurement would consist of detecting only those neutrons born at the source which arrive at the detector without interacting with any structural material in between. Experimentally, this can be difficult if not impossible, and depends on the facility, and the detector location. Collimation between the source and detector can greatly improve neutron signals, but may or may not be viable, depending on the facility. Therefore neutrons born at the source can and do undergo scattering off structural material and arrive at the detector, thereby "clouding" the pure signal, and making analysis of the plasma conditions at the source more difficult. One of the versatile aspects of this process described herein, however, is that the user -- upon suspecting certain materials to be contributors to neutron scattering – can actually *test* if they are indeed a cause of concern. By changing cells' importances to zero in the input deck (so that neutrons are killed when entering the cell) and changing the material that occupies the cells to a void, the user can then run the code, plot the light output and examine the detector response. The user can also identify whether photons or neutrons are responsible for any changes seen in the output, because the post-processing code can be easily modified to look at just the contribution of light output made from neutrons, photons, or both. This is illustrated in Figure 44. While the "mode" card in the input deck was turned on for both neutrons and photons, the source was a DD fusion neutron source and photons could only be produced by n,gamma capture reactions, therefore, virtually all the signal was produced from neutrons. As can be seen, following the primary neutron signal, there are two "humps" caused by neutrons scattering into the detector later in time. The first "hump" is caused by neutrons scattering in through the sides of the pig, and the second "hump" is from neutrons scattering off the elevator floor.

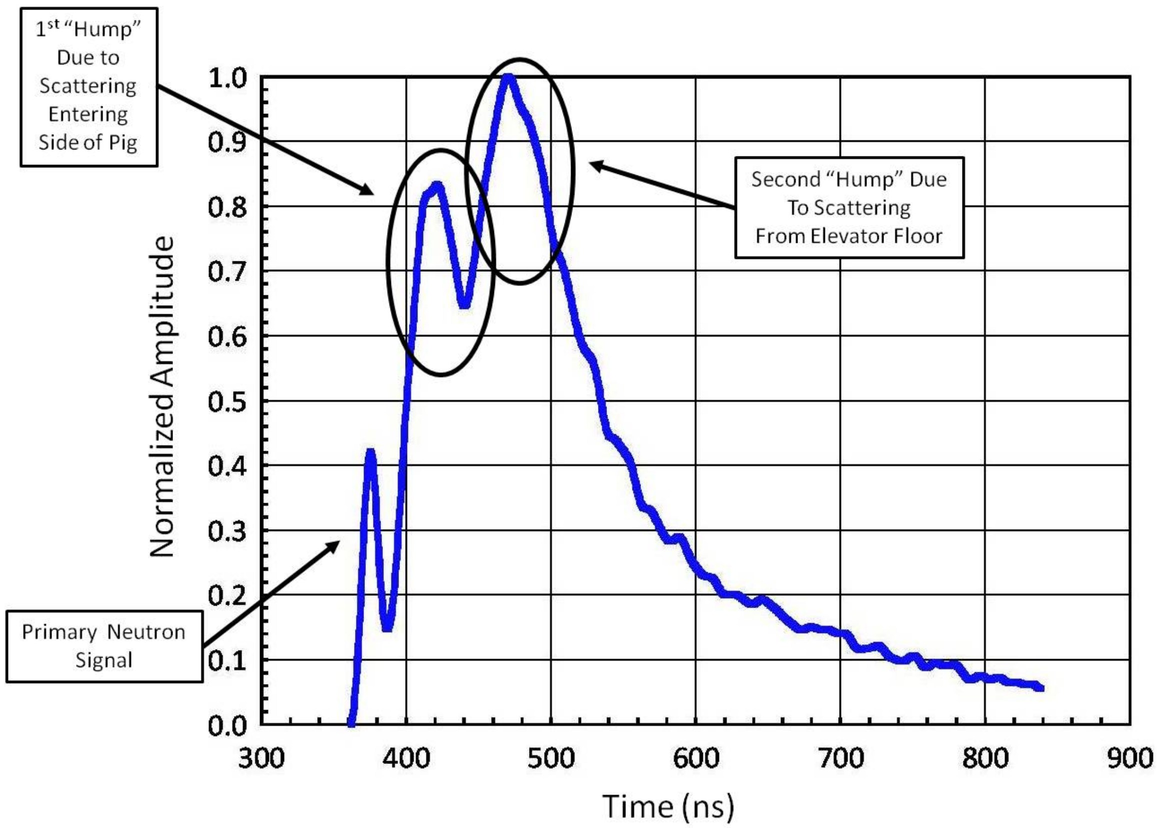

Figure 44. Neutron scattering after the primary pulse for detector location "D" in Figure 1. As can be seen, the first "hump" is from neutrons scattering through the side of the pig, and the second "hump" is caused from neutrons scattering off the elevator floor and arriving at the detector later in time.

The input deck was then modified by changing all the neutron importances for all the cells comprising the elevator floor to zero, and changing the cells of the elevator from steel to a void. This causes all neutrons that interact with the elevator to be "killed" (i.e., removed from the problem). The result is shown in Figure 45. Note the second “hump” which was at ~ 470 ns is now gone, confirming that it is indeed due to neutrons scattering off the elevator floor. The first “hump” is still there, indicating that neutrons are still scattering in through the sides of the pig.

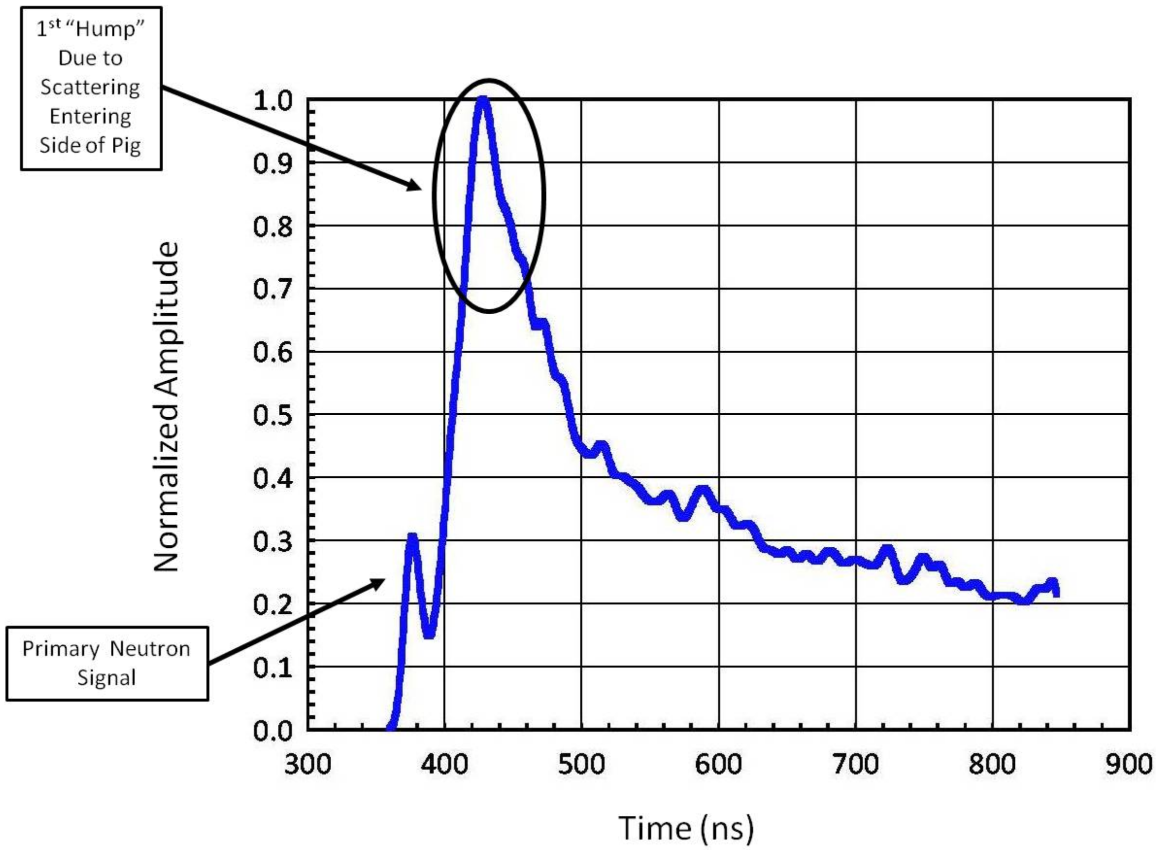

Figure 45. The elevator was made into a “kill” zone – i.e., any neutrons interacting with it were removed from the problem. The second “hump” seen in Figure 44 at ~470 ns is now gone, indicating that the elevator was indeed a cause of the second “hump”. The first “hump” is still there, indicating that neutrons are still scattering in through the sides of the pig.

The input deck was again modified by changing all the cell importances that comprised the sides of the pig to zero and changing their material from steel to a void (this is in addition to the elevator as shown in Figure 45). The result is shown in Figure 46. Note the first “hump” which appeared at ~430 ns is now gone, indicating that neutrons were indeed scattering in through the sides of the pig. All that is left is the primary neutron signal.

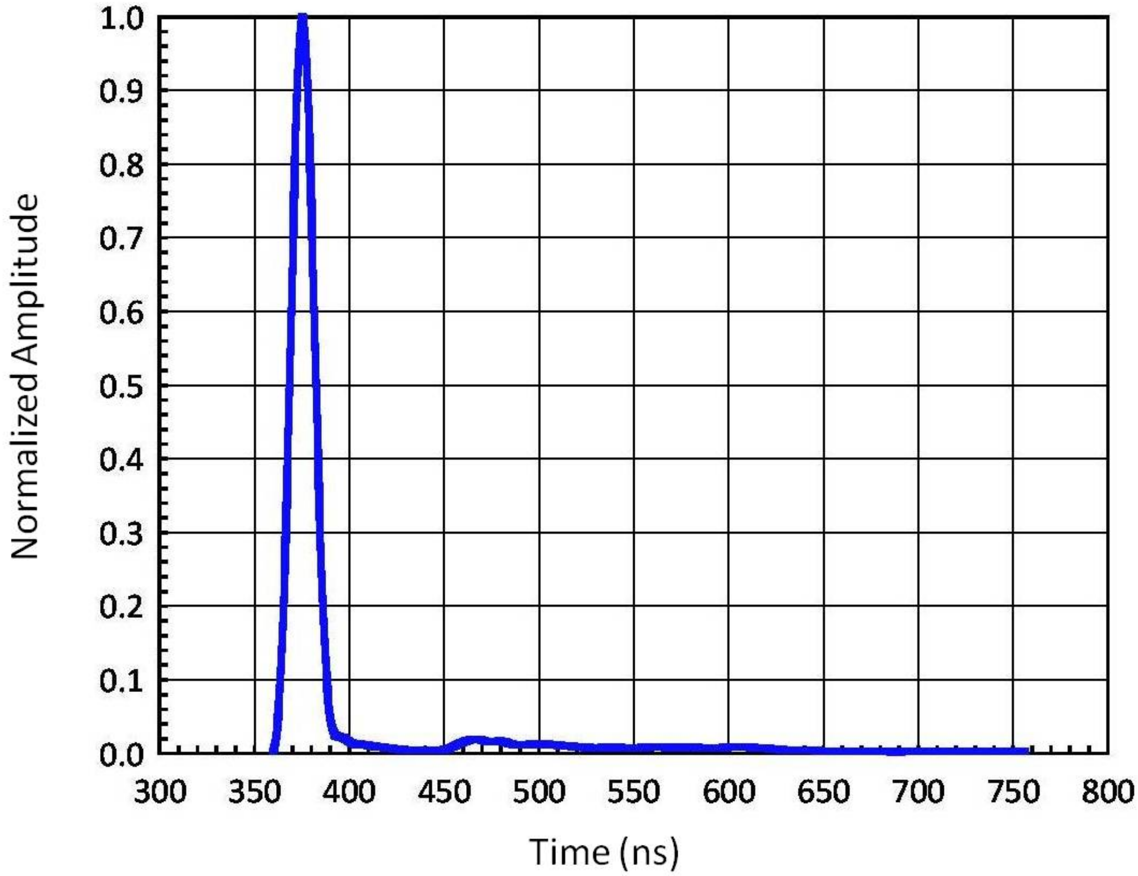

Figure 46. For the nTOF detector located at position "D" in Figure 1, both the elevator and the sides of the pig have been made into "kill" zones, thereby removing neutrons that interact with them, indicating that both the elevator and the sides of the pig were the contributors to scattering peaks later in time. All that is left above is the primary neutron peak.

In this way, this technique can be very useful in identifying sources of neutron scattering, and mitigating them if possible (by removing hardware that is a source of scattering near a detector, for example) or by adding neutron shielding in key areas identified by the code.

CHAPTER 12

CONCLUSIONS

A novel method of modeling the neutron time of flight (nTOF) detector response in current mode to inertial confinement fusion experiments has been presented. This process was first developed and then applied to the axial neutron time of flight detectors at the Z-Facility. First, the Z-Facility was modeled between the source and detector locations, which encompassed over 2400 cells and 900 surfaces with a user-modified version of MCNP, namely MCPN-PoliMi, which was developed by Enrico Padovani and Sara Pozzi in 2002. In order to obtain good statistics, many variance reduction techniques were utilized. MCNP-PoliMi simulates the detection of neutrons and photons in a plastic scintillator, and produces a collision data output table containing information of the incident particle (neutron or photon), target nucleus (hydrogen or carbon), energy deposited (MeV) and the time at which it occurred (shakes, [30]). A post-processing code was written to read this collision data output table. This converted the energy deposited by neutron and photon interactions in the plastic scintillator (i.e., nTOF detector) into light output, in units of MeVee (electron equivalent) vs time. A monoenergetic neutron case of 2.45 MeV was run at each detector location and convolved with the experimental time response found at the Idaho Accelerator Center (IAC) using their 15 MeV short pulse Linac with a 50 ps pulse width. This was done to provide both *timing and neutron impulse response information*. The resulting waveform was convolved with the simulated data and compared with the empirical results at each detector location, and was shown to be in good agreement.

For each detector, an experiment was performed, first without a neutron collimator below the source, and then with a neutron collimator fielded below the source. It was shown that the addition of the collimator resulted in greatly reducing the second scattering peak in both detector signals, but also reduced shallow-angle scattering in the bottom nTOF by 26.1%, and 18.4% in the top nTOF.

Then, as an additional step, the time response was deconvolved out of the empirical data. The contribution due to scattering was found by running a "Ideal Case" (i.e., nothing between the source and scintillator at each detector location); then a "Full Scale" geometry was run with all the structure added, and then subtracting one from the other. This scattering contribution was then subtracted from the empirical data. The resulting waveform was transformed from *dN/dt* to *dN/dE*, in order to produce neutron spectra for each detector location (Top and Bottom nTOF) and for each configuration (without collimator and with collimator).

The method developed here can be used to simulate the detector response of *any* nTOF detector, with any digitized resolution, at any facility. It has been found useful to address key issues such as scattering, which always plays a role in neutron detection when using nTOF detectors. It can be used to identify sources of scattering as well, and to improve neutron signals by modeling effective collimation. It is hoped by the author that this method will prove to be a useful tool in future modeling of experiments, where "clean" neutron signals will provide the greatest amount of information from whence they came.

FUTURE WORK

The techniques described herein have been shown to be extremely valuable in analyzing the data from dynamic holhraum experiments on Sandia National Laboratories' Z-machine. These techniques allowed the true neutron pulse shapes in the bottom nTOF detectors to be deconvolved from measured signals which in turn allows the determination of the neutron spectrum, the plasma ion temperature and the neutron yield. Since z-pinch fusion plasmas have historically been dominated by beam generated fusion reactions [31] which will result in there being an angular dependence in the neutron spectrum, it is important to apply this technique to the two (now three) side nTOF detectors, as well as the bottom two detectors, to better assess whether the neutrons observed are produced by a thermal plasma, beams, or a combination of the two.

These techniques could also be applied to other ICF facilities such as those at LLE [32] and LLNL [33]. This would include expanding the approach to include analyzing nTOF signals that measure the 14.1 MeV neutrons from the reaction:

$$D + T \rightarrow \propto (3.5\, MeV) + n(14.1\, MeV) \tag{34}$$

This D-T reaction will be the reaction of choice for all ignition experiments since this reaction has the highest reaction cross section of all fusion reactions and the peak of the cross section occurs at the lowest ion energy. In addition to helping to analyze nTOF signals as on Z, an example of another potential application would be to help in the transfer of nTOF detector calibrations between facilities. For example, nTOF detectors have been calibrated at LLE for use on NIF. Since the scattering environment at LLE is not the same as at NIF, however, the transfer of the calibration is not straight forward. The use of the techniques described in this dissertation should be of great help in transferring these calibrations.

In addition to allowing the measurements of neutron yields, ion temperatures, and neutron spectra, nTOF detectors can be used to measure another extremely important parameter in inertial confinement fusion experiments: the ρR of the fuel (g/cm2). Here ρ is the fuel density (g/cm^3) and R is the radius of fuel (cm), which is assumed to be spherical. For D-T fuel, the optimum value of ρR is ~ 3g/cm^2 [34]. For low values of ρR, disassembly of the pellet becomes an issue, and for high values of ρR, fuel depletion becomes an issue. For fusion to be an energetically viable energy source most of the D-T fuel must be heated, not by the laser driver (for example), but by the fusion reactions themselves. Since most neutrons escape with little or no interactions, this self-heating of the fuel will rely on the energy deposition of the 3.5 MeV alpha particles in the fuel. It is envisioned that the laser will create a hot spot in the central core which ignites the fuel and that the resulting alphas will create a "burn wave" that propagates outward through cold fuel. For typical fuel masses, the ρR must be increased by a factor of about twenty over "normal", solid D-T values to simply support a burn propagation wave and over a factor of one hundred to attain optimal burn conditions (This later condition corresponds to increasing the fuel density by about a factor of a thousand over solid density). Thus, the ρR attained in a pellet implosion is an extremely critical measure of pellet performance [35].

Unfortunately, ρR is a difficult quantity to measure. One potential way to measure the ρR of D-T fuel is to measure the neutron "down scattered fraction" or *dsf*. Most of the 14.1 MeV neutrons born in the fusion reactions escape the fuel without interacting. If high ρRs are attained, however, a small fraction of the neutrons will down-scatter in the fuel and exit the fuel with energies lower than the initial 14.1 MeV that they are born with. The fraction of scattered neutrons observed will be a measure of the fuel ρR, so if the *dsf* can be measured, the fuel ρR can be calculated. Since the scattered neutrons have less energy, they will travel more slowly to the nTOF detector so the detector's response to these neutrons will be separated in time from those of the primary pulse which will allow their measurement. However, the fact that the scattered neutrons will have lower energies also means that, neutron for neutron, they will induce less light output in the nTOF detector. Thus, to get the true *dsf* the light output of the respective signals must be adjusted for neutron energy – something that can be readily accomplished by the use of the techniques described herein.

These techniques can also be applied to ρR measurements of D-D fusion experiments. In the case of D-D fusion there are two reactions of roughly equal probability:

$$D + D \ \rightarrow He^3(0.82\ MeV) + n\ (2.45\ MeV) \qquad (35)$$

$$D + D \ \rightarrow T(1.01\ MeV) + \ p(3.04\ MeV) \qquad (36)$$

The product tritium of equation 36 can react with the deuterium fuel and drive the D-T reaction above (equation 34). The ratio of D-D to D-T reactions is a function of the ρR of the fuel, so measuring the ratio of D-D to D-T neutrons will give a measure of the fuel

ρR. As above, the difference in energies of the 2.45 MeV D-D neutrons and the 14.1 MeV D-T neutrons means that the two signals will be well-separated in time at an nTOF detector. Again, by properly adjusting the light output of the two signals for the different neutron energies using the techniques described in this dissertation, the ratio of D-D to D-T reactions can be measured, which, in turn will yield the fuel ρR.

ICF applications are also requiring scintillators with ever-faster time responses. This need leads to the introduction of novel scintillation materials. For example, the primary *dsf* nTOF detector at NIF uses xylene as the scintillation material. This material (or other "exotic" materials that might be used) may not have the same light output curve as typical plastic scintillators (equations 2 and 3, page 10; also Figure 7, page 11). Thus, to fully generalize the techniques discussed herein will require the experimental verification of the light output curves of all the scintillation materials being used.

The technique described herein has also been used to model the effectiveness of a new collimator design. It has been shown that the addition of a collimator did indeed improve the neutron signals but there was still room for improvement. Therefore, a new collimator design was undertaken, to be more massive than the first, and was shown with modeling that it was much more effective at eliminating neutrons that would contribute to scattering into the detectors later in time. This is shown in full in Appendix F.

APPENDICIES

APPENDIX A

MCNP-PoliMi INPUT DECK

```
INPUT DECK
c
c      BOTTOM nTOF W/ TIVAR COLLIMATOR
c
c      CELLS:
1      0 905 -1 -23
2      4 -8.96 1 -2 -11 665
3      4 -8.96 1 -2 11 -12
4      0 2 -3 -12
5      4 -8.96 3 -4 -11 665
6      4 -8.96 3 -4 11 -12
7      0 4 -5 -12
8      4 -8.96 5 -6 -11 665
9      4 -8.96 5 -6 11 -12
10     0 6 -7 -12
11     4 -8.96 7 -8 -11 665
12     4 -8.96 7 -8 11 -12
13     0 8 -9 -23
14     0 9 -10 -11
15     1 -7.9 9 -10 11 -12
16     1 -7.9 9 -10 12 -23
17     1 -7.9 9 -10 -22 23
18     1 -7.9 10 -13 -24 25
19     1 -7.9 10 -13 24 -12
20     1 -7.9 10 -13 12 -23
21     1 -7.9 10 -13 23 -22
c
22     2 -19.2 13 -27 25 -24   $ **************
23     2 -19.2 27 -28 25 -24
24     2 -19.2 28 -29 25 -24
25     2 -19.2 29 -30 25 -24
26     2 -19.2 30 -31 25 -24   $ Tungsten Insert
27     2 -19.2 31 -32 25 -24
28     2 -19.2 32 -33 25 -24
29     2 -19.2 33 -34 25 -24
30     2 -19.2 34 -35 25 -24
31     2 -19.2 35 -36 25 -24   $ **************
c
32     3 -0.93 13 -27 24 -12   $ TIVAR COLLIMATOR
33     3 -0.93 13 -27 12 -141
34     3 -0.93 27 -28 24 -12
35     3 -0.93 27 -28 12 -141
36     3 -0.93 28 -29 24 -12
37     3 -0.93 28 -29 12 -141
38     3 -0.93 29 -30 24 -12
39     3 -0.93 29 -30 12 -141
40     3 -0.93 30 -31 24 -12
41     3 -0.93 30 -31 12 -141
42     3 -0.93 31 -32 24 -12
43     3 -0.93 31 -32 12 -141
44     3 -0.93 32 -33 24 -12
45     3 -0.93 32 -33 12 -758
46     3 -0.93 33 -34 24 -12
47     3 -0.93 33 -34 12 -758
48     3 -0.93 34 -35 24 -12
49     3 -0.93 34 -35 12 -758
50     3 -0.93 35 -36 24 -12
51     3 -0.93 35 -36 12 -758  $ TIVAR COLLIMATOR
c
52     0 46 -74 -23    $ Void Inside Collimator Cone
c
53     2 -19.2 36 -37 25 -24     $ **********************
c
54     3 -0.93 36 -37 24 -12
```

```
55     3 -0.93 36 -37 12 -140
56     3 -0.93 36 -37 140 -758
c
57     2 -19.2 37 -38 25 -24
c
58     3 -0.93 37 -38 24 -12
59     3 -0.93 37 -38 12 -140
60     3 -0.93 37 -38 140 -758
c
61     2 -19.2 38 -39 25 -24   $ Part of 10" Tungsten Insert
c
62     3 -0.93 38 -39 24 -12
63     3 -0.93 38 -39 12 -140
64     3 -0.93 38 -39 140 -758
c
65     2 -19.2 39 -40 25 -24
c
66     3 -0.93 39 -40 24 -12
67     3 -0.93 39 -40 12 -140
68     3 -0.93 39 -40 140 -758
c
69     2 -19.2 40 -41 25 -24   $ Part of 10" Tungsten Insert
c
70     3 -0.93 40 -41 24 -12
71     3 -0.93 40 -41 12 -140
72     3 -0.93 40 -41 140 -758
c
73     2 -19.2 41 -42 25 -24   $ Part of 10" Tungsten Insert
c
74     3 -0.93 41 -42 24 -12
75     3 -0.93 41 -42 12 -140
76     3 -0.93 41 -42 140 -758
c
77     2 -19.2 42 -43 25 -24   $ Part of 10" Tungsten Insert
c
78     3 -0.93 42 -43 24 -12
79     3 -0.93 42 -43 12 -140
80     3 -0.93 42 -43 140 -758
c
81     2 -19.2 43 -44 25 -24   $ Part of 10" Tungsten Insert
c
82     3 -0.93 43 -44 24 -12
83     3 -0.93 43 -44 12 -140
84     3 -0.93 43 -44 140 -758
c
85     2 -19.2 44 -45 25 -24   $ Part of 10" Tungsten Insert
c
86     3 -0.93 44 -45 24 -12
87     3 -0.93 44 -45 12 -140
88     3 -0.93 44 -45 140 -758
c
89     2 -19.2 45 -46 25 -24   $ Part of 10" Tungsten Insert
c
90     3 -0.93 45 -46 24 -12
91     3 -0.93 45 -46 12 -140
92     3 -0.93 45 -46 140 -758  $ End of 10" Tungsten/TIVAR
c
c 93    0 46 -54 -23
c
c 94    0 47 -48 25 -24
c 95    0 48 -49 25 -24
c 96    0 49 -50 25 -24
c 97    0 50 -51 25 -24
c 98    0 51 -52 25 -24
c 99    0 52 -53 25 -24
c 100   0 53 -54 25 -24
c
101   0 13 -46 -25     $ Void inside collimator
c
c 102   0 55 -56 25 -24   $ TIVAR Collimator
c 103   0 56 -57 25 -24
c 104   0 57 -58 25 -24
```

```
c 105   0 58 -59 25 -24
c 106   0 59 -60 25 -24
c 107   0 60 -61 25 -24
c 108   0 61 -62 25 -24
c 109   0 62 -63 25 -24
c 110   0 63 -64 25 -24
c 111   0 64 -65 25 -24
c 112   0 65 -66 25 -24  $ *************************
c
c 113   0 46 -47 24 -142        $ *************************
c 114   0 46 -47 142 -140
c 115   0 46 -47 140 -141
c 116   0 47 -48 24 -142
c 117   0 47 -48 142 -140
c 118   0 47 -48 140 -141
c 119   0 48 -49 24 -142
c 120   0 48 -49 142 -140
c 121   0 48 -49 140 -141
c 122   0 49 -50 24 -142
c 123   0 49 -50 142 -140
c 124   0 49 -50 140 -141       $ Cells where more TIVAR
c 125   0 50 -51 24 -142        $ can be added to the
c 126   0 50 -51 142 -140       $ 25.4 cm (10 in) length
c 127   0 50 -51 140 -141
c 128   0 51 -52 24 -142
c 129   0 51 -52 142 -140
c 130   0 51 -52 140 -141
c 131   0 52 -53 24 -142
c 132   0 52 -53 142 -140
c 133   0 52 -53 140 -141
c 134   0 53 -54 24 -142
c 135   0 53 -54 142 -140
c 136   0 53 -54 140 -141      $ *************************
c
c 137   0 66 -74 -23            $ *************************
c 138   0 139 -67 25 -24
c 139   0 139 -67 24 -142
c 140   0 67 -68 -25
c 141   0 67 -68 25 -24
c 142   0 67 -68 24 -142
c 143   0 68 -69 -25
c 144   0 68 -69 25 -24
c 145   0 68 -69 24 -142
c 146   0 69 -70 -25
c 147   0 69 -70 25 -24
c 148   0 69 -70 24 -142         $ Cells where more TIVAR
c 149   0 70 -71 -25             $ can be added to the
c 150   0 70 -71 25 -24          $ 50.8 cm (20 in) length
c 151   0 70 -71 24 -142
c 152   0 71 -72 -25
c 153   0 71 -72 25 -24
c 154   0 71 -72 24 -142
c 155   0 72 -73 -25
c 156   0 72 -73 25 -24
c 157   0 72 -73 24 -142
c 158   0 73 -74 -25
c 159   0 73 -74 25 -24
c 160   0 73 -74 24 -142    $ ************************
c
c 161   0 54 -66 142 -23
c
162   1 -7.9 13 -27 23 -22    $ ************************
163   1 -7.9 27 -28 23 -22
164   1 -7.9 28 -29 23 -22
165   1 -7.9 29 -30 23 -22
166   1 -7.9 30 -31 23 -22
167   1 -7.9 31 -32 23 -22
168   1 -7.9 32 -33 23 -22
169   1 -7.9 33 -34 23 -22
170   1 -7.9 34 -35 23 -22
171   1 -7.9 35 -36 23 -22
172   1 -7.9 36 -37 23 -22
```

```
173    1 -7.9 37 -38 23 -22
174    1 -7.9 38 -39 23 -22
175    1 -7.9 39 -40 23 -22
176    1 -7.9 40 -41 23 -22
177    1 -7.9 41 -42 23 -22
178    1 -7.9 42 -43 23 -22
179    1 -7.9 43 -44 23 -22
180    1 -7.9 44 -45 23 -22
181    1 -7.9 45 -46 23 -22
182    1 -7.9 46 -47 23 -22
183    1 -7.9 47 -48 23 -22
184    1 -7.9 48 -49 23 -22
185    1 -7.9 49 -50 23 -22
186    1 -7.9 50 -51 23 -22
187    1 -7.9 51 -52 23 -22
188    1 -7.9 52 -53 23 -22
189    1 -7.9 53 -54 23 -22
190    1 -7.9 54 -55 23 -22
191    1 -7.9 55 -56 23 -22
192    1 -7.9 56 -57 23 -22
193    1 -7.9 57 -58 23 -22
194    1 -7.9 58 -59 23 -22
195    1 -7.9 59 -60 23 -22
196    1 -7.9 60 -61 23 -22
197    1 -7.9 61 -62 23 -22
198    1 -7.9 62 -63 23 -22
199    1 -7.9 63 -64 23 -22
200    1 -7.9 64 -65 23 -22      $ MITL Cone
201    1 -7.9 65 -66 23 -22
202    1 -7.9 66 -67 23 -22
203    1 -7.9 67 -68 23 -22
204    1 -7.9 68 -69 23 -22
205    1 -7.9 69 -70 23 -22
206    1 -7.9 70 -71 23 -22
207    1 -7.9 71 -72 23 -22
208    1 -7.9 72 -73 23 -22
209    1 -7.9 73 -74 23 -22
210    1 -7.9 74 -75 23 -22
211    1 -7.9 75 -76 23 -22
212    1 -7.9 76 -77 23 -22
213    1 -7.9 77 -78 23 -22
214    1 -7.9 78 -79 23 -22
215    1 -7.9 79 -80 23 -22
216    1 -7.9 80 -81 23 -22
217    1 -7.9 81 -82 23 -22
218    1 -7.9 82 -83 23 -22
219    1 -7.9 83 -84 23 -22
220    1 -7.9 84 -85 23 -22
221    1 -7.9 85 -86 23 -22
222    1 -7.9 86 -87 23 -22
223    1 -7.9 87 -88 23 -22
224    1 -7.9 88 -89 23 -22
225    1 -7.9 89 -90 23 -22
226    1 -7.9 90 -91 23 -22
227    1 -7.9 91 -92 23 -22
228    1 -7.9 92 -93 23 -22
229    1 -7.9 93 -94 23 -22
230    1 -7.9 94 -95 23 -22
231    1 -7.9 95 -96 23 -22
232    1 -7.9 96 -97 23 -22
233    1 -7.9 97 -98 23 -22
234    1 -7.9 98 -99 23 -22
235    1 -7.9 99 -100 23 -22
236    1 -7.9 100 -101 23 -22
237    1 -7.9 101 -102 23 -22
238    1 -7.9 102 -103 23 -22
239    1 -7.9 103 -104 23 -22
240    1 -7.9 104 -105 23 -22
241    1 -7.9 105 -106 23 -22
242    1 -7.9 106 -107 23 -22
243    1 -7.9 107 -108 23 -22
244    1 -7.9 108 -109 23 -22
```

```
245   1 -7.9 109 -110 23 -22
246   1 -7.9 110 -111 23 -22
247   1 -7.9 111 -112 23 -22
248   1 -7.9 112 -113 23 -22
249   1 -7.9 113 -114 23 -22
250   1 -7.9 114 -115 23 -22
251   1 -7.9 115 -116 23 -22
252   1 -7.9 116 -117 23 -22
253   1 -7.9 117 -16 23 -22     $ *********************************
c
254   1 -7.9 16 -119 20 -21          $ *********************************
255   1 -7.9 119 -120 20 -21
256   1 -7.9 120 -121 20 -21
257   1 -7.9 121 -122 20 -21
258   1 -7.9 122 -123 20 -21
259   1 -7.9 123 -124 20 -21
260   1 -7.9 124 -125 20 -21
261   1 -7.9 125 -126 20 -21          $ Bottom Cylinder of MITLs
262   1 -7.9 126 -127 20 -21
263   1 -7.9 127 -128 20 -21
264   1 -7.9 128 -129 20 -21
265   1 -7.9 129 -130 20 -21
266   1 -7.9 130 -131 20 -21
267   1 -7.9 131 -132 20 -21
268   1 -7.9 132 -133 20 -21
269   1 -7.9 133 -134 20 -21
270   1 -7.9 134 -135 20 -21
271   1 -7.9 135 -17 20 -21           $ *********************************
c
c 272   0 9 -17 22 -21              $ Don't need -- see cell 481
c 273   0 106 -106 -25                $ Inside Collimator Cone (25)
274   0 106 -16 -23
275   0 16 -17 -20
c
276   6 -1.032 18 -460 -137        $ TOP nTOF Scintillator Cell
c                                     Either BC-418 or BC-422Q --
c                                     Same Density and Ratio
c
277   0 671 -672 137 -931            $ Pig Cell
c 278   0 66 -139 -25              $ Tally Cell at Collimator Exit
c 279   0 66 -139 25 -24
c 280   0 66 -139 24 -142
c
c 281   0 1 -3 144 -146              $ ************************
c 282   0 3 -5 144 -146              $ Void Cells around outside
c 283   0 5 -7 144 -146              $ of MITL Cone (22 & 23)
c 284   0 7 -9 144 -146              $ ************************
c
285   0 17 -149 -20
c
286   0 434 -430 680 -21 #2291
c
287   0 13 -32 141 -23
c 288   0 27 -28 141 -23
c 289   0 28 -29 141 -23
c 290   0 29 -30 141 -23
c 291   0 30 -31 141 -23
c 292   0 31 -32 141 -23
c
c 293   0 32 -33 141 -23
c 294   0 33 -34 141 -23
c 295   0 34 -35 141 -23
c 296   0 35 -36 141 -23
c 297   0 36 -37 141 -23
c 298   0 37 -38 141 -23
c 299   0 38 -39 141 -23
c 300   0 39 -40 141 -23
c 301   0 40 -41 141 -23
c 302   0 41 -42 141 -23
c 303   0 42 -43 141 -23
c 304   0 43 -44 141 -23
c 305   0 44 -45 141 -23
```

```
c 306   0 45 -46 141 -23
c
c 307   0 46 -47 141 -23
c 308   0 47 -48 141 -23
c 309   0 48 -49 141 -23
c 310   0 49 -50 141 -23
c 311   0 50 -51 141 -23
c 312   0 51 -52 141 -23
c 313   0 52 -53 141 -23
c 314   0 53 -54 141 -23
c
c 315   0 54 -55 24 -142    $ ****************************
c 316   0 55 -56 24 -142
c 317   0 56 -57 24 -142
c 318   0 57 -58 24 -142
c 319   0 58 -59 24 -142    $ More Tivar to "Shadow" the
c 320   0 59 -60 24 -142    $ pig to twice it's radius
c 321   0 60 -61 24 -142    $ (from 54.61 cm to 109.22 cm)
c 322   0 61 -62 24 -142
c 323   0 62 -63 24 -142
c 324   0 63 -64 24 -142
c 325   0 64 -65 24 -142
c 326   0 65 -66 24 -142    $ ****************************
c
c 327   0 66 -139 142 -23
c 328   0 139 -74 142 -23
c 329   0 67 -68 142 -23
c 330   0 68 -69 142 -23
c 331   0 69 -70 142 -23
c 332   0 70 -71 142 -23
c 333   0 71 -72 142 -23
c 334   0 72 -73 142 -23
c 335   0 73 -74 142 -23
c
336   0 74 -106 -23         $ *****************************
c 337   0 74 -75 25 -24
c 338   0 74 -75 24 -142
c 339   0 74 -75 142 -23
c 340   0 75 -76 -25
c 341   0 75 -76 25 -24
c 342   0 75 -76 24 -142
c 343   0 75 -76 142 -23
c 344   0 76 -77 -25
c 345   0 76 -77 25 -24
c 346   0 76 -77 24 -142
c 347   0 76 -77 142 -23
c 348   0 77 -78 -25
c 349   0 77 -78 25 -24
c 350   0 77 -78 24 -142
c 351   0 77 -78 142 -23
c 352   0 78 -79 -25
c 353   0 78 -79 25 -24
c 354   0 78 -79 24 -142
c 355   0 78 -79 142 -23
c 356   0 79 -80 -25
c 357   0 79 -80 25 -24
c 358   0 79 -80 24 -142
c 359   0 79 -80 142 -23
c 360   0 80 -81 -25
c 361   0 80 -81 25 -24
c 362   0 80 -81 24 -142
c 363   0 80 -81 142 -23
c 364   0 81 -82 -25
c 365   0 81 -82 25 -24
c 366   0 81 -82 24 -142
c 367   0 81 -82 142 -23
c 368   0 82 -83 -25
c 369   0 82 -83 25 -24
c 370   0 82 -83 24 -142
c 371   0 82 -83 142 -23
c 372   0 83 -84 -25
c 373   0 83 -84 25 -24
```

```
c 374    0 83 -84 24 -142
c 375    0 83 -84 142 -23
c 376    0 84 -85 -25
c 377    0 84 -85 25 -24          $ Cells where more TIVAR
c 378    0 84 -85 24 -142         $ Can be added to Collimator
c 379    0 84 -85 142 -23
c 380    0 85 -86 -25
c 381    0 85 -86 25 -24
c 382    0 85 -86 24 -142
c 383    0 85 -86 142 -23
c 384    0 86 -87 -25
c 385    0 86 -87 25 -24
c 386    0 86 -87 24 -142
c 387    0 86 -87 142 -23
c 388    0 87 -88 -25
c 389    0 87 -88 25 -24
c 390    0 87 -88 24 -142
c 391    0 87 -88 142 -23
c 392    0 88 -89 -25
c 393    0 88 -89 25 -24
c 394    0 88 -89 24 -142
c 395    0 88 -89 142 -23
c 396    0 89 -90 -25
c 397    0 89 -90 25 -24
c 398    0 89 -90 24 -142
c 399    0 89 -90 142 -23
c 400    0 90 -91 -25
c 401    0 90 -91 25 -24
c 402    0 90 -91 24 -142
c 403    0 90 -91 142 -23
c 404    0 91 -92 -25
c 405    0 91 -92 25 -24
c 406    0 91 -92 24 -142
c 407    0 91 -92 142 -23
c 408    0 92 -93 -25
c 409    0 92 -93 25 -24
c 410    0 92 -93 24 -142
c 411    0 92 -93 142 -23
c 412    0 93 -94 -25
c 413    0 93 -94 25 -24
c 414    0 93 -94 24 -142
c 415    0 93 -94 142 -23
c 416    0 94 -95 -25
c 417    0 94 -95 25 -24
c 418    0 94 -95 24 -142
c 419    0 94 -95 142 -23
c 420    0 95 -96 -25
c 421    0 95 -96 25 -24
c 422    0 95 -96 24 -142
c 423    0 95 -96 142 -23
c 424    0 96 -97 -25
c 425    0 96 -97 25 -24
c 426    0 96 -97 24 -142
c 427    0 96 -97 142 -23
c 428    0 97 -98 -25
c 429    0 97 -98 25 -24
c 430    0 97 -98 24 -142
c 431    0 97 -98 142 -23
c 432    0 98 -99 -25
c 433    0 98 -99 25 -24
c 434    0 98 -99 24 -142
c 435    0 98 -99 142 -23
c 436    0 99 -100 -25
c 437    0 99 -100 25 -24
c 438    0 99 -100 24 -142
c 439    0 99 -100 142 -23
c 440    0 100 -101 -25
c 441    0 100 -101 25 -24
c 442    0 100 -101 24 -142
c 443    0 100 -101 142 -23
c 444    0 101 -102 -25
c 445    0 101 -102 25 -24
```

```
c 446   0 101 -102 24 -142
c 447   0 101 -102 142 -23
c 448   0 102 -103 -25
c 449   0 102 -103 25 -24
c 450   0 102 -103 24 -142
c 451   0 102 -103 142 -23
c 452   0 103 -104 -25
c 453   0 103 -104 25 -24
c 454   0 103 -104 24 -142
c 455   0 103 -104 142 -23
c 456   0 104 -105 -25
c 457   0 104 -105 25 -24
c 458   0 104 -105 24 -142
c 459   0 104 -105 142 -23
c 460   0 105 -106 -25
c 461   0 105 -106 25 -24
c 462   0 105 -106 24 -142
c 463   0 105 -106 142 -23         $ ******************************
c
c 464   0 671 -672 669 -25          $ Ring around Scintillator the size
                                      of collimator hole
465   1 -7.9 1 -2 23 -22         $ *****************************
466   1 -7.9 2 -3 23 -22
467   1 -7.9 3 -4 23 -22
468   1 -7.9 4 -5 23 -22
469   1 -7.9 5 -6 23 -22
470   1 -7.9 6 -7 23 -22
471   1 -7.9 7 -8 23 -22
472   1 -7.9 8 -9 23 -22         $ *****************************
c
473   0 1 -8 12 -23
c
c 474   0 3 -4 12 -23              $ Void Cells on inside top
c 475   0 5 -6 12 -23              $ of MITL Cone (22 & 23)
c 476   0 7 -8 12 -23
c
c 477   0 2 -3 22 -143
c 478   0 4 -5 22 -143             $ Void Cells on outside top
c 479   0 6 -7 22 -143             $ of MITL Cone (22 & 23)
c 480   0 8 -9 22 -143
c
481   0 909 -145 144 -146          $ Void b/w 2nd MITL Cone and Stack
482   0 908 -16 22 -143            $ Void b/w 1st & 2nd MITL Cone
483   0 16 -145 21 -143
484   0 145 -149 21 -146         $ Void b/w MITL Cyl #1 and Stack
485   0 149 -675 -146          $ Void b/w MITL #1 & Bottom of Stack
c
486   0 663 -734 -147            $ Void b/w Stack and Detector
c
487   1 -7.9 1 -2 143 -144       $ *******************************
488   1 -7.9 2 -3 143 -144
489   1 -7.9 3 -4 143 -144
490   1 -7.9 4 -5 143 -144
491   1 -7.9 5 -6 143 -144
492   1 -7.9 6 -7 143 -144
493   1 -7.9 7 -8 143 -144
494   1 -7.9 8 -9 143 -144
495   1 -7.9 9 -10 143 -144
496   1 -7.9 10 -13 143 -144
497   1 -7.9 13 -27 143 -144
498   1 -7.9 27 -28 143 -144
499   1 -7.9 28 -29 143 -144
500   1 -7.9 29 -30 143 -144
501   1 -7.9 30 -31 143 -144
502   1 -7.9 31 -32 143 -144
503   1 -7.9 32 -33 143 -144
504   1 -7.9 33 -34 143 -144
505   1 -7.9 34 -35 143 -144
506   1 -7.9 35 -36 143 -144
507   1 -7.9 36 -37 143 -144
508   1 -7.9 37 -38 143 -144
509   1 -7.9 38 -39 143 -144
```

```
510    1 -7.9 39 -40 143 -144
511    1 -7.9 40 -41 143 -144
512    1 -7.9 41 -42 143 -144
513    1 -7.9 42 -43 143 -144
514    1 -7.9 43 -44 143 -144
515    1 -7.9 44 -45 143 -144
516    1 -7.9 45 -46 143 -144
517    1 -7.9 46 -47 143 -144
518    1 -7.9 47 -48 143 -144
519    1 -7.9 48 -49 143 -144
520    1 -7.9 49 -50 143 -144
521    1 -7.9 50 -51 143 -144
522    1 -7.9 51 -52 143 -144
523    1 -7.9 52 -53 143 -144
524    1 -7.9 53 -54 143 -144
525    1 -7.9 54 -55 143 -144
526    1 -7.9 55 -56 143 -144
527    1 -7.9 56 -57 143 -144
528    1 -7.9 57 -58 143 -144
529    1 -7.9 58 -59 143 -144
530    1 -7.9 59 -60 143 -144      $ 2nd MITL CONE
531    1 -7.9 60 -61 143 -144
532    1 -7.9 61 -62 143 -144
533    1 -7.9 62 -63 143 -144
534    1 -7.9 63 -64 143 -144
535    1 -7.9 64 -65 143 -144
536    1 -7.9 65 -66 143 -144
537    1 -7.9 66 -67 143 -144
538    1 -7.9 67 -68 143 -144
539    1 -7.9 68 -69 143 -144
540    1 -7.9 69 -70 143 -144
541    1 -7.9 70 -71 143 -144
542    1 -7.9 71 -72 143 -144
543    1 -7.9 72 -73 143 -144
544    1 -7.9 73 -74 143 -144
545    1 -7.9 74 -75 143 -144
546    1 -7.9 75 -76 143 -144
547    1 -7.9 76 -77 143 -144
548    1 -7.9 77 -78 143 -144
549    1 -7.9 78 -79 143 -144
550    1 -7.9 79 -80 143 -144
551    1 -7.9 80 -81 143 -144
552    1 -7.9 81 -82 143 -144
553    1 -7.9 82 -83 143 -144
554    1 -7.9 83 -84 143 -144
555    1 -7.9 84 -85 143 -144
556    1 -7.9 85 -86 143 -144
557    1 -7.9 86 -87 143 -144
558    1 -7.9 87 -88 143 -144
559    1 -7.9 88 -89 143 -144
560    1 -7.9 89 -90 143 -144
561    1 -7.9 90 -91 143 -144
562    1 -7.9 91 -92 143 -144
563    1 -7.9 92 -93 143 -144
564    1 -7.9 93 -94 143 -144
565    1 -7.9 94 -95 143 -144
566    1 -7.9 95 -96 143 -144
567    1 -7.9 96 -97 143 -144
568    1 -7.9 97 -98 143 -144
569    1 -7.9 98 -99 143 -144
570    1 -7.9 99 -100 143 -144
571    1 -7.9 100 -101 143 -144
572    1 -7.9 101 -102 143 -144
573    1 -7.9 102 -103 143 -144
574    1 -7.9 103 -104 143 -144
575    1 -7.9 104 -105 143 -144
576    1 -7.9 105 -106 143 -144
577    1 -7.9 106 -107 143 -144
578    1 -7.9 107 -108 143 -144
579    1 -7.9 108 -109 143 -144
580    1 -7.9 109 -110 143 -144
581    1 -7.9 110 -111 143 -144
```

```
582    1 -7.9 111 -112 143 -144
583    1 -7.9 112 -113 143 -144
584    1 -7.9 113 -114 143 -144
585    1 -7.9 114 -115 143 -144
586    1 -7.9 115 -116 143 -144
587    1 -7.9 116 -117 143 -144
588    1 -7.9 117 -16 143 -144
589    1 -7.9 16 -119 143 -144
590    1 -7.9 119 -120 143 -144
591    1 -7.9 120 -121 143 -144
592    1 -7.9 121 -122 143 -144
593    1 -7.9 122 -123 143 -144
594    1 -7.9 123 -124 143 -144
595    1 -7.9 124 -125 143 -144
596    1 -7.9 125 -126 143 -144
597    1 -7.9 126 -127 143 -144
598    1 -7.9 127 -145 143 -144      $ *************************
c
599    1 -7.9 17 -150 20 -21         $ *************************
600    1 -7.9 150 -151 20 -21
601    1 -7.9 151 -152 20 -21
602    1 -7.9 152 -153 20 -21
603    1 -7.9 153 -154 20 -21
604    1 -7.9 154 -155 20 -21
605    1 -7.9 155 -156 20 -21
606    1 -7.9 156 -157 20 -21
607    1 -7.9 157 -158 20 -21
608    1 -7.9 158 -159 20 -21
609    1 -7.9 159 -160 20 -21
610    1 -7.9 160 -161 20 -21
611    1 -7.9 161 -162 20 -21
612    1 -7.9 162 -163 20 -21        $ Cylinder Extention on MITL #1
613    1 -7.9 163 -164 20 -21
614    1 -7.9 164 -165 20 -21
615    1 -7.9 165 -166 20 -21
616    1 -7.9 166 -167 20 -21
617    1 -7.9 167 -168 20 -21
618    1 -7.9 168 -169 20 -21
619    1 -7.9 169 -170 20 -21
620    1 -7.9 170 -171 20 -21
621    1 -7.9 171 -172 20 -21
622    1 -7.9 172 -173 20 -21
623    1 -7.9 173 -174 20 -21
624    1 -7.9 174 -175 20 -21
625    1 -7.9 175 -176 20 -21
626    1 -7.9 176 -177 20 -21
627    1 -7.9 177 -178 20 -21
628    1 -7.9 178 -179 20 -21
629    1 -7.9 179 -149 20 -21        $ *************************
c
c 630   0 149 -148 146 -147        $ Stack
c
631    0 434 -430 21 -147 680 -684           $ Void at end to cover expansion
c                                     of Stack
c
632    1 -7.9 1 -2 146 -147     $ **************************
633    1 -7.9 2 -3 146 -147
634    1 -7.9 3 -4 146 -147
635    1 -7.9 4 -5 146 -147
636    1 -7.9 5 -6 146 -147
637    1 -7.9 6 -7 146 -147
638    1 -7.9 7 -8 146 -147
639    1 -7.9 8 -9 146 -147
640    1 -7.9 9 -10 146 -147
641    1 -7.9 10 -13 146 -147
642    1 -7.9 13 -27 146 -147
643    1 -7.9 27 -28 146 -147
644    1 -7.9 28 -29 146 -147
645    1 -7.9 29 -30 146 -147
646    1 -7.9 30 -31 146 -147
647    1 -7.9 31 -32 146 -147
648    1 -7.9 32 -33 146 -147
```

649	1	-7.9	33	-34	146	-147
650	1	-7.9	34	-35	146	-147
651	1	-7.9	35	-36	146	-147
652	1	-7.9	36	-37	146	-147
653	1	-7.9	37	-38	146	-147
654	1	-7.9	38	-39	146	-147
655	1	-7.9	39	-40	146	-147
656	1	-7.9	40	-41	146	-147
657	1	-7.9	41	-42	146	-147
658	1	-7.9	42	-43	146	-147
659	1	-7.9	43	-44	146	-147
660	1	-7.9	44	-45	146	-147
661	1	-7.9	45	-46	146	-147
662	1	-7.9	46	-47	146	-147
663	1	-7.9	47	-48	146	-147
664	1	-7.9	48	-49	146	-147
665	1	-7.9	49	-50	146	-147
666	1	-7.9	50	-51	146	-147
667	1	-7.9	51	-52	146	-147
668	1	-7.9	52	-53	146	-147
669	1	-7.9	53	-54	146	-147
670	1	-7.9	54	-55	146	-147
671	1	-7.9	55	-56	146	-147
672	1	-7.9	56	-57	146	-147
673	1	-7.9	57	-58	146	-147
674	1	-7.9	58	-59	146	-147
675	1	-7.9	59	-60	146	-147
676	1	-7.9	60	-61	146	-147
677	1	-7.9	61	-62	146	-147
678	1	-7.9	62	-63	146	-147
679	1	-7.9	63	-64	146	-147
680	1	-7.9	64	-65	146	-147
681	1	-7.9	65	-66	146	-147
682	1	-7.9	66	-67	146	-147
683	1	-7.9	67	-68	146	-147
684	1	-7.9	68	-69	146	-147
685	1	-7.9	69	-70	146	-147
686	1	-7.9	70	-71	146	-147
687	1	-7.9	71	-72	146	-147
688	1	-7.9	72	-73	146	-147
689	1	-7.9	73	-74	146	-147
690	1	-7.9	74	-75	146	-147
691	1	-7.9	75	-76	146	-147
692	1	-7.9	76	-77	146	-147
693	1	-7.9	77	-78	146	-147
694	1	-7.9	78	-79	146	-147
695	1	-7.9	79	-80	146	-147
696	1	-7.9	80	-81	146	-147
697	1	-7.9	81	-82	146	-147
698	1	-7.9	82	-83	146	-147
699	1	-7.9	83	-84	146	-147
700	1	-7.9	84	-85	146	-147
701	1	-7.9	85	-86	146	-147
702	1	-7.9	86	-87	146	-147
703	1	-7.9	87	-88	146	-147
704	1	-7.9	88	-89	146	-147
705	1	-7.9	89	-90	146	-147
706	1	-7.9	90	-91	146	-147
707	1	-7.9	91	-92	146	-147
708	1	-7.9	92	-93	146	-147
709	1	-7.9	93	-94	146	-147
710	1	-7.9	94	-95	146	-147
711	1	-7.9	95	-96	146	-147
712	1	-7.9	96	-97	146	-147
713	1	-7.9	97	-98	146	-147
714	1	-7.9	98	-99	146	-147
715	1	-7.9	99	-100	146	-147
716	1	-7.9	100	-101	146	-147
717	1	-7.9	101	-102	146	-147
718	1	-7.9	102	-103	146	-147
719	1	-7.9	103	-104	146	-147
720	1	-7.9	104	-105	146	-147

721	1	-7.9	105	-106	146	-147
722	1	-7.9	106	-107	146	-147
723	1	-7.9	107	-108	146	-147
724	1	-7.9	108	-109	146	-147
725	1	-7.9	109	-110	146	-147
726	1	-7.9	110	-111	146	-147
727	1	-7.9	111	-112	146	-147
728	1	-7.9	112	-113	146	-147
729	1	-7.9	113	-114	146	-147
730	1	-7.9	114	-115	146	-147
731	1	-7.9	115	-116	146	-147
732	1	-7.9	116	-117	146	-147
733	1	-7.9	117	-16	146	-147
734	1	-7.9	16	-119	146	-147
735	1	-7.9	119	-120	146	-147
736	1	-7.9	120	-121	146	-147
737	1	-7.9	121	-122	146	-147
738	1	-7.9	122	-123	146	-147
739	1	-7.9	123	-124	146	-147
740	1	-7.9	124	-125	146	-147
741	1	-7.9	125	-126	146	-147
742	1	-7.9	126	-127	146	-147
743	1	-7.9	127	-128	146	-147
744	1	-7.9	128	-129	146	-147
745	1	-7.9	129	-130	146	-147
746	1	-7.9	130	-131	146	-147
747	1	-7.9	131	-132	146	-147
748	1	-7.9	132	-133	146	-147
749	1	-7.9	133	-134	146	-147
750	1	-7.9	134	-135	146	-147
751	1	-7.9	135	-17	146	-147
752	1	-7.9	17	-150	146	-147
753	1	-7.9	150	-151	146	-147
754	1	-7.9	151	-152	146	-147
755	1	-7.9	152	-153	146	-147
756	1	-7.9	153	-154	146	-147
757	1	-7.9	154	-155	146	-147
758	1	-7.9	155	-156	146	-147
759	1	-7.9	156	-157	146	-147
760	1	-7.9	157	-158	146	-147
761	1	-7.9	158	-159	146	-147
762	1	-7.9	159	-160	146	-147
763	1	-7.9	160	-161	146	-147
764	1	-7.9	161	-162	146	-147
765	1	-7.9	162	-163	146	-147
766	1	-7.9	163	-164	146	-147
767	1	-7.9	164	-165	146	-147
768	1	-7.9	165	-166	146	-147
769	1	-7.9	166	-167	146	-147
770	1	-7.9	167	-168	146	-147
771	1	-7.9	168	-169	146	-147
772	1	-7.9	169	-170	146	-147
773	1	-7.9	170	-171	146	-147
774	1	-7.9	171	-172	146	-147
775	1	-7.9	172	-173	146	-147
776	1	-7.9	173	-174	146	-147
777	1	-7.9	174	-175	146	-147
778	1	-7.9	175	-176	146	-147
779	1	-7.9	176	-177	146	-147
780	1	-7.9	177	-178	146	-147
781	1	-7.9	178	-179	146	-147
782	1	-7.9	179	-149	146	-147
783	1	-7.9	149	-180	146	-147
784	1	-7.9	180	-181	146	-147
785	1	-7.9	181	-182	146	-147
786	1	-7.9	182	-183	146	-147
787	1	-7.9	183	-184	146	-147
788	1	-7.9	184	-185	146	-147
789	1	-7.9	185	-186	146	-147
790	1	-7.9	186	-187	146	-147
791	1	-7.9	187	-188	146	-147
792	1	-7.9	188	-189	146	-147

```
793     1 -7.9 189 -190 146 -147
794     1 -7.9 190 -191 146 -147
795     1 -7.9 191 -192 146 -147
796     1 -7.9 192 -193 146 -147
797     1 -7.9 193 -194 146 -147
798     1 -7.9 194 -195 146 -147
799     1 -7.9 195 -196 146 -147
800     1 -7.9 196 -197 146 -147
801     1 -7.9 197 -198 146 -147
802     1 -7.9 198 -199 146 -147
803     1 -7.9 199 -200 146 -147
804     1 -7.9 200 -201 146 -147
805     1 -7.9 201 -202 146 -147
806     1 -7.9 202 -203 146 -147
807     1 -7.9 203 -204 146 -147
808     1 -7.9 204 -205 146 -147
809     1 -7.9 205 -206 146 -147
810     1 -7.9 206 -207 146 -147
811     1 -7.9 207 -208 146 -147
812     1 -7.9 208 -209 146 -147
813     1 -7.9 209 -210 146 -147
814     1 -7.9 210 -211 146 -147
815     1 -7.9 211 -212 146 -147
816     1 -7.9 212 -213 146 -147
817     1 -7.9 213 -214 146 -147
818     1 -7.9 214 -215 146 -147
819     1 -7.9 215 -216 146 -147
c
820     1 -7.9 216 -217 146 -147
821     1 -7.9 217 -218 146 -147
822     1 -7.9 218 -219 146 -147
823     1 -7.9 219 -220 146 -147
824     1 -7.9 220 -221 146 -147
825     1 -7.9 221 -222 146 -147
826     1 -7.9 222 -223 146 -147
827     1 -7.9 223 -224 146 -147
828     1 -7.9 224 -225 146 -147
829     1 -7.9 225 -226 146 -147
830     1 -7.9 226 -227 146 -147
831     1 -7.9 227 -228 146 -147
832     1 -7.9 228 -229 146 -147
833     1 -7.9 229 -230 146 -147
834     1 -7.9 230 -231 146 -147
835     1 -7.9 231 -232 146 -147
836     1 -7.9 232 -233 146 -147
837     1 -7.9 233 -234 146 -147
838     1 -7.9 234 -235 146 -147
839     1 -7.9 235 -236 146 -147
840     1 -7.9 236 -237 146 -147
841     1 -7.9 237 -238 146 -147
842     1 -7.9 238 -239 146 -147
843     1 -7.9 239 -240 146 -147
844     1 -7.9 240 -241 146 -147
845     1 -7.9 241 -242 146 -147
846     1 -7.9 242 -243 146 -147
847     1 -7.9 243 -244 146 -147
848     1 -7.9 244 -245 146 -147
849     1 -7.9 245 -246 146 -147
850     1 -7.9 246 -247 146 -147
851     1 -7.9 247 -248 146 -147          $ THE STACK
852     1 -7.9 248 -249 146 -147
853     1 -7.9 249 -250 146 -147
854     1 -7.9 250 -251 146 -147
855     1 -7.9 251 -252 146 -147
856     1 -7.9 252 -253 146 -147
857     1 -7.9 253 -254 146 -147
858     1 -7.9 254 -255 146 -147
859     1 -7.9 255 -256 146 -147
860     1 -7.9 256 -257 146 -147
861     1 -7.9 257 -258 146 -147
862     1 -7.9 258 -259 146 -147
863     1 -7.9 259 -260 146 -147
```

864	1	-7.9	260	-261	146	-147
865	1	-7.9	261	-262	146	-147
866	1	-7.9	262	-263	146	-147
867	1	-7.9	263	-264	146	-147
868	1	-7.9	264	-265	146	-147
869	1	-7.9	265	-266	146	-147
870	1	-7.9	266	-267	146	-147
871	1	-7.9	267	-268	146	-147
872	1	-7.9	268	-269	146	-147
873	1	-7.9	269	-270	146	-147
874	1	-7.9	270	-271	146	-147
875	1	-7.9	271	-272	146	-147
876	1	-7.9	272	-273	146	-147
877	1	-7.9	273	-274	146	-147
878	1	-7.9	274	-275	146	-147
879	1	-7.9	275	-276	146	-147
880	1	-7.9	276	-277	146	-147
881	1	-7.9	277	-278	146	-147
882	1	-7.9	278	-279	146	-147
883	1	-7.9	279	-280	146	-147
884	1	-7.9	280	-281	146	-147
885	1	-7.9	281	-282	146	-147
886	1	-7.9	282	-283	146	-147
887	1	-7.9	283	-284	146	-147
888	1	-7.9	284	-285	146	-147
889	1	-7.9	285	-286	146	-147
890	1	-7.9	286	-287	146	-147
891	1	-7.9	287	-288	146	-147
892	1	-7.9	288	-289	146	-147
893	1	-7.9	289	-290	146	-147
894	1	-7.9	290	-291	146	-147
895	1	-7.9	291	-292	146	-147
896	1	-7.9	292	-293	146	-147
897	1	-7.9	293	-294	146	-147
898	1	-7.9	294	-295	146	-147
899	1	-7.9	295	-296	146	-147
900	1	-7.9	296	-297	146	-147
901	1	-7.9	297	-298	146	-147
902	1	-7.9	298	-299	146	-147
903	1	-7.9	299	-300	146	-147
904	1	-7.9	300	-301	146	-147
905	1	-7.9	301	-302	146	-147
906	1	-7.9	302	-303	146	-147
907	1	-7.9	303	-304	146	-147
908	1	-7.9	304	-305	146	-147
909	1	-7.9	305	-306	146	-147
910	1	-7.9	306	-307	146	-147
911	1	-7.9	307	-308	146	-147
912	1	-7.9	308	-309	146	-147
913	1	-7.9	309	-310	146	-147
914	1	-7.9	310	-311	146	-147
915	1	-7.9	311	-312	146	-147
916	1	-7.9	312	-313	146	-147
917	1	-7.9	313	-314	146	-147
918	1	-7.9	314	-315	146	-147
919	1	-7.9	315	-316	146	-147
920	1	-7.9	316	-317	146	-147
921	1	-7.9	317	-318	146	-147
922	1	-7.9	318	-319	146	-147
923	1	-7.9	319	-320	146	-147
924	1	-7.9	320	-321	146	-147
925	1	-7.9	321	-322	146	-147
926	1	-7.9	322	-323	146	-147
927	1	-7.9	323	-324	146	-147
928	1	-7.9	324	-325	146	-147
929	1	-7.9	325	-326	146	-147
930	1	-7.9	326	-327	146	-147
931	1	-7.9	327	-328	146	-147
932	1	-7.9	328	-329	146	-147
933	1	-7.9	329	-330	146	-147
934	1	-7.9	330	-331	146	-147
935	1	-7.9	331	-332	146	-147

936	1	-7.9	332	-333	146	-147
937	1	-7.9	333	-334	146	-147
938	1	-7.9	334	-335	146	-147
939	1	-7.9	335	-336	146	-147
940	1	-7.9	336	-337	146	-147
941	1	-7.9	337	-338	146	-147
942	1	-7.9	338	-339	146	-147
943	1	-7.9	339	-340	146	-147
944	1	-7.9	340	-341	146	-147
945	1	-7.9	341	-342	146	-147
946	1	-7.9	342	-343	146	-147
947	1	-7.9	343	-344	146	-147
948	1	-7.9	344	-345	146	-147
949	1	-7.9	345	-346	146	-147
950	1	-7.9	346	-347	146	-147
951	1	-7.9	347	-348	146	-147
952	1	-7.9	348	-349	146	-147
953	1	-7.9	349	-350	146	-147
954	1	-7.9	350	-351	146	-147
955	1	-7.9	351	-352	146	-147
956	1	-7.9	352	-353	146	-147
957	1	-7.9	353	-354	146	-147
958	1	-7.9	354	-355	146	-147
959	1	-7.9	355	-356	146	-147
960	1	-7.9	356	-357	146	-147
961	1	-7.9	357	-358	146	-147
962	1	-7.9	358	-359	146	-147
963	1	-7.9	359	-360	146	-147
964	1	-7.9	360	-361	146	-147
965	1	-7.9	361	-362	146	-147
966	1	-7.9	362	-363	146	-147
967	1	-7.9	363	-364	146	-147
968	1	-7.9	364	-365	146	-147
969	1	-7.9	365	-366	146	-147
970	1	-7.9	366	-367	146	-147
971	1	-7.9	367	-368	146	-147
972	1	-7.9	368	-369	146	-147
973	1	-7.9	369	-370	146	-147
974	1	-7.9	370	-371	146	-147
975	1	-7.9	371	-372	146	-147
976	1	-7.9	372	-373	146	-147
977	1	-7.9	373	-374	146	-147
978	1	-7.9	374	-375	146	-147
979	1	-7.9	375	-376	146	-147
980	1	-7.9	376	-377	146	-147
981	1	-7.9	377	-378	146	-147
982	1	-7.9	378	-379	146	-147
983	1	-7.9	379	-380	146	-147
984	1	-7.9	380	-381	146	-147
985	1	-7.9	381	-382	146	-147
986	1	-7.9	382	-383	146	-147
987	1	-7.9	383	-384	146	-147
988	1	-7.9	384	-385	146	-147
989	1	-7.9	385	-386	146	-147
990	1	-7.9	386	-387	146	-147
991	1	-7.9	387	-388	146	-147
992	1	-7.9	388	-389	146	-147
993	1	-7.9	389	-390	146	-147
994	1	-7.9	390	-391	146	-147
995	1	-7.9	391	-392	146	-147
996	1	-7.9	392	-393	146	-147
997	1	-7.9	393	-394	146	-147
998	1	-7.9	394	-395	146	-147
999	1	-7.9	395	-396	146	-147
1000	1	-7.9	396	-397	146	-147
1001	1	-7.9	397	-398	146	-147
1002	1	-7.9	398	-399	146	-147
1003	1	-7.9	399	-400	146	-147
1004	1	-7.9	400	-401	146	-147
1005	1	-7.9	401	-402	146	-147
1006	1	-7.9	402	-403	146	-147
1007	1	-7.9	403	-404	146	-147

```
1008  1 -7.9 404 -405 146 -147
1009  1 -7.9 405 -406 146 -147
1010  1 -7.9 406 -407 146 -147
1011  1 -7.9 407 -408 146 -147
1012  1 -7.9 408 -409 146 -147
1013  1 -7.9 409 -410 146 -147
1014  1 -7.9 410 -411 146 -147
1015  1 -7.9 411 -412 146 -147
1016  1 -7.9 412 -413 146 -147
1017  1 -7.9 413 -414 146 -147
1018  1 -7.9 414 -415 146 -147
1019  1 -7.9 415 -416 146 -147
1020  1 -7.9 416 -417 146 -147
1021  1 -7.9 417 -418 146 -147
1022  1 -7.9 418 -419 146 -147
1023  1 -7.9 419 -420 146 -147
1024  1 -7.9 420 -421 146 -147
1025  1 -7.9 421 -422 146 -147
1026  1 -7.9 422 -423 146 -147
1027  1 -7.9 423 -424 146 -147
1028  1 -7.9 424 -425 146 -147
1029  1 -7.9 425 -426 146 -147
1030  1 -7.9 426 -427 146 -147
1031  1 -7.9 427 -148 146 -147    $ *****************************
c
1032  2 -19.2 434 -435 431 -432
1033  2 -19.2 435 -436 431 -432
1034  2 -19.2 436 -437 431 -432
1035  2 -19.2 437 -438 431 -432
1036  2 -19.2 438 -439 431 -432
1037  2 -19.2 439 -440 431 -432
1038  2 -19.2 440 -441 431 -432
1039  2 -19.2 441 -442 431 -432
1040  2 -19.2 442 -443 431 -432
1041  2 -19.2 443 -444 431 -432
1042  2 -19.2 444 -445 431 -432
1043  2 -19.2 445 -18 431 -432
1044  2 -19.2 18 -460 431 -432
1045  2 -19.2 460 -446 431 -432
1046  2 -19.2 446 -447 431 -432
1047  2 -19.2 447 -448 431 -432
1048  2 -19.2 448 -449 431 -432
1049  2 -19.2 449 -428 431 -432
1050  2 -19.2 428 -429 431 -432
c 1051  5 -11.34 428 -429 459 -431
1052  5 -11.34 428 -429 458 -431
1053  5 -11.34 428 -429 457 -458
1054  5 -11.34 428 -429 456 -457
1055  5 -11.34 428 -429 455 -456
1056  5 -11.34 428 -429 454 -455
1057  5 -11.34 428 -429 453 -454
1058  5 -11.34 428 -429 452 -453
1059  5 -11.34 428 -429 451 -452
1060  5 -11.34 428 -429 450 -451
1061  5 -11.34 428 -429 137 -450
1062  5 -11.34 428 -429 461 -137
c
1063  5 -11.34 434 -435 432 -433
1064  5 -11.34 435 -436 432 -433
1065  5 -11.34 436 -437 432 -433
1066  5 -11.34 437 -438 432 -433
1067  5 -11.34 438 -439 432 -433
1068  5 -11.34 439 -440 432 -433
1069  5 -11.34 440 -441 432 -433
1070  5 -11.34 441 -442 432 -433
1071  5 -11.34 442 -443 432 -433
1072  5 -11.34 443 -444 432 -433
1073  5 -11.34 444 -445 432 -433
1074  5 -11.34 445 -18 432 -433
1075  5 -11.34 18 -460 432 -433
1076  5 -11.34 460 -446 432 -433
1077  5 -11.34 446 -447 432 -433
```

```
1078  5 -11.34 447 -448 432 -433
1079  5 -11.34 448 -449 432 -433
1080  5 -11.34 449 -428 432 -433
1081  5 -11.34 428 -429 432 -433
1082  5 -11.34 429 -430 432 -433
1083  2 -19.2 429 -430 431 -432
c 1084  2 -19.2 429 -430 459 -431
1085  2 -19.2 429 -430 458 -431
1086  2 -19.2 429 -430 457 -458
1087  2 -19.2 429 -430 456 -457
1088  2 -19.2 429 -430 455 -456
1089  2 -19.2 429 -430 454 -455
1090  2 -19.2 429 -430 453 -454
1091  2 -19.2 429 -430 452 -453
1092  2 -19.2 429 -430 451 -452
1093  2 -19.2 429 -430 450 -451
1094  2 -19.2 429 -430 137 -450
1095  2 -19.2 429 -430 461 -137
c
1096  0 471 -671 -431
1097  0 672 -428 -431
c
1098  5 -11.34 428 -429 -461
1099  2 -19.2 429 -430 -461
c
c 1100  2 -19.2 462 -463 431 -432
c 1101  2 -19.2 463 -464 431 -432
c 1102  2 -19.2 464 -465 431 -432
c 1103  2 -19.2 465 -466 431 -432
c 1104  2 -19.2 466 -467 431 -432
c 1105  2 -19.2 467 -468 431 -432
c 1106  2 -19.2 468 -469 431 -432
c 1107  2 -19.2 469 -470 431 -432
c 1108  2 -19.2 470 -471 431 -432
c
1109  2 -19.2 471 -472 431 -432
1110  2 -19.2 472 -473 431 -432
1111  2 -19.2 473 -474 431 -432
1112  2 -19.2 474 -475 431 -432
1113  2 -19.2 475 -476 431 -432
1114  2 -19.2 476 -477 431 -432
1115  2 -19.2 477 -478 431 -432
1116  2 -19.2 478 -479 431 -432
1117  2 -19.2 479 -480 431 -432
1118  2 -19.2 480 -481 431 -432
1119  2 -19.2 481 -434 431 -432
c
c 1120  5 -11.34 462 -463 432 -433
c 1121  5 -11.34 463 -464 432 -433
c 1122  5 -11.34 464 -465 432 -433
c 1123  5 -11.34 465 -466 432 -433
c 1124  5 -11.34 466 -467 432 -433
c 1125  5 -11.34 467 -468 432 -433
c 1126  5 -11.34 468 -469 432 -433
c 1127  5 -11.34 469 -470 432 -433
c 1128  5 -11.34 470 -471 432 -433
c
1129  5 -11.34 471 -472 432 -433
1130  5 -11.34 472 -473 432 -433
1131  5 -11.34 473 -474 432 -433
1132  5 -11.34 474 -475 432 -433
1133  5 -11.34 475 -476 432 -433
1134  5 -11.34 476 -477 432 -433
1135  5 -11.34 477 -478 432 -433
1136  5 -11.34 478 -479 432 -433
1137  5 -11.34 479 -480 432 -433
1138  5 -11.34 480 -481 432 -433
1139  5 -11.34 481 -434 432 -433
c
1140  0 471 -434 680 -147
c
1141  2 -19.2 489 -488 431 -432     $ ********************************
```

```
1142  2 -19.2 488 -487 431 -432
1143  2 -19.2 487 -486 431 -432
1144  2 -19.2 486 -485 431 -432
1145  2 -19.2 485 -484 431 -432
1146  2 -19.2 484 -483 431 -432
1147  2 -19.2 483 -482 431 -432    $ Pig made 8" longer for a total
1148  2 -19.2 482 -471 431 -432    $ length of 48"
1149  5 -11.34 489 -488 432 -433
1150  5 -11.34 488 -487 432 -433
1151  5 -11.34 487 -486 432 -433
1152  5 -11.34 486 -485 432 -433
1153  5 -11.34 485 -484 432 -433
1154  5 -11.34 484 -483 432 -433
1155  5 -11.34 483 -482 432 -433
1156  5 -11.34 482 -471 432 -433     $ ********************************
c
1157  5 -11.34 499 -498 137 -450     $ ********************************
1158  5 -11.34 499 -498 450 -451
c
1159  1 -7.9 499 -498 451 -452
1160  1 -7.9 499 -498 452 -453
1161  1 -7.9 499 -498 453 -454
1162  1 -7.9 499 -498 454 -455
1163  1 -7.9 499 -498 455 -456
1164  1 -7.9 499 -498 456 -457
1165  1 -7.9 499 -498 457 -458
1166  1 -7.9 499 -498 458 -431
1167  1 -7.9 499 -498 431 -432
1168  1 -7.9 499 -498 432 -433
c
1169  2 -19.2 498 -497 137 -450
1170  2 -19.2 498 -497 450 -451
1171  2 -19.2 498 -497 451 -452
1172  2 -19.2 498 -497 452 -453
1173  2 -19.2 498 -497 453 -454
1174  2 -19.2 498 -497 454 -455
1175  2 -19.2 498 -497 455 -456
1176  2 -19.2 498 -497 456 -457
1177  2 -19.2 498 -497 457 -458
1178  2 -19.2 498 -497 458 -431
1179  2 -19.2 498 -497 431 -432
1180  2 -19.2 498 -497 432 -433
1181  2 -19.2 497 -496 137 -450
1182  2 -19.2 497 -496 450 -451
1183  2 -19.2 497 -496 451 -452
1184  2 -19.2 497 -496 452 -453
1185  2 -19.2 497 -496 453 -454
1186  2 -19.2 497 -496 454 -455
1187  2 -19.2 497 -496 455 -456
1188  2 -19.2 497 -496 456 -457
1189  2 -19.2 497 -496 457 -458
1190  2 -19.2 497 -496 458 -431
1191  2 -19.2 497 -496 431 -432
1192  2 -19.2 497 -496 432 -433
1193  2 -19.2 496 -495 137 -450
1194  2 -19.2 496 -495 450 -451
1195  2 -19.2 496 -495 451 -452
1196  2 -19.2 496 -495 452 -453
1197  2 -19.2 496 -495 453 -454
1198  2 -19.2 496 -495 454 -455
1199  2 -19.2 496 -495 455 -456
1200  2 -19.2 496 -495 456 -457
1201  2 -19.2 496 -495 457 -458
1202  2 -19.2 496 -495 458 -431
1203  2 -19.2 496 -495 431 -432
1204  2 -19.2 496 -495 432 -678    $ 10" TUNGSTEN PLUG WITH A 3" DIA HOLE
1205  2 -19.2 495 -494 137 -450
1206  2 -19.2 495 -494 450 -451
1207  2 -19.2 495 -494 451 -452
1208  2 -19.2 495 -494 452 -453
1209  2 -19.2 495 -494 453 -454
1210  2 -19.2 495 -494 454 -455
```

```
1211  2 -19.2 495 -494 455 -456
1212  2 -19.2 495 -494 456 -457
1213  2 -19.2 495 -494 457 -458
1214  2 -19.2 495 -494 458 -431
1215  2 -19.2 495 -494 431 -432
1216  2 -19.2 495 -494 432 -678
1217  2 -19.2 494 -493 137 -450
1218  2 -19.2 494 -493 450 -451
1219  2 -19.2 494 -493 451 -452
1220  2 -19.2 494 -493 452 -453
1221  2 -19.2 494 -493 453 -454
1222  2 -19.2 494 -493 454 -455
1223  2 -19.2 494 -493 455 -456
1224  2 -19.2 494 -493 456 -457
1225  2 -19.2 494 -493 457 -458
1226  2 -19.2 494 -493 458 -431
1227  2 -19.2 494 -493 431 -432
1228  1 -7.9 494 -493 432 -678
1229  2 -19.2 493 -492 137 -450
1230  2 -19.2 493 -492 450 -451
1231  2 -19.2 493 -492 451 -452
1232  2 -19.2 493 -492 452 -453
1233  2 -19.2 493 -492 453 -454
1234  2 -19.2 493 -492 454 -455
1235  2 -19.2 493 -492 455 -456
1236  2 -19.2 493 -492 456 -457
1237  2 -19.2 493 -492 457 -458
1238  2 -19.2 493 -492 458 -431
1239  2 -19.2 493 -492 431 -432
1240  1 -7.9 493 -492 432 -678
1241  2 -19.2 492 -491 137 -450
1242  2 -19.2 492 -491 450 -451
1243  2 -19.2 492 -491 451 -452
1244  2 -19.2 492 -491 452 -453
1245  2 -19.2 492 -491 453 -454
1246  2 -19.2 492 -491 454 -455
1247  2 -19.2 492 -491 455 -456
1248  2 -19.2 492 -491 456 -457
1249  2 -19.2 492 -491 457 -458
1250  2 -19.2 492 -491 458 -431
1251  1 -7.9 492 -491 431 -432
1252  1 -7.9 492 -491 432 -433
1253  2 -19.2 491 -490 137 -450
1254  2 -19.2 491 -490 450 -451
1255  2 -19.2 491 -490 451 -452
1256  2 -19.2 491 -490 452 -453
1257  2 -19.2 491 -490 453 -454
1258  2 -19.2 491 -490 454 -455
1259  2 -19.2 491 -490 455 -456
1260  2 -19.2 491 -490 456 -457
1261  2 -19.2 491 -490 457 -458
1262  2 -19.2 491 -490 458 -431
1263  1 -7.9 491 -490 431 -432
1264  1 -7.9 491 -490 432 -433
1265  2 -19.2 490 -937 137 -450
1266  2 -19.2 490 -489 450 -451
1267  2 -19.2 490 -489 451 -452
1268  2 -19.2 490 -489 452 -453
1269  2 -19.2 490 -489 453 -454
1270  2 -19.2 490 -489 454 -455
1271  2 -19.2 490 -489 455 -456
1272  2 -19.2 490 -489 456 -457
1273  2 -19.2 490 -489 457 -458
1274  1 -7.9 490 -489 458 -431
1275  1 -7.9 490 -489 431 -432
1276  1 -7.9 490 -489 432 -433    $ ************************************
c
1277  0 496 -489 -137              $ 3" diameter hole thru Tungsten Plug
c
1278  0 668 -471 -431              $ Void on inside of Pig
c
1279  0 679 -471 680 -147              $ Void on outside of Pig
```

```
c
1280  5 -11.34 499 -498 -461       $ *************************************
1281  5 -11.34 499 -498 461 -137
1282  5 -11.34 498 -497 -461
1283  5 -11.34 498 -497 461 -137   $  3" Pb PLUG
1284  5 -11.34 497 -496 -461
1285  5 -11.34 497 -496 461 -137   $ ************************************
c
1286  1 -7.9 496 -495 678 -433
c
1287  1 -7.9 495 -494 678 -433
1288  1 -7.9 494 -493 678 -433
1289  1 -7.9 493 -492 678 -433
1290  1 -7.9 499 -498 433 -508
c 1291  5 -11.34 506 -505 451 -452
c 1292  5 -11.34 506 -505 452 -453
c 1293  5 -11.34 506 -505 453 -454
c 1294  5 -11.34 505 -504 -461
c 1295  5 -11.34 505 -504 461 -137
c 1296  5 -11.34 505 -504 137 -450
c 1297  5 -11.34 505 -504 450 -451
c 1298  5 -11.34 505 -504 451 -452
c 1299  5 -11.34 505 -504 452 -453
c 1300  5 -11.34 505 -504 453 -454
c
1301  5 -11.34 504 -503 -461
1302  5 -11.34 504 -503 461 -137
1303  5 -11.34 504 -503 137 -450
1304  5 -11.34 504 -503 450 -451
1305  5 -11.34 504 -503 451 -452
1306  5 -11.34 504 -503 452 -453
1307  5 -11.34 504 -503 453 -454
1308  5 -11.34 503 -502 -461        $ 8 INCHES OF Pb
1309  5 -11.34 503 -502 461 -137
1310  5 -11.34 503 -502 137 -450
1311  5 -11.34 503 -502 450 -451
1312  5 -11.34 503 -502 451 -452
1313  5 -11.34 503 -502 452 -453
1314  5 -11.34 503 -502 453 -454
1315  5 -11.34 502 -501 -461
1316  5 -11.34 502 -501 461 -137
1317  5 -11.34 502 -501 137 -450
1318  5 -11.34 502 -501 450 -451
1319  5 -11.34 502 -501 451 -452
1320  5 -11.34 502 -501 452 -453
1321  5 -11.34 502 -501 453 -454
1322  5 -11.34 501 -500 -461
1323  5 -11.34 501 -500 461 -137
1324  5 -11.34 501 -500 137 -450
1325  5 -11.34 501 -500 450 -451
1326  5 -11.34 501 -500 451 -452
1327  5 -11.34 501 -500 452 -453
1328  5 -11.34 501 -500 453 -454
1329  5 -11.34 500 -499 -461
1330  5 -11.34 500 -499 461 -137
1331  5 -11.34 500 -499 137 -450
1332  5 -11.34 500 -499 450 -451
1333  5 -11.34 500 -499 451 -452
1334  5 -11.34 500 -499 452 -453
1335  5 -11.34 500 -499 453 -454   $ ************************************
c
1336  0 504 -499 782 -147
c
1337  5 -11.34 489 -488 433 -508
1338  5 -11.34 488 -487 433 -508
1339  5 -11.34 487 -486 433 -508
1340  5 -11.34 486 -485 433 -508
1341  5 -11.34 485 -484 433 -508
1342  5 -11.34 484 -483 433 -508
1343  5 -11.34 483 -482 433 -508
1344  5 -11.34 482 -471 433 -508
c
```

```
c 1345  5 -11.34 462 -463 433 -508
c 1346  5 -11.34 463 -464 433 -508
c 1347  5 -11.34 464 -465 433 -508
c 1348  5 -11.34 465 -466 433 -508
c 1349  5 -11.34 466 -467 433 -508
c 1350  5 -11.34 467 -468 433 -508
c 1351  5 -11.34 468 -469 433 -508
c 1352  5 -11.34 469 -470 433 -508
c 1353  5 -11.34 470 -471 433 -508
c
1354  5 -11.34 471 -472 433 -508
1355  5 -11.34 472 -473 433 -508
1356  5 -11.34 473 -474 433 -508
1357  5 -11.34 474 -475 433 -508
1358  5 -11.34 475 -476 433 -508
1359  5 -11.34 476 -477 433 -508
1360  5 -11.34 477 -478 433 -508
1361  5 -11.34 478 -479 433 -508
1362  5 -11.34 479 -480 433 -508
1363  5 -11.34 480 -481 433 -508
1364  5 -11.34 481 -434 433 -508
1365  5 -11.34 434 -435 433 -508
1366  5 -11.34 435 -436 433 -508
1367  5 -11.34 436 -437 433 -508
1368  5 -11.34 437 -438 433 -508
1369  5 -11.34 438 -439 433 -508
1370  5 -11.34 439 -440 433 -508
1371  5 -11.34 440 -441 433 -508
1372  5 -11.34 441 -442 433 -508
1373  5 -11.34 442 -443 433 -508
1374  5 -11.34 443 -444 433 -508
1375  5 -11.34 444 -445 433 -508
1376  5 -11.34 445 -18 433 -508
1377  5 -11.34 18 -460 433 -508
1378  5 -11.34 460 -446 433 -508
1379  5 -11.34 446 -447 433 -508
1380  5 -11.34 447 -448 433 -508
1381  5 -11.34 448 -449 433 -508
1382  5 -11.34 449 -428 433 -508
1383  5 -11.34 428 -429 433 -508
1384  5 -11.34 429 -430 433 -508
c
1385  1 -7.9 489 -488 508 -509
1386  1 -7.9 488 -487 508 -509
1387  1 -7.9 487 -486 508 -509
1388  1 -7.9 486 -485 508 -509
1389  1 -7.9 485 -484 508 -509
1390  1 -7.9 484 -483 508 -509
1391  1 -7.9 483 -482 508 -509
1392  1 -7.9 482 -471 508 -509
c
c 1393  1 -7.9 462 -463 508 -509
c 1394  1 -7.9 463 -464 508 -509
c 1395  1 -7.9 464 -465 508 -509
c 1396  1 -7.9 465 -466 508 -509
c 1397  1 -7.9 466 -467 508 -509
c 1398  1 -7.9 467 -468 508 -509
c 1399  1 -7.9 468 -469 508 -509
c 1400  1 -7.9 469 -470 508 -509
c 1401  1 -7.9 470 -471 508 -509
c
1402  1 -7.9 471 -472 508 -509
1403  1 -7.9 472 -473 508 -509
1404  1 -7.9 473 -474 508 -509
1405  1 -7.9 474 -475 508 -509
1406  1 -7.9 475 -476 508 -509
1407  1 -7.9 476 -477 508 -509
1408  1 -7.9 477 -478 508 -509
1409  1 -7.9 478 -479 508 -509
1410  1 -7.9 479 -480 508 -509
1411  1 -7.9 480 -481 508 -509
1412  1 -7.9 481 -434 508 -509
```

```
1413  1 -7.9 434 -435 508 -509
1414  1 -7.9 435 -436 508 -509
1415  1 -7.9 436 -437 508 -509
1416  1 -7.9 437 -438 508 -509
1417  1 -7.9 438 -439 508 -509
1418  1 -7.9 439 -440 508 -509
1419  1 -7.9 440 -441 508 -509
1420  1 -7.9 441 -442 508 -509
1421  1 -7.9 442 -443 508 -509
1422  1 -7.9 443 -444 508 -509
1423  1 -7.9 444 -445 508 -509
1424  1 -7.9 445 -18 508 -509
1425  1 -7.9 18 -460 508 -509
1426  1 -7.9 460 -446 508 -509
1427  1 -7.9 446 -447 508 -509
1428  1 -7.9 447 -448 508 -509
1429  1 -7.9 448 -449 508 -509
1430  1 -7.9 449 -428 508 -509
1431  1 -7.9 428 -429 508 -509
1432  1 -7.9 429 -430 508 -509
c
1433  0 499 -498 508 -147
c
1434  1 -7.9 498 -497 508 -509
1435  1 -7.9 497 -496 508 -509
1436  1 -7.9 496 -495 508 -509
1437  1 -7.9 495 -494 508 -509
1438  1 -7.9 494 -493 508 -509
1439  1 -7.9 493 -492 508 -509
1440  1 -7.9 492 -491 508 -509
1441  1 -7.9 491 -490 508 -509
1442  1 -7.9 490 -489 508 -509
c 1443  1 -7.9 499 -498 433 -508
1444  1 -7.9 498 -497 433 -508
1445  1 -7.9 497 -496 433 -508
1446  1 -7.9 496 -495 433 -508
1447  1 -7.9 495 -494 433 -508
1448  1 -7.9 494 -493 433 -508
1449  1 -7.9 493 -492 433 -508
1450  1 -7.9 492 -491 433 -508
1451  1 -7.9 491 -490 433 -508
1452  1 -7.9 490 -489 433 -508
c
1453  0 32 -46 758 -23
c
c ********************* ADDITION OF BOTTOM LID ***************************
C
1500  1 -7.9 600 -148 601 -146
1501  1 -7.9 600 -148 602 -601
1502  1 -7.9 600 -148 603 -602
1503  1 -7.9 600 -148 604 -603
1504  1 -7.9 600 -148 605 -604
1505  1 -7.9 600 -148 606 -605
1506  1 -7.9 600 -148 607 -606
1507  1 -7.9 600 -148 608 -607
1508  1 -7.9 600 -148 609 -608
1509  1 -7.9 600 -148 610 -609
1510  1 -7.9 600 -148 611 -610
1511  1 -7.9 600 -148 612 -611
1512  1 -7.9 600 -148 613 -612
1513  1 -7.9 600 -148 614 -613
1514  1 -7.9 600 -148 615 -614
1515  1 -7.9 600 -148 616 -615
1516  1 -7.9 600 -148 617 -616
1517  1 -7.9 600 -148 618 -617
1518  1 -7.9 600 -148 619 -618
1519  1 -7.9 600 -148 620 -619
1520  1 -7.9 600 -148 621 -620
1521  1 -7.9 600 -148 622 -621
1522  1 -7.9 600 -148 623 -622
1523  1 -7.9 600 -148 624 -623
1524  1 -7.9 600 -148 625 -624
```

```
1525  1 -7.9 600 -148 626 -625
1526  1 -7.9 600 -148 627 -626
1527  0 600 -148 628 -627
1528  0 600 -148 629 -628
1529  0 600 -148 630 -629
1530  0 600 -148 631 -630
1531  0 600 -148 632 -631
1532  0 600 -148 633 -632
1533  0 600 -148 634 -633
1534  0 600 -148 635 -634
1535  0 600 -148 636 -635
1536  0 600 -148 637 -636
1537  0 600 -148 638 -637
1538  0 600 -148 639 -638
1539  0 600 -148 640 -639
1540  0 600 -148 641 -640
1541  0 600 -148 642 -641
1542  0 600 -148 643 -642
1543  0 600 -148 644 -643
1544  0 600 -148 645 -644
1545  0 600 -148 646 -645
1546  0 600 -148 647 -646
1547  0 600 -148 648 -647
1548  0 600 -148 649 -648
1549  0 600 -148 759 -649
1550  0 600 -148 758 -759
1551  0 600 -148 757 -758
1552  0 600 -148 756 -757
1553  0 600 -148 755 -756
1554  0 600 -148 754 -755
1555  0 600 -148 753 -754
1556  0 600 -148 752 -753
1557  0 600 -148 751 -752
1558  0 600 -148 750 -751
1559  0 600 -148 749 -750
1560  0 600 -148 748 -749
1561  0 600 -148 665 -748      $ END OF BOTTOM LID
c
1562  8 -7.84 148 -662 625 -624   $ 3 FOOT DIAGNOSTIC FLANGE
1563  8 -7.84 148 -662 626 -625
1564  8 -7.84 148 -662 627 -626   $ NOTE: CHANGED FROM STAINLESS STEEL
1565  8 -7.84 148 -662 628 -627   $ TO ORDINARY STEEL (97.96% Fe, 2.04% C)
1566  8 -7.84 148 -662 629 -628
1567  8 -7.84 148 -662 630 -629
1568  8 -7.84 148 -662 631 -630
1569  8 -7.84 148 -662 632 -631
1570  8 -7.84 148 -662 633 -632
1571  8 -7.84 148 -662 634 -633
1572  8 -7.84 148 -662 635 -634
1573  8 -7.84 148 -662 636 -635
1574  8 -7.84 148 -662 637 -636
1575  8 -7.84 148 -662 638 -637
1576  8 -7.84 148 -662 639 -638
1577  8 -7.84 148 -662 640 -639
1578  8 -7.84 148 -662 641 -640
1579  8 -7.84 148 -662 642 -641
1580  8 -7.84 148 -662 643 -642
1581  8 -7.84 148 -662 644 -643
1582  8 -7.84 148 -662 645 -644
1583  8 -7.84 148 -662 646 -645
1584  8 -7.84 148 -662 647 -646
1585  8 -7.84 148 -662 648 -647
1586  8 -7.84 148 -662 649 -648
1587  8 -7.84 148 -662 759 -649
1588  8 -7.84 148 -662 758 -759
1589  8 -7.84 148 -662 757 -758
1590  8 -7.84 148 -662 756 -757
1591  8 -7.84 148 -662 755 -756
1592  8 -7.84 148 -662 754 -755
1593  8 -7.84 148 -662 753 -754
1594  8 -7.84 148 -662 752 -753
1595  8 -7.84 148 -662 751 -752
```

```
1596  8 -7.84 148 -662 750 -751
1597  8 -7.84 148 -662 749 -750        $ 3 INCH RADIUS VOIDED
1598  8 -7.84 148 -662 748 -749
1599  8 -7.84 148 -662 665 -748
c
1600  8 -7.84 664 -600 628 -627  $ 1/2" SHIELD PLATE (VACUUM SIDE)
1601  8 -7.84 664 -600 629 -628
1602  8 -7.84 664 -600 630 -629  $ NOTE: CHANGED FROM STAINLESS STEEL
1603  8 -7.84 664 -600 631 -630  $ TO ORDINARY STEEL (97.96% Fe, 2.04% C)
1604  8 -7.84 664 -600 632 -631
1605  8 -7.84 664 -600 633 -632
1606  8 -7.84 664 -600 634 -633
1607  8 -7.84 664 -600 635 -634
1608  8 -7.84 664 -600 636 -635
1609  8 -7.84 664 -600 637 -636
1610  8 -7.84 664 -600 638 -637
1611  8 -7.84 664 -600 639 -638
1612  8 -7.84 664 -600 640 -639
1613  8 -7.84 664 -600 641 -640
1614  8 -7.84 664 -600 642 -641
1615  8 -7.84 664 -600 643 -642
1616  8 -7.84 664 -600 644 -643
1617  8 -7.84 664 -600 645 -644
1618  8 -7.84 664 -600 646 -645
1619  8 -7.84 664 -600 647 -646
1620  8 -7.84 664 -600 648 -647
1621  8 -7.84 664 -600 649 -648
1622  8 -7.84 664 -600 759 -649
1623  8 -7.84 664 -600 758 -759
1624  8 -7.84 664 -600 757 -758
1625  8 -7.84 664 -600 756 -757
1626  8 -7.84 664 -600 755 -756
1627  8 -7.84 664 -600 754 -755
1628  8 -7.84 664 -600 753 -754
1629  8 -7.84 664 -600 752 -753
1630  8 -7.84 664 -600 751 -752
1631  8 -7.84 664 -600 750 -751
1632  8 -7.84 664 -600 749 -750
1633  8 -7.84 664 -600 748 -749
1634  8 -7.84 664 -600 665 -748  $ END OF 1/2" SHIELD PLATE
c
c **** CHANGING PORTIONS OF BOTTOM LID TO STEEL AS OPPOSED
c      TO STAINLESS STEEL:
c
1635  8 -7.84 662 -663 766 -767  $ 0.7" THICK, 8" DIA FLANGE
1636  0 662 -663 765 -766  $ THIS IS THE FLANGE WE
1637  0 662 -663 764 -765  $ "SEE" THROUGH W/ nTOF
1638  0 662 -663 763 -764  $ ** END OF 8" DIA FLANGE **
c
1639  0 664 -600 624 -146     $ VOID B/W STACK AND 9/16" SHIELD PLATE
1640  0 148 -662 624 -147     $ VOID B/W OUTER STACK AND 8" FLANGE
c
c 1641  0 662 -507 -147     $ VOID B/W AIR SIDE OF LID TO TOP OF 8" Pb
c
1642  6 -1.032 666 -667 -137  $ TOP nTOF SCINTILLATOR
c
1643  7 -2.7 489 -666 -137    $ 1/8" ALUMINUM (DETECTOR HOUSING)
1644  7 -2.7 667 -668 -137    $ 1/8" ALUMINUM (DETECTOR HOUSING)
c
1645  0 489 -668 935 -431  $ VOID AROUND TOP nTOF INSIDE PIG
c
1646  8 -7.84 664 -600 -665  $ 9/16" SHIELD PLATE
1647  0 600 -148 -665       $ BOTTOM LID
1648  8 -7.84 148 -662 -665       $ 3' DIAGNOSTIC FLANGE
c
c  **** NOTE: STEEL AS OPPOSED TO STAINLESS STEEL:
c
1649  0 662 -663 -763  $ 8" FLANGE (nTOF SEE THRU)
c
1650  0 662 -663 767 -147
c
1651  7 -2.7 489 -670 137 -935  $ TOP nTOF ALUMINUM HOUSING
```

```
1652  7 -2.7 670 -668 137 -935  $ TOP nTOF ALUMINUM HOUSING
c
1653  7 -2.7 671 -673 456 -669 929 -930 $ OUTTER LIGHTGUIDE ALUMINUM HOUSING
1654  7 -2.7 673 -672 456 -669 929 -930 $ OUTTER LIGHTGUIDE ALUMINUM HOUSING
1655  7 -2.7 671 -18 -137       $ BOTTOM nTOF ALUMINUM HOUSING
1656  7 -2.7 460 -672 -137      $ BOTTOM nTOF ALUMINUM HOUSING
c
c ****** END OF BOTTOM LID ADDITION *******
c
c
1657  0 10 -13 -25   $ VOID B/L BOTTOM BLAST SHIELD
c
1658  0 1 -2 -665   $ 2" HOLE THRU COPPER PLATES
1659  0 3 -4 -665   $ "   "     "    "      "
1660  0 5 -6 -665   $ "   "     "    "      "
1661  0 7 -8 -665   $ "   "     "    "      "
c
1662  4 -8.96 675 -664 628 -627   $ 9/16" COPPER SHIELD PLATE
1663  4 -8.96 675 -664 629 -628
1664  4 -8.96 675 -664 630 -629
1665  4 -8.96 675 -664 631 -630
1666  4 -8.96 675 -664 632 -631
1667  4 -8.96 675 -664 633 -632
1668  4 -8.96 675 -664 634 -633
1669  4 -8.96 675 -664 635 -634
1670  4 -8.96 675 -664 636 -635
1671  4 -8.96 675 -664 637 -636
1672  4 -8.96 675 -664 638 -637
1673  4 -8.96 675 -664 639 -638
1674  4 -8.96 675 -664 640 -639
1675  4 -8.96 675 -664 641 -640
1676  4 -8.96 675 -664 642 -641
1677  4 -8.96 675 -664 643 -642
1678  4 -8.96 675 -664 644 -643
1679  4 -8.96 675 -664 645 -644
1680  4 -8.96 675 -664 646 -645
1681  4 -8.96 675 -664 647 -646
1682  4 -8.96 675 -664 648 -647
1683  4 -8.96 675 -664 649 -648
1684  4 -8.96 675 -664 759 -649
1685  4 -8.96 675 -664 758 -759
1686  4 -8.96 675 -664 757 -758
1687  4 -8.96 675 -664 756 -757
1688  4 -8.96 675 -664 755 -756
1689  4 -8.96 675 -664 754 -755
1690  4 -8.96 675 -664 753 -754
1691  4 -8.96 675 -664 752 -753
1692  4 -8.96 675 -664 751 -752
1693  4 -8.96 675 -664 750 -751
1694  4 -8.96 675 -664 749 -750
1695  4 -8.96 675 -664 748 -749
1696  4 -8.96 675 -664 665 -748
1697  4 -8.96 675 -664 -665      $ 9/16" COPPER SHIELD PLATE
c
1698  0 675 -664 624 -146
c
1699  1 -7.9 664 -600 627 -626   $ 9/16" SS SHIELD PLATE
1700  1 -7.9 664 -600 626 -625   $  "     "    "     "
1701  1 -7.9 664 -600 625 -624   $  "     "    "     "
1702  4 -8.96 675 -664 627 -626  $  "     Cu   "     "
1703  4 -8.96 675 -664 626 -625  $  "     "    "     "
1704  4 -8.96 675 -664 625 -624  $  "     "    "     "
c
1705  8 -7.84 676 -677 -760       $ ELEVATOR FLOOR
1706  8 -7.84 676 -677 760 -761
1707  8 -7.84 676 -677 761 -748
1708  8 -7.84 676 -677 748 -749
1709  8 -7.84 676 -677 749 -750
1710  8 -7.84 676 -677 750 -751
1711  8 -7.84 676 -677 751 -752
1712  8 -7.84 676 -677 752 -753
1713  8 -7.84 676 -677 753 -754
```

```
1714  8 -7.84 676 -677 754 -755
1715  8 -7.84 676 -677 755 -756
1716  8 -7.84 676 -677 756 -762
1717  8 -7.84 676 -677 762 -757
1718  8 -7.84 676 -677 757 -758
1719  8 -7.84 676 -677 758 -759
1720  8 -7.84 676 -677 759 -649
1721  8 -7.84 676 -677 649 -648
1722  8 -7.84 676 -677 648 -647
1723  8 -7.84 676 -677 647 -646
1724  8 -7.84 676 -677 646 -645
1725  8 -7.84 676 -677 645 -644
1726  8 -7.84 676 -677 644 -643
1727  8 -7.84 676 -677 643 -642
1728  8 -7.84 676 -677 642 -641
1729  8 -7.84 676 -677 641 -640
1730  8 -7.84 676 -677 640 -639
1731  8 -7.84 676 -677 639 -638
1732  8 -7.84 676 -677 638 -637
1733  8 -7.84 676 -677 637 -636
1734  8 -7.84 676 -677 636 -635
1735  8 -7.84 676 -677 635 -634
1736  8 -7.84 676 -677 634 -633
1737  8 -7.84 676 -677 633 -632
1738  8 -7.84 676 -677 632 -631
1739  8 -7.84 676 -677 631 -630
1740  8 -7.84 676 -677 630 -629
1741  8 -7.84 676 -677 629 -628
1742  8 -7.84 676 -677 628 -627
1743  8 -7.84 676 -677 627 -626
1744  8 -7.84 676 -677 626 -625
1745  8 -7.84 676 -677 625 -624
1746  8 -7.84 676 -677 624 -623
1747  8 -7.84 676 -677 623 -622
1748  8 -7.84 676 -677 622 -621
1749  8 -7.84 676 -677 621 -620
1750  8 -7.84 676 -677 620 -619
1751  8 -7.84 676 -677 619 -618
1752  8 -7.84 676 -677 618 -617
1753  8 -7.84 676 -677 617 -616
1754  8 -7.84 676 -677 616 -615
1755  8 -7.84 676 -677 615 -614
1756  8 -7.84 676 -677 614 -613
1757  8 -7.84 676 -677 613 -612
1758  8 -7.84 676 -677 612 -611
1759  8 -7.84 676 -677 611 -610
1760  8 -7.84 676 -677 610 -609
1761  8 -7.84 676 -677 609 -608
1762  8 -7.84 676 -677 608 -607
1763  8 -7.84 676 -677 607 -606
1764  8 -7.84 676 -677 606 -605
1765  8 -7.84 676 -677 605 -604
1766  8 -7.84 676 -677 604 -603
1767  8 -7.84 676 -677 603 -602
1768  8 -7.84 676 -677 602 -601
1769  8 -7.84 676 -677 601 -146
1770  8 -7.84 676 -677 146 -147     $ ELEVATOR FLOOR
c
1771  0 430 -784 -147 #2287 #2288 #2289 #2290 #2291 #2292 &
 #2293 #2294
c     $ VOID B/W BOTTOM OF PIG AND ELEVATOR FLOOR
c
c
1772  1 -7.9 679 -495 681 -682 -680 683 #1436 #1446 #1286 #1204 $ SIDE PLATES
1773  1 -7.9 681 -682 495 -494 -680 683 #1437 #1447 #1287 #1216 $ ON PIG
1774  1 -7.9 681 -682 494 -493 -680 683 #1438 #1448 #1288 #1228
1775  1 -7.9 681 -682 493 -492 -680 683 #1439 #1449 #1289 #1240
1776  1 -7.9 681 -682 492 -491 -680 683 #1440 #1450 #1252
1777  1 -7.9 681 -682 491 -490 -680 683 #1441 #1451 #1264
1778  1 -7.9 681 -682 490 -489 -680 683 #1442 #1452 #1276
1779  1 -7.9 681 -682 489 -488 -680 683 #1385 #1337 #1149
1780  1 -7.9 681 -682 488 -487 -680 683 #1386 #1338 #1150
```

```
1781  1 -7.9 681 -682 487 -486 -680 683 #1387 #1339 #1151
1782  1 -7.9 681 -682 486 -485 -680 683 #1388 #1340 #1152
1783  1 -7.9 681 -682 485 -484 -680 683 #1389 #1341 #1153
1784  1 -7.9 681 -682 484 -483 -680 683 #1390 #1342 #1154
1785  1 -7.9 681 -682 483 -482 -680 683 #1391 #1343 #1155
1786  1 -7.9 681 -682 482 -471 -680 683 #1392 #1344 #1156
1787  1 -7.9 681 -682 471 -472 -680 683 #1402 #1354 #1129
1788  1 -7.9 681 -682 472 -473 -680 683 #1403 #1355 #1130
1789  1 -7.9 681 -682 473 -474 -680 683 #1404 #1356 #1131
1790  1 -7.9 681 -682 474 -475 -680 683 #1405 #1357 #1132
1791  1 -7.9 681 -682 475 -476 -680 683 #1406 #1358 #1133
1792  1 -7.9 681 -682 476 -477 -680 683 #1407 #1359 #1134
1793  1 -7.9 681 -682 477 -478 -680 683 #1408 #1360 #1135
1794  1 -7.9 681 -682 478 -479 -680 683 #1409 #1361 #1136
1795  1 -7.9 681 -682 479 -480 -680 683 #1410 #1362 #1137
1796  1 -7.9 681 -682 480 -481 -680 683 #1411 #1363 #1138
1797  1 -7.9 681 -682 481 -434 -680 683 #1412 #1364 #1139
1798  1 -7.9 681 -682 434 -435 -680 683 #1413 #1365 #1063
1799  1 -7.9 681 -682 435 -436 -680 683 #1414 #1366 #1064
1800  1 -7.9 681 -682 436 -437 -680 683 #1415 #1367 #1065
1801  1 -7.9 681 -682 437 -438 -680 683 #1416 #1368 #1066
1802  1 -7.9 681 -682 438 -439 -680 683 #1417 #1369 #1067
1803  1 -7.9 681 -682 439 -440 -680 683 #1418 #1370 #1068
1804  1 -7.9 681 -682 440 -441 -680 683 #1419 #1371 #1069
1805  1 -7.9 681 -682 441 -442 -680 683 #1420 #1372 #1070
1806  1 -7.9 681 -682 442 -443 -680 683 #1421 #1373 #1071
1807  1 -7.9 681 -682 443 -444 -680 683 #1422 #1374 #1072
1808  1 -7.9 681 -682 444 -445 -680 683 #1423 #1375 #1073
1809  1 -7.9 681 -682 445 -18 -680 683 #1424 #1376 #1074
1810  1 -7.9 681 -682 18 -460 -680 683 #1425 #1377 #1075
1811  1 -7.9 681 -682 460 -446 -680 683 #1426 #1378 #1076
1812  1 -7.9 681 -682 446 -447 -680 683 #1427 #1379 #1077
1813  1 -7.9 681 -682 447 -448 -680 683 #1428 #1380 #1078
1814  1 -7.9 681 -682 448 -449 -680 683 #1429 #1381 #1079
1815  1 -7.9 681 -682 449 -428 -680 683 #1430 #1382 #1080
1816  1 -7.9 681 -682 428 -429 -680 683 #1431 #1383 #1081
1817  1 -7.9 681 -682 429 -430 -680 683 #1432 #1384 #1082
c
1818  0 498 -679 509 -147
c
1819  0 679 -430 -680 683 -681 -147  $ VOIDS AROUND PIG
c
1820  0 679 -430 -680 683 682 -147
c
1821  0 679 -430 -685 684 -681 -147 #2289
c
1822  0 679 -430 -685 684 682 -147 #2291
c
1823  0 679 -430 -683 685 509 -147
c
C 1823  0 679 -430 -683 685 509 -147
c
c 1824  0 679 -430 681 -682 684 509
c
1824  0 679 -471 -684 -147
1825  0 471 -434 -684 -147
1826  0 434 -430 -684 -21 #2287 #2289 #2291
c
1827  1 -7.9 679 -495 681 -682 -685 684 #1436 #1446 #1286 #1204 $ SIDE PLATES
ON PIG
1828  1 -7.9 681 -682 495 -494 -685 684 #1437 #1447 #1287 #1216
1829  1 -7.9 681 -682 494 -493 -685 684 #1438 #1448 #1288 #1228
1830  1 -7.9 681 -682 493 -492 -685 684 #1439 #1449 #1289 #1240
1831  1 -7.9 681 -682 492 -491 -685 684 #1440 #1450 #1252
1832  1 -7.9 681 -682 491 -490 -685 684 #1441 #1451 #1264
1833  1 -7.9 681 -682 490 -489 -685 684 #1442 #1452 #1276
1834  1 -7.9 681 -682 489 -488 -685 684 #1385 #1337 #1149
1835  1 -7.9 681 -682 488 -487 -685 684 #1386 #1338 #1150
1836  1 -7.9 681 -682 487 -486 -685 684 #1387 #1339 #1151
1837  1 -7.9 681 -682 486 -485 -685 684 #1388 #1340 #1152
1838  1 -7.9 681 -682 485 -484 -685 684 #1389 #1341 #1153
1839  1 -7.9 681 -682 484 -483 -685 684 #1390 #1342 #1154
```

```
1840  1 -7.9 681 -682 483 -482 -685 684 #1391 #1343 #1155
1841  1 -7.9 681 -682 482 -471 -685 684 #1392 #1344 #1156
1842  1 -7.9 681 -682 471 -472 -685 684 #1402 #1354 #1129
1843  1 -7.9 681 -682 472 -473 -685 684 #1403 #1355 #1130
1844  1 -7.9 681 -682 473 -474 -685 684 #1404 #1356 #1131
1845  1 -7.9 681 -682 474 -475 -685 684 #1405 #1357 #1132
1846  1 -7.9 681 -682 475 -476 -685 684 #1406 #1358 #1133
1847  1 -7.9 681 -682 476 -477 -685 684 #1407 #1359 #1134
1848  1 -7.9 681 -682 477 -478 -685 684 #1408 #1360 #1135
1849  1 -7.9 681 -682 478 -479 -685 684 #1409 #1361 #1136
1850  1 -7.9 681 -682 479 -480 -685 684 #1410 #1362 #1137
1851  1 -7.9 681 -682 480 -481 -685 684 #1411 #1363 #1138
1852  1 -7.9 681 -682 481 -434 -685 684 #1412 #1364 #1139
1853  1 -7.9 681 -682 434 -435 -685 684 #1413 #1365 #1063
1854  1 -7.9 681 -682 435 -436 -685 684 #1414 #1366 #1064
1855  1 -7.9 681 -682 436 -437 -685 684 #1415 #1367 #1065
1856  1 -7.9 681 -682 437 -438 -685 684 #1416 #1368 #1066
1857  1 -7.9 681 -682 438 -439 -685 684 #1417 #1369 #1067
1858  1 -7.9 681 -682 439 -440 -685 684 #1418 #1370 #1068
1859  1 -7.9 681 -682 440 -441 -685 684 #1419 #1371 #1069
1860  1 -7.9 681 -682 441 -442 -685 684 #1420 #1372 #1070
1861  1 -7.9 681 -682 442 -443 -685 684 #1421 #1373 #1071
1862  1 -7.9 681 -682 443 -444 -685 684 #1422 #1374 #1072
1863  1 -7.9 681 -682 444 -445 -685 684 #1423 #1375 #1073
1864  1 -7.9 681 -682 445 -18 -685 684 #1424 #1376 #1074
1865  1 -7.9 681 -682 18 -460 -685 684 #1425 #1377 #1075
1866  1 -7.9 681 -682 460 -446 -685 684 #1426 #1378 #1076
1867  1 -7.9 681 -682 446 -447 -685 684 #1427 #1379 #1077
1868  1 -7.9 681 -682 447 -448 -685 684 #1428 #1380 #1078
1869  1 -7.9 681 -682 448 -449 -685 684 #1429 #1381 #1079
1870  1 -7.9 681 -682 449 -428 -685 684 #1430 #1382 #1080
1871  1 -7.9 681 -682 428 -429 -685 684 #1431 #1383 #1081
1872  1 -7.9 681 -682 429 -430 -685 684 #1432 #1384 #1082
c
1873  0 434 -430 21 -147 680
1874  0 434 -430 21 -147 -684
c
1875  9 -0.915 686 -504 -454 453  $ 6 INCHES POLY ON TOP OF Pb
1876  9 -0.915 686 -504 -453 452
1877  9 -0.915 686 -504 -452 451
1878  9 -0.915 686 -504 -451 692
c 1879  9 -0.915 686 -504 -450 692
c
c 1880  9 -0.915 686 -504 -137 692
c 1881  0 686 -504 -692     $ CTR HOLE THRU POLY
c
1882  9 -0.915 687 -686 -454 453
1883  9 -0.915 687 -686 -453 452
1884  9 -0.915 687 -686 -452 451
1885  9 -0.915 687 -686 -451 692
c 1886  9 -0.915 687 -686 -450 692
c
c 1887  9 -0.915 687 -686 -137 692
c 1888  0 687 -686 -692     $ CTR HOLE THRU POLY
c
1889  9 -0.915 688 -687 -454 453
1890  9 -0.915 688 -687 -453 452
1891  9 -0.915 688 -687 -452 451
1892  9 -0.915 688 -687 -451 692
c 1893  9 -0.915 688 -687 -450 692
c
c 1894  9 -0.915 688 -687 -137 692
c 1895  0 688 -687 -692     $ CTR HOLE THRU POLY
c
1896  9 -0.915 689 -688 -454 453
1897  9 -0.915 689 -688 -453 452
1898  9 -0.915 689 -688 -452 451
1899  9 -0.915 689 -688 -451 692
c 1900  9 -0.915 689 -688 -450 692
c
c 1901  9 -0.915 689 -688 -137 692
c 1902  0 689 -688 -692     $ CTR HOLE THRU POLY
```

```
c
1903  9 -0.915 690 -689 -454 453
1904  9 -0.915 690 -689 -453 452
1905  9 -0.915 690 -689 -452 451
1906  9 -0.915 690 -689 -451 692
c 1907  9 -0.915 690 -689 -450 692
c
c 1908  9 -0.915 690 -689 -137 692
c 1909  0 690 -689 -692     $ CTR HOLE THRU POLY
c
1910  9 -0.915 691 -690 -454 453
1911  9 -0.915 691 -690 -453 452
1912  9 -0.915 691 -690 -452 451
1913  9 -0.915 691 -690 -451 692
c 1914  9 -0.915 691 -690 -450 692
c
c 1915  9 -0.915 691 -690 -137 692
c 1916  0 691 -690 -692  $ CTR HOLE THRU POLY; END OF 6 INCHES POLY ON TOP OF
Pb
c
1917  0 695 -504 433 -147  $ Void b/w poly and stack
c
1918  9 -0.915 693 -691 -454 453  $ 3 FOOT STACK OF POLY
1919  9 -0.915 693 -691 -453 452
1920  9 -0.915 693 -691 -452 451
1921  9 -0.915 693 -691 -451 692
c 1922  9 -0.915 693 -691 -450 692
c 1923  9 -0.915 693 -691 -137 692
1924  9 -0.915 694 -693 -454 453
1925  9 -0.915 694 -693 -453 452
1926  9 -0.915 694 -693 -452 451
1927  9 -0.915 694 -693 -451 692
c 1928  9 -0.915 694 -693 -450 692
c 1929  9 -0.915 694 -693 -137 692
1930  9 -0.915 695 -694 -454 453
1931  9 -0.915 695 -694 -453 452
1932  9 -0.915 695 -694 -452 451
1933  9 -0.915 695 -694 -451 692
c 1934  9 -0.915 695 -694 -450 692
c 1935  9 -0.915 695 -694 -137 692
1936  9 -0.915 696 -695 -454 453
1937  9 -0.915 696 -695 -453 452
1938  9 -0.915 696 -695 -452 451
1939  9 -0.915 696 -695 -451 692
c 1940  9 -0.915 696 -695 -450 692
c 1941  9 -0.915 696 -695 -137 692
1942  9 -0.915 697 -696 -454 453
1943  9 -0.915 697 -696 -453 452
1944  9 -0.915 697 -696 -452 451
1945  9 -0.915 697 -696 -451 692
c 1946  9 -0.915 697 -696 -450 692
c 1947  9 -0.915 697 -696 -137 692
c
1948  9 -0.915 698 -697 -454 453
1949  9 -0.915 698 -747 -453 692
1950  9 -0.915 747 -697 -453 692
c
c 1951  9 -0.915 698 -697 -451 692
c 1952  9 -0.915 698 -697 -450 692
c 1953  9 -0.915 698 -697 -137 692
c
1954  9 -0.915 699 -698 -454 453
1955  9 -0.915 699 -746 -453 692
1956  9 -0.915 746 -698 -453 692
c
c 1957  9 -0.915 699 -698 -451 692
c 1958  9 -0.915 699 -698 -450 692
c 1959  9 -0.915 699 -698 -137 692
c
1960  9 -0.915 700 -699 -454 453
1961  9 -0.915 700 -745 -453 692
1962  9 -0.915 745 -699 -453 692
```

```
c
c 1963  9 -0.915 700 -699 -451 692
c 1964  9 -0.915 700 -699 -450 692
c 1965  9 -0.915 700 -699 -137 692
c
1966  9 -0.915 701 -700 -454 453
1967  9 -0.915 701 -744 -453 692
1968  9 -0.915 744 -700 -453 692
c
c 1969  9 -0.915 701 -700 -451 692
c 1970  9 -0.915 701 -700 -450 692
c 1971  9 -0.915 701 -700 -137 692
c
1972  9 -0.915 702 -701 -454 453
1973  9 -0.915 702 -743 -453 692
1974  9 -0.915 743 -701 -453 692
c
c 1975  9 -0.915 702 -701 -451 692
c 1976  9 -0.915 702 -701 -450 692
c 1977  9 -0.915 702 -701 -137 692
c
1978  9 -0.915 703 -702 -454 453
1979  9 -0.915 703 -742 -453 692
1980  9 -0.915 742 -702 -453 692
c
c 1981  9 -0.915 703 -702 -451 692
c 1982  9 -0.915 703 -702 -450 692
c 1983  9 -0.915 703 -702 -137 692
c
1984  9 -0.915 704 -703 -454 453
1985  9 -0.915 704 -741 -453 692
1986  9 -0.915 741 -703 -453 692
c
c 1987  9 -0.915 704 -703 -451 692
c 1988  9 -0.915 704 -703 -450 692
c 1989  9 -0.915 704 -703 -137 692
c
1990  9 -0.915 705 -704 -454 453
1991  9 -0.915 705 -740 -453 692
1992  9 -0.915 740 -704 -453 692
c
c 1993  9 -0.915 705 -704 -451 692
c 1994  9 -0.915 705 -704 -450 692
c 1995  9 -0.915 705 -704 -137 692
c
1996  9 -0.915 706 -705 -454 453
1997  9 -0.915 706 -739 -453 692
1998  9 -0.915 739 -705 -453 692
c
c 1999  9 -0.915 706 -705 -451 692
c 2000  9 -0.915 706 -705 -450 692
c 2001  9 -0.915 706 -705 -137 692
c
2002  9 -0.915 707 -706 -454 453
2003  9 -0.915 707 -738 -453 692
2004  9 -0.915 738 -706 -453 692
c
c 2005  9 -0.915 707 -706 -451 692
c 2006  9 -0.915 707 -706 -450 692
c 2007  9 -0.915 707 -706 -137 692
c
2008  9 -0.915 708 -707 -454 453
2009  9 -0.915 708 -737 -453 692
2010  9 -0.915 737 -707 -453 692
c
c 2011  9 -0.915 708 -707 -451 692
c 2012  9 -0.915 708 -707 -450 692
c 2013  9 -0.915 708 -707 -137 692
c
2014  9 -0.915 709 -708 -454 453
2015  9 -0.915 709 -736 -453 692
2016  9 -0.915 736 -708 -453 692
```

```
c
c 2017  9 -0.915 709 -708 -451 692
c 2018  9 -0.915 709 -708 -450 692
c 2019  9 -0.915 709 -708 -137 692
c
2020  9 -0.915 710 -709 -454 453
2021  9 -0.915 710 -723 -453 692
2022  9 -0.915 723 -709 -453 692
c
c 2023  9 -0.915 710 -709 -451 692
c 2024  9 -0.915 710 -709 -450 692
c 2025  9 -0.915 710 -709 -137 692
c
2026  9 -0.915 711 -710 -454 453
2027  9 -0.915 711 -724 -453 692
2028  9 -0.915 724 -710 -453 692
c
c 2029  9 -0.915 711 -710 -451 692
c 2030  9 -0.915 711 -710 -450 692
c 2031  9 -0.915 711 -710 -137 692
c
2032  9 -0.915 712 -711 -454 453
2033  9 -0.915 712 -725 -453 692
2034  9 -0.915 725 -711 -453 692
c
c 2035  9 -0.915 712 -711 -451 692
c 2036  9 -0.915 712 -711 -450 692
c 2037  9 -0.915 712 -711 -137 692
c
2038  9 -0.915 713 -712 -454 453
2039  9 -0.915 713 -726 -453 692
2040  9 -0.915 726 -712 -453 692
c
c 2041  9 -0.915 713 -712 -451 692
c 2042  9 -0.915 713 -712 -450 692
c 2043  9 -0.915 713 -712 -137 692
c
2044  9 -0.915 714 -713 -454 453
2045  9 -0.915 714 -727 -453 692
2046  9 -0.915 727 -713 -453 692
c
c 2047  9 -0.915 714 -713 -451 692
c 2048  9 -0.915 714 -713 -450 692
c 2049  9 -0.915 714 -713 -137 692
c
2050  9 -0.915 715 -714 -454 453
2051  9 -0.915 715 -728 -453 692
2052  9 -0.915 728 -714 -453 692
c
c 2053  9 -0.915 715 -714 -451 692
c 2054  9 -0.915 715 -714 -450 692
c 2055  9 -0.915 715 -714 -137 692
c
2056  9 -0.915 716 -715 -454 453
2057  9 -0.915 716 -729 -453 692
2058  9 -0.915 729 -715 -453 692
c
c 2059  9 -0.915 716 -715 -451 692
c 2060  9 -0.915 716 -715 -450 692
c 2061  9 -0.915 716 -715 -137 692
c
2062  9 -0.915 717 -716 -454 453
2063  9 -0.915 717 -730 -453 692
2064  9 -0.915 730 -716 -453 692
c
c 2065  9 -0.915 717 -716 -451 692
c 2066  9 -0.915 717 -716 -450 692
c 2067  9 -0.915 717 -716 -137 692
c
2068  9 -0.915 718 -717 -454 453
2069  9 -0.915 718 -731 -453 692
2070  9 -0.915 731 -717 -453 692
```

```
c
c 2071  9 -0.915 718 -717 -451 692
c 2072  9 -0.915 718 -717 -450 692
c 2073  9 -0.915 718 -717 -137 692
c
2074  9 -0.915 719 -718 -454 453
2075  9 -0.915 719 -732 -453 692
2076  9 -0.915 732 -718 -453 692
c
c 2077  9 -0.915 719 -718 -451 692
c 2078  9 -0.915 719 -718 -450 692
c 2079  9 -0.915 719 -718 -137 692
c
2080  9 -0.915 720 -719 -454 453
2081  9 -0.915 720 -733 -453 692
2082  9 -0.915 733 -719 -453 692
c
c 2083  9 -0.915 720 -719 -451 692
c 2084  9 -0.915 720 -719 -450 692
c 2085  9 -0.915 720 -719 -137 692
c
2086  9 -0.915 734 -720 -454 452
2087  9 -0.915 734 -720 -451 692
2088  9 -0.915 734 -720 -452 451
c
c 2089  9 -0.915 721 -720 -451 692
c 2090  9 -0.915 721 -720 -450 692
c 2091  9 -0.915 721 -720 -137 692
c
c 2092  9 -0.915 722 -721 -454 453
c 2093  9 -0.915 722 -735 -453 692
c 2094  9 -0.915 735 -721 -453 692
c
c 2095  9 -0.915 722 -721 -451 692
c 2096  9 -0.915 722 -721 -450 692
c 2097  9 -0.915 722 -721 -137 692
c
2098  0 734 -504 -692  $ VOID INSIDE POLY
c
2099  9 -0.915 706 -739 454 -455  $ 4th SECTION POLY
2100  9 -0.915 707 -706 454 -455
2101  9 -0.915 708 -707 454 -455
2102  9 -0.915 709 -708 454 -455
2103  9 -0.915 710 -709 454 -455
2104  9 -0.915 711 -710 454 -455
2105  9 -0.915 712 -711 454 -455
2106  9 -0.915 713 -712 454 -455
2107  9 -0.915 714 -713 454 -455
2108  9 -0.915 715 -714 454 -455
2109  9 -0.915 716 -715 454 -455
c
2110  0 716 -739 455 -147
c
2111  1 -7.9 -799 #1771      $ 16" DIA SS PLATE
c
c 2112    1 -7.9 784 -785 760 -761  $ @ BOTTOM OF YOKE
c 2113    1 -7.9 784 -785 761 -748  $ (WHERE YOKE SWIVELS)
c 2114    1 -7.9 784 -785 748 -749
c 2115    1 -7.9 784 -785 749 -750
c 2116    1 -7.9 784 -785 750 -751
c 2117    1 -7.9 784 -785 751 -752
c 2118    1 -7.9 784 -785 752 -753
c 2119    1 -7.9 784 -785 753 -754
c
2120    0 784 -785 799 -147 #1826 #1874 #2287 #2288 #2286
c
c 2121    8 -7.84 785 -786 -760     $ 1/2" PLATE OF PIG
c 2122    8 -7.84 785 -786 760 -761 $ CHASSIS
c 2123    8 -7.84 785 -786 761 -748
c 2124    8 -7.84 785 -786 748 -749
c 2125    8 -7.84 785 -786 749 -750
c 2126    8 -7.84 785 -786 750 -751
```

```
c 2127    8 -7.84 785 -786 751 -752
c 2128    8 -7.84 785 -786 752 -753
c 2129    8 -7.84 785 -786 753 -754
c 2130    8 -7.84 785 -786 754 -755
c 2131    8 -7.84 785 -786 755 -756
c 2132    8 -7.84 785 -786 756 -762
c 2133    8 -7.84 785 -786 762 -757
c 2134    8 -7.84 785 -786 757 -758
c 2135    8 -7.84 785 -786 758 -759
c 2136    8 -7.84 785 -786 759 -649
c 2137    8 -7.84 785 -786 649 -648
c 2138    8 -7.84 785 -786 648 -647
c 2139    8 -7.84 785 -786 647 -646
c 2140    8 -7.84 785 -786 646 -645
c 2141    8 -7.84 785 -786 645 -644
c 2142    8 -7.84 785 -786 644 -643
c 2143    8 -7.84 785 -786 643 -642
c
2144     0 785 -786 792 -147 #2288 #2286 #2287
2145     0 786 -676 -147 #1874 #2286 $ #2144
c
c 2146  8 -7.84 785 -786 642 -641
c
2147  9 -0.915 500 -499 780 -781    $ BEGINNING OF 30.5" DIA
2148  9 -0.915 500 -499 508 -780    $ BORATED POLY PIECE (RIGHT
2149  9 -0.915 500 -499 433 -508    $ NOW, IT'S JUST POLY)
2150  9 -0.915 500 -499 432 -433    $ AROUND Pb, RESTING ON TOP
2151  9 -0.915 500 -499 458 -432    $ OF PIG
2152  9 -0.915 500 -499 457 -458
2153  9 -0.915 500 -499 456 -457
2154  9 -0.915 500 -499 455 -456
2155  9 -0.915 500 -499 454 -455
2156  9 -0.915 501 -500 780 -781
2157  9 -0.915 501 -500 508 -780
2158  9 -0.915 501 -500 433 -508
2159  9 -0.915 501 -500 432 -433
2160  9 -0.915 501 -500 458 -432
2161  9 -0.915 501 -500 457 -458
2162  9 -0.915 501 -500 456 -457
2163  9 -0.915 501 -500 455 -456
2164  9 -0.915 501 -500 454 -455
2165  9 -0.915 502 -501 780 -781
2166  9 -0.915 502 -501 508 -780
2167  9 -0.915 502 -501 433 -508
2168  9 -0.915 502 -501 432 -433
2169  9 -0.915 502 -501 458 -432
2170  9 -0.915 502 -501 457 -458
2171  9 -0.915 502 -501 456 -457
2172  9 -0.915 502 -501 455 -456
2173  9 -0.915 502 -501 454 -455
2174  9 -0.915 503 -502 780 -781
2175  9 -0.915 503 -502 508 -780
2176  9 -0.915 503 -502 433 -508
2177  9 -0.915 503 -502 432 -433
2178  9 -0.915 503 -502 458 -432
2179  9 -0.915 503 -502 457 -458
2180  9 -0.915 503 -502 456 -457
2181  9 -0.915 503 -502 455 -456
2182  9 -0.915 503 -502 454 -455
2183  9 -0.915 504 -503 780 -781
2184  9 -0.915 504 -503 508 -780
2185  9 -0.915 504 -503 433 -508
2186  9 -0.915 504 -503 432 -433
2187  9 -0.915 504 -503 458 -432
2188  9 -0.915 504 -503 457 -458
2189  9 -0.915 504 -503 456 -457
2190  9 -0.915 504 -503 455 -456
2191  9 -0.915 504 -503 454 -455
c
2192  9 -0.915 504 -503 781 -782
2193  9 -0.915 503 -502 781 -782
2194  9 -0.915 502 -501 781 -782
```

```
2195   9 -0.915 501 -500 781 -782
2196   9 -0.915 500 -499 781 -782    $ END OF 30.5" DIA POLY
c
2197   9 -0.915 686 -504 432 -433    $ BEGINNING OF 2, 2FT DIA
2198   9 -0.915 686 -504 458 -432    $ PIECES OF POLY ON TOP
2199   9 -0.915 686 -504 457 -458    $ OF Pb
2200   9 -0.915 686 -504 456 -457
2201   9 -0.915 686 -504 455 -456
2202   9 -0.915 686 -504 454 -455
2203   9 -0.915 687 -686 432 -433
2204   9 -0.915 687 -686 458 -432
2205   9 -0.915 687 -686 457 -458
2206   9 -0.915 687 -686 456 -457
2207   9 -0.915 687 -686 455 -456
2208   9 -0.915 687 -686 454 -455
2209   9 -0.915 688 -687 432 -433
2210   9 -0.915 688 -687 458 -432
2211   9 -0.915 688 -687 457 -458
2212   9 -0.915 688 -687 456 -457
2213   9 -0.915 688 -687 455 -456
2214   9 -0.915 688 -687 454 -455
2215   9 -0.915 689 -688 432 -433
2216   9 -0.915 689 -688 458 -432
2217   9 -0.915 689 -688 457 -458
2218   9 -0.915 689 -688 456 -457
2219   9 -0.915 689 -688 455 -456
2220   9 -0.915 689 -688 454 -455
2221   9 -0.915 690 -689 432 -433
2222   9 -0.915 690 -689 458 -432
2223   9 -0.915 690 -689 457 -458
2224   9 -0.915 690 -689 456 -457
2225   9 -0.915 690 -689 455 -456
2226   9 -0.915 690 -689 454 -455
2227   9 -0.915 691 -690 432 -433
2228   9 -0.915 691 -690 458 -432
2229   9 -0.915 691 -690 457 -458
2230   9 -0.915 691 -690 456 -457
2231   9 -0.915 691 -690 455 -456
2232   9 -0.915 691 -690 454 -455
2233   9 -0.915 693 -691 432 -433
2234   9 -0.915 693 -691 458 -432
2235   9 -0.915 693 -691 457 -458
2236   9 -0.915 693 -691 456 -457
2237   9 -0.915 693 -691 455 -456
2238   9 -0.915 693 -691 454 -455
2239   9 -0.915 694 -693 432 -433
2240   9 -0.915 694 -693 458 -432
2241   9 -0.915 694 -693 457 -458
2242   9 -0.915 694 -693 456 -457
2243   9 -0.915 694 -693 455 -456
2244   9 -0.915 694 -693 454 -455
2245   9 -0.915 695 -694 432 -433
2246   9 -0.915 695 -694 458 -432
2247   9 -0.915 695 -694 457 -458
2248   9 -0.915 695 -694 456 -457
2249   9 -0.915 695 -694 455 -456
2250   9 -0.915 695 -694 454 -455
c
2251   0 734 -716 454 -147
c
2252   9 -0.915 696 -695 456 -457
2253   9 -0.915 696 -695 455 -456
2254   9 -0.915 696 -695 454 -455
2255   9 -0.915 697 -696 456 -457
2256   9 -0.915 697 -696 455 -456
2257   9 -0.915 697 -696 454 -455
2258   9 -0.915 698 -697 456 -457
2259   9 -0.915 698 -697 455 -456
2260   9 -0.915 698 -697 454 -455
2261   9 -0.915 699 -698 456 -457
2262   9 -0.915 699 -698 455 -456
2263   9 -0.915 699 -698 454 -455
```

```
2264  9 -0.915 700 -699 456 -457
2265  9 -0.915 700 -699 455 -456
2266  9 -0.915 700 -699 454 -455
2267  9 -0.915 701 -700 456 -457
2268  9 -0.915 701 -700 455 -456
2269  9 -0.915 701 -700 454 -455
2270  9 -0.915 702 -701 456 -457
2271  9 -0.915 702 -701 455 -456
2272  9 -0.915 702 -701 454 -455
2273  9 -0.915 703 -702 456 -457
2274  9 -0.915 703 -702 455 -456
2275  9 -0.915 703 -702 454 -455
2276  9 -0.915 704 -703 456 -457
2277  9 -0.915 704 -703 455 -456
2278  9 -0.915 704 -703 454 -455
2279  9 -0.915 705 -704 456 -457
2280  9 -0.915 705 -704 455 -456
2281  9 -0.915 705 -704 454 -455
2282  9 -0.915 739 -705 456 -457
2283  9 -0.915 739 -705 455 -456
2284  9 -0.915 739 -705 454 -455
c
2285  0 739 -695 457 -147
c
2286  8 -7.84 -792 $ #2120
c
2287  8 -7.84 -793 #2286 #2145 #2290
c
2288  8 -7.84 -794 #2286 #2145 #2292
c
2289  8 -7.84 -795 #2290
c
2290  8 -7.84 -796
c
2291  8 -7.84 -797 #2292
c
2292  8 -7.84 -798
c
2293  8 -7.84 -800 801
c
2294  0 -801
c
2295  1 -7.9 -1 900 23 -22   $ INNER MITL EXTENSION
2296  1 -7.9 -900 901 23 -22
2297  1 -7.9 -901 902 23 -22
2298  1 -7.9 -902 903 23 -22
2299  1 -7.9 -903 904 23 -22
2300  1 -7.9 -904 905 23 -22
c 2301  0 144 -146 -1 909
2302  0 -928 26 -147
2303  1 -7.9 -1 900 -144 143   $ OUTER MITL EXTENSION
2304  1 -7.9 -900 901 -144 143
2305  1 -7.9 -901 902 -144 143
2306  1 -7.9 -902 903 -144 143
2307  1 -7.9 -903 904 -144 143
2308  1 -7.9 -904 905 -144 143
2309  1 -7.9 -905 906 -144 143
2310  1 -7.9 -906 907 -144 143
2311  1 -7.9 -907 908 -144 143
c
2312  1 -7.9 -1 900 -147 146  $ EXTENSION OF STACK
2313  1 -7.9 -900 901 -147 146
2314  1 -7.9 -901 902 -147 146
2315  1 -7.9 -902 903 -147 146
2316  1 -7.9 -903 904 -147 146
2317  1 -7.9 -904 905 -147 146
2318  1 -7.9 -905 906 -147 146
2319  1 -7.9 -906 907 -147 146
2320  1 -7.9 -907 908 -147 146
c
2321  1 -7.9 -909 908 144 -752
2322  1 -7.9 -909 908 752 -753
```

```
2323  1 -7.9 -909 908 753 -754
2324  1 -7.9 -909 908 754 -755
2325  1 -7.9 -909 908 755 -756
2326  1 -7.9 -909 908 756 -757
2327  1 -7.9 -909 908 757 -758
2328  1 -7.9 -909 908 758 -759
2329  1 -7.9 -909 908 759 -649
2330  1 -7.9 -909 908 649 -648
2331  1 -7.9 -909 908 648 -647
2332  1 -7.9 -909 908 647 -646
2333  1 -7.9 -909 908 646 -645
2334  1 -7.9 -909 908 645 -644
2335  1 -7.9 -909 908 644 -643
2336  1 -7.9 -909 908 643 -642
2337  1 -7.9 -909 908 642 -641
2338  1 -7.9 -909 908 641 -640
2339  1 -7.9 -909 908 640 -639
2340  1 -7.9 -909 908 639 -638
2341  1 -7.9 -909 908 638 -637
2342  1 -7.9 -909 908 637 -636
2343  1 -7.9 -909 908 636 -635
2344  1 -7.9 -909 908 635 -634
2345  1 -7.9 -909 908 634 -633
2346  1 -7.9 -909 908 633 -632
2347  1 -7.9 -909 908 632 -631
2348  1 -7.9 -909 908 631 -630
2349  1 -7.9 -909 908 630 -629
2350  1 -7.9 -909 908 629 -628
2351  1 -7.9 -909 908 628 -627
2352  1 -7.9 -909 908 627 -626
2353  1 -7.9 -909 908 626 -625
2354  1 -7.9 -909 908 625 -624
2355  1 -7.9 -909 908 624 -623
2356  1 -7.9 -909 908 623 -622
2357  1 -7.9 -909 908 622 -621
2358  1 -7.9 -909 908 621 -620
2359  1 -7.9 -909 908 620 -619
2360  1 -7.9 -909 908 619 -618
2361  1 -7.9 -909 908 618 -617
2362  1 -7.9 -909 908 617 -616
2363  1 -7.9 -909 908 616 -615
2364  1 -7.9 -909 908 615 -614
2365  1 -7.9 -909 908 614 -613
2366  1 -7.9 -909 908 613 -612
2367  1 -7.9 -909 908 612 -611
2368  1 -7.9 -909 908 611 -610
2369  1 -7.9 -909 908 610 -609
2370  1 -7.9 -909 908 609 -608
2371  1 -7.9 -909 908 608 -607
2372  1 -7.9 -909 908 607 -606
2373  1 -7.9 -909 908 606 -605
2374  1 -7.9 -909 908 605 -604
2375  1 -7.9 -909 908 604 -603
2376  1 -7.9 -909 908 603 -602
2377  1 -7.9 -909 908 602 -601
2378  1 -7.9 -909 908 601 -146
c
2379  0 -905 908 -22
c
2380  1 -7.9 754 -926 -908 910  $ DEBRIS SHIELD (1/2" THICK SS)
2381  1 -7.9 754 -926 -910 911
2382  1 -7.9 754 -926 -911 912
2383  1 -7.9 754 -926 -912 913
2384  1 -7.9 754 -926 -913 914
2385  1 -7.9 754 -926 -914 915
2386  1 -7.9 754 -926 -915 916
2387  1 -7.9 754 -926 -916 917
2388  1 -7.9 754 -926 -917 918
2389  1 -7.9 754 -926 -918 919
2390  1 -7.9 754 -926 -919 920
2391  1 -7.9 754 -926 -920 921
2392  1 -7.9 754 -926 -921 922
```

```
2393  1 -7.9 754 -926 -922 923
2394  1 -7.9 754 -926 -923 924
2395  4 -8.96 -924 925 -760     $ COPPER LID ON DEBRIS SHIELD
2396  4 -8.96 -924 925 760 -761
2397  4 -8.96 -924 925 761 -748
2398  4 -8.96 -924 925 748 -749
2399  4 -8.96 -924 925 749 -750
2400  4 -8.96 -924 925 750 -751
2401  4 -8.96 -924 925 751 -752
2402  4 -8.96 -924 925 752 -753
2403  4 -8.96 -924 925 753 -754
2404  4 -8.96 -924 925 754 -755  $ COPPER LID ON DEBRIS SHIELD
2405  1 -7.9 -927 924 926 -762   $ RINGS ON TOP OF DEBRIS SHIELD
2406  1 -7.9 -925 928 926 -762
2407  0 -908 924 -754 936            $ VOID INSIDE DEBRIS SHIELD
2408  0 -908 927 926 -762
2409  0 -924 925 755 -762
2410  0 -908 928 762 -146
2411  0 -925 928 -926
c
2412  1 -7.9 146 -147 -908 910   $ EXTENSION OF STACK TO TOP OF
2413  1 -7.9 146 -147 -910 911   $ DEBRIS SHIELD
2414  1 -7.9 146 -147 -911 912
2415  1 -7.9 146 -147 -912 913
2416  1 -7.9 146 -147 -913 914
2417  1 -7.9 146 -147 -914 915
2418  1 -7.9 146 -147 -915 916
2419  1 -7.9 146 -147 -916 917
2420  1 -7.9 146 -147 -917 918
2421  1 -7.9 146 -147 -918 919
2422  1 -7.9 146 -147 -919 920
2423  1 -7.9 146 -147 -920 921
2424  1 -7.9 146 -147 -921 922
2425  1 -7.9 146 -147 -922 923
2426  1 -7.9 146 -147 -923 924
2427  1 -7.9 146 -147 -924 925
2428  1 -7.9 146 -147 -925 928
c
2429  10 -1.19 18 -460 931 -452 929 -930
2430  10 -1.19 18 -460 452 -454 929 -930
2431  10 -1.19 18 -460 454 -456 929 -930
2432  7 -2.7 671 -18 931 -456 929 -930
2433  7 -2.7 460 -672 931 -456 929 -930
2434  0 671 -672 669 -431 933 -932
2435  7 -2.7 671 -672 933 -929 -669
2436  7 -2.7 671 -672 930 -932 -669
2437  0 671 -672 932 -431
2438  0 671 -672 -933 -431
c
2439  0 -936  $ LOCATION OF SOURCE
c
2440  0 937 -489 137 -450
c
c 2441  0 26 -677 147 -938     $ OUTSIDE MACHINE
c 2442  0 -26 939 -938         $   "        "
c 2443  0 677 -940 -938        $   "        "
c 2444  0 -939:940:938         $ UNIVERSE OUTSIDE -- KILL ZONE
c 2445  0 941 -942 -943 944 -945   $ COOKIE-CUTTER CELL
c
2441  0 -26:677:147                $ Universe outside -- Kill Zone

c  ***************************************************************************
c     SURFACES
1     py 0.0
2     py 0.635
3     py 1.905
4     py 2.54
5     py 3.81
6     py 4.445
7     py 5.715
8     py 6.35
9     py 7.62
```

```
10    py 8.89
11    cy 3.175              $ 2.5" hole thru top SS plate
12    cy 8.89
13    py 10.16
c 14    py 35.16
c 15    py 58.89
16    py 127.6096
17    py 150.0632
18    1 py 56.48544
c 19    py 719.62
20    cy 121.963180
21    cy 125.215904
22    ky -28.909206 0.64 1   $ Outer MITL Cone
23    ky -24.843329 0.64 1   $ Inner MITL Cone
24    cy 6.35                $ Cylinder to match original
c                              Tungsten insert
25    ky -129.54 0.000517 1  $ Collimator Cone
c
26    py -62.0   $ Plane above Debris Shield
27    py 11.43
28    py 12.7
29    py 13.97
30    py 15.24
31    py 16.51
32    py 17.78
33    py 19.05
34    py 20.32
35    py 21.59
36    py 22.86
37    py 24.13
38    py 25.4
39    py 26.67
40    py 27.94
41    py 29.21
42    py 30.48
43    py 31.75
44    py 33.02
45    py 34.29
46    py 35.56
47    py 36.83
48    py 38.1
49    py 39.37
50    py 40.64
51    py 41.91
52    py 43.18
53    py 44.45
54    py 45.72
55    py 46.99
56    py 48.26
57    py 49.53
58    py 50.8
59    py 52.07
60    py 53.34
61    py 54.61
62    py 55.88
63    py 57.15
64    py 58.42
65    py 59.69
66    py 60.96
67    py 62.23
68    py 63.5
69    py 64.77
70    py 66.04
71    py 67.31
72    py 68.58
73    py 69.85
74    py 71.12
75    py 72.39
76    py 73.66
77    py 74.93
78    py 76.2
79    py 77.47
```

```
80     py 78.74
81     py 80.01
82     py 81.28
83     py 82.55
84     py 83.82
85     py 85.09
86     py 86.36
87     py 87.63
88     py 88.9
89     py 90.17
90     py 91.44
91     py 92.71
92     py 93.98
93     py 95.25
94     py 96.52
95     py 97.79
96     py 99.06
97     py 100.33
98     py 101.6
99     py 102.87
100    py 104.14
101    py 105.41
102    py 106.68
103    py 107.95
104    py 109.22
105    py 110.49
106    py 111.76
107    py 113.0
108    py 114.3
109    py 115.57
110    py 116.84
111    py 118.11
112    py 119.38
113    py 120.65
114    py 121.92
115    py 123.19
116    py 124.46
117    py 125.73
c 118    py 127.6096
119    py 128.8796
120    py 130.1496
121    py 131.4196
122    py 132.6896
123    py 133.9596
124    py 135.2296
125    py 136.4996
126    py 137.7696
127    py 139.0396
128    py 140.3096
129    py 141.5796
130    py 142.8496
131    py 144.1196
132    py 145.3896
133    py 146.6596
134    py 147.9296
135    py 149.1996
c 136    py 150.0632
137    1 cy 3.81                   $ OUTER DIA OF SCINTILLATOR
c 138    cy 54.61
139    py 60.97
140    cy 18.0
141    ky -20.777452 0.64 1    $ Cone for space b/w TIVAR & MITL
142    ky -30.48 0.021207 1    $ TIVAR cone to shadow pig
c                              to twice it's radius
c
143    ky -30.545720 0.6780965 1    $ Inner MITL Cone #2
144    ky -35.541454 0.6780965 1    $ Outer MITL Cone #2
145    py 139.336834                $ Base of MITL Cone #2
146    cy 160.02                    $ Radius of Stack (5' 3")
147    cy 162.56                    $ Outer radius of stack (1" thick)
148    py 500.4562                  $ Bottom of Stack
149    py 188.55436                 $ Bottom of MITL #1 Cylinder
```

```
c
150    py 151.3332
151    py 152.6032
152    py 153.8732
153    py 155.1432
154    py 156.4132
155    py 157.6832
156    py 158.9532
157    py 160.2232
158    py 161.4932
159    py 162.7632
160    py 164.0332
161    py 165.3032
162    py 166.5732
163    py 167.8432
164    py 169.1132
165    py 170.3832
166    py 171.6532
167    py 172.9232
168    py 174.1332
169    py 175.4632
170    py 176.7332
171    py 178.0032
172    py 179.2732
173    py 180.5432
174    py 181.8132
175    py 183.0832
176    py 184.3532
177    py 185.6232
178    py 186.8932
179    py 188.1632
c
180    py 190.0
181    py 191.25
182    py 192.5
183    py 193.75
184    py 195.0
185    py 196.25
186    py 197.5
187    py 198.75
188    py 200.0
189    py 201.25
190    py 202.5
191    py 203.75
192    py 205.0
193    py 206.25
194    py 207.5
195    py 208.75
196    py 210.0
197    py 211.25
198    py 212.5
199    py 213.75
200    py 215.0
201    py 216.25
202    py 217.5
203    py 218.75
204    py 220.0
205    py 221.25
206    py 222.5
207    py 223.75
208    py 225.0
209    py 226.25
210    py 227.5
211    py 228.75
212    py 230.0
213    py 231.25
214    py 232.5
215    py 233.75
216    py 235.0
c
217    py 236.25
218    py 237.5
```

```
219    py  238.75
220    py  240.0
221    py  241.25
222    py  242.5
223    py  243.75
224    py  245.0
225    py  246.25
226    py  247.5
227    py  248.75
228    py  250.0
229    py  251.25
230    py  252.5
231    py  253.75
232    py  255.0
233    py  256.25
234    py  257.5
235    py  258.75
236    py  260.0
237    py  261.25
238    py  262.5
239    py  263.75
240    py  265.0
241    py  266.25
242    py  267.5
243    py  268.75
244    py  270.0
245    py  271.25
246    py  272.5
247    py  273.75
248    py  275.0
249    py  276.25
250    py  277.5
251    py  278.75
252    py  280.0
253    py  281.25
254    py  282.5
255    py  283.75
256    py  285.0
257    py  286.25
258    py  287.5
259    py  288.75
260    py  290.0
261    py  291.25
262    py  292.5
263    py  293.75
264    py  295.0
265    py  296.25
266    py  297.5
267    py  298.75
268    py  300.0
269    py  301.25
270    py  302.5
271    py  303.75
272    py  305.0
273    py  306.25
274    py  307.5
275    py  308.75
276    py  310.0
277    py  311.25
278    py  312.5
279    py  313.75
280    py  315.0
281    py  316.25
282    py  317.5
283    py  318.75
284    py  320.0
285    py  321.25
286    py  322.5
287    py  323.75
288    py  325.0
289    py  326.25
290    py  327.5
```

```
291     py 328.75
292     py 330.0
293     py 331.25
294     py 332.5
295     py 333.75
296     py 335.0
297     py 336.25
298     py 337.5
299     py 338.75
300     py 340.0
301     py 341.25
302     py 342.5
303     py 343.75
304     py 345.0
305     py 346.75
306     py 347.5
307     py 348.75
308     py 350.0
309     py 351.25
310     py 352.5
311     py 353.75
312     py 355.0
313     py 356.25
314     py 357.5
315     py 358.75
316     py 360.0
317     py 361.25
318     py 362.5
319     py 363.75
320     py 365.0
321     py 366.25
322     py 367.5
323     py 368.75
324     py 370.0
325     py 371.25
326     py 372.5
327     py 373.75
328     py 375.0
329     py 376.25
330     py 377.5
331     py 378.75
332     py 380.0
333     py 381.25
334     py 382.5
335     py 383.75
336     py 385.0
337     py 386.25
338     py 387.5
339     py 388.75
340     py 390.0
341     py 391.25
342     py 392.5
343     py 393.75
344     py 395.0
345     py 396.25
346     py 397.5
347     py 398.75
348     py 400.0
349     py 401.25
350     py 402.5
351     py 403.75
352     py 405.0
353     py 406.25
354     py 407.5
355     py 408.75
356     py 410.0
357     py 411.25
358     py 412.5
359     py 413.75
360     py 415.0
361     py 416.25
362     py 417.5
```

```
363    py 418.75
364    py 420.0
365    py 421.25
366    py 422.5
367    py 423.75
368    py 425.0
369    py 426.25
370    py 427.5
371    py 428.75
372    py 430.0
373    py 431.25
374    py 432.5
375    py 433.75
376    py 435.0
377    py 436.25
378    py 437.5
379    py 438.75
380    py 440.0
381    py 441.25
382    py 442.5
383    py 443.75
384    py 445.0
385    py 446.25
386    py 447.5
387    py 448.75
388    py 450.0
389    py 451.25
390    py 452.5
391    py 453.75
392    py 455.0
393    py 456.25
394    py 457.5
395    py 458.75
396    py 460.0
397    py 461.25
398    py 462.5
399    py 463.75
400    py 465.0
401    py 466.25
402    py 467.5
403    py 468.75
404    py 470.0
405    py 471.25
406    py 472.5
407    py 473.75
408    py 475.0
409    py 476.25
410    py 477.5
411    py 478.75
412    py 480.0
413    py 481.25
414    py 482.5
415    py 483.75
416    py 485.0
417    py 486.25
418    py 487.5
419    py 488.75
420    py 490.0
421    py 491.25
422    py 492.5
423    py 493.75
424    py 495.0
425    py 496.25
426    py 497.5
427    py 498.75
c
428    1 py 71.72544
429    1 py 74.26544
430    1 py 76.80544  $ BOTTOM OF PIG
431    1 cy 26.67    $ ID of Pb/W "Box"; 21" ID
432    1 cy 27.94
433    1 cy 30.48
```

```
c
434   1 py 26.00544
435   1 py 28.54544
436   1 py 31.08544
437   1 py 33.62544
438   1 py 36.16544
439   1 py 38.70544
440   1 py 41.24544
441   1 py 43.78544
442   1 py 46.32544
443   1 py 48.86544
444   1 py 51.40544
445   1 py 53.94544
446   1 py 61.56544
447   1 py 64.10544
448   1 py 66.64544
449   1 py 69.18544
450   1 cy 5.08
451   1 cy 7.62
452   1 cy 10.16
453   1 cy 12.7
454   1 cy 15.24
455   1 cy 17.78
456   1 cy 20.32
457   1 cy 22.86
458   1 cy 25.40
c 459   cy 27.94  $ Same as 432
460   1 py 59.025440
461   1 cy 1.27
c
c 462   py 719.5225
c
c 463   py 699.78
c 464   py 702.32
c 465   py 704.86
c 466   py 707.40
c 467   py 709.94
c 468   py 712.48
c 469   py 715.02
c 470   py 717.56
c
471   1 py -1.934560
c
472   1 py 0.0   $ PIVOT POINT OF PIG
473   1 py 3.14544
474   1 py 5.68544
475   1 py 8.22544
476   1 py 10.76544
477   1 py 13.30544
478   1 py 15.84544
479   1 py 18.38544
480   1 py 20.92544
481   1 py 23.46544
c
482   1 py -5.05206
483   1 py -7.59206
484   1 py -10.13206
485   1 py -12.67206
486   1 py -15.21206
487   1 py -17.75206
488   1 py -20.29206
489   1 py -22.83206
490   1 py -25.37206
491   1 py -27.91206
492   1 py -30.45206
493   1 py -32.99206
494   1 py -35.53206
495   1 py -38.07206
496   1 py -40.61206
497   1 py -43.15206
498   1 py -45.69206
499   1 py -48.23206
```

```
c
500   1 py -50.77206
501   1 py -53.31206
502   1 py -55.85206
503   1 py -58.39206
c
504   1 py -60.93206
c
c 505   py 636.28
c 506   py 633.74
c 507   py 631.20
508   1 cy 33.02
c
509   1 cy 34.29    $ RADIUS OF PIG
c
c 510   cy 30.48     $ Outer dia of TIVAR (2ft dia); same as 433
c
c   ******************* BOTTOM LID ADDITION ***********************
c
600   py 498.5512  $ Vacuum Side of Bottom Lid (3/4" thick)
601   cy 157.48
602   cy 154.94
603   cy 152.40
604   cy 149.86
605   cy 147.32
606   cy 144.78
607   cy 142.24
608   cy 139.70
609   cy 137.16
610   cy 134.62
611   cy 132.08
612   cy 129.54
613   cy 127.00
614   cy 124.46
615   cy 121.92
616   cy 119.38
617   cy 116.84
618   cy 114.30
619   cy 111.76
620   cy 109.22
621   cy 106.68
622   cy 104.14
623   cy 101.60
624   cy 99.06
625   cy 96.52
626   cy 93.98
627   cy 91.44
628   cy 88.90
629   cy 86.36
630   cy 83.82
631   cy 81.28
632   cy 78.74
633   cy 76.20
634   cy 73.66
635   cy 71.12
636   cy 68.58
637   cy 66.04
638   cy 63.50
639   cy 60.96
640   cy 58.42
641   cy 55.88
642   cy 53.34
643   cy 50.80
644   cy 48.26
645   cy 45.72
646   cy 43.18
647   cy 40.64
648   cy 38.10
649   cy 35.56
c 650   cy 33.02  $ SAME AS 508
c 651   cy 30.48  $ SAME AS 433
c 652   cy 27.94  $ SAME AS 432
```

```
c 653   cy 25.40  $ SAME AS 458
c 654   cy 22.86  $ SAME AS 457
c 655   cy 20.32  $ SAME AS 456
c 656   cy 17.78  $ SAME AS 455
c 657   cy 15.24  $ SAME AS 454
c 658   cy 12.70  $ SAME AS 453
c 659   cy 10.16  $ SAME AS 452
c 660   cy 7.62  $ SAME AS 451
c 661   cy 5.08   $ SAME AS 450
662   py 502.3612
663   py 504.1392
664   py 497.12245  $ 9/16" SHIELD PLATE
665   cy 2.54
666   1 py -22.51456
667   1 py -19.97456
668   1 py -19.65706  $ ****** END OF BOTTOM LID ADDITION ******
c
669   1 cy 20.955
670   1 py -21.24456
c
671   1 py 56.16794
672   1 py 59.34294
673   1 py 57.75544
c
c 674   cy 2.54  $ 2" HOLE THRU COPPER PLATES
c
675   py 495.6937  $ 9/16" COPPER PLATE ABOVE SHIELD PLATE
c
676   py 850.275   $ ELEVATOR FLOOR 20.25" B/L PIG
677   py 852.815   $ THICKNESS OF ELEVATOR (1")
c
678   1 cy 29.21  $ TO "STAGGER" W PLUG
c
679   1 py -39.34206
c
c     *************************************************
c     NOTE: SIDE PLATES ON PIG ARE IN CORRECT POSITION
c     (i.e., ON SIDES WHERE YOKE ATTACHES)
c
680   pz 35.56    $ OUTER PLANE OF SIDE PLATES ON PIG
c
681   1 px -19.685    $ WIDTH OF SIDE PLATES 7.75"
682   1 px 19.685     $   "   "    "    "     "
683   pz 28.076768
c
684   pz -35.56   $ OUTER PLANE OF SIDE PLATES ON PIG
685   pz -28.076768
c
c     *************************************************
c
686   1 py -63.47206
687   1 py -66.01206
688   1 py -68.55206
689   1 py -71.09206
690   1 py -73.63206
c
691   1 py -76.17206
c
692   1 cy 3.811  $ SURFACE 692 TRANSFORMED BELOW
c
693   1 py -78.71206
694   1 py -81.25206
695   1 py -83.15706
696   1 py -86.01456
697   1 py -88.87206
698   1 py -91.41206
699   1 py -93.95206
700   1 py -96.49206
701   1 py -99.03206
702   1 py -101.57206
703   1 py -104.11206
704   1 py -106.65206
```

```
705   1 py -109.19206
706   1 py -111.73206
707   1 py -114.27206
708   1 py -116.81206
709   1 py -119.35206
710   1 py -121.89206
711   1 py -124.43206
712   1 py -126.97206
713   1 py -129.51206
714   1 py -132.05206
715   1 py -134.59206
716   1 py -136.49706
717   1 py -139.67206
718   1 py -142.21206
719   1 py -144.75206
720   1 py -147.29206
c 721   1 py -149.83206
c 722   1 py -152.37206
c
723   1 py -120.62206
724   1 py -123.16206
725   1 py -125.70206
726   1 py -128.24206
727   1 py -130.78206
728   1 py -133.32206
729   1 py -135.86206
730   1 py -138.40206
731   1 py -140.94206
732   1 py -143.48206
733   1 py -146.02206
734   1 py -148.56206
c 735   1 py -151.10206
c
736   1 py -118.08206
737   1 py -115.54206
738   1 py -113.00206
739   1 py -110.46206
740   1 py -107.92206
741   1 py -105.38206
742   1 py -102.84206
743   1 py -100.30206
744   1 py -97.76206
745   1 py -95.22206
746   1 py -92.68206
747   1 py -90.14206
c
748   cy 5.08   $ SAME AS 450 B/F TRANSLATION
749   cy 7.62   $  "    " 451  "        "
750   cy 10.16  $  "    " 452  "        "
751   cy 12.7   $  "    " 453  "        "
752   cy 15.24  $  "    " 454  "        "
753   cy 17.78  $  "    " 455  "        "
754   cy 20.32  $  "    " 456  "        "
755   cy 22.86  $  "    " 457  "        "
756   cy 25.4   $  "    " 458  "        "
757   cy 27.94  $  "    " 432  "        "
758   cy 30.48  $  "    " 433  "        "
759   cy 33.02  $  "    " 508  "        "
760   cy 1.27   $  "    " 461  "        "
761   cy 3.81   $  "    " 137  "        "
762   cy 26.67  $  "    " 431  "        "
c
763   c/y 27.94 0 2.54  $ x z R
764   c/y 27.94 0 5.08
765   c/y 27.94 0 7.62
766   c/y 27.94 0 10.16
767   c/y 27.94 0 12.7
c
c 768   1 py -154.91206  $ SURFACES FOR 4 FOOT
c 769   1 py -157.45206  $ POLY COLLIMATOR
c 770   1 py -159.99206  $ (TURNS OUT, 4 FEET IS
c 771   1 py -162.53206  $ TOO LONG)
```

```
c 772   1 py -165.07206
c 773   1 py -167.61206
c 774   1 py -170.15206
c 775   1 py -172.69206
c 776   1 py -175.23206
c 777   1 py -177.77206
c 778   1 py -180.31206
c 779   1 py -182.85206
c
780   1 cy 35.56
781   1 cy 38.1
c
782   1 cy 38.735
c
784   py 819.82456001
785   py 822.3645999     $ 822.2
786   py 823.634567
c
c 787   cy 55.88
c
c 788   px 55.88
c 789   pz 55.88
c
c 790   px -55.88
c 791   pz -55.88
c
c    BOTTOM CHASSIS OF PIG:
c
792  BOX -41.91 822.36456001 -41.91001  83.820001 0 0  0 1.27 0  0 0 83.82
c
793  2 BOX -39.437617 -13.9699901 0  83.82 0 0  0 16.001 0  0 0 1.2701
c
794  3 BOX -39.437617 -13.970001 -1.3  83.82001 0 0  0 16 0  0 0 1.27
c
795  BOX -41.91 801 -54.1  83.82 0 0  0 11.43 0   0 0 1.27001
c
796  BOX -41.91 811.59 -54.101  83.8201 0 0  0 1.27 0   0 0 3.29
c
797  BOX -41.91 801 52.9  83.81999 0 0  0 11.43 0   0 0 1.27
c
798  BOX -41.91 811.5 50.87  83.820001 0 0  0 1.27 0   0 0 3.3
c
799  BOX -19.85 819.82456 -19.587517 39.7002 0 0  0 2.54 0  0 0 39.7002
c
c    BOTTOM OF YOKE: 4" x 8" x 1/4"
c
800  BOX -10.16 809.66456 -39.37  20.32 0 0  0 10.16 0  0 0 78.74
c
801  BOX -9.525 810.29956 -39.37  19.05 0 0  0 8.89 0  0 0 78.74
c
c   **** SURFACES TO EXTEND MITL CONES/DEBRIS SHIELD ****
900  py -1.82
901  py -4.36
902  py -6.9
903  py -9.44
904  py -11.98
905  py -14.521
906  py -17.061
907  py -19.601
908  py -21.2985
909  py -18.7585
910  py -23.8385
911  py -26.3785
912  py -28.9185
913  py -31.4585
914  py -33.9985
915  py -36.5385
916  py -39.0785
917  py -41.6185
918  py -44.1585
919  py -46.6985
920  py -49.2385
```

```
921  py -51.7785
922  py -54.3185
923  py -56.8585
924  py -57.4935  $ Top Inside Height of Copper Lid
925  py -60.0335  $ Top of Copper Lid (1" Thick)
926  cy 21.54     $ OD of DEBRIS SHIELD
927  py -56.2235
928  py -61.3035
c
929  1 pz -5.08
930  1 pz 5.08
931  1 cy 4.65
932  1 pz 5.715
933  1 pz -5.715
934  1 cz 62.8
935  1 cy 4.1275
936  sy -30.48 0.5  $ sy y R -- Location of Source
937  1 py -24.10206
c
c 938  cy 300.0
c 939  py -200.0
c 940  py 1000.0
c
c 941  py -100.0  $ Top of Cookie Cutter Cell
c 942  py 900.0  $ Bottom of Cookie Cutter Cell
c 943  4 px 0.001
c 944  4 pz 0.001
c 945  cy 180.0

c     isotropic fusion point source at (0,-30.48,0)
c
mode  n p
c
sdef  par=1 erg=d2 pos=0 -30.48 0 $ dir=d1 vec=0 1 0
c
c si1   -1 0.173648 1          $ Cone Bias -1 cos(theta) +1
c sp1   0 0.586824 0.413176    $ Cone Bias (theta = 80 deg)
c sb1   0 0.001 0.999          $ Cone Bias
sp2   -4 -0.002 -2           $ -4 Fusion Source; 0.002 MeV = 2keV;
c                              2 is DD Source, 1 is DT Source
c
c   Air at Sea Level (TO ILLUSTRATE SOURCE LOCATION)
c m11 7014.50c -0.765  &
c    8016.50c -0.235
c
c  Tungsten
m2 74000.55c 1
c
c  SCINTILLATOR [BC-418 OR BC-422Q]
m6 1001.60c 1.1 6000.60c 1          $ NOTE: CHANGED FROM .50c TO .60c
c
c  Copper Plates
m4 29000.50c 1
c
c  Lead
m5 82000.50c 1
c
c  Aluminum G-15 (MCNP5 Manual)
m7 13027.50c 1
c
c  High Molecular Weight Polyethelyne
c  TIVAR 1000
m3 1001.50c 2 6000.50c 1
c
c  Steel (FOR BOTTOM LID; 97.96% Fe, 2.04% C)
m8 26000.55c -0.9796 6000.50c -0.0204
c
c  Polyethylene Collimator on top of Pig (C2H4)
m9 1001.50c 4 6000.50c 2
c
c   Lucite Light Guides (Density = 1.19 g/cc)
m10 1001.60c -0.080538 6000.60c -0.599848 8016.60c -0.319614
```

```
c
c  Stainless Steel (67.5% Fe, 19% Cr, 10% Ni, 2% Mn, 1% Si, 0.5% Cu) G-13
m1 26000.55c -67.5  24000.50c -19.0  28000.50c -10.0  25055.51c -2.0 &
   14000.51c -1.0  29000.50c -0.5
c
c   ******************************************
c   CELL IMPORTANCES:
c
imp:n 1 1943r 0
c
imp:p 1 1943r 0
c
c   ******************************************
c
c **** CELL TRANSFORMATION CARD ****************
c    (FOR HOLE THRU POLY & PIG -- 3.0 DEGREE TILT)
c    PIG IS SET AT ACTUAL FIELDED POSITION, 3 DEG OFF AXIS
c
c     ORIGIN OF x', y', z' COORD SYSTEM:
c     39.437617 722.03456 0
c
c     HOWEVER, PUTTING PIG BACK ON AXIS,
c     SO NO TRANSFORMATION
c
c     x - x': 360.0 DEGREES
c     y - x': 270.0 DEGREES
c     z - x': 90    DEGREES
c
c     x - y': 90.0  DEGREES
c     y - y': 360.0 DEGREES
c     z - y': 90    DEGREES
c
c     x - z': 90 DEGREES
c     y - z': 90 DEGREES
c     z - z': 0  DEGREES
c
c
*TR1  39.437617 722.03456 0  357.0 267.0 90  87.0 357.0 90  90 90 0  1
c
c  ****************************
c
c **** CELL TRANSFORMATION CARDS (FOR PART OF CHASSIS) ****
c
*TR2  -2.472383 822.36456 -41.91  0 90 90  90 45 45 90 135 45 1
c
*TR3  -2.472383 822.36456 41.91  0 90 90  90 45 45 90 45 45 1
c
c  *** TRANSFORMATION FOR COOKIE CUTTER CELL ****
c
*TR4  0 0 0   45 90 135  90 0 90   135 90 225
c  ****************************
c  WEIGHT WINDOW GENERATOR CARD
c
WWG 5 0  $ Ask WW Generator to find weights
c          5 - Tally ; 1 - Source Cell; 0 - Use mesh-based
c          generator (MESH Card)
c
c  MESH-BASED WEIGHT WINDOW GENERATOR:
c
c  NOTE: ORIGIN AT LOWER LEFT; IMESH, JMESH, KMESH ARE COORDINATES
c        OF UPPER RIGHT, COVERING ALL GEOMETRY.
c
mesh geom rec origin -163 -62.5 -163 ref 0 -62.4 0
c
c **** NOTE: FOR MCNP4C, 2 COARSE MESHES PER DIRECTION ARE REQ'D!! ****
c
     imesh 0.0  163        iints   25  25  $ 2 COARSE MESHES B/W -163 TO 0.0
c                                               AND 0.0 TO +163
     jmesh 395.9  853      jints   25  25  $ 2 COARSE MESHES B/W -62.5 TO 395.9
c                                            AND 395.9 TO 853 <== TO ELEVATOR!!
     kmesh 0.0  163        kints   25  25  $ 2 COARSE MESHES B/W -163 TO 0.0
c                                            AND 0.0 TO 163
```

```
c
c      ****************************************
c
c      WEIGHT WINDOW PARAMETER CARD
c
c      WWP:n 4j -1    $ <=== -1 TO GET WT WINDOW LOWER BOUNDS
c                       FROM EXTERNAL WWINP FILE
c
c
c      ********** DXTRAN CARD ******************
c        **** TOP nTOF ****
c
c        NOTE: DIFFERENT COORDS x,y,z SINCE
c        TRANSFORMING PIG TO 3 DEGREE TILT
c
c        x          y   z  RI1 RI2 DWC1  DWC2 DPWT
c        |          |   |  |   |    |     |    |
DXT:n 42.464451 779.79 0 4.6 4.6 1000.0 0.0 0.001
c
c      1000.0 = UPPER WT CUTOFF IN SPHERE (DWC1)
c      0.0    = LOWER WT CUTOFF IN SPHERE (DWC2)
c      0.001  = MINIMUM PHOTON WT (DPWT)
c
c      *****************************************
c
c      ******** FORCED COLLISIONS CARD *********
c            FOR CELL 276 (SCINTILLATOR)
c
c      w/ xi = -1, FORCED COLLISION ONLY APPLIES
c            TO PARTICLES ENTERING THE CELL
c
c           xi = -1
c                |
FCL:n 0 204R -1 0 1738R
c
c
c
c      *****************************************
c       VOLUME CARD FOR SCINTILLATOR CELL (276)
c      (NEED TO INCLUDE IT B/C OF TRANSFORMATION;
c       F4 AND F6 TALLIES BELOW NEED IT)
c
VOL 205J 115.83333 1739J
c
c      *****************************************
c      PHOTON PRODUCTION BIAS CARD (PIKMT)
c
c      (LOOKING AT NEUTRON-INDUCED PHOTON PRODUCTION
c       NOTE: ALL PHOTON PRODUCTION DONE WITH NORMAL
c       SAMPLING TECHNIQUES)
c
c      PIKMT ZAID(1) ipik(1) mt(1) pmt(1)
c
c      ZAID FOR H
c        |
c        |   ipik > 0, photon production is biased for ZAID(1);
c        |   |
c        |   |         [if ipik = 0, photons produced from ZAID(1)
c        |   |         are done with normal sampling techniques]
c        |   |
c        |   |   MT = reaction identifier for the photon-production
c        |   |   |    to be sampled (in this case, 102 = n,gamma;
c        |   |   |    (only used if ipik>0)
c        |   |   |
c        |   |   | Controls the frequency with which the specified
c        |   |   | MT reactions are sampled (only used if ipik>0)
c        |   |   |  |
PIKMT 1001 0  $ 102 1
c
c       6000 0  $ <== photons produced from Carbon
c
c       13027 0 $ <== photons produced from Aluminum
```

```
c
c       26000 0 $ <== photons produced from Iron
c
c       74000 0 $ <== photons produced from Tungsten
c
c       82000 0 $ <== photons produced from Lead
c
c      *****************************************
c      PHOTON WEIGHT CARD (PWT) (COMMENTED OUT)
c
c      [CONTROLS THE NUMBER AND WEIGHT OF NEUTRON-INDUCED PHOTONS
c      PRODUCED AT NEUTRON COLLISIONS.  ONLY PROMPT PHOTONS ARE
c      PRODUCED FROM NEUTRON COLLISIONS.  DELAYED GAMMAS ARE
c      NEGLECTED BY MCNP.]
c
c      PWT W1 W2 W3 ... WI (DEFAULT VALUE: Wi = -1)
c
c      PWT  -1 1943r 0
c
c      *******************************************
c   TALLY n FLUX @ DETECTOR AND PIG:
c
c      F4 @ Detector:
f4:n   276
t4     35.5 36 36.1 36.2 36.3 36.4 36.5 36.6 36.7 36.8
       36.9 37.0 37.1 37.2 37.3 37.4 37.5 37.6 37.7 37.8
       37.9 38.0 38.1 38.2 38.3 38.4 38.5 38.6 38.7 38.8
       38.9 39.0 39.1 39.2 39.3 39.4 39.5 39.6 39.7 39.8
       39.9 40.0 40.1 40.2 40.3 40.4 40.5 40.6 40.7 40.8
       40.9 41.0 41.1 41.2 41.3 41.4 41.5 41.6 41.7 41.8
       41.9 42.0 42.1 42.2 42.3 42.4 42.5 42.6 42.7 42.8
       42.9 43.0 43.1 43.2 43.3 43.4 43.5 43.6 43.7 43.8
       43.9 44.0 44.1 44.2 44.3 44.4 44.5 44.6 44.7 44.8
       44.9 45.0 45.1 45.2 45.3 45.4 45.5 45.6 45.7 45.8
       45.9 46.0 46.1 46.2 46.3 46.4 46.5 46.6 46.7 46.8
       46.9 47.0 47.1 47.2 47.3 47.4 47.5 47.6 47.7 47.8
       47.9 48.0 48.1 48.2 48.3 48.4 48.5 48.6 48.7 48.8
       48.9 49.0 49.1 49.2 49.3 49.4 49.5 49.6 49.7 49.8
       49.9 50.0 50.1 50.2 50.3 50.4 50.5 50.6 50.7 50.8
       50.9 51.0 55.0 60.0 65.0 70.0 75.0 80.0 85.0 t
c
c      ********************************************************
c      POINT DETECTOR RIGHT IN THE MIDDLE OF THE SCINTILLATOR
c
c      Fn:pl x y z R0
c
c        x           y   z  R0
c        |           |   |  |
F5:n   42.464451 779.79 0 4.6
c
c                            $ 43.47 = x COORD OF PT DETECTOR
c                              (SAME AS DXTRAN SPHERE)
c
c                            $ 779.79 = Y COORD OF PT DETECTOR
c                              (SAME AS DXTRAN SPHERE)
c
c                            $ 0 = Z COORD OF PT DETECTOR
c
c                            $ R0 = RADIUS OF SPHERE OFEXCLUSION
c                        (INCLUDES SCINTILLATOR AND ALUMINUM SHELL;
c                         SAME AS DXTRAN SPHERE ABOVE)
c
c      *********************************************************
c
c      F6 ENERGY DEPOSITED IN SCINTILLATOR
f6:n   276
t6     35.5 36 36.1 36.2 36.3 36.4 36.5 36.6 36.7 36.8
       36.9 37.0 37.1 37.2 37.3 37.4 37.5 37.6 37.7 37.8
       37.9 38.0 38.1 38.2 38.3 38.4 38.5 38.6 38.7 38.8
       38.9 39.0 39.1 39.2 39.3 39.4 39.5 39.6 39.7 39.8
       39.9 40.0 40.1 40.2 40.3 40.4 40.5 40.6 40.7 40.8
       40.9 41.0 41.1 41.2 41.3 41.4 41.5 41.6 41.7 41.8
```

```
      41.9 42.0 42.1 42.2 42.3 42.4 42.5 42.6 42.7 42.8
      42.9 43.0 43.1 43.2 43.3 43.4 43.5 43.6 43.7 43.8
      43.9 44.0 44.1 44.2 44.3 44.4 44.5 44.6 44.7 44.8
      44.9 45.0 45.1 45.2 45.3 45.4 45.5 45.6 45.7 45.8
      45.9 46.0 46.1 46.2 46.3 46.4 46.5 46.6 46.7 46.8
      46.9 47.0 47.1 47.2 47.3 47.4 47.5 47.6 47.7 47.8
      47.9 48.0 48.1 48.2 48.3 48.4 48.5 48.6 48.7 48.8
      48.9 49.0 49.1 49.2 49.3 49.4 49.5 49.6 49.7 49.8
      49.9 50.0 50.1 50.2 50.3 50.4 50.5 50.6 50.7 50.8
      50.9 51.0 55.0 60.0 65.0 70.0 75.0 80.0 85.0 t
c
c
nps   1.0E+07     $ 10 Million Particles
c
PRINT   $ Print All Tables
c
cut:n 85 0     $ Time cutoff --
c                lower energy cutoff is zero MeV
c
c *********************** MCNP-POLIMI INFORMATION *************************
c
c
PHYS:N J 20.0
c
PHYS:P 0 1 1
c
CUT:P 85 J 0    $ CUT:P CARD JUST LIKE CUT:N CARD ABOVE (85 SHAKES)
c
IDUM 0 0 0 0 J 1 1 276
c
c   1st 0 -- SOURCE ENTIRELY DEFINED IN SDEF CARD
c   2ND 0 -- n'S SAMPLED AS IN STANDARD MCNP
c   3RD 0 -- n COLLISION AND PHOTON PRODUCTION NOT CORRELATED (STD MCNP)
c   4TH 0 -- FOR PHOTON EMISSION @ TIME OF FISSION FOR ALL FISSIONS
c   5TH J -- NOT USED
c   6TH 1 -- COLLISIONS PRINT OUT FOR HISTORIES IN AT LEAST "1" DETECTOR CELL
c   7TH 1 -- NUMBER OF CELLS (DETECTORS) FOR WHICH COLLISION DATA IS REQ'D
c   8TH 276 -- CELL NUMBER FOR COLLISION DATA PRINTOUT
c
RDUM 0.0 0.0      $ ENERGY DEP BY n'S MUST EXCEED 0.0 eV TO BE PRINTED
c                     "     "  "  p's  "       "   0.0  " "  "     "
c
FILES 21 DUMN1
c
c ***************************************************************************


c MESH TALLY   $ NO MESH TALLY TO SAVE TIME
tmesh
  rmesh1:n flux
    cora1 -162.56 100i 162.56
    corb1 -30.48 100i 739.84
    corc1 -162.56 162.56
endmd

c NOTE: REMOVING TRAKS AND POPUL MESH TALLIES
C       TO SHORTEN RUN TIME
  rmesh11:n traks
    cora11 -162.56 100i 162.56
    corb11 -30.48 100i 739.84
    corc11 -162.56 162.56
  rmesh21:n popul
    cora21 -162.56 100i 162.56
    corb21 -30.48 100i 739.84
    corc21 -162.56 162.56
endmd
```

APPENDIX B

THE nTOF POST-PROCESSING CODE

```
% Loads and analyzes MCNP-POLIMI output file

% nTOF -- THIS READS THE .DAT INPUT FILE
% AND CALCULATES THE LIGHT OUTPUT VS TIME IN SHAKES
%
% 15 columns of ascii output file have the following information:
% # of Start Event, Part #, Part Type, Reaction type (Ntyn), ZAID
collision nucleus, detector cell #,
% energy rel (MeV), time (shakes), x, y, z, wgt, generation #, #
scatterings, mtp or code, energy of
% particle prior to present collision

% note: in the variable names p=photon; n=neutron
%
%
% **************** GLOBAL VARIABLES
*********************************************
%
global  lonc ncal pcal data tmax nTOF coll maxrow
%
%
***********************************************************************
*******

disp(' ')
disp(' *** nTOF POST-PROCESSING CODE ***')
disp(' ')
%
% ****************************** INPUT BLOCK
******************************
%
%
%
%
% ****************** LIGHT OUTPUT OPTIONS ************************
%
% Light Output for n on hydrogen
ncal=[0.0364   0.125 0];
% Light Output for n on Carbon
lonc=0.02;
% Light Output for Gamma on Electron
lop=1;
% Parameters for Line in Calib: photons
pcal=[lop   0];
%
%
% ****************************** INPUT BLOCK
******************************
%
filen=input(' Please enter the file name:  ','s');  % file name
```

```
if isempty(which(filen)), disp(['        ----->  ERROR: file ',filen,'
not found']), return, end
%
disp(' ')
%
nTOF=input(' Is this the Top nTOF (1) or Bottom nTOF (2)?:  ');
%
disp(' ')
%
coll=input(' Is the Tivar Collimator in place? (1) yes, or (0) no:  ');
%
disp(' ')
%
tmin=input(' Enter minimum time in shakes to plot: ');
%
disp(' ')
tmax=input(' Enter max time in shakes to plot: ');
%
disp(' ')
%
digitres=input(' Enter digitizer resolution in (ns): ');
digitres=digitres/10.0;  % Conversion from ns to shakes
disp(' ')
%
writefile=input(' Write results to file ? (0) no (1) yes:  ');

tic   % starts the stopwatch timer
%
***********************************************************************
*
%
%                         BEGIN POSTPROCESSING
%
format loose
format long
disp(' *****************************************')
data=load(filen);  % load data file
%
% nrow gets # of rows in data file
% ncol gets # of columns in data file
%
[nrow,ncol]=size(data);
%
newrow=nrow;
%
disp(' ')
disp(' Successfully loaded file')
    %
disp(' ')
disp([' Number of rows in file = ',int2str(nrow)])
%
disp(' ')
disp([' tmax = ', num2str(tmax),' shakes']);
disp(' ')
%
bps = 1.0/digitres;   % bins per shake
%
```

```
disp([' bps = ', num2str(bps), ' bins per shake'])
disp(' ')
%
TOF = 0.0;

if(nTOF == 2)
   TOF = (809)/(2.166 * 10);  % Arrival time in shakes at bottom
                              % Detector
elseif(nTOF == 1)
   TOF = (730)/(2.166 * 10);  % Arrival time in shakes at top
                              % Detector
end
%
disp([' TOF = ', num2str(TOF) ' shakes (Arrival Time)'])
disp(' ')
%
disp([' tmin = ', num2str(tmin), ' Shakes (Start Time to Plot)'])
disp(' ')
%
maxrow = (tmax - tmin)* bps; % Maximum number of rows needed for 200 ps
                            % time bins to plot from neutron arrival
                            % time at detector to tmax
%
maxrow = int16(maxrow) + 1; % Converting to Integer & adding 1
%
disp([' maxrow = ', num2str(maxrow), ' maximum rows required'])
disp(' ')
%
 if any(diff(data(:,8))<0)
    data=sortrows(data,8);   % sort in terms of increasing times
 end
%
% disp(' ')
disp(' Successfully sorted file in terms of increasing times')
%
%
disp(' ')
disp(' **************************************************')
%
%
lout=zeros(nrow,1);  % loads lout with zeros
%
%  **************************** LIGHT OUTPUT
****************************
%   convert energy depositions to light (lout)
   for j=1:nrow
      if data(j,3)==1                         % particle = neutron
         if data(j,5)==1001                     % nucleus  = hydrogen
            lout(j)=polyval(ncal,data(j,7));      % light output for
energy dep.
            %
         elseif floor(data(j,5)/1000)==6       % nucleus = carbon
            lout(j)=data(j,7)*lonc;               % light output =
energy deposited * light
            %
         else disp(['! error, the struck nucleus is unknown  ',
int2str(data(j,5))])
```

```
         end
      elseif (data(j,3)==2 || data(j,3)==3) % particle = photon
           lout(j)=polyval(pcal,data(j,7));        % light output for
energy dep.
           %
      else disp(['! error, the incident particle is unknown  ',
int2str(data(j,3))])
      end
   end
 %
disp(' ')
disp(' Successfully converted energy depositions to light')
%
outputtime=zeros(nrow,1);  % loads outputtime with zeros
outputLO=zeros(nrow,1);  % loads outputLO with zeros
outputboth=zeros(nrow,2);  % loads outputboth with zeros
%
%
timeout1=zeros(maxrow,1);   % loads zeros into timeout1
lightout1=zeros(maxrow,1);  % loads zeros into lightout1
%
% ********* BEFORE SUMMING PULSES *********
for j=tmin:nrow
    outputtime(j,1) = data(j,8);  % time in shakes (x-values)
    %
    outputLO(j,1) = lout(j);     % Light Output in MeVee
    %
    outputboth(j,1) = data(j,8);
    outputboth(j,2) = lout(j);
    %
end
%
%
timebin = zeros(maxrow,1);  % loads timebin with zeros
%
timebin(1,1) = outputtime(tmin,1); % timebin gets 1st value of
outputtime
%
disp(' ')
disp([' First Time Bin = ', num2str(timebin(1,1))])
disp(' ')
%
disp(' Loading Timebin with bins equal to digitizer resolution from
first value in the data')

% LOADS TIMEBIN WITH 200 ps TIME BINS STARTING AT THE FIRST VALUE
% IN THE DATA
%
for j = 1:maxrow
    timebin(j + 1, 1) = timebin(j,1) + digitres;
end
%
disp(' ')
disp(' Summing Pulses')
    % ************** SUMMING PULSES *******************
    for j = tmin: nrow
```

```
          for i = 1: maxrow

            if((outputtime(j,1) >= timebin(i,1)) && ((outputtime(j,1)<=
timebin(i + 1,1))))

              lightout1(i,1) = lightout1(i,1) + outputLO(j,1);

            end

         end

     end

disp(' ')
disp(' Assigning Time to Middle of Bin')
     %  ASSIGNING TIME TO MIDDLE OF BIN:
     for j = 1:maxrow                         % k

          timeout1(j,1) = timebin(j,1) + digitres/2.0;

     end
%
lightout=zeros(maxrow,1);
timeout=zeros(maxrow,1);
timelight=zeros(maxrow,2);

for j=1:maxrow
   timelight(j,1) = timeout1(j,1);
   timelight(j,2) = lightout1(j,1);
   lightout(j,1) = lightout1(j,1);
   timeout(j,1) = timeout1(j,1);
end
%
%
plottools('on', 'figurepalette')
%
% PLOTS LIGHT OUTPUT VS TIME:
%
plot(timeout,lightout)
%
xlabel('Time (shakes)');
ylabel('Light Output (MeVee)');
xlim([tmin tmax]);  % FOR BOTTOM nTOF, STARTING AT 30 SHAKES IS FINE
%
if(nTOF==1 && coll==1)
    title('Top nTOF in Basement Pig with Tivar Collimator');
elseif(nTOF==1 && coll==0)
    title('Top nTOF in Basement Pig with no Tivar Collimator');
elseif(nTOF==2 && coll==1)
    title('Bottom nTOF in Basement Pig with Tivar Collimator');
elseif(nTOF==2 && coll==0)
    title('Bottom nTOF in Basement Pig with no Tivar Collimator');
end
%
```

```
% write results to file
%
if writefile==1
%
    ind1=find(filen=='.');  % If '.' in filename, ind1=# of characters
%                             up to '.'
    if ind1
        root=filen(1:ind1-1);  % root=filename w/o '.'
    else
    root=filen;          % elseif no '.', root=filename
    end
%
dlmwrite(root, timelight);  % Writes matrix timelight into ASCII format
%                             file using default delimiter ',' to
%                             separate matrix elements; starting at the
%                             first column and first row of filename.
%                             ASCII file takes the name of root (the
%                             filename input at the beginning)
%
end
%
disp(' ')
disp(' Got to here -- end of program')
%
disp(' ')
toc   % ends the stopwatch timer
disp(' ')
%
return
```

APPENDIX C

THE CONVOLUTION ("FOLDING IN") CODE

```
% This program folds in a time response of 7.5 ns of our nTOF
% detectors into the calculated values of the detector response
% found with MCNP-PoliMi and postmain_ntof_U (the post-processor)

disp(' ')
filen=input(' Please enter the MCNP-PoliMi Calculated file name:
','s');  % file name
if isempty(which(filen)), disp(['        ----->  ERROR: file ',filen,'
not found']), return, end
disp(' ')

Fold=input(' Fold in A Gaussian (1) or Actual Time Response (2)?: ');
disp(' ')

tmin=input(' Enter minimum time in shakes to plot: ');
disp(' ')

tmax=input(' Enter max time in shakes to plot: ');
disp(' ')

fileout=input(' Please enter the name you wish for the output file:
','s');  % file name
disp(' ')

writefile=input(' Write results to file ? (0) no (1) yes:  ');

tic   % starts the stopwatch timer

format loose
format long
disp(' *****************************************')
disp(' ')
zzz=load(filen);  % load data file
%
% nrow gets # of rows in data file
% ncol gets # of columns in data file
%
[nrow,ncol]=size(zzz);

% *************** FOLDING IN THE GAUSSIAN ************************

if(Fold==1);

   FWHM=input(' Please enter the FWHM of the Gaussian in ns: ');
   disp(' ')

   Half_FWHM = FWHM / 2.0;
   FWHM = FWHM/10.0;  % Converting to Shakes
```

```
   digitres=input(' Enter digitizer resolution in (ns): ');
   disp(' ')

   widths=input(' Please enter the number of Half-Widths Per Side: ');
   disp(' ')

   Sigma = FWHM /(realsqrt(8 * log(2)));
   disp([' Sigma = ', num2str(Sigma)]);
   disp(' ')

% Sigma = 0.318495675;

% Integral = 0.399175132;

   start = Half_FWHM * widths;
   disp([' start = ', num2str(start)]);
   disp(' ')

   begin = start * 10.0;
   begin = floor(begin);
   begin = begin/100.0;

   disp([' begin = ', num2str(begin)]);
   disp(' ')

   finish = abs(begin);
   disp([' finish = ', num2str(finish)]);
   disp(' ')

   Half = (start)/digitres;
   disp([' Half = ', num2str(Half)]);
   disp(' ')

   digitres=digitres/10.0;  % Conversion from ns to shakes
   disp([' digitres in shakes = ', num2str(digitres)]);
   disp(' ')

   one_side = Half * 2.0;
   disp([' one_side = ', num2str(one_side)]);
   disp(' ')

   one_side = floor(one_side);
   disp([' one_side rounded down = ', num2str(one_side)]);
   disp(' ')

   width = one_side + 1; % Width of Gaussian
   disp([' width = ', num2str(width)]);
   disp(' ')

   Gaussian=zeros(width,1);  % Loads Guassian with zeros

   SumGaussian = zeros(1,1);

% k=0;
```

```
   l=0;
   j=1;

% disp(' nargin = ', int2str(nargin));

% ************** CALCULATING THE GAUSSIAN *******************
   for i = -begin:digitres:finish;

    % disp([' i = ', num2str(i)]);

       Gaussian(j,1) = exp(-((i .^ 2)/(2 * (Sigma .^ 2))));

    % disp([' Gaussian(', int2str(j),',1)', ' = ',
num2str(Gaussian(j,1))]);

       SumGaussian(1,1) = (Gaussian(j,1) + SumGaussian(1,1));

    % disp([' SumGaussian = ', num2str(SumGaussian(1,1))]);

       j = j + 1;

   end
% ************* SUMMING THE GAUSSIAN *********************
% ************ TO CALCULATE THE INTEGRAL ******************
   SumGaussian(1,1) = SumGaussian(1,1) * 0.02;

   disp(' ');
   disp([' SumGaussian = ', num2str(SumGaussian(1,1))]);
   disp(' ');


% *************** LOADING THE LARGE ARRAY ********************
   k = 1;
   maxcol = nrow + width;

   disp([' maxcol = ', int2str(maxcol)]);

   NewGaussian = zeros(nrow,maxcol);

   for n = 1:nrow;

       Constant = zzz(n,2)/SumGaussian(1,1);

    % disp([' Constant = ', num2str(Constant)]);

        for m = 1:width;

            NewGaussian(n,m) = Constant * Gaussian(m,1);

% disp(' ');
% disp([' NewGaussian(',int2str(n) ',' int2str(m),') =
',num2str(NewGaussian(n,m))]);
% disp(' ');
```

```
          end

      end
      NewGaussianFinal = zeros(nrow,maxcol);
      p = width;
   % *************** SHIFTING DATA IN ROWS **************
      for i = 2:nrow;

          for j = p:-1:1;

       % disp([' j = ', int2str(j)]);
            NewGaussianFinal(i,i-1+j) = NewGaussian(i,j);

       % NewGaussian(i,j+1) = NewGaussian(i,j);

   % disp([' NewGaussianFinal(', int2str(i),',',int2str(i-1+j),') = ',
   num2str(NewGaussianFinal(i,i-1+j))]);

          end

      end

   maxcol = nrow + width;
   NewSum = zeros(1,maxcol);

   % **************** SUMMING COLUMNS IN NEWGAUSSIAN ************
      for p = 1:maxcol;

          for q = 1:nrow;

              NewSum(1,p) = NewGaussianFinal(q,p) + NewSum(1,p);
      % disp([' NewSum(1,',int2str(p),') = ', num2str(NewSum(1,p))]);
          end

   % disp([' NewSum(1,',int2str(p),') = ', num2str(NewSum(1,p))]);

      end

      lightout=zeros(maxcol,1);
      timeout=zeros(maxcol,1);
      timelight=zeros(maxcol,2);

      for j=1:nrow
         timelight(j,1) = zzz(j,1);
         timeout(j,1) = zzz(j,1);

      % disp([' timeout(', int2str(j),', 1) = ', num2str(timeout(j,1))]);
      end

      disp(' ***************************************** ');

      for j=1:maxcol;
```

```
      timelight(j,2) = NewSum(1,j);
      lightout(j,1) = NewSum(1,j);

   % disp([' lightout(', int2str(j),', 1) = ',
num2str(lightout(j,1))]);
   end
%
   Integral=zeros(1,1);
   for i=1:maxcol;
%
       Integral(1,1) = (lightout(i,1) + Integral(1,1));
    % disp([' Integral = ', num2str(Integral(1,1))]);
   end

   disp([' Integral = ', num2str(Integral(1,1))]);

   plottools('on', 'figurepalette')
%
   % PLOTS LIGHT OUTPUT VS TIME:
%
   plot(timeout,lightout)

   xlabel('Time (shakes)');
   ylabel('Light Output (MeVee)');
   xlim([tmin tmax]);  % FOR BOTTOM nTOF, STARTING AT 30 SHAKES IS FINE

% **************** FOLDING IN ACTUAL TIME RESPONSE
***********************

elseif(Fold==2);

   Detector_TRF=input(' Please enter the Detector Time Response File:
', 's');
   disp(' ')

   digitres=input(' Enter digitizer resolution in (ns): ');
   disp(' ')

   digitres=digitres/10.0;  % Conversion from ns to shakes
   disp([' digitres in shakes = ', num2str(digitres)]);
   disp(' ')

   format loose
   format short
   disp(' ****************************************')
   disp(' ')
   zzz=load(filen);  % load data file
   %
   % nrow gets # of rows in data file
   % ncol gets # of columns in data file
   %
   [nrow,ncol]=size(zzz);

   xxx=load(Detector_TRF); % Loads Detector Time Response File
   [width,col]=size(xxx);  % width is number of rows in Detector_TRF
```

```
   disp([' nrow = ', int2str(nrow)]);
   disp(' ')
   disp([' width = ', int2str(width)]);

   SumGaussian = zeros(1,1);

% k=0;
   l=0;
   j=1;

   for i = 1:width;

       SumGaussian(1,1) = (xxx(i,2) + SumGaussian(1,1));

   end
   % ************* SUMMING THE GAUSSIAN **********************
   % ************ TO CALCULATE THE INTEGRAL ******************
   SumGaussian(1,1) = SumGaussian(1,1) * digitres;

   disp(' ');
   disp([' SumGaussian = ', num2str(SumGaussian(1,1),'%12.7f\n')]);
   disp(' ');


   % *************** LOADING THE LARGE ARRAY ********************
   k = 1;
   maxcol = nrow + width;

   disp([' maxcol = ', int2str(maxcol)]);

   NewGaussian = zeros(nrow,maxcol);

   for n = 1:nrow;

       Constant = zzz(n,2)/SumGaussian(1,1);

       % disp([' Constant = ', num2str(Constant,'%12.7f\n')]);
       % disp(' ')

       Constant = Constant * 1.0E04;

       % disp([' Constant = ', num2str(Constant,'%12.7f\n')]);
       % disp(' ')

       Constant = round(Constant);

       % disp([' Constant = ', num2str(Constant,'%12.7f\n')]);
       % disp(' ')

       Constant = Constant/1.0E04;

       % disp([' Constant = ', num2str(Constant,'%12.7f\n')]);
```

```
        for m = 1:width;

            NewGaussian(n,m) = Constant * xxx(m,2);

% disp(' ');
% disp([' NewGaussian(',int2str(n) ',' int2str(m),') =
',num2str(NewGaussian(n,m))]);
% disp(' ');

        end

   end
   NewGaussianFinal = zeros(nrow,maxcol);
   p = width;
   % **************** SHIFTING DATA IN ROWS **************
   for i = 2:nrow;

       for j = p:-1:1;

    % disp([' j = ', int2str(j)]);
       NewGaussianFinal(i,i-1+j) = NewGaussian(i,j);

    NewGaussian(i,j+1) = NewGaussian(i,j);

% disp([' NewGaussianFinal(', int2str(i),',',int2str(i-1+j),') = ',
num2str(NewGaussianFinal(i,i-1+j))]);

       end

   end

   maxcol = nrow + width;
   NewSum = zeros(1,maxcol);

   % ***************** SUMMING COLUMNS IN NEWGAUSSIAN *************
   for p = 1:maxcol;

       for q = 1:nrow;

           NewSum(1,p) = NewGaussianFinal(q,p) + NewSum(1,p);
   % disp([' NewSum(1,',int2str(p),') = ', num2str(NewSum(1,p))]);
       end

% disp([' NewSum(1,',int2str(p),') = ', num2str(NewSum(1,p))]);

   end

   lightout=zeros(maxcol,1);
   timeout=zeros(maxcol,1);
   timelight=zeros(maxcol,2);

   for j=1:nrow
```

```
      timelight(j,1) = zzz(j,1);
      timeout(j,1) = zzz(j,1);

   % disp([' timeout(', int2str(j),', 1) = ', num2str(timeout(j,1))]);
   end

   disp(' ***************************************** ');

   for j=1:maxcol;
      timelight(j,2) = NewSum(1,j);
      lightout(j,1) = NewSum(1,j);

      % disp([' lightout(', int2str(j),', 1) = ',
num2str(lightout(j,1))]);
   end
%
   Integral=zeros(1,1);
   for i=1:maxcol;
%
       Integral(1,1) = (lightout(i,1) + Integral(1,1));
    % disp([' Integral = ', num2str(Integral(1,1))]);
   end

   disp([' Integral = ', num2str(Integral(1,1))]);

   plottools('on', 'figurepalette')
%
% PLOTS LIGHT OUTPUT VS TIME:
%
   plot(timeout,lightout)

   xlabel('Time (shakes)');
   ylabel('Light Output (MeVee)');
   xlim([tmin tmax]);  % FOR BOTTOM nTOF, STARTING AT 30 SHAKES IS FINE

end

if writefile==1
%
    ind1=find(fileout=='.');  % If '.' in filename, ind1=# of
characters
%                             up to '.'
    if ind1
       root=fileout(1:ind1-1);  % root=filename w/o '.'
    else
       root=fileout;          % elseif no '.', root=filename
    end
%
dlmwrite(root, timelight);  % Writes matrix timelight into ASCII format
%                             file using default delimiter ',' to
%                             separate matrix elements; starting at the
%                             first column and first row of filename.
%                             ASCII file takes the name of root (the
%                             filename input at the beginning)
```

```
end

disp(' ')
disp(' Got to here -- end of program')
%
disp(' ')
toc   % ends the stopwatch timer
disp(' ')
%
return
```

APPENDIX D

THE DECONVOLUTION ("UNFOLDING") CODE

```
      PROGRAM deconvlv
!C     driver for routine convlv
      INTEGER N,N2,M
      REAL PI
      !C
      PARAMETER (N = 2048, M = 2046, N2 = 4096, pi = 3.14159265, NMAX=4096)
      INTEGER i,ISIGN
      DIMENSION DATA(N),RESPNS(M),RESP(N),ANS(N2),FOLD(N),TIME(N)
      REAL Time1, Amp1, Time2, Amp2
      REAL RESPNST(N)

      CHARACTER*80 FNAME
      CHARACTER*80 FNAMER

ISIGN = -1

!C    INPUT THE FOLDED IN FILE NAME ON THE TERMINAL
!C
      WRITE (*,2)
2     FORMAT ()
      WRITE (*,*) '  ENTER FOLDED IN FILE NAME OF DETECTOR DATA: '
      READ (*,'(A)') FNAME
      OPEN(UNIT=3,FILE=FNAME,STATUS='OLD')

      OPEN(UNIT = 8, FILE = 'Unfold_Output')    ! Open Output File

!C    READ IN DATA (TIME IN SHAKES AND AMPLITUDE):


      DO i=1,N

      READ(3,10,END=20) Time1, Amp1     ! THIS READS THE FOLDED-IN DETECTOR
                                        ! FILE OF ANY LENGTH AND STORES THE
10    FORMAT(F7.4, 1x, F11.6)           ! VALUES IN AN ARRAY "FOLD";
                                        ! F8.4,T16,F14.8


      TIME (i)  = Time1
      FOLD (i) = Amp1
      DATA(i) = Amp1


      WRITE(*,12)  i,  Amp1
12    FORMAT('FOLD(1,',i6,') = ', 3x, F11.6)
      WRITE(*,13) i, Time1
13    FORMAT('TIME(1,',i6, ') = ', 3x, F7.4)


      END DO

20    ENDFILE(UNIT=3)

! *******************************************************

      WRITE(8,21) FNAME
21    FORMAT(A)
```

```
      DO i = 1, N

        WRITE(8,22) TIME(i), FOLD(i)

22      FORMAT(F7.4, 3x, F11.9)

     END DO

! *****************************************************

!C   INPUT THE RESPONSE FUNCTION OF THE DETECTOR

     WRITE(*,23)
23   FORMAT()
     WRITE (*,*) '  ENTER RESPONSE FUNCTION OF DETECTOR: '
     READ (*,'(A)') FNAMER

     OPEN(UNIT=7,FILE=FNAMER,STATUS='OLD')


     DO i=1,M

      READ(7,30,END=40) Time2, Amp2

30   FORMAT(F6.3, T8, F9.6)


     RESPNST(i) = Time2
     RESPNS(i) = Amp2
     RESP(i) = Amp2

     WRITE(*,31)  i,  Time2
31   FORMAT(' Time2(1,',i4,') = ', 3x, F6.3)

     WRITE(*,32) i, Amp2
32   FORMAT(' Amp2(1,',i4, ') = ', 3x, F9.4)


     END DO

40   ENDFILE(UNIT=7)

! *******************************************************
     WRITE(8,41)
41   FORMAT()

     WRITE(8,42) FNAMER
42   FORMAT(A)

     DO i = 1, M

        WRITE(8,43) RESPNST(i), RESPNS(i)

43      FORMAT(F6.3, 3x, F8.6)

     END DO

      call convlv(DATA,N,RESP,M,ISIGN,ANS)

! ************** PRINT ANSWER OUT HERE *********************
```

```
! ***********************************************************
     WRITE(8,44)
44   FORMAT()

     WRITE(8,45) '  PROGRAM UNFOLD RESULTS: '
45   FORMAT(A)

     DO i = 1, N

        WRITE(8,46) TIME(i), ANS(i)

46      FORMAT(3x,F10.6, 3X, F13.6, 3x, F13.6)

     END DO

     WRITE(*,47)
47   FORMAT()

     WRITE(*,48)'  PROGRAM UNFOLD RESULTS:'
48   FORMAT(A)

      DO i = 1, N

        WRITE(*,49) TIME(i), ANS(i)

49      FORMAT(3x,F10.6, 3X,F13.6, 3x, E13.6)

      END DO

      END

      SUBROUTINE convlv(data,n,respns,m,isign,ans)
      INTEGER isign,m,n,NMAX
      REAL data(n),respns(n)
      COMPLEX ans(n)
      PARAMETER (NMAX=4096)
CU    USES realft,twofft
      INTEGER i,no2
      COMPLEX fft(NMAX)
      do 11 i=1,(m-1)/2
        respns(n+1-i)=respns(m+1-i)
11    continue
      do 12 i=(m+3)/2,n-(m-1)/2
        respns(i)=0.0
12    continue
      call twofft(data,respns,fft,ans,n)
      no2=n/2
      do 13 i=1,no2+1
        if (isign.eq.1) then
          ans(i)=fft(i)*ans(i)/no2
        else if (isign.eq.-1) then
          if (abs(ans(i)).eq.0.0) pause
     *'deconvolving at response zero in convlv'
          ans(i)=fft(i)/ans(i)/no2
        else
          pause 'no meaning for isign in convlv'
        endif
13    continue
      ans(1)=cmplx(real(ans(1)),real(ans(no2+1)))
      call realft(ans,n,-1)
```

```
      return
      END

      SUBROUTINE four1(data,nn,isign)
      INTEGER isign,nn
      REAL data(2*nn)
      INTEGER i,istep,j,m,mmax,n
      REAL tempi,tempr
      DOUBLE PRECISION theta,wi,wpi,wpr,wr,wtemp
      n=2*nn
      j=1
      do 11 i=1,n,2
        if(j.gt.i)then
          tempr=data(j)
          tempi=data(j+1)
          data(j)=data(i)
          data(j+1)=data(i+1)
          data(i)=tempr
          data(i+1)=tempi
        endif
        m=nn
1       if ((m.ge.2).and.(j.gt.m)) then
          j=j-m
          m=m/2
        goto 1
        endif
        j=j+m
11    continue
      mmax=2
2     if (n.gt.mmax) then
        istep=2*mmax
        theta=6.28318530717959d0/(isign*mmax)
        wpr=-2.d0*sin(0.5d0*theta)**2
        wpi=sin(theta)
        wr=1.d0
        wi=0.d0
        do 13 m=1,mmax,2
          do 12 i=m,n,istep
            j=i+mmax
            tempr=sngl(wr)*data(j)-sngl(wi)*data(j+1)
            tempi=sngl(wr)*data(j+1)+sngl(wi)*data(j)
            data(j)=data(i)-tempr
            data(j+1)=data(i+1)-tempi
            data(i)=data(i)+tempr
            data(i+1)=data(i+1)+tempi
12        continue
          wtemp=wr
          wr=wr*wpr-wi*wpi+wr
          wi=wi*wpr+wtemp*wpi+wi
13      continue
        mmax=istep
      goto 2
      endif
      return
      END
```

```fortran
      SUBROUTINE realft(data,n,isign)
      INTEGER isign,n
      REAL data(n)
CU    USES four1
      INTEGER i,i1,i2,i3,i4,n2p3
      REAL c1,c2,h1i,h1r,h2i,h2r,wis,wrs
      DOUBLE PRECISION theta,wi,wpi,wpr,wr,wtemp
      theta=3.141592653589793d0/dble(n/2)
      c1=0.5
      if (isign.eq.1) then
        c2=-0.5
        call four1(data,n/2,+1)
      else
        c2=0.5
        theta=-theta
      endif
      wpr=-2.0d0*sin(0.5d0*theta)**2
      wpi=sin(theta)
      wr=1.0d0+wpr
      wi=wpi
      n2p3=n+3
      do 11 i=2,n/4
        i1=2*i-1
        i2=i1+1
        i3=n2p3-i2
        i4=i3+1
        wrs=sngl(wr)
        wis=sngl(wi)
        h1r=c1*(data(i1)+data(i3))
        h1i=c1*(data(i2)-data(i4))
        h2r=-c2*(data(i2)+data(i4))
        h2i=c2*(data(i1)-data(i3))
        data(i1)=h1r+wrs*h2r-wis*h2i
        data(i2)=h1i+wrs*h2i+wis*h2r
        data(i3)=h1r-wrs*h2r+wis*h2i
        data(i4)=-h1i+wrs*h2i+wis*h2r
        wtemp=wr
        wr=wr*wpr-wi*wpi+wr
        wi=wi*wpr+wtemp*wpi+wi
11    continue
      if (isign.eq.1) then
        h1r=data(1)
        data(1)=h1r+data(2)
        data(2)=h1r-data(2)
      else
        h1r=data(1)
        data(1)=c1*(h1r+data(2))
        data(2)=c1*(h1r-data(2))
        call four1(data,n/2,-1)
      endif
      return
      END
```

```fortran
      SUBROUTINE twofft(data1,data2,fft1,fft2,n)
      INTEGER n
      REAL data1(n),data2(n)
      COMPLEX fft1(n),fft2(n)
CU    USES four1
      INTEGER j,n2
      COMPLEX h1,h2,c1,c2
      c1=cmplx(0.5,0.0)
      c2=cmplx(0.0,-0.5)
      do 11 j=1,n
        fft1(j)=cmplx(data1(j),data2(j))
11    continue
      call four1(fft1,n,1)
      fft2(1)=cmplx(aimag(fft1(1)),0.0)
      fft1(1)=cmplx(real(fft1(1)),0.0)
      n2=n+2
      do 12 j=2,n/2+1
        h1=c1*(fft1(j)+conjg(fft1(n2-j)))
        h2=c2*(fft1(j)-conjg(fft1(n2-j)))
        fft1(j)=h1
        fft1(n2-j)=conjg(h1)
        fft2(j)=h2
        fft2(n2-j)=conjg(h2)
12    continue
      return
      END
```

APPENDIX E

IDAHO ACCELERATOR CENTER LAYOUT

Shown in Figure 47 is the layout of the experiments that were performed at the Idaho Accelerator Center located at Idaho State University in Pocatello, Idaho [24]. The goal was to measure the time response of nTOF detectors using 50 ps pulses of x-rays. Initially the nTOFs were placed in the "Great Hall" which housed the 15 MeV linac itself but the data had a high degree of background due to scattering, therefore the nTOFs were moved into the "Shielded Cell" – a room separated from the Great Hall by two 30.48 cm (1 ft) thick concrete walls separated by 1.2192 m (4 ft) of earth, through which

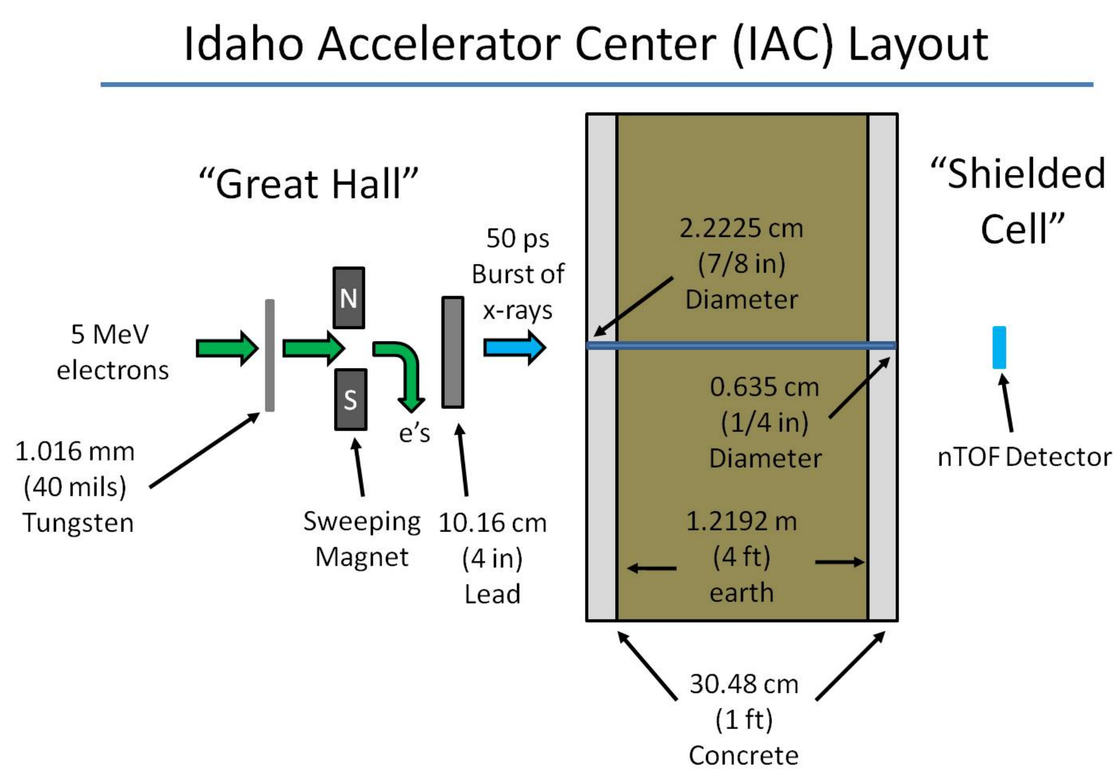

Figure 47. Idaho Accelerator Center (IAC) Layout. The "Great Hall" housed the 15 MeV Linac. The nTOF detectors were placed in the "Shielded Cell" behind two 30.48 cm (1 ft) thick walls separated by 1.292 m (4 ft) of earth. The entrance aperture in the Great Hall was 2.2225 cm (7/8 in) diameter and the exit aperture in the Shielded Cell was 0.635 cm (1/4 in). This geometry provided good data with very little background. The goal was to measure the time response of the detectors using 50 ps bursts of x-rays.

a narrow collimator ran from the Great Hall into the Shielded Cell. The entrance aperture of the collimator was 2.2225 cm (7/8 in) and the exit aperture was 0.635 cm (1/4 in). The data obtained from the nTOFs placed in the Shielded Cell was quite good, and shown in Figure 48.

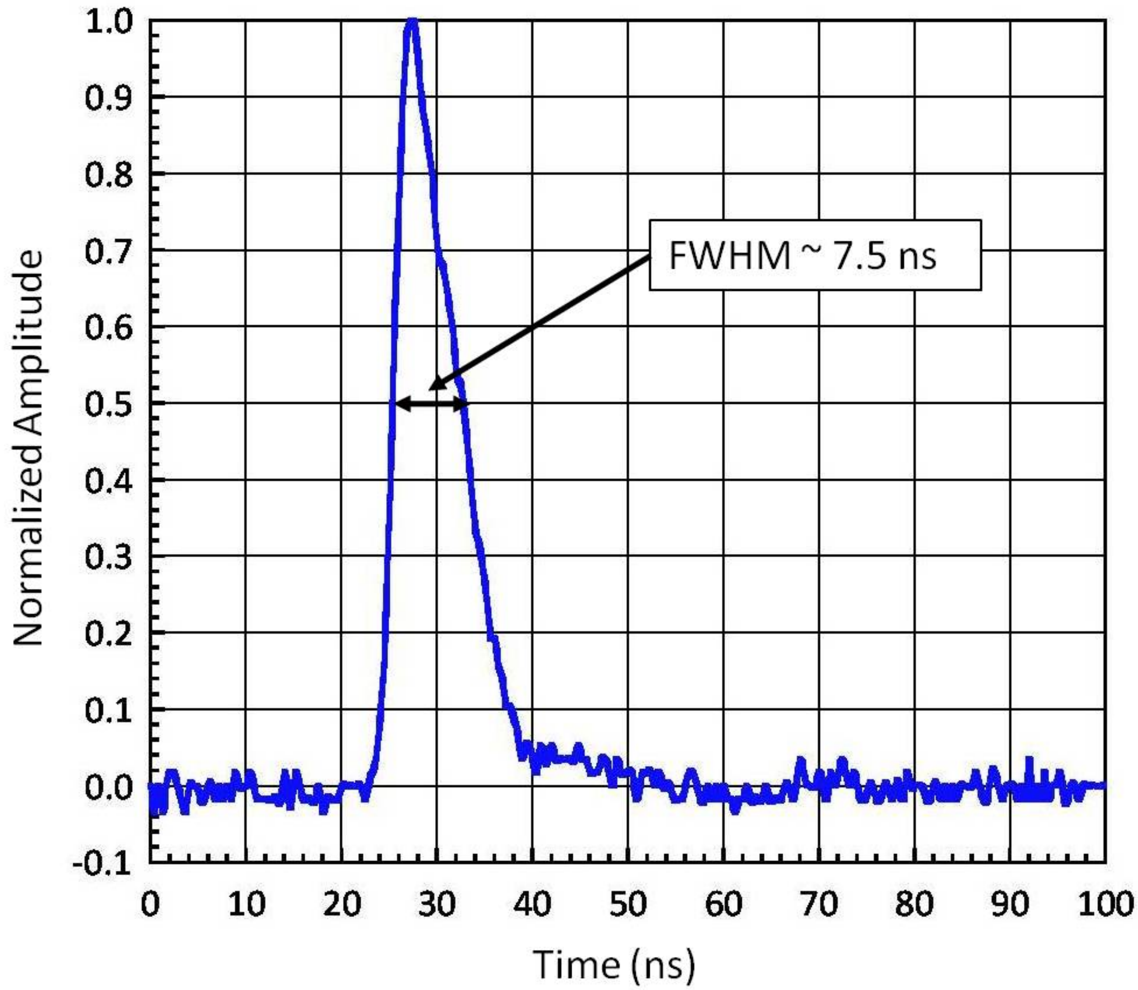

Figure 48. Experimental Time response found at the Idaho Accelerator Center (IAC) using 50 ps bursts of x-rays. The full width at half maxima is approximately 7.5 ns. This data was obtained in the "Shielded Cell" (see Figure 47) where the background was quite low due to the extensive amount of shielding and narrow collimation.

It was found that the best results were obtained when the linac operated at 400 mA, and pulsed 5 MeV electrons into 1.016 mm (40 mils) of tungsten. A sweeping magnet removed the electrons out of the beam, leaving only the 50 ps bursts of x-rays which were attenuated by 10.16 cm (4 in) of lead. The x-rays were collimated through two 30.48 cm (1 ft) thick concrete walls and 1.2192 m (4 ft) of earth, then entered the shielded cell. The data was recorded on a Tektronix TDS7254B 2.5 GHz, 4 channel digital phosphor digitizer [19] in an average over several pulses (typically 32). In this way, the time response of four nTOF detectors was found with a nominal value of a full width at half maxima to be 7.5 ns.

APPENDIX F

NEW COLLIMATOR DESIGN

In the 2006 – 2007 timeframe, the Z-Machine was refurbished, and attention was paid to upgrading all diagnostics. It was known that the addition of the collimator under target chamber center greatly improved neutron signals as shown in this work; however, there was room for improvement. Therefore, a design of a new collimator was undertaken, to have a great deal more mass than the first one. Figure 49 shows the model of the first collimator that was shown to improve signals on shot z1549.

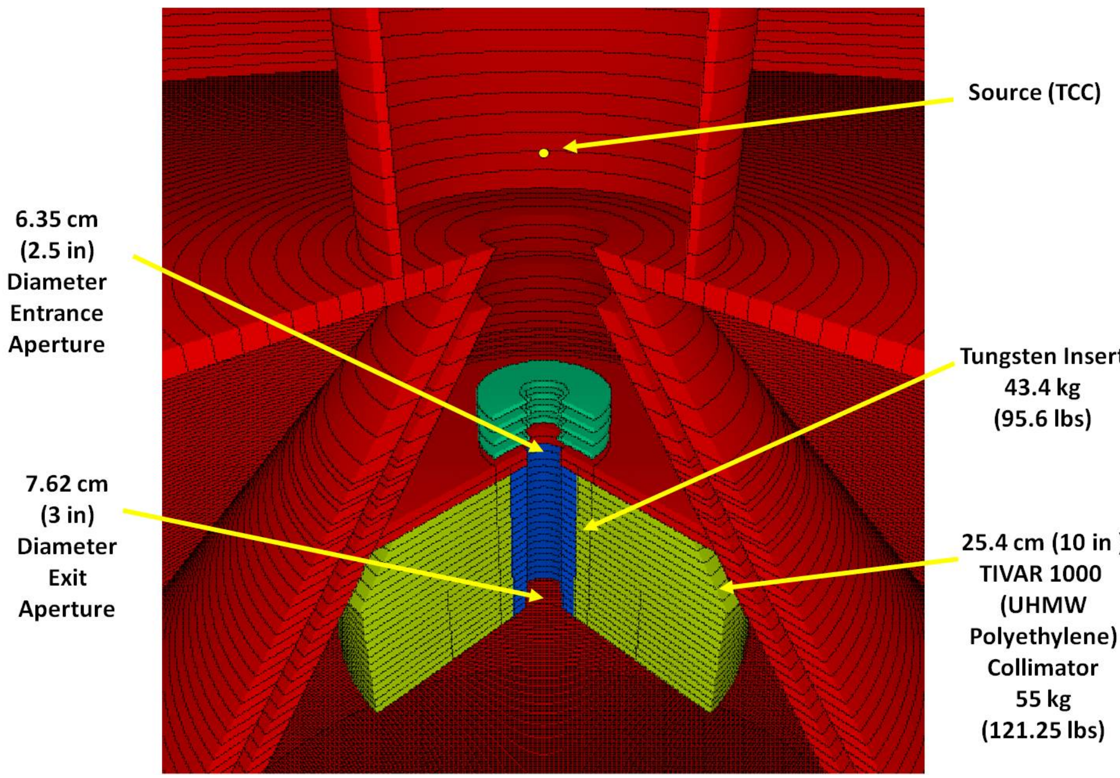

Figure 49. The model of the first neutron collimator used on the Z-machine. It was 30.48 cm (12 in) in radius and 25.4 cm (10 in) tall, made out of ultra-high molecular weight polyethylene (TIVAR 1000) [27]. It had a entrance aperture of 6.35 cm (2.5 in), and an exit aperture of 7.62 cm (3 in). It weighed 55 kg (121.25 lbs); the tungsten insert weighed 43.4 kg (95.6 lbs). It was installed on the machine in sections.

Figure 50 shows the design of the new collimator. The radius was increased – the top radius is 24.75 cm (9.74 in) and the bottom radius is 45 cm (17.7 in). Also, a cylinder of ultra-high molecular weight polyethylene (TIVAR 1000) [27] 38.1 cm (15 in) was added along the axis, giving it a mushroom appearance. The aperture along the Z-axis was 3.81 cm (1.5 in) in diameter (note that this is half the diameter of the previous collimator's exit aperture, or 7.62 cm (3 in)). The mass of the new collimator was 109.5 kg (241.3 lbs), and the mass of the tungsten insert was 8.3 kg (18.4 lbs). Since the

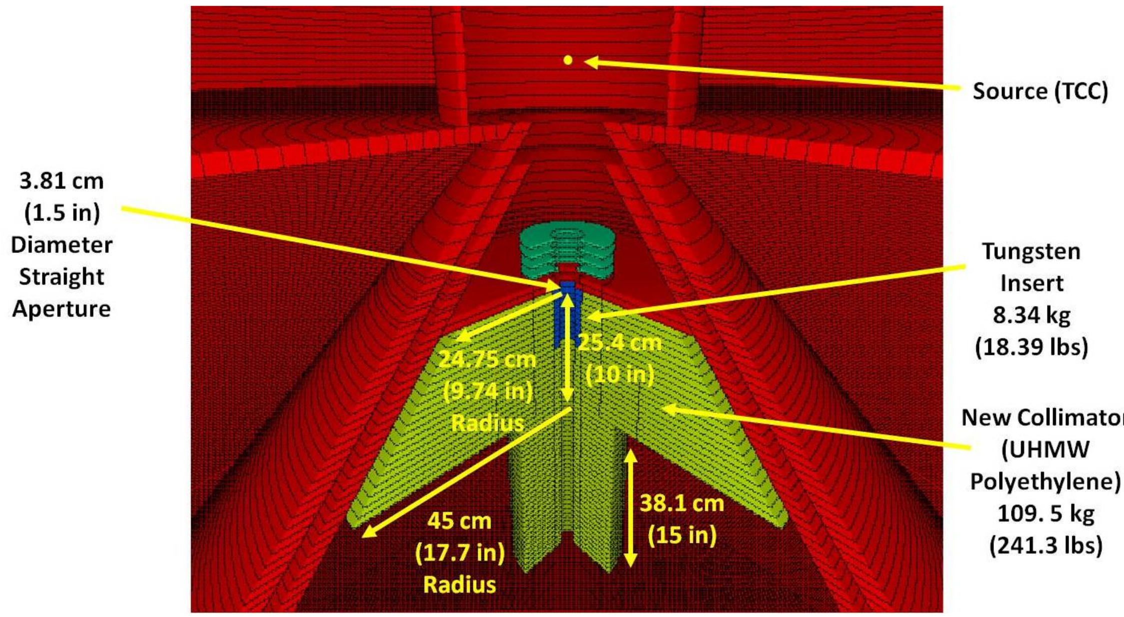

Figure 50. The new collimator design. The top radius is 24.75 cm (9.74 in) and the bottom radius is 45 cm (17.7 in). A cylinder of ultra-high molecular weight polyethylene (TIVAR 1000) [27] was added along the axis, giving it a mushroom appearance. The aperture along the Z-axis was 3.81 cm (1.5 in) in diameter and did not taper. The mass of the collimator was 109.5 kg (241.3 lbs), and the mass of the tungsten insert was 8.3 kg (18.4 lbs). Since the collimator had to be installed on the machine by hand by the center section, it was installed in sections due to its massive weight.

collimator had to be installed on the machine by hand by the center section, it was installed in sections due to its massive weight.

The model with the old collimator (Figure 49) is shown in Figure 51 for the bottom nTOF (location “D” in Figure 1). Of note is the additional, second scattering peak that occurs later in time, at about 460 ns.

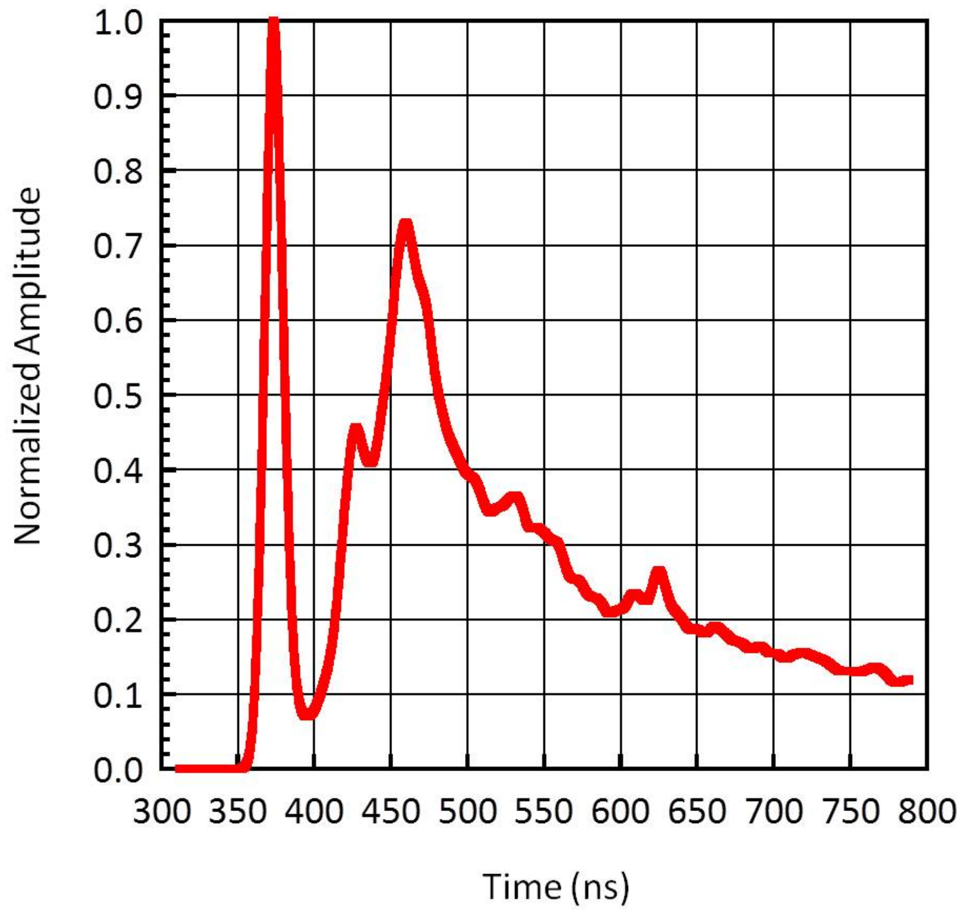

Figure 51. The model with the old collimator (Figure 49) for the bottom nTOF (location “D” in Figure 1). Despite the fact that the addition of the old collimator improved the signal, there is still a second scattering peak which occurs later in time at about 460 ns.

The model with the new collimator (Figure 50) is shown in Figure 52 for the bottom nTOF (location “D” in Figure 1). Note that the second scattering peak in Figure 51 goes away, leaving a very clean neutron signal.

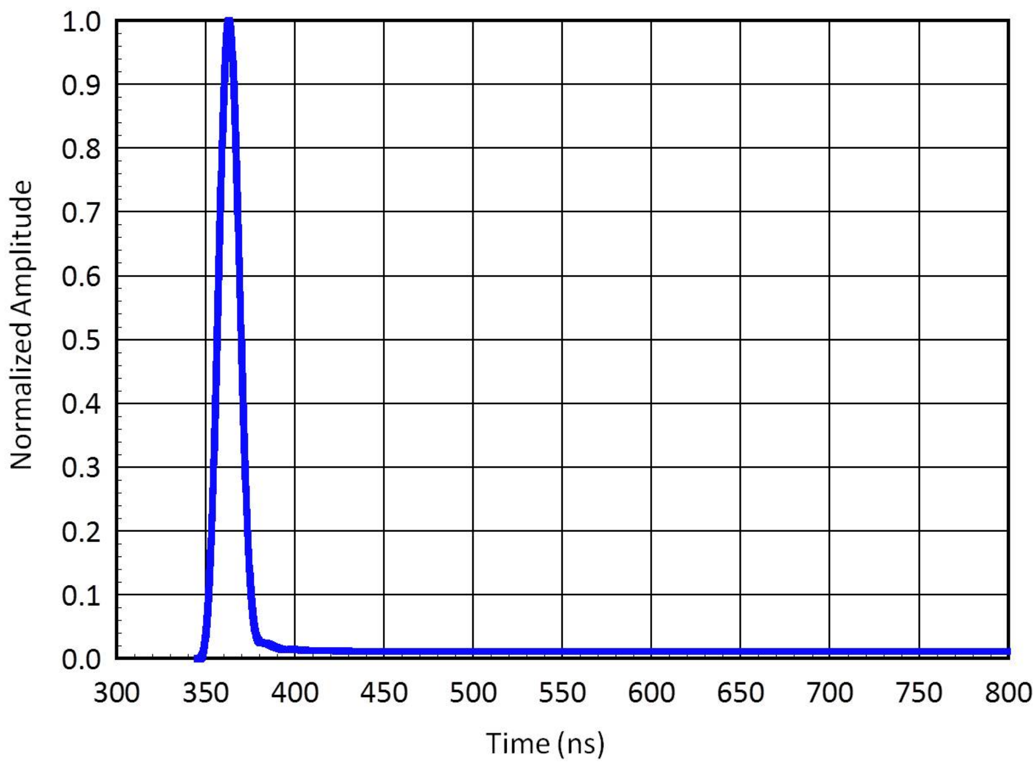

Figure 52. The model with the new collimator (Figure 50) for the bottom nTOF (location "D" in Figure 1). Note that the second scattering peak shown in Figure 51 has gone away, leaving a very clean neutron signal.

Figure 53 shows the model of the old collimator (Figure 49) for the top nTOF (location "C" in Figure 1). Although the old collimator did improve the signal, there is still some scattering later in time, past the primary neutron peak. Figure 54 shows the model of the new collimator (Figure 50) for the top nTOF (location "C" in Figure 1). Note that the scattering later in time is greatly reduced, showing that the additional mass of the new collimator was necessary to improve the neutron signal.

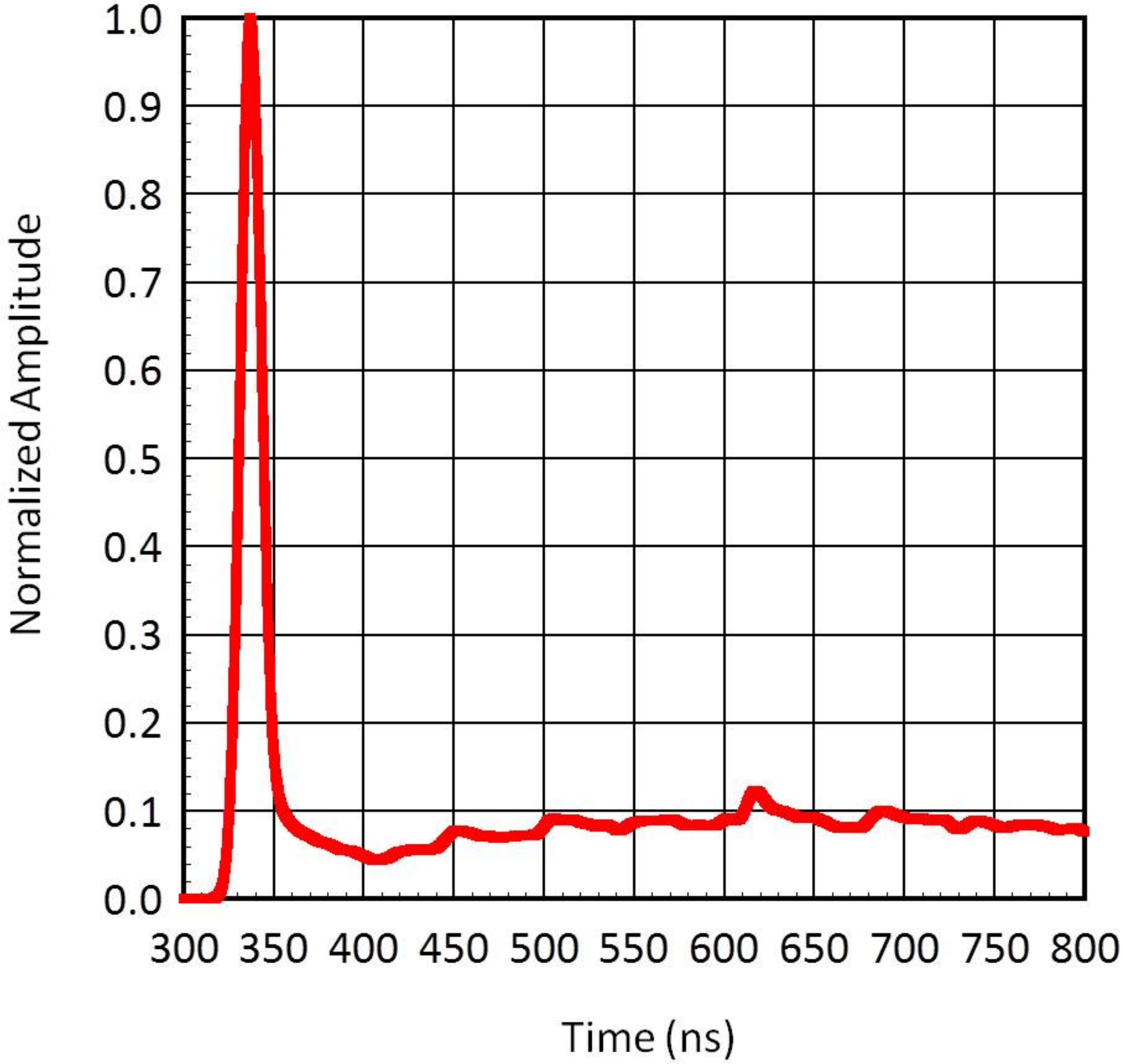

Figure 53. The model of the old collimator (Figure 49) for the top nTOF (location "C" in Figure 1). Although the addition of the old collimator did improve the signal, there is still scattering later in time past the primary neutron peak.

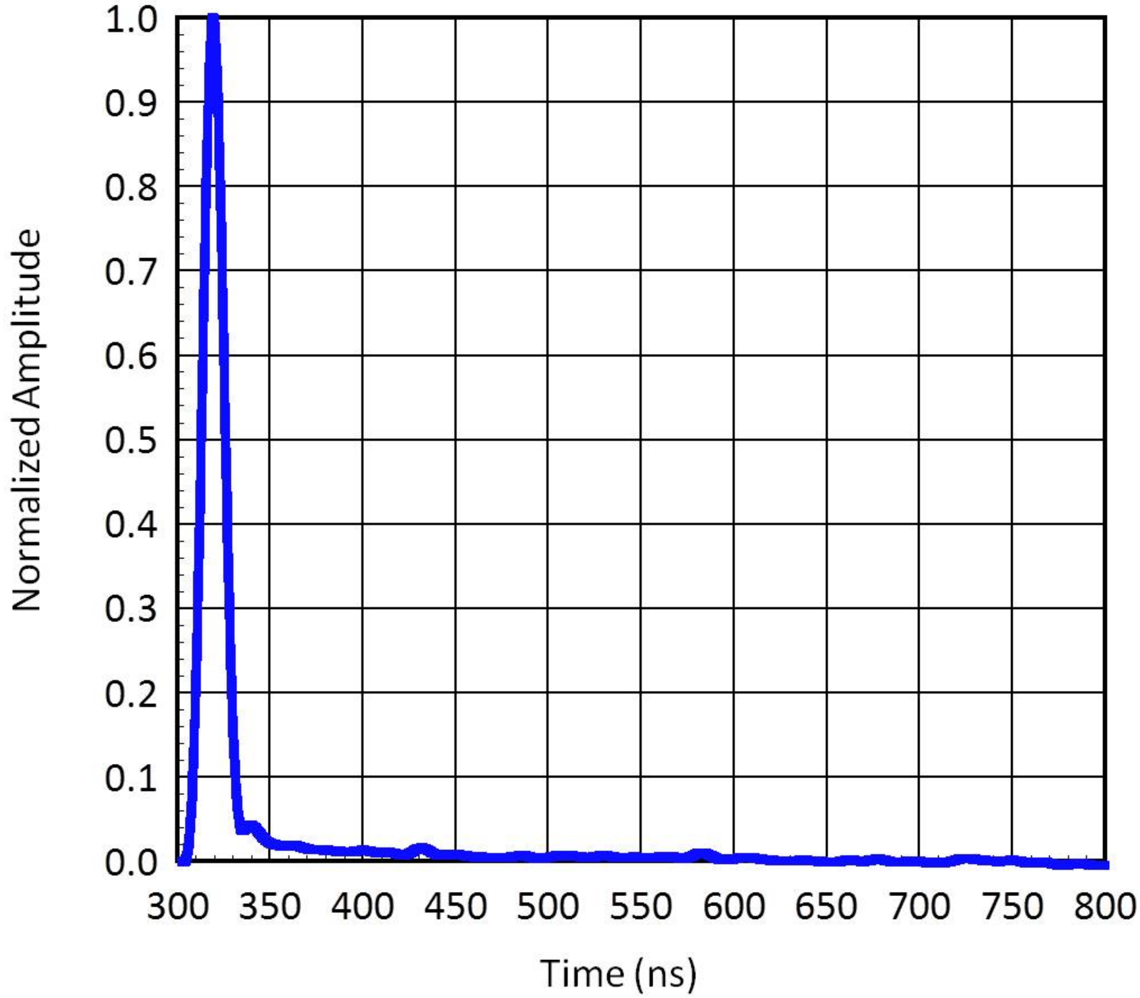

Figure 54. The model with the new collimator for the top nTOF (location "C" in Figure 1). Note that the scattering later in time is greatly reduced, showing that the additional mass of the new collimator was necessary to improve the neutron signal.

REFERENCES

[1] Matzen, K., Phys. Plasmas **4**, 1519 (1997).

[2] Spielman, R. B., *et al., Proceedings of the 9th IEEE Pulse Power Conference*, Albuquerque, NM, edited by R. White and K. Prestwich (Institute of Electrical and Electronics Engineers, New York, 1995), p. 396.

[3] J. Nuckolls *et al*., Nature **239**, 139 (1972).

[4] T. J. Nash *et al*., Phys. Plasmas **6**, 2023 (1999).

[5] J.F. Briesmeister (Ed). MCNP – A General Monte Carlo N-Particle Transport Code, Version 4C, LA-13709-M, Los Alamos National Laboratory, April 2000.

[6] S.A. Pozzi, E. Padovani, M. Marsequerra, Nucl. Instr. and Meth. A 513 (2003) 550-558.

[7] J.T. Mihalczo, J.A. Mullens, J.K. Mattingly, T.E. Valentine, Nucl. Instr. and Meth. A 450 (1998) 531.

[8] S.A. Pozzi, J.K. Mattingly, J.T. Mihalczo, E. Padovani, "Validation of the MCNP-PoliMi Code for the Simulation of Nuclear Safeguards Experiments on Uranium and Plutonium

Metal," Nuclear Mathematical and Computational Sciences: A Century in Review, A Century Anew, Gatlinburg, Tennessee, April 6 – 11, 2003, on CD-ROM, American Nuclear Society, LaGrange Park, IL., 2003.

[9] E. Padovani, S.A. Pozzi, MCNP-PoliMi ver.1.0 User's Manual, CESNEF-021125, Library of Nuclear Engineering Department, Politecnico di Milano, November 2002.

[10] Knoll, G.F., Radiation Detection and Measurement, John Wiley and Sons, NY., 1979.

[11] 1 MeVee = amount of light produced by 1 MeV deposited by a Compton scattered electron.

[12] Birks, J.B., The Theory and Practice of Scintillation Counting, Pergamon Press, NY., 1964.

[13] M. Marseguerra, E. Padovani, S.A. Pozzi, M.D. Ros, Nucl. Inst. and Meth. B 213 (2004) 289-293.

[14] N.R. Stanton, "A Monte Carlo Program for Calculating Neutron Detection Efficiencies in Plastic Scintillator, "Ohio State University Preprint COO-1545-92, Columbus, OH, USA, 1971.

[15] J.B. Czirr, D.R. Nygren, C.D. Zafiratos, Nucl. Instr. and Meth. 31 (1964) 226 – 232.

[16] V.V. Verbinski, W.R. Burrus, T.A. Love, W. Zobel and N.W. Hill, Nucl. Instr. and Meth. 65 (1968) 8 – 25.

[17] S.A. Pozzi, J.A. Mullens, and J.T. Mihalczo, " Analysis of neutron and photon detection position for the calibration of plastic (BC-420) and liquid (BC-501) scintillators, " Nucl. Inst. and Meth. A 524/1-3 pp. 92-101, 2004.

[18] D.B. Pelowitz (Ed), " MCNPX User's Manual," Version 2.5.0, LA-CP-05-0369, Los Alamos National Laboratory, April 2005.

[19] Tektronix Corporation, Beaverton, OR 97077.

[20] J.S. Hendricks and T.E. Booth, " MCNP Variance Reduction Overview, " Radiation Transport Group X-6, LANL, 87544, Los Alamos, NM, 1985.

[21] Shultis, J.K., and Faw, R.E., " An MCNP Primer, " Dept. of Mechanical and Nuclear Engineering, Kansas State University, Manhattan, KS 66506, 2004.

[22] Savitsky, A., and Golay, M. J. E., "Smoothing and Differentiation of Data by Simplified Least Squares Procedures," Analytical Chemistry 36, (8): 1627 – 1639.

[23] For more information, see “Savitzky-Golay smoothing filter” at http://en.wikeipedia.org

[24] For a summary of IAC facilities and contact information, see http://www.iac.isu.edu

[25] W.H. Press, S.A. Teukolsky, W.T. Vetterling, and B.P. Flannery, NUMERIAL RECIPES in FORTRAN, The Art of Scientific Computing, 2nd Ed., Cambridge University Press, 1992.

[26] J.R. Taylor, An Introduction to Error Analysis, 2nd ed., University Science Books, Sausalito, CA, 1997.

[27] For a summary TIVAR 1000 properties and contact information, see http://www.quadrantplastics.com

[28] National Security Technologies, North Las Vegas Operations, North Las Vegas, Nevada.

[29] Personal Correspondence with Dr. Carlos Ruiz, PMTS, of Sandia National Laboratories.

[30] 1 shake = 10^{-08} sec = 10 ns.

[31] C.L. Ruiz, G.W. Cooper, S.A. Slutz, J.E. Bailey, G.A. Chandler, T.J. Nash, T.A. Mehlhorn, R.R. Leeper, D. Fehl, A.J. Nelson, J. Franklin, and L. Ziegler, Physical Review Letters, **93**, 1, 2 July 2004.

[32] T.R. Boehly, D.L. Brown, R.S. Craxton, R.L. Keck, J.P. Knauer, J.H. Kelly, T.J. Kessler, S.A. Kumpan, S.J. Loucks, S.A. Letzring, F.J. Marshall, R.L. McCrory, S.F.B. Mose, W. Seka, J.M. Soures, and C.P. Verdon, "Initial performance results of the OMEGA laser system," *Opt. Commun*., vol. 133, pp. 495-506, 1997.

[33] E.I. Moses, "The National Ignition Facility: Status and plans for the experimental program," *Fusion Sci. Technol*., vol 44, pp. 11-18, 2003.

[34] Duderstadt and Moses, Inertial Confinement Fusion, John Wiley and Sons, Inc., Madison, WI, 1982.

[35] J. A. Frenje, D. T. Casey, C. K. Li, J. R. Rygg, F. H. Seguin, R. D. Petrasso, V. Yu. Glebov, D. D. Meyerhofer, T. C. Sangster, S. Hatchett, S. Haan, C. Cerjan, O. Landen, M. Moran, P. Song, D. C. Wilson, and R. J. Leeper, Rev. Sci. Instrum. **79**, 10E502 (2008).